UNIVERSITY OF KWAZULU-NATAL

The Evolution of Galaxies in Sunyaev-Zel'dovich Selected Galaxy Clusters from ACT DR5

by

Damien Cole Ragavan

Submitted in fulfilment of the academic requirements of Masters of Science in Applied Mathematics

in the

School of Mathematics, Statistics and Computer Science

University of KwaZulu-Natal

Westville

South Africa

February 6, 2023

As the candidate's supervisor, I have approved this thesis for submission.

Name: _____ Signature: _____ Date: _____

"By faith we understand that the entire Universe was formed at God’s command, that what we now see did not come from anything that can be seen." – Hebrews 11:3

Abstract

The galaxy luminosity function (LF) describes the number of galaxies per unit volume as a function of their luminosity. Accurate measurements of the LF can tell us how environmental processes influence the properties of current galaxy populations, helping us obtain clues as to which processes are important in shaping galaxy formation and evolution. Deriving LFs in clusters is generally a simple task since they provide a rich collection of galaxies at the same distance, and the density with respect to the surrounding environment is high enough to identify members both photometrically and spectroscopically.

We examine the galaxy population of 3008 Sunyaev-Zel'dovich (SZ)-selected galaxy clusters, drawn from the Atacama Cosmology Telescope Data Release 5 (ACT DR5) sample, by measuring their composite r-band LFs from $0.20 < z < 0.80$ using optical data from the ninth data release of the Dark Energy Camera Legacy Survey (DECaLS DR9). This type of study has never been performed on this specific cluster sample over this chunk of cosmic time. Taking advantage of accurate photometry from DECaLS, we used photometric redshifts to construct redshift-binned and mass-binned composite LFs over the apparent magnitude range of $17.0 < m_r < 22.5$. Cluster membership was determined probabilistically using galaxy photometric redshift probability distributions. An LF of each cluster was weighted according to the richness and number of contributing galaxies to construct the composite LF. A single Schechter function was fitted to 12 redshift-binned composite LFs and 12 low-mass and high-mass subset LFs. A χ^2 minimization technique was then used to estimate the best-fit parameters, m^* and α, from the Schechter model.

For our total redshift-binned LFs, we obtained a characteristic magnitude of $m^* = 18.51 \pm 0.02$, and faint-end slope of $\alpha = -1.18 \pm 0.01$ at $\langle z \rangle = 0.225$. At $\langle z \rangle = 0.775$, we obtained: $m^* = 20.62 \pm 0.23$ and $\alpha = -2.19 \pm 0.10$. We find a strong and significant ($\approx 10.1\sigma$) evolution of α with redshift for the total composite LFs.

Low-mass and high-mass subsets were defined by selecting the top and bottom 25 %

of clusters by mass in each redshift bin. For the low-mass subsets, we obtained Schechter best-fit parameters of (m^*, α) = (18.52 $\pm$ 0.05, -1.18 $\pm$ 0.01) at $\langle z \rangle = 0.225$, and ($m^*$, α) = (20.14 $\pm$ 1.82, -2.36 $\pm$ 0.83) at $\langle z \rangle = 0.775$. For the high-mass subset, we found best-fit parameters of (m^*, α) = (18.48 $\pm$ 0.03, -1.15 $\pm$ 0.01) at $\langle z \rangle = 0.225$, and ($m^*$, α) = (21.14 $\pm$ 0.55, -2.05 $\pm$ 0.30) at $\langle z \rangle = 0.775$. The key result from the mass subsets is that they are consistent ($< 1\sigma$) with the total redshift-binned LFs, implying no dependence in α or m^* with cluster mass.

Our composite LFs reveal a trend of M^* becoming brighter and α becoming steeper with redshift, with α being poorly constrained in our high redshift bins. Our faint-end slopes appear to be considerably steeper than the slopes measured in previous literature. We attribute the steepness in our faint-end slopes to be a result of measuring our LFs in the r-band, and that this samples bluer rest-frame wavelengths than for our lower redshift samples. We notice an excess of bright galaxies above the Schechter function fit in many of our LFs, especially in the mid-redshift bins of our sample. We conclude that our cluster LFs are in disagreement with previous field studies we made comparisons to, which measured a steeper α than us at a lower redshift than what our sample covers. This is consistent with previous studies that suggested that the cluster LF is different from the field LF, especially in redder passbands.

Declaration: Plagiarism

I, Damien Cole Ragavan, declare that:

1. the research reported in this dissertation, except where otherwise indicated or acknowledged, is my original work;

2. this dissertation has not been submitted in full or in part for any degree or examination to any other university;

3. this dissertation does not contain other persons' data, pictures, graphs or other information, unless specifically acknowledged as being sourced from other persons;

4. this dissertation does not contain other persons' writing, unless specifically acknowledged as being sourced from other researchers. Where other written sources have been quoted, then:

   a) their words have been re-written but the general information attributed to them has been referenced;

   b) where their exact words have been used, their writing has been placed inside quotation marks, and referenced;

5. this dissertation does not contain text, graphics or tables copied and pasted from the Internet, unless specifically acknowledged, and the source being detailed in the dissertation and in the References sections.

Signature: _____

Date: _____

Acknowledgements

I would like to firstly thank my Lord and saviour Jesus Christ, without Him, none of this would be possible. A special thank you to my supervisor, Prof. Matt Hilton, for all his continuous assistance, patience, and guidance throughout this project. Thank you for the weekly meetings and constant feedback, which made this project much more manageable. I would also like to thank my parents, Jerome and Chireen, and my sister, Caitlyn, for all their support and encouragement. A special thank you to Kabelo Kesebonye for his constant assistance and support in this project. Thank you to Prof. Siva and my fellow NASSP colleagues for all their advice and assistance throughout. A thank you to all my friends, whose names are too numerous to mention, for their support and motivation. Finally, I would like to thank NASSP-UKZN and the NRF for their financial support and for granting me this opportunity to complete my master's dissertation under them.

Contents

List of Figures

List of Tables

Chapter 1

Introduction

In this thesis, we examine the galaxy population of Sunyaev-Zel'dovich selected clusters by measuring their optical luminosity functions. By measuring the shape of the galaxy luminosity function in a number of environments, one is able to obtain clues as to which processes are essential in shaping galaxy evolution. In this chapter, we provide an introduction to cosmology, galaxies and their properties, galaxy clusters, and cluster detection methods. We also describe the Sunyaev-Zel'dovich effect and introduce the galaxy luminosity function.

1.1 Introduction to Cosmology

Cosmology is a discipline focused on the history of the Universe in both its structure and evolution. A fundamental basis for cosmology is the cosmological principle. The cosmological principle assumes that the Universe is homogeneous and isotropic. Studies of the clustering of galaxies and temperature changes in the cosmic microwave background have confirmed these assumptions (e.g., Bennett et al., 2013; Planck Collaboration et al., 2014b; Alam et al., 2016). In addition, it is assumed that the same laws of physics hold everywhere within the Universe.

1.1.1 Expansion of the Universe

In the early twentieth century, the first set of descriptive equations about the Universe was derived from Einstein's theory of general relativity, which redefined the understanding of gravity. The most interesting implication of this new formulation was that space-time was not in equilibrium, but rather expanding or contracting. He introduced a constant, termed the cosmological constant (Λ), into his equations to counteract the expansion or contraction. A more substantial model was introduced by Alexander Friedmann (Friedmann, 1924), who solved Einstein's equations without assuming the Universe was static and produced a set of equations in which the Universe expanded from a single point. In this model, the expansion of the Universe is dictated by some curvature parameter (k). Friedmann (1924) defined three scenarios in the Universe: (i) if $k = 0$, then the density of matter (Ω) in the Universe is equal to the critical value at which the Universe will expand forever at a decreasing rate; (ii) if $k > 0$ (referred to as a "closed" Universe) then it would cease expansion and cause the Universe to collapse backwards to a "big crunch"; and (iii) if $k < 0$ (referred to as an "open" Universe) then there would not be a sufficient gravitational attraction to stop expansion and the Universe expands forever.

In 1926, Edwin Hubble (Hubble, 1926) confirmed that there existed other galaxies like our own and that the observable Universe was larger than previously expected. More importantly, the radiation from the faraway galaxies was systematically redshifted, which, interpreted as a Doppler effect, suggested that they were moving away from us at great speed. Georges Lemaître solved this puzzle in 1927 (Lemaître, 1927), by calculating the exact solutions of Einstein's equations by assuming a positively curved space, time-varying matter density and pressure, and a non-zero cosmological constant. He obtained a model with perpetual accelerated expansion. The great novelty was that Lemaître provided the first interpretation of cosmological redshifts in terms of space expansion, instead of a real motion of galaxies: space was constantly expanding and consequently increased the apparent separations between galaxies. This idea proved to be one of the most significant discoveries of the century.

Friedmann's model was later accompanied by Edwin Hubble's discovery that the Universe was in fact expanding (Hubble, 1929). By measuring the distances to nearby galaxies using standard candles, such as Cepheid variable stars, and comparing these distances to the galaxies' redshifts, Hubble (1929) showed that the further away a galaxy was the faster its rate of recession. Hubble's Law was inevitably derived from this relation, in which the speed of recession and distance are directly proportional and are related by Hubble's constant (H_0) in the equation $v = H_0 d$. This linear relationship (shown in figure 1.1.1) is a consequence of observing a Universe that is constantly expanding. Modern measurements have placed H_0 to be in the range of 65 - 75 $\mathrm{kms^{-1}Mpc^{-1}}$ (e.g., Freedman et al., 2001; Hinshaw et al., 2013; Planck Collaboration et al., 2016b; Abbott et al., 2017; Planck Collaboration et al., 2020).

In the local Universe, one of the most reliable measurements of H_0 comes from Type Ia supernovae (e.g., Freedman et al., 2009; Riess et al., 2016; Dhawan et al., 2018), which rely on primary distance indicators for their zero-point calibration (e.g., Cepheids and geometrical distances). Type Ia supernovae (SNe Ia) are supernovae that occur in binary star systems in which one of the stars is a white dwarf. The other star can be anything from a giant star to an even smaller white dwarf. SNe Ia are useful observation probes into the early Universe and its structure since their luminosities are similar. These sources have characteristic light curves which can be standardised and can thus be used to measure cosmological distances. Large numbers of SNe Ia have been discovered with the Supernova Legacy Survey (SNLS; Astier et al., 2006), providing constraints on the matter density of the Universe, Ω_m, and the dark energy equation of state, w_X, assuming a flat universe. Observations of SNe Ia provided the first significant evidence that the Universe is expanding at an accelerated rate, providing the first evidence for dark energy (Riess et al., 1998; Perlmutter et al., 1999).

The early discovery of the expansion of the Universe was swiftly succeeded by attempts to theorize how the Universe came to be. These attempts all led to one prevailing model called the Big Bang Theory.

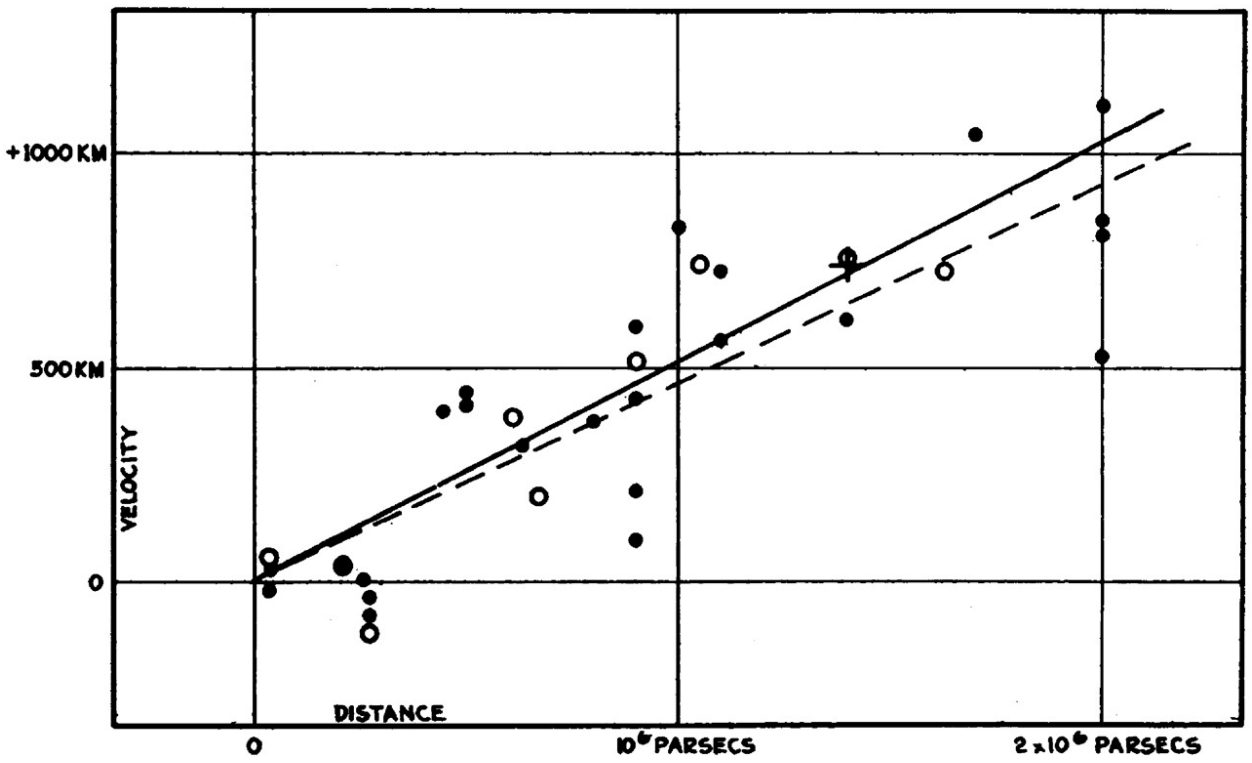

Figure 1.1.1: A plot representing the linear relationship between the velocity and distance to galaxies from Hubble (1929). Radial velocities, corrected for solar motion are plotted against distances estimated from evolved stars and average luminosities of nebulae in a cluster.

1.1.2 The Big Bang Theory

The Big Bang Theory (BBT) is a cosmological description of the development of the Universe, stating that the entirety of the elements in the Universe originated from a hot, dense plasma, beginning in an epoch of radiation dominance. Although successful, there were initial concerns with the theory. One of these was that there has not been enough time allocation in a standard Big Bang model for radiation to travel from one region of the Universe to the other. This is a problem since the Universe appears to have the same temperature in opposing directions. Another concern was that the model gives no explanation for the observed flatness of the Universe. These concerns were eventually reconciled when the idea of 'inflation' was proposed by Alan Guth in 1981 (Guth, 1981). This theory allows for a small

enough region for radiation to travel across before an exponential expansion in the volume of space. Inflation predicts that space has zero curvature (i.e., flat) and the required mass-energy for this to be true is larger than the mass-energy apparently available in baryonic matter.

A spatially-flat Universe is mainly composed of dark energy ($\approx 68\%$) and dark matter ($\approx 27\%$), with a small amount of baryonic matter, which is matter composed of baryons, ($\approx 5\%$) [1]. Unlike normal matter, dark matter is a hypothesised form that does not interact with the electromagnetic field. This means it neither absorbs nor emits electromagnetic radiation, making it difficult to detect. The noticeable presence of dark matter was first predicted by Fritz Zwicky in 1933 (Zwicky, 1933), who linked the line-of-sight radial velocities of galaxies within a galaxy cluster to the mass of the cluster. By making observations of galaxies within the Coma cluster, Zwicky (1933) discovered large line-of-sight radial velocities which could not be explained by visible matter, but rather by a non-detectable form of matter - i.e., dark matter. A number of subsequent studies on galaxies and galaxy clusters have confirmed this existence through observations of galaxy rotation curves (e.g., Rubin et al., 1980; Begeman, 1987; Salucci et al., 2007; Kauffmann et al., 2015; Brook & Shankar, 2015), gravitational lensing (e.g., Bartelmann & Schneider, 2001; Coe et al., 2010; Kilbinger et al., 2013; Caminha et al., 2022), stellar dynamics (e.g., Bridges et al., 2006; Thomas et al., 2011 Sweet et al., 2015; van Houdt et al., 2021), and distributions of intracluster gas (e.g., Sarazin, 1986; Brighenti & Mathews, 2002; Babyk et al., 2012).

The currently most accepted model for the Universe is a flat ΛCDM (cold dark matter) Big Bang model (Planck Collaboration et al., 2014a) where the expansion of the Universe is accelerating due to the cosmological constant Λ and the age of the Universe is ≈ 13.8 billion years. Cold dark matter (CDM) is a hypothetical type of dark matter that moves slowly compared to the speed of light. In the CDM theory (Peebles, 1982), structure grows hierarchically, with small objects collapsing under their self-gravity first and merging in a continuous hierarchy to form larger and more massive objects. This model accounts for

[1] https://science.nasa.gov/astrophysics/focus-areas/what-is-dark-energy

the accelerated expansion of the Universe, the large-scale matter distribution within the Universe, the amount of hydrogen distributed throughout the cosmos, and the existence and structure of the cosmic microwave background radiation.

1.1.3 The Cosmic Microwave Background

In the beginning, approximately 13.8 billion years ago, when the Universe was very young, it was extremely dense and hot, with temperatures greater than 10^{32}K, and filled with hydrogen plasma and radiation (Anderson, 2015). As it expanded, this plasma and radiation cooled. After approximately 380000 years it had cooled sufficiently for neutral hydrogen atoms to form, giving rise to the recombination epoch (Sunyaev & Zeldovich, 1970; Farhang et al., 2012). Unlike the plasma, these new atoms could not scatter the thermal radiation, making the Universe transparent and resulting in photons freely moving through space. Ever since, these energetic photons have been propagating through space, being stretched by the expansion of the Universe. This has led to an increase in their wavelength, as they grow less energetic. This radiation has since been redshifted down to a spectrum with T $\approx$ 2.725 K (Fixsen, 2009). This is the origin of the cosmic microwave background (CMB) radiation (Gawiser & Silk, 2000).

The existence of the CMB was first postulated in the late 1940s by George Gamow (Gamow, 1948), Ralph Alpher and Robert Herman (Alpher & Herman, 1948), who were investigating the nucleosynthesis of light elements in the early Universe. They discovered that extremely hot temperatures were needed to synthesise these elements and leftover radiation from the Big Bang would permeate and be detectable even today. It wasn't until 1965 when the first CMB detection was made by Arno Penzias and Robert Wilson who, through the construction of the Dicke radiometer (Dicke, 1946), detected an excess antenna temperature which they could not account for (Penzias & Wilson, 1965). Dicke et al. (1965) confirmed that this excess temperature was in fact due to the CMB.

Since it was first detected, CMB detections by telescopes and ground-based instruments have indicated temperature fluctuations (as shown in figure 1.1.2) in this background radi-

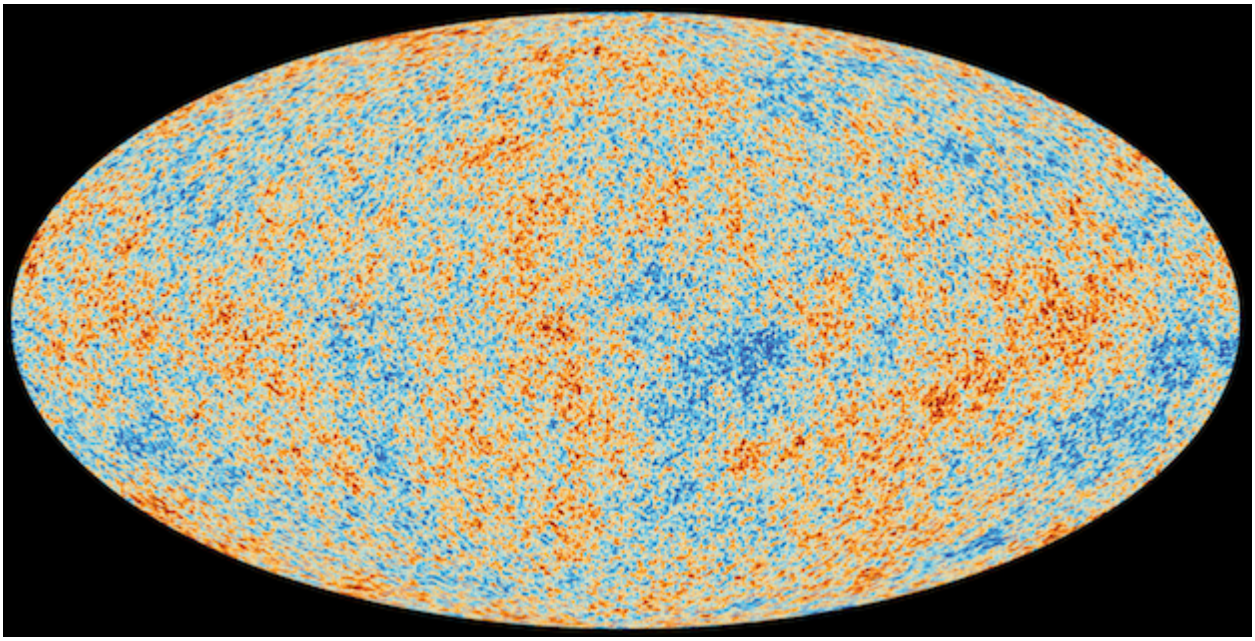

Figure 1.1.2: The anisotropies of the CMB, as observed by ESA's Planck mission. The CMB is a snapshot of the oldest light in our cosmos and displays tiny temperature fluctuations that correspond to regions of slightly different densities, representing the seeds of all the stars and galaxies today. This image is based on data from the final release of the Planck Legacy mission, published in July 2018. Source: https://sci.esa.int/web/planck/-/60500-plancks-view-of-the-cosmic-microwave-background

ation (e.g., Wilkinson Microwave Anisotropy Probe (WMAP), Bennett et al., 2003; Planck satellite, Bouchet, 2009; South Pole Telescope, Ruhl et al., 2004; Atacama Cosmology Telescope, Kosowsky, 2006). An interesting discovery made from CMB measurements is that it has a near-perfect blackbody spectrum (Mather et al., 1990). This feature cemented the consensus that the CMB was a remnant of the Big Bang (Peebles et al., 1991). Studies of these fluctuations can help constrain basic parameters describing the Big Bang model, as well as provide us with information about the origin of galaxies, clusters of galaxies, and large-scale structures of galaxies (Bennett et al., 2003). We discuss the structure of galaxies, including their properties and evolution, in the next section.

1.2 Galaxies

The large-scale structure of the Universe consists of voids and filaments, that can be broken down into superclusters, clusters, galaxy groups, and subsequently into galaxies. Galaxies are gravitationally bound systems consisting of dark matter, stars, stellar remnants, and the interstellar medium (ISM). The ISM usually consists of gas, dust, and other matter and radiation that exists between star systems in a galaxy. Galaxies can range from hosting fewer than 100 million stars (dwarf galaxies) to around 100 trillion stars. The largest galaxies are the brightest cluster galaxies (BCGs) found in galaxy clusters. BCGs include the most massive galaxies in the Universe and are generally elliptical galaxies which lie close to the geometric and kinematical centre of their host galaxy cluster. Some BCGs can be classified as central dominant (cD) type galaxies (Tonry, 1987; Katayama et al., 2003; Seigar et al., 2007), which are known to be supergiant ellipticals or central dominant galaxies characterized by a large halo of stars.

It is estimated that there are $\approx 2 \times 10^{12}$ (two trillion) or more galaxies in the observable Universe, with most being far less massive than the Milky Way (Conselice et al., 2016). Properties of galaxies such as their size, mass, morphology, and colour contribute to their evolution. We examine the morphological and colour properties of galaxies, in turn, below.

1.2.1 Morphology

Galaxy morphological classification is a historically used system by astronomers to divide galaxies into groups based on their visual appearance or shape. There are multiple schemes available which can be used to classify galaxies, with the most popular being the Hubble sequence or tuning fork (Hubble, 1926; Hubble, 1927; Hubble, 1936) which splits galaxies into two distinct categories: elliptical and spiral (or disk) galaxies (shown in figure 1.2.1). Lenticular galaxies (Sandage, 1961) are an intermediate type of galaxy that lies between the two categories. Historically, the left end (ellipticals) of Hubble's sequence is dubbed as 'early-type' galaxies and the right (spirals) as 'late-type' galaxies, although this has nothing to do with galaxy evolution as it is understood today.

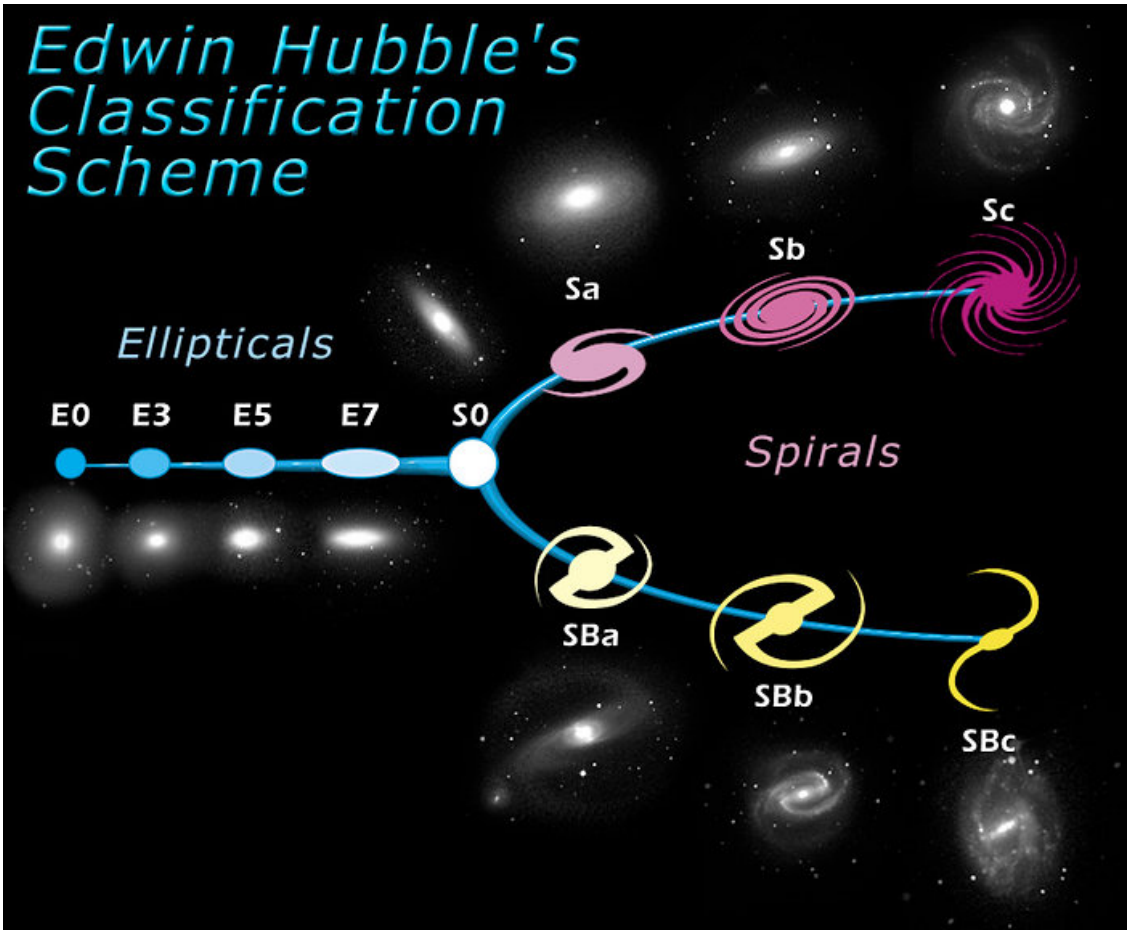

Figure 1.2.1: Tuning-fork style diagram of the Hubble sequence for galaxies. The left end depicts the different types of elliptical galaxies (E), while the right shows normal and barred spiral (S) galaxies. The region on the scale between elliptical and spiral galaxies is reserved for lenticular galaxies (S0). Source: https://esahubble.org/images/heic9902o/

Hubble's classification is still one of the predominant classification models and has since been built upon (e.g., De Vaucouleurs, 1959a; Sandage, 1961; Buta & Combes, 1996). Additional classification schemes have also been established based on either spectral properties or kinematics (Johnson & Morgan, 1953; Emsellem et al., 2007; Emsellem et al., 2011; Schulze et al., 2018; Krajnović et al., 2020). One popular addition to the tuning fork was the de Vaucouleurs system, which distinguishes between spiral and irregular galaxies, and adds variety to the spiral structure by considering rings (De Vaucouleurs, 1959a).

As figure 1.2.1 depicts, spiral galaxies are subdivided into distinct types. Independent of their type, they all host spiral arms, which are characterised by an abundance of star formation, and lie within a galactic disc. Hence, spiral arms are associated with young and bright stellar populations, making their structures well-defined. Furthermore, $\approx 25-50\%$ of local spiral galaxies provide proof of a galactic bar, with some galaxies hosting numerous bar structures (Aguerri et al., 2009; Masters et al., 2011; Cheung et al., 2013; Lee et al., 2019). Unlike the spiral arms, the inner regions (often referred to as the bulge) of spiral galaxies are associated with an excess of light as compared to the exponential disk profile and are characterised by an old stellar population.

On the other hand, elliptical galaxies are smooth, well-defined systems with a continuously declining brightness distribution. Most elliptical galaxies are characterised by older, low-mass stellar populations. Hence, they provide evidence for minimal star formation activity. De Vaucouleurs (1958) introduced the quantitative decomposition of the luminosity distribution which allowed for the surface brightness profiles of spiral galaxies to be resolved into a spheroidal (or bulge) component associated with elliptical galaxies (De Vaucouleurs, 1948; De Vaucouleurs, 1953) and exponential disk characteristics of spiral galaxies (Patterson, 1940; De Vaucouleurs, 1959b).

To date, millions of stars in galactic regions (e.g., halo, disk, bulge, bar) of the Milky Way have been spectroscopically surveyed (e.g., Yan et al., 2022), producing an increasingly detailed picture of general galactic characteristics and specific assembly histories (Eisenstein et al., 2011). The different types of stars found in galaxy stellar populations also have an effect on the various colours we observe in galaxies. In the next section, we discuss the colour properties of galaxies.

1.2.2 Colour

The more massive a star is, the shorter its lifetime and the higher its temperature is, i.e., the bluer it appears (Schaller et al., 1992; Da Costa et al., 2010; Gvaramadze et al., 2017). Since high-mass stars are short-lived, the blue colour found within galactic regions is associated

with ongoing star formation. Therefore, a young stellar population has an average colour that is blue since most of the light is coming from the hot stars. Spiral galaxies, which are characterised by high star formation activity in their spiral arms and disks, are typically associated with the colour blue (Kennicutt, 1989; Martin & Kennicutt, 2001) and younger stellar populations. On the other hand, low-mass stars are cooler in temperature, and as a result, appear red in colour. An old stellar population is red since most of the hot, blue stars have died off and turned into red giant stars, leaving behind the bright cool stars that supply most of the light. Elliptical galaxies, which are associated with low star formation, are known hosts of older stellar populations, and thus typically appear red (Martig et al., 2009).

A big step in broadening our understanding of the differences between galaxies was provided by the colour separation observed between spiral and elliptical galaxies (Baum, 1959). Additional observations and analysis have resulted in the colour-magnitude diagram (Chester & Roberts, 1964; Chiosi, 1967; Visvanathan & Sandage, 1977; Tully et al., 1982). The colour-magnitude or colour-mass diagram shows the relationship between optical colour and absolute magnitude, or absolute magnitude and galaxy mass. As shown in figure 1.2.2, this diagram is divided into three distinct regions: (top) the 'red sequence'; (middle) the 'green valley'; and (bottom) the 'blue cloud'. The 'red sequence' (or RS) contains mostly elliptical (red) galaxies. The existence of the red sequence has been known for over 50 years (Baum, 1959), and the form of the rest of the distribution has become clear over the decades (e.g., Visvanathan, 1981), with a large increase in our knowledge coming from large galaxy catalogues with accurate photometry produced by the Sloan Digital Sky Survey (SDSS; Strateva et al., 2001; Bell et al., 2003). The 'blue cloud' includes mostly spiral (blue) galaxies, as expected. The region between these two distributions lies an underpopulated area known as the 'green valley', indicating that the transition from star-forming to quiescent happens on shorter timescales compared to the periods of star formation and quiescence (Brammer et al., 2009; Loh et al., 2010). However, more recent observations indicate that the distribution of galaxy colour is more continuous and varied, calling the existence of a singular pathway

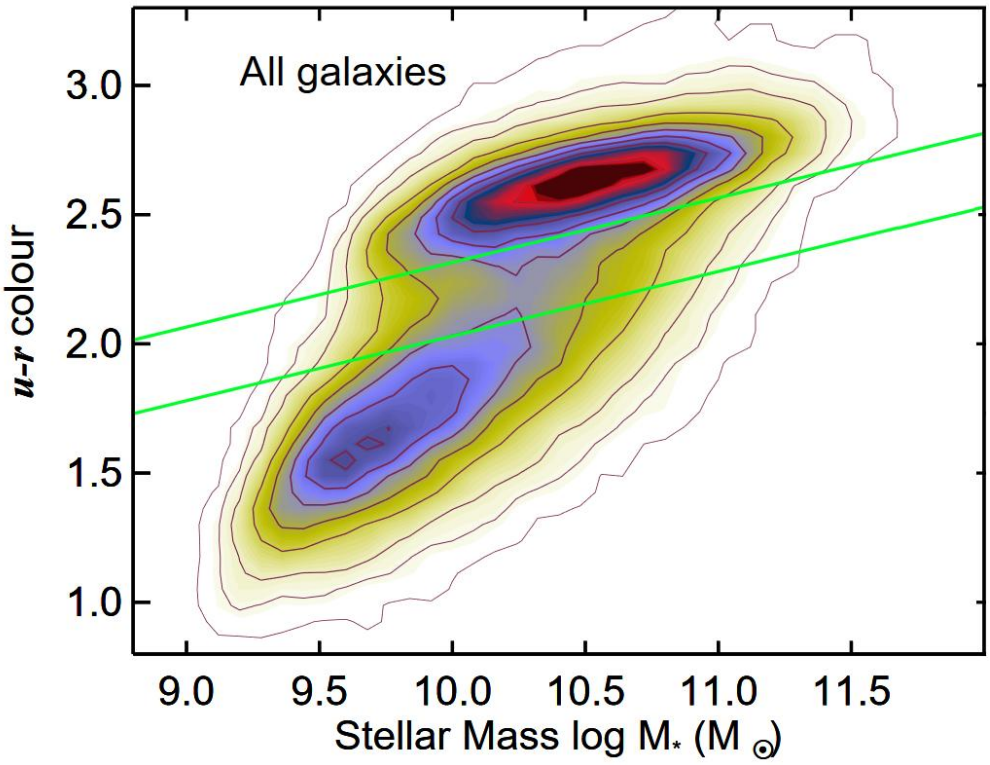

Figure 1.2.2: A u - r colour-stellar mass diagram from Schawinski et al. (2014) based on SDSS (Abazajian et al., 2009), the Galaxy Evolution Explorer (GALEX) (Martin et al., 2005), and Galaxy Zoo (Lintott et al., 2008; Lintott et al., 2011) data. The upper region shows the region referred to as the red sequence, while the lower region is referred to as the blue cloud, each displaying the associated apparent colour. The transition region between the two solid green lines is referred to as the green valley.

through the green valley into question (Schawinski et al., 2014; Smethurst et al., 2015; Eales et al., 2018). These colour distributions depend on the way galaxies evolve over time and the processes that have generated the variety of structures observed in galaxies. We discuss the origin and evolution of galaxies in the next section.

1.2.3 Galaxy formation and evolution

Galaxies are thought to begin as small clouds of stars and dust swirling through space. As other clouds of stars and gas get close, gravity sends these objects careening into one another and knits them into larger spinning packs (Pillepich et al., 2017). Subsequent collisions can cling material toward a galaxy's outskirts, creating extensive spiral arms filled with colonies of stars. At the end of the dark ages, as the Universe was slowly re-ionised, the first galaxies were formed. As primordial over-densities grow via gravitational attraction, baryons condense within dark matter halos. Gas is accreted from (what later is known as) the intergalactic medium (IGM) forming the interstellar medium (ISM) and the enveloping circum-galactic medium (CGM) (Dayal & Ferrara, 2018).

Galaxy formation is dependent on non-linear density fluctuations and initial conditions, such as redshift, density and composition (Peebles, 1993; Mo et al., 2010; Silk et al., 2014). Although all galaxies form via gravitational instabilities (Dayal & Ferrara, 2018) within a broader dark matter halo, the individual processes quickly diverge thereafter (Mo et al., 2010). In the current paradigm, the initial formation of star-forming disks (at low and intermediate masses) is suggested to occur through cold-mode accretion, which means that most gas is accreted at temperatures lower than the halo virial temperature ($T \leq 10^4$ K) (Katz & Gunn, 1991; Birnboim & Dekel, 2003; Kereš et al., 2005; Benson & Bower, 2011; Woods et al., 2014; Dayal & Ferrara, 2018). High-mass systems, on the other hand, are dominated by the previously assumed standard paradigm of hot-mode accretion (Kereš et al., 2005; Ocvirk et al., 2008), during which a large amount of gas falling into the dark matter halo is shock heated to the halo virial temperature (Dayal & Ferrara, 2018). Depending on the specific temperature, gas settles into disks of varying scale height (Yoachim & Dalcanton, 2006). The colder the gas, the denser it may become, resulting in thinner disks where a majority of star formation occurs (Mo et al., 1998). After stars are formed in the thin disk, they experience gradual dynamic heating leading to older stellar populations being associated with larger galactic scale heights (Binney & Tremaine, 2011). After the formation of a gaseous disk and the associated influx in star formation, galaxy formation depends on

environmental conditions, such as the mass, composition, and manner in which matter is accreted.

Typically, star formation occurs in the densest regions in giant molecular clouds. Feedback processes (thermal or kinetic) have an impact on these regions and, thus, influence galactic star formation. Two such feedback mechanisms are defined: (i) positive feedback (boosts star formation), and (ii) negative feedback (quenches star formation). Sources of positive feedback include turbulence (Elmegreen & Scalo, 2004; Ostriker & Shetty, 2011; Pan et al., 2016) and chemical enrichment by stars (Nomoto et al., 2013; Hansen et al., 2020). Negative feedback mechanisms include stellar radiation (Ceverino & Klypin, 2009; Hopkins et al., 2014; Emerick et al., 2018), supernovae (Vecchia & Schaye, 2012; Sarmento & Scannapieco, 2022), and active galactic nuclei (AGN) (Fabian, 2012; Cicone et al., 2014; Cielo et al., 2018). Feedback mechanisms generally have varying effects depending on galactic properties, such as stellar masses. At low stellar masses, supernovae-driven winds can accelerate (diffuse) gas to high velocities and expel vast amounts from the galaxy (Matzner, 2002; Ostriker et al., 2010; Ostriker & Shetty, 2011; Puchwein & Springel, 2013). While expelling large amounts of diffuse gas has no immediate effect on star formation, it does impact the reservoir of gas available for future star formation. As galaxy mass increases, AGN feedback, i.e. the intense non-stellar emission associated with the accretion onto supermassive black holes, becomes increasingly important (Kormendy et al., 2009). In massive galaxies the AGN can deposit vast amounts of energy into the ISM, thereby suppressing star formation (Best et al., 2007; Somerville et al., 2008; Puchwein & Springel, 2013); Smith et al., 2020). AGN feedback also plays an important role in shaping the galaxy luminosity function - the number density of galaxies of different luminosity (Bower et al., 2006). Although the detailed processes driving the intense nuclear activity are not fully understood (Steinborn et al., 2018), it is well established that galaxy mergers can trigger AGN feedback.

Galaxy mergers are violent, inelastic collisions of two or more galaxies (as shown in figure 1.2.3), and are extended events in a galaxy's evolution (Boylan-Kolchin et al., 2008). It is currently well-established that mergers can impact the star formation rate (SFR) of galaxies

Figure 1.2.3: Snapshots of galaxies at six different stages of the merging process, courtesy of the Hubble Space Telescope (HST). One merger could take millions of years to complete, so the individual stages are illustrated with different images from 59 new images of colliding galaxies from HST. Source: https://sci.esa.int/web/hubble/-/42637-merger-stages-of-interacting-galaxies

in different ways. Mergers have been found to increase (Rodríguez Montero et al., 2019; Baron et al., 2020; Silva et al., 2021), not impact (Pearson et al., 2019), and decrease (Wu et al., 2020; Ellison et al., 2022) the SFR on different timescales, depending on the properties of the specific merger. Potentially merger-triggered mechanisms which impact the SFR include facilitating the central galactic black hole growth (Schawinski et al., 2014; McAlpine et al., 2017), thus leading to possibly strong AGN feedback (Hopkins et al., 2013; Park et al., 2018; Chadayammuri et al., 2021). Mergers are typically associated with intermediate and lower-density environments. They are rare in higher-density environments because galaxies

in galaxy clusters have a high-velocity dispersion (Menci & Fusco-Femiano, 1996; Gnedin, 2003) and interacting galaxies require sufficiently slow relative velocities to merge (Binney & Tremaine, 1987).

Once galaxies are formed, they usually attract each other by gravity and merge to form larger galaxies. The galaxies can then, by gravity, group together to form filaments and clusters. As we will discuss in the next section, galaxy clusters play a pivotal role in shaping galaxy evolution and structure.

1.3 Galaxy clusters

Galaxy clusters are the most massive gravitationally bound systems in the Universe and are normally composed of hundreds of galaxies, dark matter, and a hot gaseous plasma known as the intracluster medium (ICM). They, therefore, represent a fair sample of the Universe as it evolves over cosmic time. We show one of the nearest rich cluster of galaxies, which is the Coma cluster, in figure 1.3.1.

Galaxy cluster formation involves multiple mechanisms on different scales. This formation process is non-linear since the primordial linear density grows sufficiently under the action of gravity to become non-linear at cluster scales. In other words, clusters grow non-linearly with time. Cluster formation models (Kaiser, 1986; Huss et al., 1999; Kravtsov & Borgani, 2012) indicate that the general process can be traced to tiny density fluctuations in the early Universe, which are amplified due to dark matter and gravity.

Another important feature of clusters is their large masses, $\approx 10^{14} - 10^{15} M_{\odot}$ (Mohr et al., 1999), which ensure that gas and stellar mass observed within them remain gravitationally bound. The majority of cluster mass ($\approx 88\%$) consists of dark matter within the radius that encloses an average density of 200 times the critical density at the cluster redshift - R_{200}. The remainder of the mass contributions come from the ICM ($\approx 10\%$), and, lastly, from the hundreds of galaxy members within the cluster (making up $\approx 2\%$) (Biviano & Salucci, 2006). Studies such as Vikhlinin et al. (2009) showed that galaxy clusters are assembled late, doubling their masses on average since $z \approx 0.5$. Similarly, they accrete half their present-day

member galaxies at $z < 0.5$ (Berrier et al., 2008).

Figure 1.3.1: A wide-field image of the region around the Coma galaxy cluster (Abell 1656) constructed from the images in the Digitized Sky Survey. NGC 4921 is the small circular galaxy below and a little to the right of the centre of the image. The field-of-view is approximately 2.7 × 2.85 degrees. North is 0.4° left of vertical and East is on the left.
Source: https://esahubble.org/images/heic0901c/

The ability of galaxies to continue forming stars is well known to depend on their local environment. Observations have revealed a relationship between the environmental density and the morphological galaxy type, known as the morphological-density relation for

galaxies (Dressler, 1980; Dressler et al., 1997; Smith et al., 2005). While field populations are dominated by actively star-forming galaxies (usually late-morphological types such as spirals (Sp) or irregular galaxies (Irr)), cluster populations are dominated by galaxies with early-type morphologies, primarily ellipticals (E) (Bahcall, 1977). This suggests that almost all galaxies in the cores of rich clusters are now passively evolving. The old and relatively homogeneous nature of their stellar populations leads to the majority of galaxies in clusters occupying relatively tight loci in colour-magnitude diagrams which have proved important to modern cluster finding algorithms (e.g., Oguri, 2014; Rykoff et al., 2014). This is evident in the Butcher-Oemler effect, which is the excess of galaxies bluer than the colour-magnitude sequence (where most elliptical galaxies lie) in clusters at $z > 0.1$ - 0.2 as compared to the richest nearby clusters (Butcher & Oemler, 1978b).

Galaxy clusters are also known to host RS (see Section 1.2.2) galaxies, which mostly house long-lived stars with low masses and red optical colours. The evolution of these galaxies could be examined by inspecting the luminosity distribution of cluster galaxies, either with the dwarf-to-giant ratio (DGR) approach (Stott et al., 2007) or with a luminosity function analysis (Zhang et al., 2019). The DGR approach offers a simple approach to quantify the relative evolution of the numbers of bright and faint galaxies by using the ratio of the number of dwarfs to giants along the red sequence and using a single number to parameterize the distribution of galaxy luminosities within a population (Stott et al., 2007). RS galaxies exhibit little star formation activity and, thus, their formation and evolution provide clues to how quenching of galaxy star formation occurs in the cluster environment (Zhang et al., 2019). As we will discuss in the next section, various processes influence the suppression of star formation within galaxy clusters.

1.3.1 Quenching mechanisms

Galaxy clusters not only influence galactic morphology but also greatly impact star formation properties of galaxies in their vicinity (Boselli & Gavazzi, 2014). Due to environmental processes, galaxies in clusters are far more likely to have reduced star formation, compared

to field galaxies (Oemler, 1974; Butcher & Oemler, 1978a). Mechanisms such as ram-pressure stripping (Gunn & Gott, 1972), galaxy harassment (Moore et al., 1996), mergers (Binney & Tremaine, 1987; Roos, 1981), and tidal interactions (White, 1980) have been proposed to quench star formation and transform star-forming galaxies into passively evolving ones. Especially relevant to the outskirts of clusters are strangulation and pre-processing, which are both related to the hot gas halo surrounding a galaxy. Strangulation is the disruption of hot halo gas inflow to the inner galactic regions, leading to a cold gas deprivation within the galaxy and hence quenching star formation on long time scales (Weinmann et al., 2006; von der Linden et al., 2010; Vaughan et al., 2020). Pre-processing involves hot halo gas being removed prior to cluster infall, usually in groups on the outskirts of galaxy clusters (Bahé et al., 2012). In both these mechanisms, it means that the hot gas halo is removed and/or heated before the cold gas within the galaxy (McCarthy et al., 2008; Bahé et al., 2013). This implies that outside the inner cluster region, the star-forming cold gas is not necessarily expelled or heated, but rather has an effect on the halo supply and thus decreases star formation (Kawata & Mulchaey, 2008).

The density of the ICM is higher in inner cluster regions, $\leq 0.5\ R_{\rm vir}$ (where $R_{\rm vir}$ is the virial radius), than anywhere else in a cluster. As a result, these regions are affected by a shorter timescale quenching mechanism known as ram-pressure stripping (Zinger et al., 2018). Ram-pressure stripping is the process whereby the galactic (cold) gas is removed due to the external gas pressure $P_{\rm ram}$ exerted by the ICM, becoming stronger than the galactic gravitational binding energy (Gunn & Gott, 1972). In addition to gas expulsion, ram-pressure may also compress gas into high-density clouds, leading to an enhancement of star formation (Vulcani et al., 2018; Roberts & Parker, 2020; Roberts et al., 2022). This compression and expulsion of cold gas in galaxies is best exemplified by jellyfish galaxies, which are gas-rich and characterised by their optically bright, star-forming, extended tails of expelled material (Poggianti et al., 2017; Sheen et al., 2017; Jaffé et al., 2018). Interestingly, there is mounting observational evidence suggesting that jellyfish galaxies (George et al., 2019; Radovich et al., 2019), as well as cluster galaxies with recent bursts of star formation

(Dressler & Gunn, 1983) host AGNs. This surprisingly high incidence, compared to the general cluster and field population, suggests that ram-pressure stripping may trigger AGN feedback via nuclear gas inflow (Poggianti et al., 2017), thereby additionally suppressing star formation after a brief episode of enhancement (George et al., 2019).

While the velocity dispersion of galaxies in galaxy clusters is too high for frequent mergers (Menci & Fusco-Femiano, 1996; Gnedin, 2003), galaxies do interact with each other. Specifically, multiple high-speed encounters between galaxies, i.e., galaxy harassment, influence star formation and are able to drive strong morphological transformations in clusters, building the lenticular and elliptical galaxy population (Moore et al., 1998). Similarly, tidal effects, which are gravitational interactions between galaxies, and between galaxies and the cluster potential, can lead to both dynamical heating and morphological transformation (Gnedin, 2003).

Galaxy clusters provide us with key information based on their characteristics such as they evolve slowly so they retain information about how the Universe formed, they are held together by gravity which makes them an excellent source of dark matter, and they act as laboratories in studying galaxy evolution (e.g., Spitzer & Baade, 1951; De Propris et al., 2003). Since they play a vital role in understanding the Universe, we take a look at the advancements in technology that have enabled us to make multiwavelength observations of galaxy clusters.

1.4 Galaxy cluster detection

In 1784, Charles Messier became one of the first people to notice the clustering of galaxies and develop a catalogue of nebulae (Jones, 1991). Shortly after, William Herschel also developed his own catalogue of nebulae, independently, in 1785 (Herschel, 1785; Herschel, 1864). However, galaxy clusters were only recognized as celestial objects at the beginning of the 20th century due to the work of Edwin Hubble (Hubble, 1925; Hubble, 1926; Hubble, 1936). Other crucial landmarks in cluster detection were: the first estimation of the mass of a galaxy cluster (the Coma cluster) by Zwicky (1933) (who also established the need for dark

matter, see Section 1.1.2), and the role of clusters as laboratories for studying the evolution of galaxies by Spitzer & Baade (1951).

Early observations of the night sky were carried out in and limited to, the optical band. The advancement of technology has rapidly improved observations and has allowed for multi-wavelength surveys (see figure 1.4.1). Bright clusters have also more recently been discovered using infrared (IR), X-ray, radio and Sunyaev-Zel'dovich observations. Each of these detection methods has advantages and disadvantages, but by combining multiwavelength data we can gain a broader understanding of galaxy clusters and eliminate bias. We discuss optical, X-ray and Sunyaev-Zel'dovich cluster detection methods below.

Figure 1.4.1: Images of galaxy cluster Abell 1835 ($z = 0.25$) at X-ray, optical and mm wavelengths. Left: X-ray image from Chandra X-ray observatory (Mantz et al., 2010), Center: Optical image from Canada France Hawaii Telescope (CFHT), Right: SZ image from Sunyaev-Zel'dovich Array. Source: https://ned.ipac.caltech.edu/level5/Sept18/Allen/Allen3.html

1.4.1 Optical

Optical and near-infrared (NIR) emission from galaxy clusters comes mostly from starlight. The main observables from optical surveys of clusters include richness, luminosity and colour. The richness of a cluster can be defined as a statistical measure of the number of galaxies within a cluster (Abell, 1958; Zwicky et al., 1961; Koester et al., 2007; Rykoff et al., 2016).

For individual cluster observations, density, luminosity and velocity dispersion profiles are observed.

The first extensive cluster catalogue was constructed by Abell (1958), based on visual inspection of photographic plates from the Palomar Observatory Sky Survey (POSS). POSS was first carried out in the 1950s using the 48-inch Oschin Schmidt telescope at Mount Palomar and became the first photographic survey of the sky (Minkowski & Abell, 1963; Reid et al., 1991). The Abell catalogue consists of 2712 galaxy clusters, with an analysed distribution of 1682 of them, and was found to be mostly complete out to $z \approx 0.20$. However, up to 25% of these clusters could be contaminated or be the results of projections (Lucey, 1983; Frenk et al., 1990; van Haarlem et al., 1997). Zwicky et al. (1961) also composed their own cluster catalogue using POSS. Although this method appeared to be simpler than Abell's, its completeness is strongly dependent on the redshift of the cluster. This is because clusters that have similar richness but different redshifts will have different overdensities. Astronomers used these two catalogues to find a way to classify clusters based on their content and richness.

Useful studies created a wide variety of classifications for clusters, such as (i) compact, medium compact, and open (Zwicky et al., 1961); (ii) cD (central galaxy dominated), B (binary), L (line), C (core), F (flat), and I (irregular) (Rood & Sastry, 1971), and (iii) spiral-rich, spiral-poor, and cD (Oemler, 1974). This can be narrowed down into two main classification categories: regular and irregular galaxy clusters. Regular clusters usually have a central concentration of galaxies, are spherically symmetric, and are dominated by E and S0 galaxies. Irregular clusters have a varying population from poor to rich, show no symmetry, and contain mixed types of galaxies.

The advancement of technology saw the introduction of digitised images and computer algorithms, which were preferred to the visual inspection of photographic plates. The Edinburgh-Durham Survey (Heydon-Dumbleton et al., 1989) was one of the first large-scale machine-based optical galaxy catalogue (around 10^6 galaxies) composed using plates taken by the UK Schmidt Telescope Unit (UKSTU) and the COSMOS microdensitometer. Lums-

den et al. (1992) later went on using this catalogue to create the Edinburgh-Durham Cluster Catalogue (EDCC), consisting of 737 clusters or groups, using a peak-finding algorithm. Maddox et al. (1988) used the SERC Automatic Plate Measuring (APM) densitometer to study 176 UKSTU plates and discovered 3.6×10^6 galaxies in a 4400 deg^2 area. This survey was later used to create a cluster catalogue presented by Dalton et al. (1992). A rapid procession of cluster surveys has resulted since. We describe some of these findings in Table 1.4.1.

A significant modern optical survey of note is the SDSS. SDSS is a major multi-spectral imaging and spectroscopic redshift survey that began operations in the early 2000s, using a 2.5 m wide-angle optical telescope at Apache Point Observatory. SDSS covers a third of the celestial sphere and provides the most complete database for low redshift clusters (Alam et al., 2015), and provides five-band photometry (u, g, r, i, and z). The currently most updated release from SDSS is the 17th release, DR17 (Abdurro'uf et al., 2022). Due to the sheer size of this survey, we have the opportunity to create large and complete cluster catalogues. Various research groups have attempted this with SDSS data previously, using cluster finding algorithms (Koester et al., 2007; Wen et al., 2009; Hao et al., 2010; Rykoff et al., 2014; Díaz-Sánchez, 2021).

The next generation of imaging surveys surpassed SDSS in various combinations of depth, solid angle coverage, and image quality. For example, the Canada-France-Hawaii Telescope Lens Survey (CFHTLS: Veillet, 2007; Heymans et al., 2012) covered 154 deg^2 in five bands, to i'= 25.5. The Dark Energy Survey (DES: Dark Energy Survey Collaboration et al., 2016) imaged 5000 deg^2 of the southern sky in five bands with the Blanco 4 m telescope, going to magnitude depths of $r \approx 24.3$ (10σ). Another ongoing survey is the Kilo-Degree Survey (KiDS: De Jong et al., 2013), which covers 1500 deg^2 in four bands to $r = 24.9$. The Hyper Suprime-Cam Subaru Strategic Program (HSC-SSP) survey goes deeper than all of these surveys, while still covering over 1000 deg^2, and including a narrow-band imaging component as well (Aihara et al., 2017).

The advantage of optical observations is that they provide the largest yield of galaxy

clusters per square degree as compared to other wavelengths. This is due to the wide field of view for most of these surveys and their greater depth. They are also essential for providing photometric redshifts for clusters detected in other wavelengths (Khedekar & Majumdar, 2013). However, the disadvantage of optical surveys is that they are vulnerable to projection effects and observations can be contaminated by line-of-sight foreground or background objects (Yee & Gladders, 2002). X-ray surveys are less prone to these projection effects and can therefore help us compose more robust cluster catalogues.

1.4.2 X-ray

X-ray emissions from galaxy clusters provide information about the cluster environment and the physical processes occurring within them. Galaxy clusters "light-up" at X-ray (as shown in figure 1.4.1) wavelengths since their gravity compresses diffuse gas, heating it up to around $10^7 - 10^8$ K (Böhringer & Werner, 2010). The main X-ray emissions from the ICM are collisional: (i) bremsstrahlung (Boldt et al., 1966; Felten et al., 1966) and (ii) recombination emission. Bremsstrahlung emission is the radiation produced by the deceleration of an electron when deflected by a proton. The emissivities of the aforementioned processes are proportional to the square of the electron density (which ranges from $\approx 10^{-1}$ cm^{-3} in cluster centres to $\approx 10^{-5}$ cm^{-3} in cluster outskirts). These low densities make modelling simpler since the X-ray-emitting plasma would be optically thin.

For survey observations, the primary X-ray observables are flux, spectral hardness and spatial extent. Early missions, such as the Extended Medium Sensitivity Survey (EMSS), were conducted in the late 1970s using X-ray imaging instruments onboard the Einstein observatory. EMSS surveyed over 778 deg^2, providing a homogeneous flux-limited sample of 835 X-ray sources (Gioia et al., 1990). The first X-ray cluster catalogues constructed for cosmological work were based on the Ariel V (Villa et al., 1976) and HEAO-1 (Friedman, 1979) all-sky surveys. These catalogues were eventually replaced by surveys taken by the ROSAT satellite, launched in June 1990 (Voges et al., 1999). A number of catalogues have

Optical detections of galaxy clusters				
Survey name	Sky coverage	Redshift	No. of clusters	Author
Palomar Distant Cluster Survey (PDCS)	5.1 $\deg^2$	$0.2 \leq z \leq 1.2$	79	Postman et al. (1996)
Palomar Transit Grism Survey (PTGS)	17.5 $\deg^2$ northern sky	most candidates: $z < 0.45$	52	Schneider et al. (1993)
LasCampanas Distant Cluster Survey (LCDCS)	130 $\deg^2$ southern sky	$0.3 \leq z \leq 1.0$	1073	Gonzalez et al. (2001)
Red-sequence Cluster Survey 1 (RCS-1)	90 $\deg^2$	$z \approx 1$	1000	Yee et al. (2007)
Red-sequence Cluster Survey 2 (RCS-2)	$\approx$ 1000 $\deg^2$	$0.1 \leq z \leq 1.0$	$\approx$ 10000	Gilbank et al. (2011)
SDSS DR6	$\approx$ 8520 $\deg^2$	$0.05 \leq z \leq 0.6$	39716	Wen et al. (2009)
SDSS DR8	$\approx$ 10000 $\deg^2$	$0.08 \leq z \leq 0.55$	25000	Rykoff et al. (2014)

Table 1.4.1: Optical detections of galaxy clusters over the past three decades.

been constructed based on the pointed observations by ROSAT, such as the ROSAT Deep Cluster Survey (Rosati et al., 1997) and the ROSAT PSPC survey (Burenin et al., 2007). On a more recent note, a German-Russian Spectrum-Roentgen-Gamma (SRG) mission, carrying the extended ROentgen Survey with an Imaging Telescope Array (eROSITA; Merloni et al., 2012), was launched at the end of 2019. The eROSITA design driving science is the detection of large samples of galaxy clusters up to redshifts $z > 1$ (Predehl et al., 2021). At the end of this programme, the eROSITA All-Sky survey in the soft X-ray band (0.2 - 2.3 keV) will be ≈ 25 times more sensitive than the ROSAT All-Sky Survey, while in the hard band (2.3 - 8 keV) it will provide the first ever true imaging survey of the full sky (Predehl et al., 2021). Modern X-ray observatories, such as Chandra (Schwartz, 2004) and XMM-Newton (Jansen et al., 2001), allow for the spatially resolved spectra of clusters to be determined precisely, allowing for measurements of the temperature and density of the ICM.

X-ray cluster surveys can also be separated into two main types: contiguous area surveys and serendipitous surveys (Gioia, 2000). The contiguous area surveys cover large areas of the sky. Examples of such surveys include the North Ecliptic Pole (NEP) survey (Henry et al., 1995), ROSAT ESO Flux Limited X-ray (REFLEX) survey (Böhringer et al., 1998), the ROSAT Brightest Cluster sample (BCS; Ebeling et al., 1998), the RASS1 Bright Sample (RASS1-BS; De Grandi et al., 1999), the Northern Rosat All-Sky (NORAS) survey (Böhringer et al., 2000), and the MAssive Cluster Survey (MACS; Ebeling et al., 2001). These surveys are used to study large-scale structures in galaxy clusters but, due to their shallowness, can not be used to identify large numbers of more massive clusters at high redshift. The serendipitous surveys use pointed data surveys to search for clusters which have the advantage of higher sensitivity but the disadvantage of a much smaller field of view, making it harder to identify large clusters. Examples of such surveys include the XMM Cluster Survey (XCS), which is based on the XMM telescope (Romer et al., 2001; Mehrtens et al., 2012), and the Chandra Multiwavelength Project (ChaMP) survey (Barkhouse et al., 2006). The various X-ray surveys carried out over the past few decades, and their comparative sensitivities and areas are shown in figure 1.4.2.

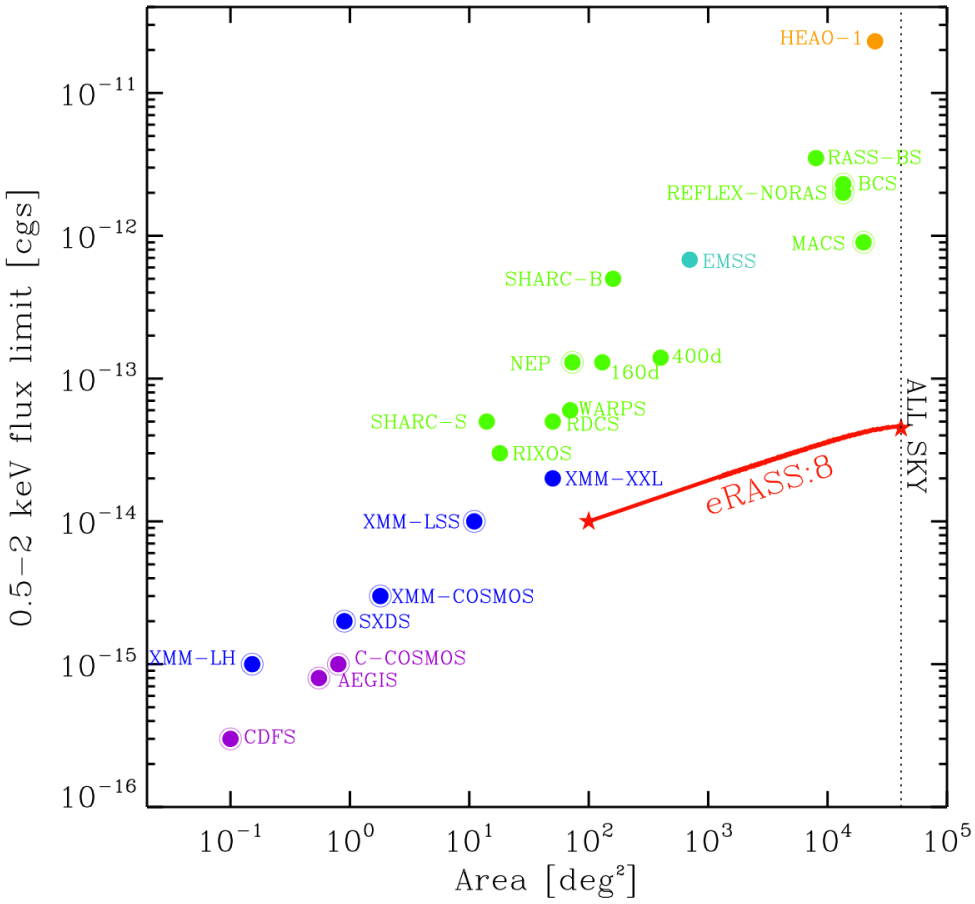

Figure 1.4.2: Comparison of sensitivity versus area for X-ray surveys, taken from Merloni et al. (2012). The red line represents the eROSITA All-Sky Survey, the orange dot is HEAO-1, green dots show all the ROSAT surveys, cyan dots show the Einstein surveys, blue is XMM-Newton, and Chandra is shown in purple. The points that have been encircled are contiguous surveys.

Galaxy clusters are the second brightest extragalactic sources in the sky, when observed in X-ray, and are easily identified because they are resolved. Projection effects are also reduced in X-ray surveys since the X-ray luminosity scales as the square of the gas density and confusion from background fluctuations is much lower (Voit, 2005). While optical observations depend on searching for cluster members to determine cluster mass, X-ray masses,

on the other hand, rely on the temperature and density of the gas which we can measure. The selection criteria for X-ray sources are also objective and quantifiable. One major, and obvious, disadvantage of X-ray surveys is that it is costly to run and maintain the missions responsible for them. A less expensive method for conducting cluster surveys that also relies on the presence of the hot ICM in clusters is the Sunyaev-Zel'dovich effect.

1.4.3 The Sunyaev-Zel'dovich effect

New generation mm-wave survey telescopes such as the Atacama Cosmology Telescope (ACT; Fowler et al., 2007), the South Pole Telescope (SPT; Carlstrom et al., 2011) and the Planck satellite mission (Planck Collaboration et al., 2014a), have made it possible to select clusters over a large portion of the sky using the Sunyaev-Zel'dovich (SZ) effect. As CMB photons pass through a galaxy cluster, they have a non-negligible chance to inverse Compton scatter off the hot (10^7 K) gas atmosphere of the cluster. This scattering boosts the photon energy and gives rise to a small frequency-dependent shift in the CMB spectrum observed through the cluster known as the thermal Sunyaev-Zel'dovich effect (Sunyaev & Zeldovich, 1970) (see figure 1.4.3).

The SZ effect was first demonstrated in pointed observations towards known clusters during the 1970s and 1980s (e.g., Sunyaev & Zeldovich, 1972; Gull & Northover, 1976; Birkinshaw et al., 978a; Birkinshaw et al., 978b; Uson, 1986). The first millimetre measurements of the SZ effect were conducted using a 140 GHz bolometer array for the Sunyaev-Zel'dovich Infrared Experiment (SuZIE), which was able to produce high signal-to-noise maps of the SZ emission in several clusters (Mauskopf et al., 2000). These bolometric detectors have very high sensitivity and are excellent at detecting the SZ effect. Another way to observe the SZ effect is to use interferometers. Due to their stability and good spatial filtering, interferometers provide high-quality images of the SZ effect. The first SZ effect detection via interferometer was made by Jones (1995), who used the Ryke telescope in Cambridge, England.

Searching for clusters using the SZ effect is now a firmly established method for cluster

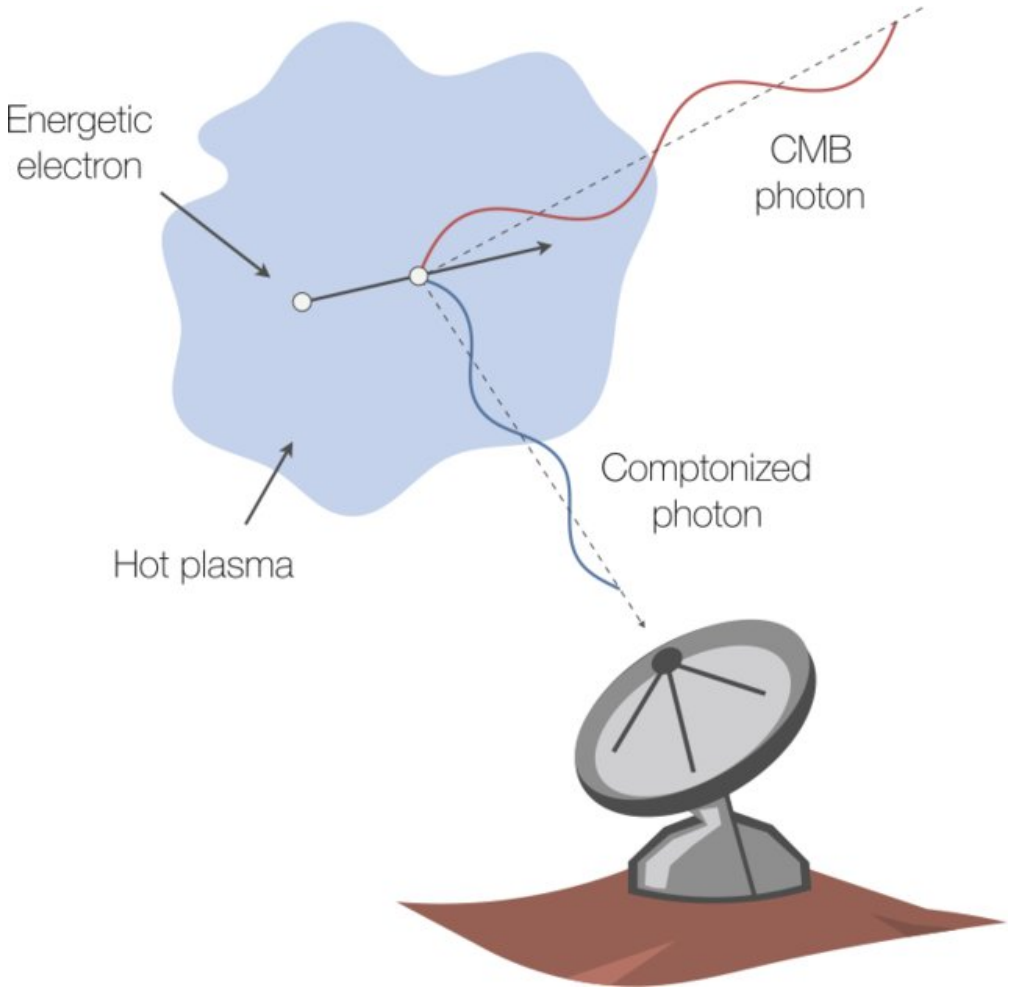

Figure 1.4.3: An updated illustration of the tSZ effect taken from Mroczkowski et al. (2019). A CMB photon (red) enters the hot ICM (light blue) from an arbitrary angle, and on average is up-scattered to higher energy (blue) by an electron (black). The largest energy is imparted on the photon when it is scattered into the direction of the incoming electron, and it is minimal when deflected into the direction opposite to the incoming electron.

detection (Hilton et al., 2018). Modern advances in technology and telescopes have allowed for SZ searches of galaxy clusters that have been made in the last two decades (Marriage et al., 2011; Bleem et al., 2015; Planck Collaboration et al., 2016a). The first large catalogues of galaxy clusters selected from blind observations of the SZ effect were made using the measurements from SPT (Staniszewski et al., 2009; Williamson et al., 2011; Bleem et al.,

2015) (see figure 1.4.4), the all-sky survey carried out by the Planck satellite mission (Planck Collaboration et al., 2014a; Planck Collaboration et al., 2016a), and from ACT (Marriage et al., 2011; Hasselfield et al., 2013; Hilton et al., 2018; Hilton et al., 2021). Unlike SPT and ACT, the Planck satellite has difficulty detecting clusters above $z \approx 0.3$ because it has a much lower spatial resolution ($\sim 10'$) than ACT or SPT ($\sim 1'$ or $\sim 2'$). Thus, clusters at $z > 0.3$ in Planck are often unresolved. Marriage et al. (2011) discovered 23 clusters detected as SZ decrements in a 455 deg^2 map of the Southern sky made with data from ACT. Hasselfield et al. (2013) reported 68 cluster galaxies detected via the SZ effect at 148 GHz in the ACT survey on the celestial equator. Hilton et al. (2018) presented a catalogue of 182 clusters detected as SZ decrements by applying a matched filter to 148 GHz maps that cover the redshift range $0.1 < z < 1.4$. The latest release from ACT consists of 4195 SZ-selected clusters presented by Hilton et al. (2021). We will be using this cluster sample in this thesis and will discuss it in more detail in the next chapter.

There are multiple advantages in choosing to select clusters through their SZ signal, compared with other methods. SZ observations and simulations have shown that the scaling relation between the SZ flux and the cluster mass is robust with low scatter (Reid & Spergel, 2006). Unlike optical and X-ray measurements, the SZ signal of a cluster does not undergo surface brightness dimming. Therefore, these surveys will be better suited in searches for massive clusters at high redshifts (Sehgal et al., 2010). Additionally, since it is a scattering effect, the distance of the scattering medium does not matter. These advantages of the SZ effect allow for the construction of effectively mass-limited cluster samples - i.e. the SZ brightness of clusters depends largely upon mass, and not on their redshift. Thus, SZ surveys can help track the evolution of the number density of massive clusters from the early Universe.

In this thesis, we investigate the galaxy luminosity function in SZ-selected clusters from the ACT DR5 sample. As will be described in the next section, the galaxy luminosity function is a valuable tool that can be used to investigate galaxy evolution in clusters.

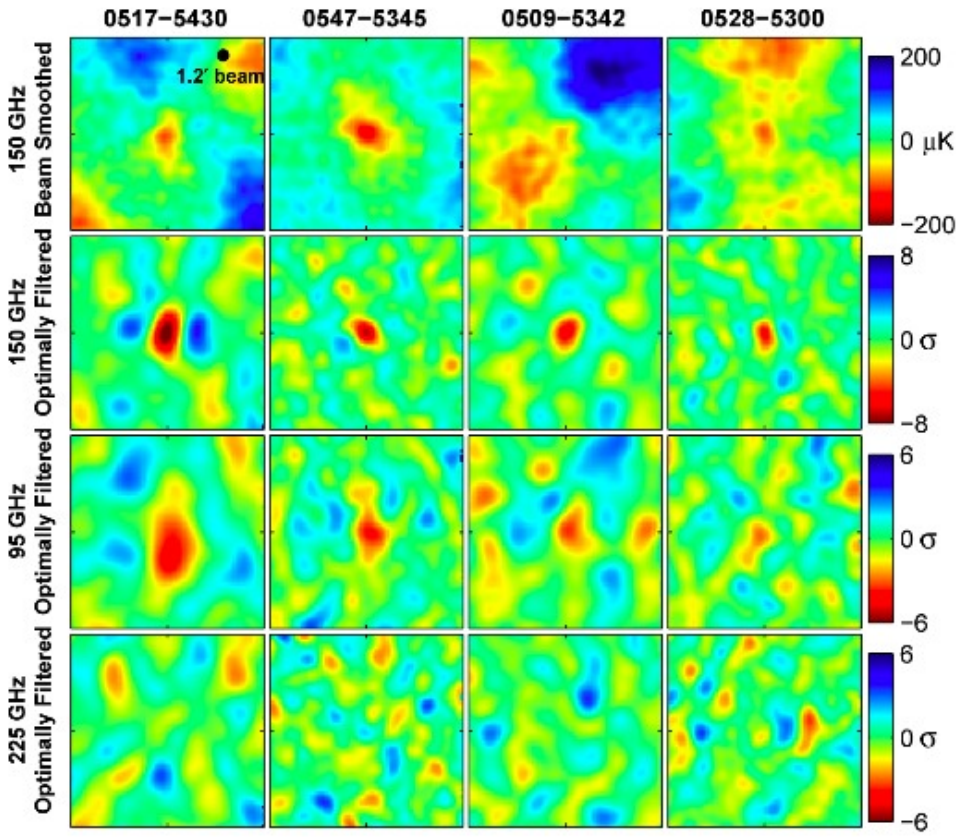

Figure 1.4.4: Images of four galaxy clusters found from the first blind SZ detections in the SPT SZ survey, taken from Staniszewski et al. (2009). In each panel, the region shown is a 20 by 20 arcmin box centred on the cluster. Each row represents a different filtered map, at different frequencies, and the scale provides detection significance in σ. Note, the clusters are not observed at 225 GHz which is close to the SZ null of 217 GHz.

1.5 Luminosity functions

The galaxy luminosity function (LF) describes the number of galaxies per unit volume as a function of the luminosity (e.g., De Propris et al., 2003). Accurate measurements of the LF can tell us how environmental processes influence the properties of current galaxy populations, helping us obtain clues as to which processes are important in shaping galaxy formation and evolution (Benson et al., 2003). The luminosity evolution is often inferred by

the variation with redshift of the LF, the fraction of blue galaxies (crucial for the Butcher-Oemler effect, see Section 1.3), and the total number of galaxies (Paolillo et al., 2001).

Deriving LFs in clusters is generally a simpler task than for field environments since clusters provide a rich collection of galaxies at the same distance, and the density with respect to the surrounding environment or field is high enough to identify members both photometrically and spectroscopically. Thus, many studies have been devoted to the LF of cluster galaxies to discover the influence of the environment on their evolution. A summary of previous studies on optical cluster LFs can be found in Table 1.5.1. Since the 1970s, there have been numerous cluster and field studies that have contributed to revealing the overall signature of the LF (e.g., Schechter, 1976; van den Bergh, 1978; Colless, 1989; De Propris et al., 2003; Mancone et al., 2010; Loveday et al., 2011; Martinet et al., 2015; Puddu et al., 2021). This trend reveals that after an exponential rise (due to a decrease in luminosity from higher luminosities), the LF turns 'off' at a characteristic magnitude (m^* or M^*) called the "knee", and then follows a power law at fainter magnitudes, known as the faint-end slope (α). The most popular parameterization fit to the LF is the Schechter function, proposed by Schechter (1976),

$$\phi(m) = 0.4\ln(10)\phi^* 10^{-0.4(m-m^*)(\alpha+1)} \exp(-10^{-0.4(m-m^*)}), \tag{1.1}$$

where ϕ^* is the normalization parameter, m^* is the characteristic apparent magnitude, and α is the faint-end slope. A schematic representation of the Schechter function is shown in figure 1.5.1. The faint-end slope is usually described as decreasing for $\alpha > -1$, flat for $\alpha = -1$ and increasing for $\alpha < -1$. α is always negative, implying a large number of galaxies with low luminosities. The Schechter function describes reasonably well the observed clusters' LFs but contamination from background galaxies can result in differences in the estimated parameters, especially in the faint-end.

Binggeli et al. (1988) originally proposed that the cluster LF is dominated by two populations, where the bright end is characterised by bright early-type (red) galaxies that follow a Gaussian-like luminosity distribution, and the faint-end is characterised by star-forming

(blue) galaxies that follow a steep power-law-like function. This has been supported by studies by Dressler et al. (1999); Adami et al. (2000); and Rakos et al. (2000). Additionally, Boyce et al. (2001) showed that the LF of Abell 868 consists of mainly three galaxy populations: luminous red and two fainter blue populations. The idea is illustrated by the fact that the cluster LFs in the redder passbands, which are presumably dominated by the old stellar populations of the early types, have much brighter M^*'s and significantly shallower slopes than those measured in bluer passbands (Goto et al., 2002). This implies that bright elliptical galaxies are more populated in dense regions, such as cluster centres. The luminosity of the BCGs or cD galaxies, which are typically giant elliptical galaxies located in cluster cores, has been shown to differ from the extrapolation of the LF of the cluster members at high luminosity (e.g., Hansen et al., 2009). This is since BCGs are not drawn from the same population as ordinary cluster galaxies (e.g., Tremaine & Richstone, 1977; Loh & Strauss, 2006; Lin et al., 2010).

Possible correlations with the presence/absence of a cD galaxy or with the Bautz-Morgan type (the BM-type classification based on the BCGs, Bautz & Morgan, 1970), are, maybe, also more interesting for their direct connection with the cluster evolutionary state. BCGs or cD galaxies are expected to be created i.) via the merger of giant galaxies in an early phase during the cluster collapse (Merritt, 1984), or ii.) in a following phase caused by the dynamical friction acting on late-comer galaxies (e.g., Ostriker & Tremaine, 1975), or iii.) via the disruption and cannibalization of many faint galaxies in the cluster cores (López-Cruz et al., 1997). The first two mechanisms might reduce the number of bright galaxies, thus shifting M^* to a fainter value (Barkhouse et al., 2007).

Cluster galaxies have been compared to field galaxies, at many different wavelengths. While some studies found the cluster LF to be indistinguishable from the field one (e.g., De Propris et al., 1998; Cortese et al., 2003; Bai et al., 2006; Agulli et al., 2014), other studies suggest it has both higher brighter characteristic magnitudes and different faint-end slopes than the field (e.g., Valotto et al., 1997; Goto et al., 2002; De Propris et al., 2003). De Propris et al. (2003) discovered that the LF of early-type galaxies in clusters is brighter

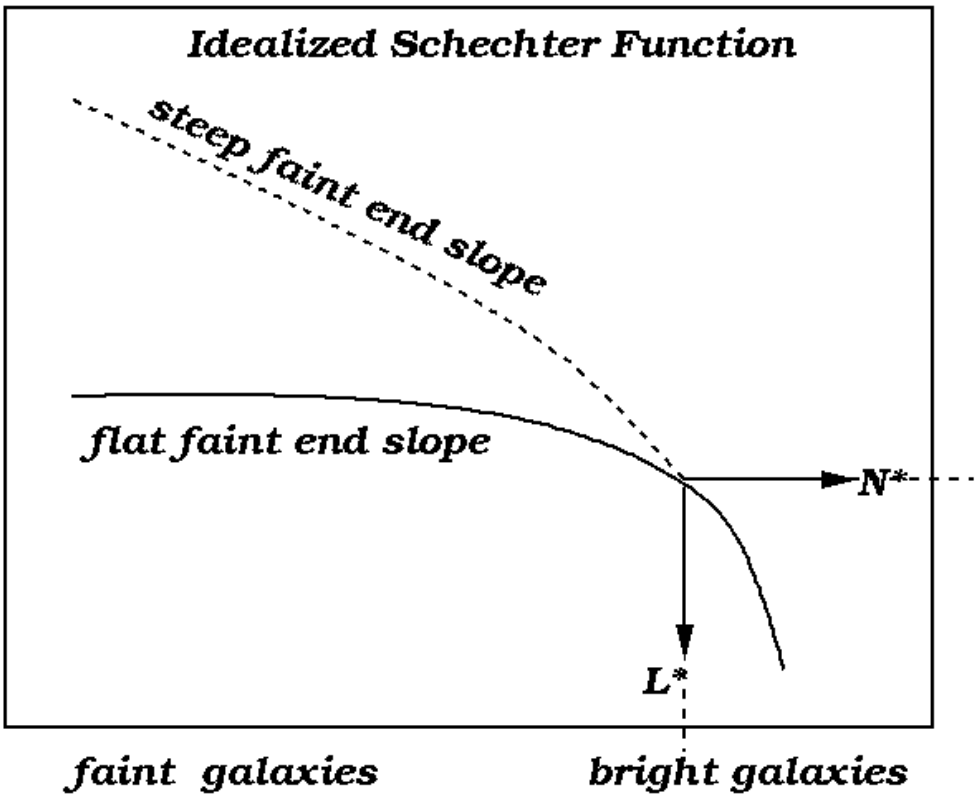

Figure 1.5.1: A schematic representation of the Schechter function describing the galaxy luminosity function. The solid line indicates a relatively flat faint-end slope, usually associated with samples that are not corrected for surface brightness selection. While the dashed line shows the case of a steep faint-end slope in which most of the galaxies in the Universe are faint/low-mass objects. Source: https://ned.ipac.caltech.edu/level5/Bothun2/Bothun6_2_1.html

and steeper than the field counterpart and that the trend of faint-end slope with spectral type is much less expressed in clusters than in the field. The differences between the field and cluster LFs for the various spectral types can be explained by suppressed star formation in the dense cluster environment, together with mergers to produce the brightest early-type galaxies (De Propris et al., 2003). The cluster environment is also richer in faint galaxies than the field (Popesso et al., 2006; Blanton et al., 2005).

Previous optical cluster LF studies						
Author/s	Survey	z	N_{clus}	Band	α	M^*
Paolillo et al. (2001)	DPOSS	$0.08 < z < 0.30$	39	g	-1.07 ± 0.08	-20.22 ± 0.15
				r	-1.11 ± 0.08	-20.67 ± 0.16
Goto et al. (2002)	SDSS CE	$0.02 < z < 0.25$	204	u	-1.40 ± 0.11	-20.84 ± 0.26
				g	-1.00 ± 0.06	-21.24 ± 0.11
				r	-0.85 ± 0.03	-21.44 ± 0.05
				i	-0.70 ± 0.05	-21.54 ± 0.08
				z	-0.58 ± 0.04	-21.59 ± 0.06
De Propris et al. (2003)	2dFGRS	$z < 0.11$	60	b_j	-1.28 ± 0.03	-20.07 ± 0.07
Popesso et al. (2006)	RASS-SDSS	$\langle z \rangle = 0.1$	69	r	-1.26 ± 0.12	-21.16 ± 0.26
Martinet et al. (2015)	DAFT/FADA	$\langle z \rangle = 0.58$	16 (Red)	R	-0.80 ± 0.14	-22.40 ± 0.20
		$\langle z \rangle = 0.62$	6 (Blue)	R	-1.32 ± 0.36	-22.40 ± 0.50
Zhang et al. (2019)	DES-SV	$0.1 \leq z < 0.4$	64	z	-0.80 ± 0.12	-22.33 ± 0.18
		$0.4 \leq z < 1.05$	27	z	-0.55 ± 0.18	-22.25 ± 0.23
Puddu et al. (2021)	AMICO/KiDS-DR3	$0.10 < z < 0.32$	755	r	-1.04 ± 0.03	-21.50 ± 0.03
		$0.32 < z < 0.46$	1182	r	-0.92 ± 0.05	-21.59 ± 0.04
		$0.46 < z < 0.55$	939	r	-0.87 ± 0.07	-21.65 ± 0.05
		$0.55 < z < 0.80$	1222	r	-0.63 ± 0.11	-21.61 ± 0.05

Table 1.5.1: Previous studies of optical cluster luminosity functions.

Previous studies did show discrepancies in various LF measurements, which is due to a combination of surface brightness selection, colour, aperture effects and local density variations (De Propris et al., 2003). Lan et al. (2016) attempted to settle the debate on the faint-end upturn by measuring the conditional LFs over a wide range of halo masses and luminosities using SDSS. By selecting galaxies in groups and clusters spanning $10^{12} - 10^{15} M_{\odot}$ in mass, and $0.01 < z < 0.05$ in redshift, they found that their conditional LFs have a characteristic r-band absolute magnitude $M_r \approx -18$ at which the slope of the LF becomes steeper toward the faint-end. This trend is consistent with earlier found observations (e.g., Popesso et al., 2006; Agulli et al., 2014; Moretti et al., 2015). Above this luminosity scale, their LFs remained flat over a few magnitudes and then declined exponentially at the bright-ends, above $M_r \approx -21$. Another recent study by Zhang et al. (2019) constrained the LF of cluster RS galaxies as a function of redshift, using ≈ 100 X-ray selected clusters in the Dark Energy

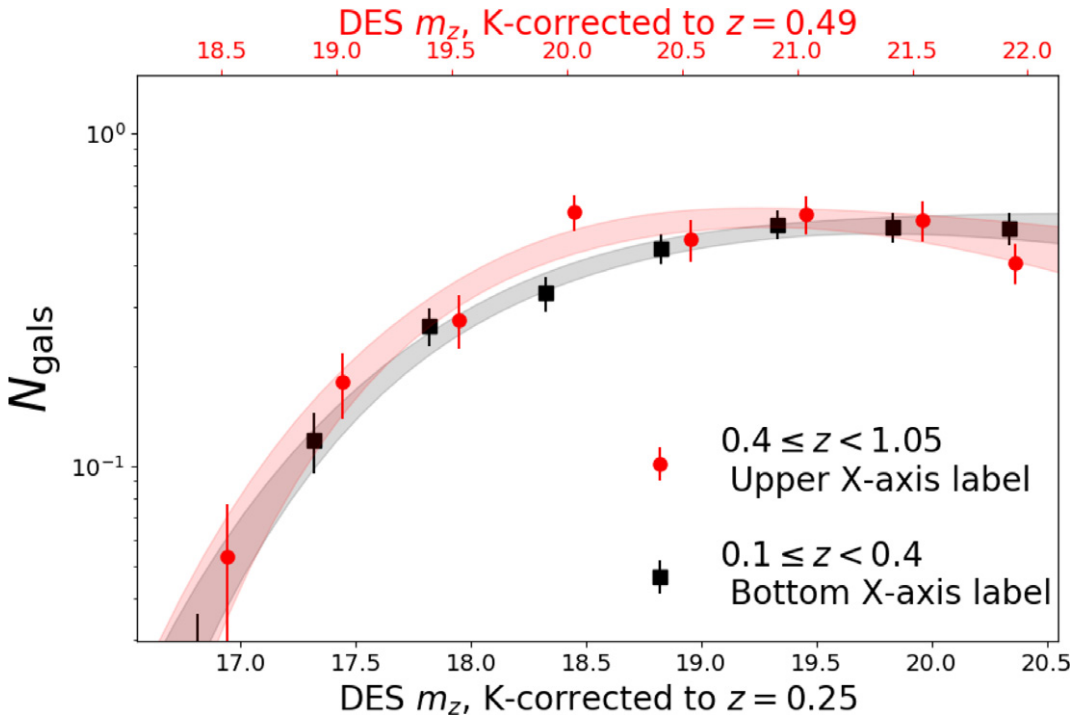

Figure 1.5.2: The RSLFs derived in two redshift bins from Zhang et al. (2019). The shaded bands show the fitted Schechter functions including 1σ fitting uncertainties. Note how the RSLF faint-end slope displays a possible redshift evolution effect.

Survey Science Verification data (DES-SV). This was the first homogeneous optical/X-ray sample large enough to constrain the evolution of the LF in redshift ($0.1 < z < 1.05$) and cluster mass ($13.5 \leq \log_{10}(M_{200\rm crit}) \sim< 15.0$). Zhang et al. (2019) fitted their red-sequence LFs (RSLFs) (shown in figure 1.5.2) with a single Schechter function to the magnitude limit of $m^* + 2$ and simultaneously modelled the mass and redshift using a hierarchical Bayesian method. They found a weak and statistically insignificant ($\approx 1.9\sigma$) evolution in the faint-end slope versus redshift.

In general, the LF of galaxies in clusters as a function of both the galaxy and cluster properties is a powerful observational test for theories of galaxy formation and evolution. We implement this tool in our quest to understand galaxy evolution within clusters.

1.6 Thesis outline

In this project we will examine the galaxy population of SZ-selected clusters drawn from the Atacama Cosmology Telescope Data Release 5 (ACT DR5; Hilton et al., 2021) sample by measuring their composite r-band luminosity functions from $0.20 < z < 0.80$, using optical data from DECaLS (Dey et al., 2019). This type of work has been done previously (see Section 1.5), but not on this cluster sample in this specific chunk of cosmic time. We will also investigate how the composite LFs evolve with redshift and cluster mass. The structure of this thesis is as follows. In Chapter 2, we describe the data and methods used for measuring the LFs. In Chapter 3, we present the results from our composite LF fits. Chapter 4 discusses our results and compares trends to previous work. We finally present a conclusion of our study in Chapter 5. Throughout this paper, we assume a flat cosmology with parameters $H_0 = 70$ km.s^{-1}Mpc^{-1}, $\Omega_\Lambda = 0.7$ and $\Omega_m = 0.3$. H_0 represents Hubble's constant, Ω_Λ represents the energy density related to the cosmological constant, and Ω_m is the matter density of the Universe at redshift zero. All magnitudes are quoted in the AB magnitude system (Oke & Gunn, 1983), unless otherwise stated.

Chapter 2

Analysis

In this chapter, we present the data we used in this project, including the cluster sample. We provide the methodology for the construction of our composite luminosity functions, including binning techniques, k-corrections, and discussing completeness corrections.

2.1 The Data

2.1.1 ACT DR5

The Atacama Cosmology Telescope (ACT) is a 6-metre mm-wave telescope located on Cerro Toco in the Atacama Desert in Chile. Initially, ACT featured a cryogenic receiver, the Millimeter Bolometer Array Camera (MBAC), that operated at three frequencies: 148 GHz, 218 GHz, and 277 GHz (Swetz et al., 2011). Each band has a field of view of $22' \times 26'$. ACT then received two receiver upgrades which enabled polarization-sensitive observations: ACTPol (Niemack et al., 2010) (2013-2016) and Advanced ACT (AdvACT; Henderson et al., 2016) (2017-2022). ACT observations ended in August 2022. With its high angular resolution, sky coverage and sensitivity, ACT was optimized for measuring angular power spectra and clusters via the tSZ effect (Thornton et al., 2016). Some of the key scientific contributions from ACT included: the discovery of the most massive galaxy cluster at $z > 0.8$ (Menanteau et al., 2012), the first measurement of the motions of clusters of galaxies using the SZ effect

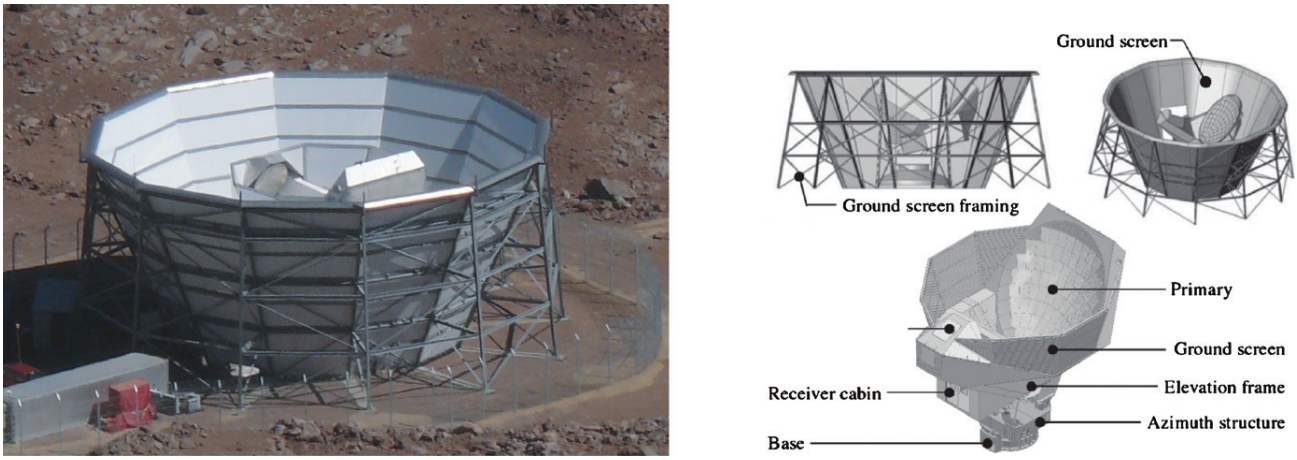

Figure 2.1.1: A picture (left) and mechanical rendering (right) of ACT and its ground screens, taken from Swetz et al. (2011). The telescope has a low profile; the full height is 12 m. The entire upper structure rotates as a unit, and the surrounding outer ground screen shields the telescope from ground emission. The primary reflector is 6 m and is surrounded by a 0.5 m guard ring.

(Hand et al., 2012), updated estimates of Hubble's constant (Aiola et al., 2020; Choi et al., 2020), and so on.

For this project, we make use of the recently updated cluster catalogue from the fifth data release (DR5) from ACT, containing 4195 galaxy clusters selected via the SZ-effect, and presented by Hilton et al. (2021). This catalogue is the largest SZ-selected cluster sample assembled to date, spanning the range $0.04 < z < 1.91$, consisting of 222 clusters with $z > 1$ and 868 newly discovered systems all within a sky coverage of ≈ 13211 deg^2. Hilton et al. (2021) adopted an SZ-signal vs mass scaling relation from Arnaud et al. (2010) and found a 90% completeness mass limit of $M_{500c} > 3.8 \times 10^{14} M_{\odot}$, evaluated at $z = 0.5$, for clusters detected at signal-to-noise ratio > 5. They selected cluster candidates by using a multi-frequency matched filter on 90 and 150 GHz maps constructed from ACT observations during the period of 2008-2018 and obtained optical confirmation and redshifts using deep, wide-area optical surveys. The ACT DR5 survey has an overlap with other deep optical weak-lensing surveys such as DES (4566 deg^2), HSC (469 deg^2) and KiDS (825 deg^2) (shown in figure 2.1.2).

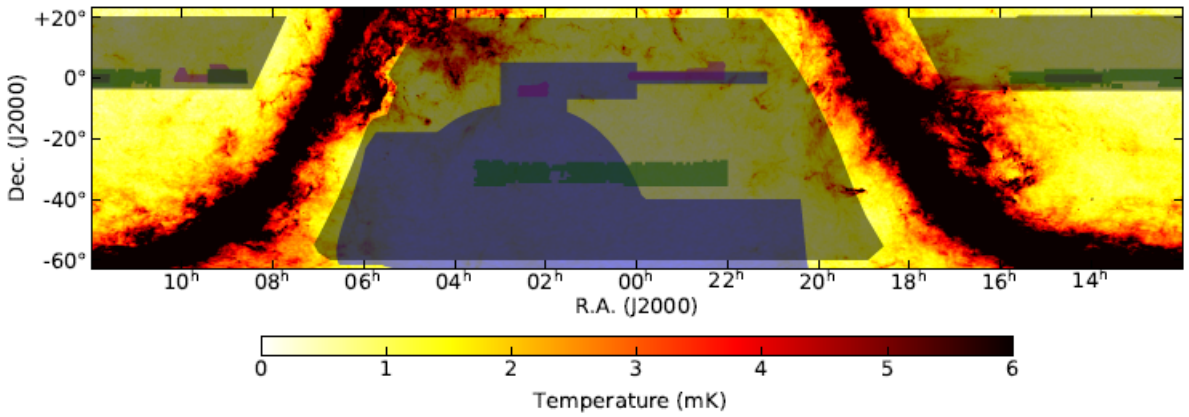

Figure 2.1.2: The ACT DR5 cluster search area, shaded in grey and covering 13211 deg^2 overlaid on the Planck 353 GHz map, which is sensitive to thermal emission by dust. The footprints of deep and wide optical surveys that will provide weak-lensing mass calibration of the cluster sample are highlighted: DES (blue); HSC (magenta); and KiDS (green) (Hilton et al., 2021).

2.1.2 DECaLS DR9

The Dark Energy Spectroscopic Instrument (DESI), which is a fixture on the Mayall Telescope at the Kitt Peak Observatory, is used for conducting spectrographic surveys of distant galaxies and measuring the effect of dark energy on the expansion of the Universe. In order to provide targets for the DESI survey, three telescopes surveyed an area of 14000 deg^2 (roughly one-third of the sky) in the g, r and z-band (Dey et al., 2019) (shown in figure 2.1.3). Those surveys were the Beijing-Arizona Sky Survey (BASS), using the Bok 2.3 m telescope, the Dark Energy Camera Legacy Survey (DECaLS), using the Blanco telescope, and the Mayall z-band Legacy Survey (MzLS), using the 4 m Mayall telescope. These three surveys were combined into the DESI Legacy Imaging Surveys, or Legacy Surveys (Dey et al., 2019).

To examine the ACT cluster population, we make use of DECaLS optical/IR data from the ninth data release (DR9) of the Legacy Surveys. DR9 does not contain any significant new observations but builds on DR8 by improving the reduction techniques and procedures used for the Legacy Surveys. DECaLS makes use of the Dark Energy Camera (DECam; Flaugher et al., 2015) located on the Blanco 4 m telescope at the Cerro Tololo Inter-American Observatory (CTIO). DECam provides optical imaging for targeting DESI, which covers both

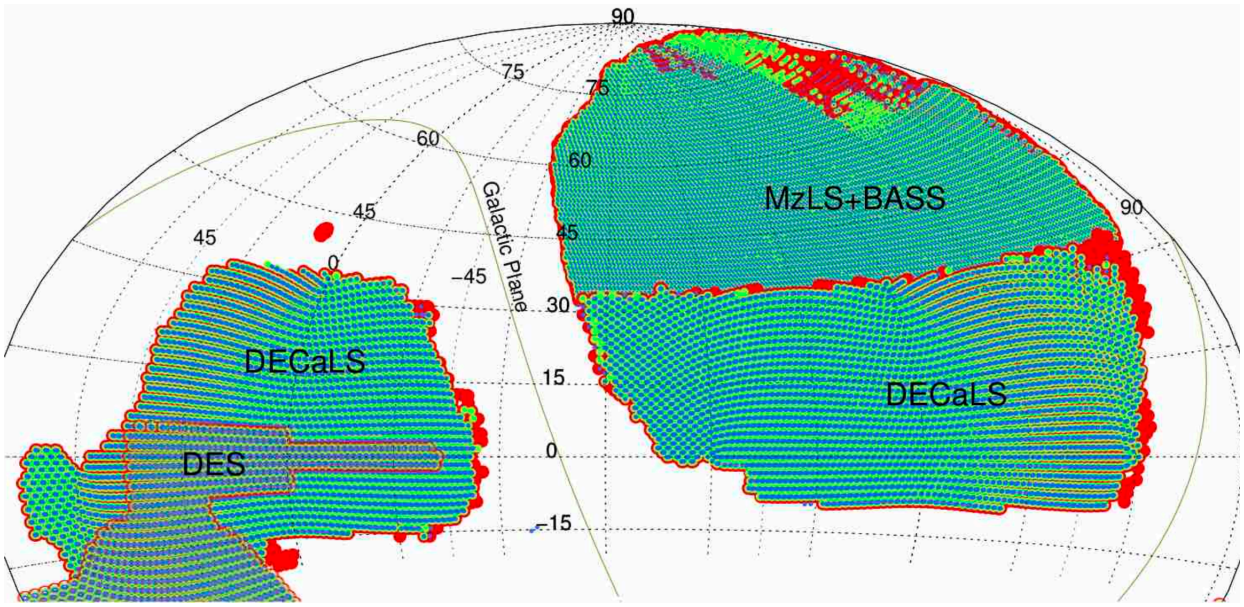

Figure 2.1.3: Complete imaging coverage of the DESI Legacy Surveys across 14000 square degrees. Red, green and blue dots represent regions, where there is at least a single z-, r-, or g-band observation, respectively. Source: https://www.desi.lbl.gov/imaging-surveys/

the North Galactic Cap region (Dec $\leq 32^0$) and South Galactic Cap region (Dec $\leq 34^0$). The combination of a large field of view and high sensitivity (400-1000 nm) for DECam makes DECaLS an efficient way to acquire photometry in the g, r and z bands. DECaLS makes use of other DECam data within the DESI footprint. The most important of these data sets are from the DES, which is an ongoing 5-band ($grizY$) photometric survey performed with DECam (Abbott et al., 2021).

DES comprises two surveys: a wide-area survey and a time-domain survey. The wide-area survey covers a large, contiguous area of sky (5000 deg^2), each part of which is observed ten times in each filter over the course of the survey; the long cumulative exposure time is needed to detect very faint galaxies, and the wide survey area enables us to detect a very large number of them.

DECaLS DR9 has a total sky coverage of 20000 deg^2 (Schlegel et al., 2021) and covers up to $z \approx 1$, with galaxy depth of ≈ 23.9 mag. in r-band magnitude (shown in figure 2.1.4).

The Legacy Surveys source catalogues also include mid-infrared photometry from the

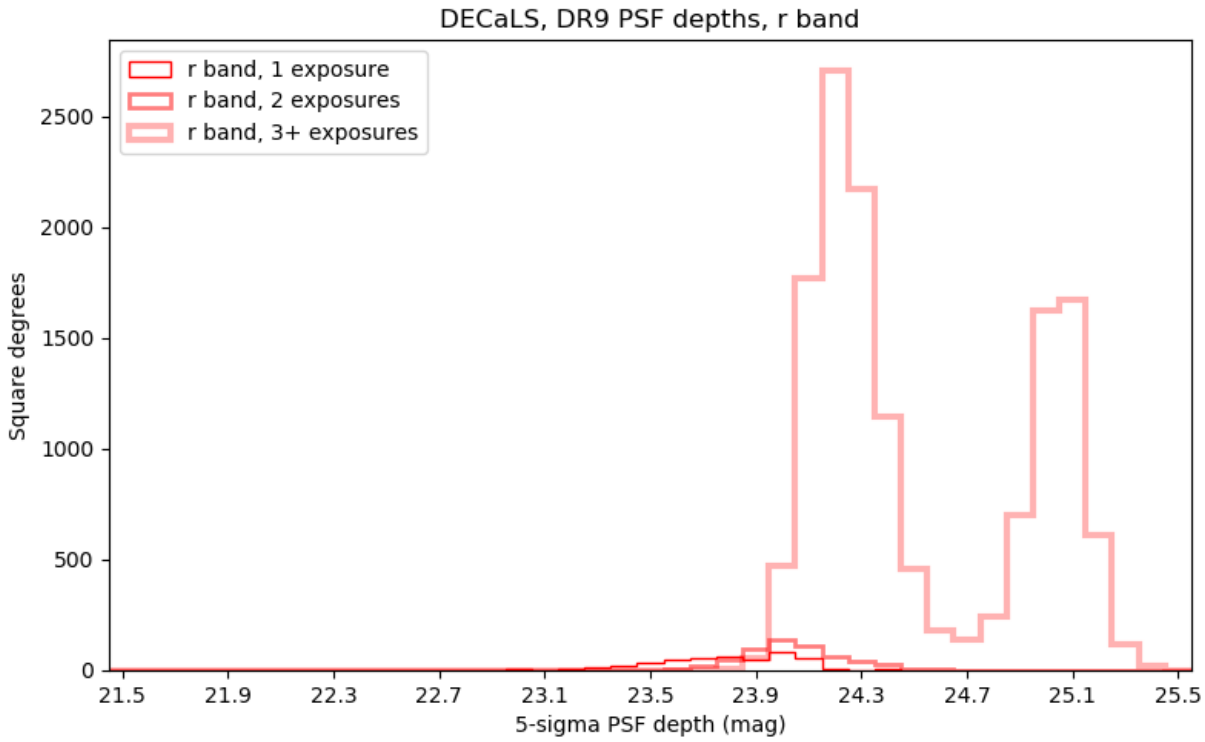

Figure 2.1.4: The r-band magnitude depths for point sources in DECaLS DR9 after different exposures. Note that a greater area of the sky is covered with more exposures. The primary reason is that most of the data here comes from DES which gets 10 exposures at each position. The shallower, one exposure part is probably DECaLS itself (i.e., the new observations they took with DECam, a separate project from DES). Source: https://www.legacysurvey.org/dr9/description/

Wide-field Infrared Survey Explorer (WISE) satellite for all optically detected sources (Dey et al., 2019). Mid-infrared imaging is critical to the DESI targeting algorithms for luminous red galaxies (LRGs) and quasars (QSOs). DESI target selection utilizes the two shortest-wavelength bands at 3.4 μm and 4.6 μm from the 4 bands (Wright et al., 2010; Cutri & et al., 2012) used by the WISE survey. Most importantly, DECaLS provides grz optical photometry for most of the ACT DR5 cluster search area footprint (10822 deg^2 of overlap; Hilton et al., 2021), making it ideal for use in this project.

2.2 Composite LFs

2.2.1 Redshift and Mass binning

Depending on the number of cluster members and the completeness of the redshift identification, the quality of individual cluster LFs can vary (De Propris et al., 2003). Rather than presenting individual cluster LFs, we derive composite cluster LFs and study variations in sub-samples binned by redshift and mass. This stacked approach makes it feasible to look for differences which are hidden by small number statistics in individual cases (De Propris et al., 2003).

As previously mentioned, our study covers a large amount of cosmic time ($0.20 < z < 0.80$). This means that we can easily bin clusters by redshift (e.g., De Propris et al., 1999; Hilton et al., 2013; Zhang et al., 2019). Due to the large number of clusters in the DR5 sample, we choose narrow redshift bins of width 0.05. This resulted in 3008 galaxy clusters selected over 12 redshift bins (see Table 2.2.1). We also select mass sub-samples within each cluster redshift bin. By selecting the top and bottom 25% of clusters by mass, we created low-mass and high-mass subsets of clusters. The details of the mass bins can be found in Table 2.2.2.

Redshift bins for composite LFs for ACT DR5 clusters			
Bin	Redshift	$N_{\rm clusters}$	Mass ($\times 10^{14} M_{\odot}$)
1	$0.20 < z < 0.25$	173	$1.94 < M_{\rm 200m} < 19.64$
2	$0.25 < z < 0.30$	225	$2.18 < M_{\rm 200m} < 20.91$
3	$0.30 < z < 0.35$	273	$2.13 < M_{\rm 200m} < 17.56$
4	$0.35 < z < 0.40$	272	$2.34 < M_{\rm 200m} < 25.42$
5	$0.40 < z < 0.45$	338	$2.36 < M_{\rm 200m} < 22.76$
6	$0.45 < z < 0.50$	294	$2.38 < M_{\rm 200m} < 11.35$
7	$0.50 < z < 0.55$	302	$2.42 < M_{\rm 200m} < 15.46$
8	$0.55 < z < 0.60$	262	$2.45 < M_{\rm 200m} < 17.54$
9	$0.60 < z < 0.65$	286	$2.49 < M_{\rm 200m} < 10.62$
10	$0.65 < z < 0.70$	227	$2.29 < M_{\rm 200m} < 8.67$
11	$0.70 < z < 0.75$	199	$2.47 < M_{\rm 200m} < 11.06$
12	$0.75 < z < 0.80$	157	$2.44 < M_{\rm 200m} < 10.76$

Table 2.2.1: Details of the redshift bins (with a bin width of 0.05) selected for our composite LFs of the ACT DR5 sample. In total, 3008 galaxy clusters were selected over the entire redshift interval. The last column shows the mass ranges of clusters per redshift interval.

Mass subsets per redshift bin				
Redshift bin	Low-mass ($\times 10^{14} M_\odot$)	$N_{\rm clusters}$	High-mass ($\times 10^{14} M_\odot$)	$N_{\rm clusters}$
$0.20 < z < 0.25$	$1.94 < M_{200\rm m} < 3.35$	47	$6.04 < M_{200\rm m} < 19.64$	37
$0.25 < z < 0.30$	$2.18 < M_{200\rm m} < 3.48$	60	$5.73 < M_{200\rm m} < 20.91$	52
$0.30 < z < 0.35$	$2.13 < M_{200\rm m} < 3.53$	72	$5.44 < M_{200\rm m} < 17.56$	62
$0.35 < z < 0.40$	$2.34 < M_{200\rm m} < 3.65$	70	$5.56 < M_{200\rm m} < 25.42$	65
$0.40 < z < 0.45$	$2.36 < M_{200\rm m} < 3.45$	89	$5.39 < M_{200\rm m} < 22.76$	77
$0.45 < z < 0.50$	$2.38 < M_{200\rm m} < 3.69$	75	$5.29 < M_{200\rm m} < 11.35$	71
$0.50 < z < 0.55$	$2.42 < M_{200\rm m} < 3.62$	78	$5.35 < M_{200\rm m} < 15.46$	73
$0.55 < z < 0.60$	$2.45 < M_{200\rm m} < 3.59$	66	$5.33 < M_{200\rm m} < 17.54$	62
$0.60 < z < 0.65$	$2.49 < M_{200\rm m} < 3.38$	73	$5.21 < M_{200\rm m} < 10.62$	65
$0.65 < z < 0.70$	$2.29 < M_{200\rm m} < 3.45$	58	$5.30 < M_{200\rm m} < 8.67$	54
$0.70 < z < 0.75$	$2.47 < M_{200\rm m} < 3.52$	50	$4.96 < M_{200\rm m} < 11.06$	46
$0.75 < z < 0.80$	$2.44 < M_{200\rm m} < 3.34$	40	$5.07 < M_{200\rm m} < 10.76$	37

Table 2.2.2: Details of the mass bins selected for our composite LFs of the ACT DR5 sample by taking the top 25 % and bottom 25 % of clusters by mass ranking. The number of clusters per mass bin are also displayed.

2.2.2 Cluster membership

To measure composite LFs, we developed a code which we call `zLF`, which is based on the `zCluster` photometric code. The `zCluster` code [2], described in Hilton et al. (2018), is used for estimating cluster photometric redshifts. The aim of `zCluster` is to use all of the photometric information available while making minimal assumptions about the optical properties of clusters such as their colours. While other methods involve the use of the colours of RS galaxies to locate clusters themselves and to estimate redshifts, the `zCluster` method avoids this. However, it does require an appropriate set of spectral templates (Hilton et al., 2018). `zCluster` has built-in support for querying large photometric surveys such as SDSS(DR7-DR12), SDSS Stripe 82 (S82), CFHTLenS, DECaLS (DR7, DR8, DR9), DES (DR1), PS1 (DR2) and KiDS (DR4). Hilton et al. (2021) found that `zCluster` was able to measure cluster redshifts out to $z \approx 1.4$ when applied to DECaLS, due to the inclusion of the WISE data.

The aim of `zLF` is to measure and plot composite LFs given an input galaxy cluster catalogue. One of the first steps in the `zCluster` code, and one which we incorporate into `zLF`, is to measure the photometric redshift (photo-z) probability distribution, *p(z)*, of each galaxy in the direction of each cluster candidate by fitting each galaxy broadband spectral energy distribution (SED) against a set of spectral templates (Hilton et al., 2021). This template-fitting method has been adopted in many codes, such as BPZ (Benítez, 2000) and EAZY (Brammer et al., 2008). For each template SED, the AB magnitude that would be observed at each redshift z_i over the range $0 < z < 3$ is calculated, in steps of 0.01 in redshift. The observed broadband SED of each galaxy is compared with each template SED at each z_i, and the $p(z)$ distribution for each galaxy is constructed from the minimum χ^2 value (over the template set) at each z_i. A magnitude-based prior is then applied that sets $p(z) = 0$ at redshifts where the r-band absolute magnitude is brighter than -24, since the probability of observing such galaxies, in reality, is extremely small (Hilton et al., 2018). The peak of the *p(z)* distribution gives the maximum-likelihood photometric redshifts for each

[2] https://github.com/ACTCollaboration/zCluster

galaxy (e.g., Benítez, 2000). Instead of using these max-likelihood photo-z's, we decided to use the full galaxy *p(z)* distributions which will offer less bias and prove to be more accurate. We retrieve the galaxy catalogues for each ACT cluster by applying `zCluster` to the DR5 catalogue and using photometry from DECaLS DR9.

Once the galaxy catalogues are retrieved, we iterate through each galaxy per cluster, while integrating over the weighted sum of the *p(z)* distributions between some range in redshift around each cluster redshift. The idea of implementing this method is that we are not actually assigning cluster membership, but instead defining a range around the cluster redshift and integrating the probability over this range. Thus, instead of stating an individual galaxy is definitely a cluster member, we are doing it probabilistically. So, even if a galaxy has a 5% chance of being a cluster member, we can add 0.05 to the galaxy count for that redshift bin. This technique was first developed by Brunner & Lubin (2000) and has since been adopted in numerous cluster LF studies (e.g., Toft et al., 2004; Rudnick et al., 2009). The range or width of the slice around which $p(z)$ is integrated should be on the order of the uncertainty in redshift for the galaxies in question. In our case, we use a $\Delta z = \pm 0.1$ slice around each cluster redshift. This range was also adopted by Rudnick et al. (2009).

The next step is to consider the relationship between galaxy luminosity and magnitude. By definition, we can measure galaxy LFs by counting the number of galaxies we find in a single band of absolute/apparent magnitude (M or m). Similarly to the redshift binning, we had the freedom to choose the width of our magnitude binning. We adopt a magnitude bin width of 0.2 mag. for the initial apparent r-band magnitude range: $17.0 < m_r < 24.5$. A narrower bin width will prevent the averaging out of any effects or trends noticeable in the composite LFs. However, there is a caveat in using apparent magnitude bins. Since our bins have a finite width, a single absolute magnitude corresponds to a range of apparent magnitudes depending on where the galaxy is located within the bin. The net effect will be to convolve the true LF with this magnitude error distribution, leading to biased estimates of the Schechter function fit parameters.

2.2.3 K-corrections

An important step to include in calculating galaxy magnitudes is k-correction. The k-correction accounts for the fact that filter passbands cover different rest-frame wavelength ranges for sources at different redshifts (Hogg et al., 2002). Since observations often measure through a single filter or bandpass, observers only measure a fraction of the total spectrum, redshifted into the frame of the observer. The application of k-correction depends on the type of spectral filter used to make observations and the shape of the spectrum. For each cluster in each bin, we k-correct galaxy r-band magnitudes, using a stellar population model from Bruzual & Charlot (2003) (BC03 hereafter), to the median redshift of each cluster bin. We compute this using the same method and model described in Hilton et al. (2013), assuming a $\tau = 0.1$ Gyr single-star burst BC03 model, formed at $z_f = 3.0$ with solar metallicity. While this k-correction will be correct for early-type galaxies in the clusters, a better approach would be to derive the k-correction from the best-fitting spectral template for a particular galaxy. However, this is beyond the scope of the work in this Master's thesis.

Once k-corrections were added to `zLF`, the next step was to determine if we required completeness corrections to our LFs.

2.2.4 Incompleteness at faint-end

Simply plotting test samples of composite LFs over $17.0 < m_r < 24.5$ revealed incompleteness at the faint-end of the luminosity function (as shown in figure 2.2.1). Incompleteness in the photometric catalogues must be compensated for to extract unbiased results. The images have finite depth, and we start failing to detect galaxies once we approach the magnitude limit of the given survey. Completeness corrections usually involve inserting synthetic point sources into cluster imaging and then running a detection algorithm to try and recover the exact same source at the predicted location (e.g., Hilton et al., 2013). The incompleteness is then corrected by weighting galaxies according to the mean incompleteness measured as a function of magnitude (Mancone et al., 2010). Completeness corrections have no real effect on the bright-end but have a huge impact on the faint-end of LFs. Our test composite LFs

reveal that there are hardly any galaxies at ≈ 24 magnitude, which is where completeness corrections would be very large. After corrections, the faint-end would shift up significantly.

However, calculating completeness corrections for DECaLS would be extremely computationally intensive and is well beyond the scope of this Master's thesis. Instead, we take a conservative approach and adopt a brighter magnitude limit where we can be certain the completeness corrections would be negligible. To confirm this limit, we look at the apparent magnitude distributions from randomly selected galaxy catalogues retrieved from DECaLS for our ACT DR5 sample (shown in figure 2.2.2). We also must consider the r-band magnitude depths for galaxies from DECaLS DR9 (see Section 2.1.2). The magnitude distributions show a galaxy depth of $m_r \approx 23.4$ magnitude, which is consistent with the DECaLS DR9 depth of 23.9 magnitude (Sridhar et al., 2020). However, adopting a magnitude limit of 23.5 magnitude to our composite LFs would not achieve the desired completeness corrections since we notice a falling-off of galaxies in our LFs at brighter magnitudes i.e. ≈ 22.5 magnitude. Thus, to avoid completeness corrections, we adopt a brighter magnitude cut and change our initial magnitude range (see Section 2.2.2) to $17.0 < m_r < 22.5$, keeping a bin width of 0.2. This results in 28 magnitude bins in total. The effect of this brighter magnitude cut can be seen in figure 2.2.3.

2.2.5 Construction of composite LFs

In our attempt to construct our composite luminosity functions, we follow a traditional method given by Colless (1989), and one adopted by many LF studies (e.g., Goto et al., 2002; De Propris et al., 2003; Hilton et al., 2005). Using the derived information from the previous sections, the following summation was carried out for each apparent magnitude bin of the composite LF,

$$N_{cj} = \frac{N_{c0}}{m_j} \sum_i \frac{N_{ij}}{N_{i0}}, \tag{2.1}$$

where N_{cj} is the number of galaxies in the jth bin of the composite LF, and m_j is the number of clusters contributing to the jth bin of the composite LF. N_{ij} is the number of galaxies

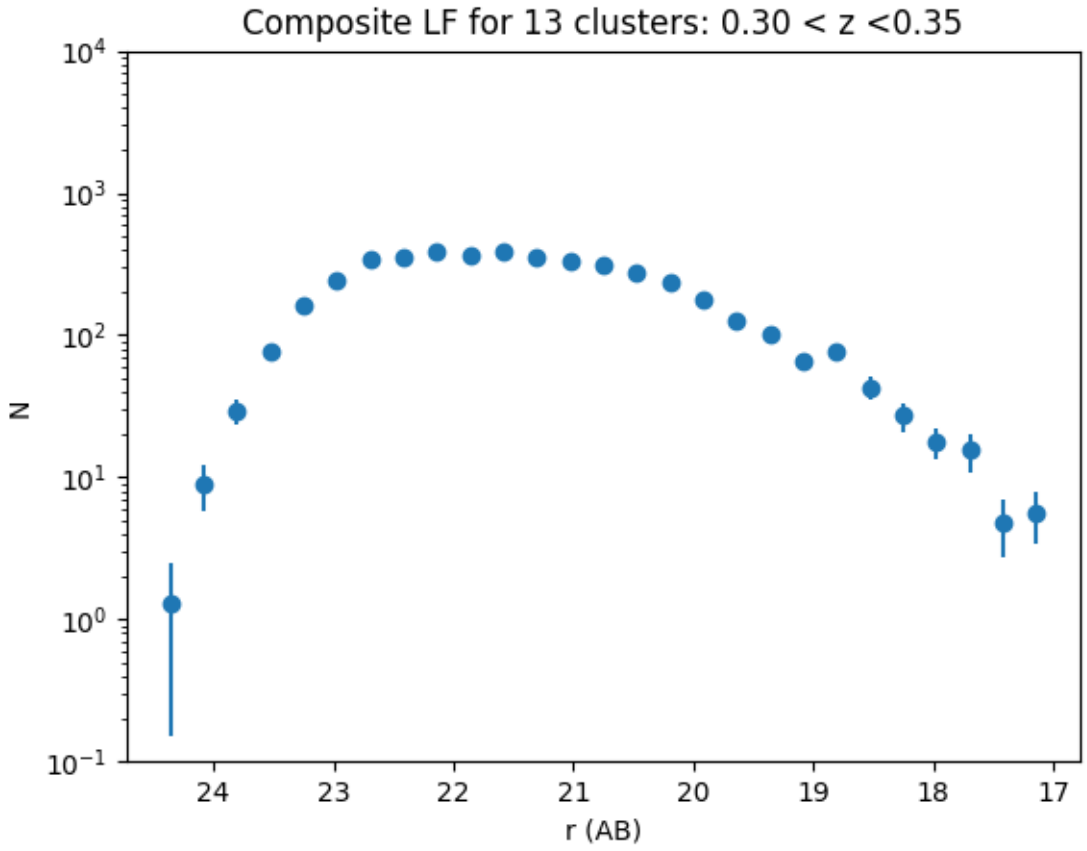

Figure 2.2.1: A composite sub-sample LF for 13 clusters in the redshift interval: $0.30 < z < 0.35$, displaying incompleteness at the faint-end ($m_r > 23$). The y-axis displays the number of galaxies or galaxy counts (N) at each magnitude. We can adopt a brighter magnitude limit to avoid completeness corrections.

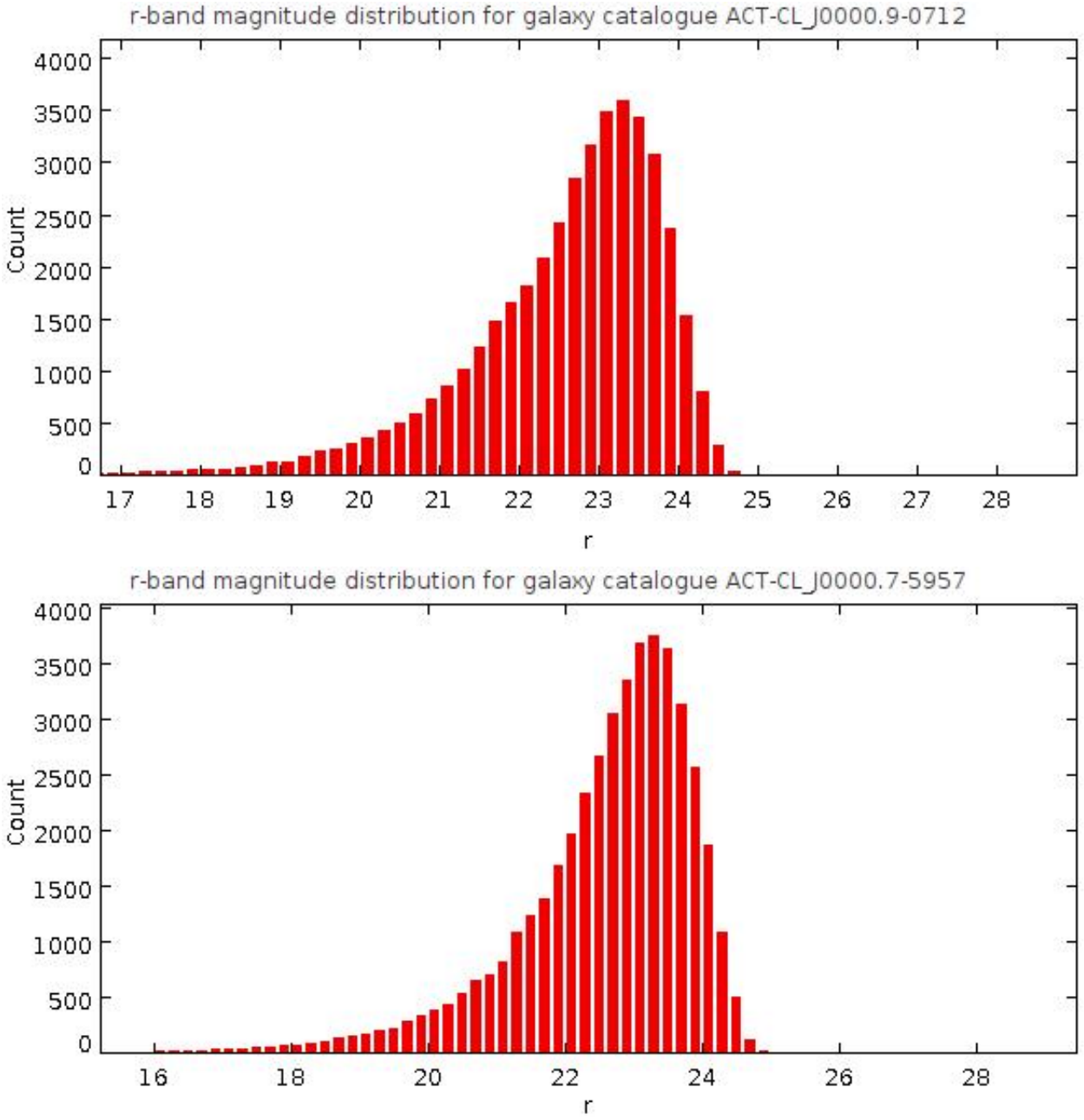

Figure 2.2.2: The apparent magnitude distributions of galaxy catalogues for two individual clusters *Top*: ACT-CLJ0000.9-0712 and *Bottom*: ACT-CLJ0000.7-5957, which we used to determine a magnitude where DECaLS should be complete (see Section 2.1.2). These distributions peak at a magnitude of ≈ 23.4.

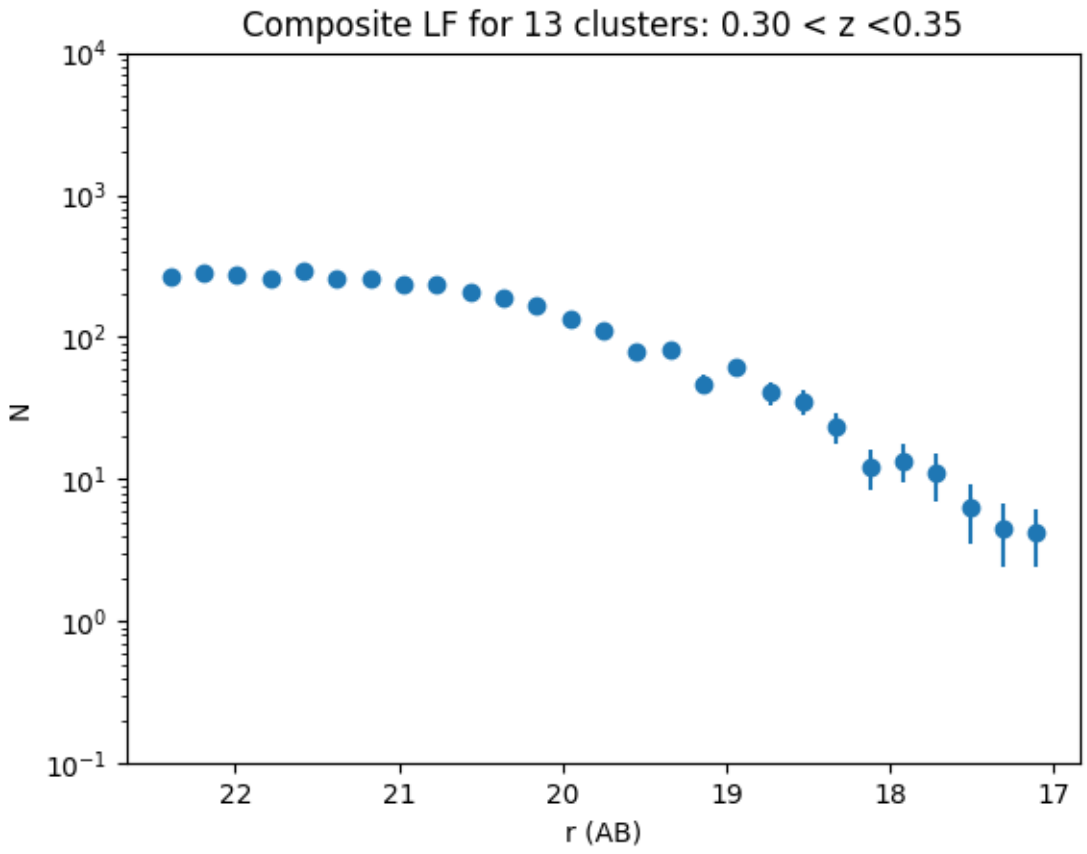

Figure 2.2.3: A composite sub-sample LF displaying the brighter magnitude cut of 22.5 we adopted to account for incompleteness at the faint-end.

contributing to the jth bin of the ith cluster LF. This was calculated by taking the sum of the $p(z)$ distributions, integrated between ± 0.1 in redshift around each cluster redshift.

N_{i0} is a normalization parameter, or cluster richness (see Section 1.4.1) estimate, for the ith cluster LF. The purpose of the richness weighting is to account for the fact that richer clusters consist of more galaxies than poorer clusters and, as a result, could dominate the composite LF. If the richness is underestimated, there will be fewer galaxies signalling that the richness estimate must be increased. Cluster richness can easily be estimated with photometric data for both massive clusters and low-mass groups. This requires two steps: (i) selecting cluster members within a defined radius, and (ii) defining an absolute magnitude limit.

Using a circle with an appropriate radius, we can select cluster members by counting the number of galaxies within it. For cluster members, we select galaxies within the approximate virial radius $R_{200\mathrm{m}}$. We calculate $R_{200\mathrm{m}}$ using the equation,

$$R_{200\mathrm{m}} = \sqrt[3]{\frac{3M_{200\mathrm{m}}}{4\pi 200\rho_m(z)}}, \tag{2.2}$$

where $M_{200\mathrm{m}}$ is the cluster mass within $R_{200\mathrm{m}}$ (with respect to the mean density), and $\rho_m(z)$ is the mean matter density of the Universe at the cluster redshift.

In order to define an absolute magnitude limit, we constructed a volume-limited galaxy sample using absolute magnitude distributions generated from DECaLS field galaxy catalogues. To generate the field catalogues, we used the `zField` [3] code, which retrieves the catalogues in a circular region centred on a user-specified right ascension (RA) and declination (dec) coordinates and then calculates the maximum likelihood photo-z's. We arbitrarily selected four field catalogues for comparison (see figure 2.2.4). Using this volume-limited sample, we adopted an absolute magnitude limit of $\approx$ - 20 magnitude, for $z < 1.0$, which is consistent across the four magnitude distributions. Only cluster members within this limit ($M_r <$ -20) were selected and their probabilities were used for our cluster richness estimates (i.e., the calculation of N_{i0}). Since the volume-limited sample covers up to $z = 1.0$, we only

[3] https://zcluster.readthedocs.io/en/latest/commands.html#zfield

include galaxies brighter than the magnitude limit.

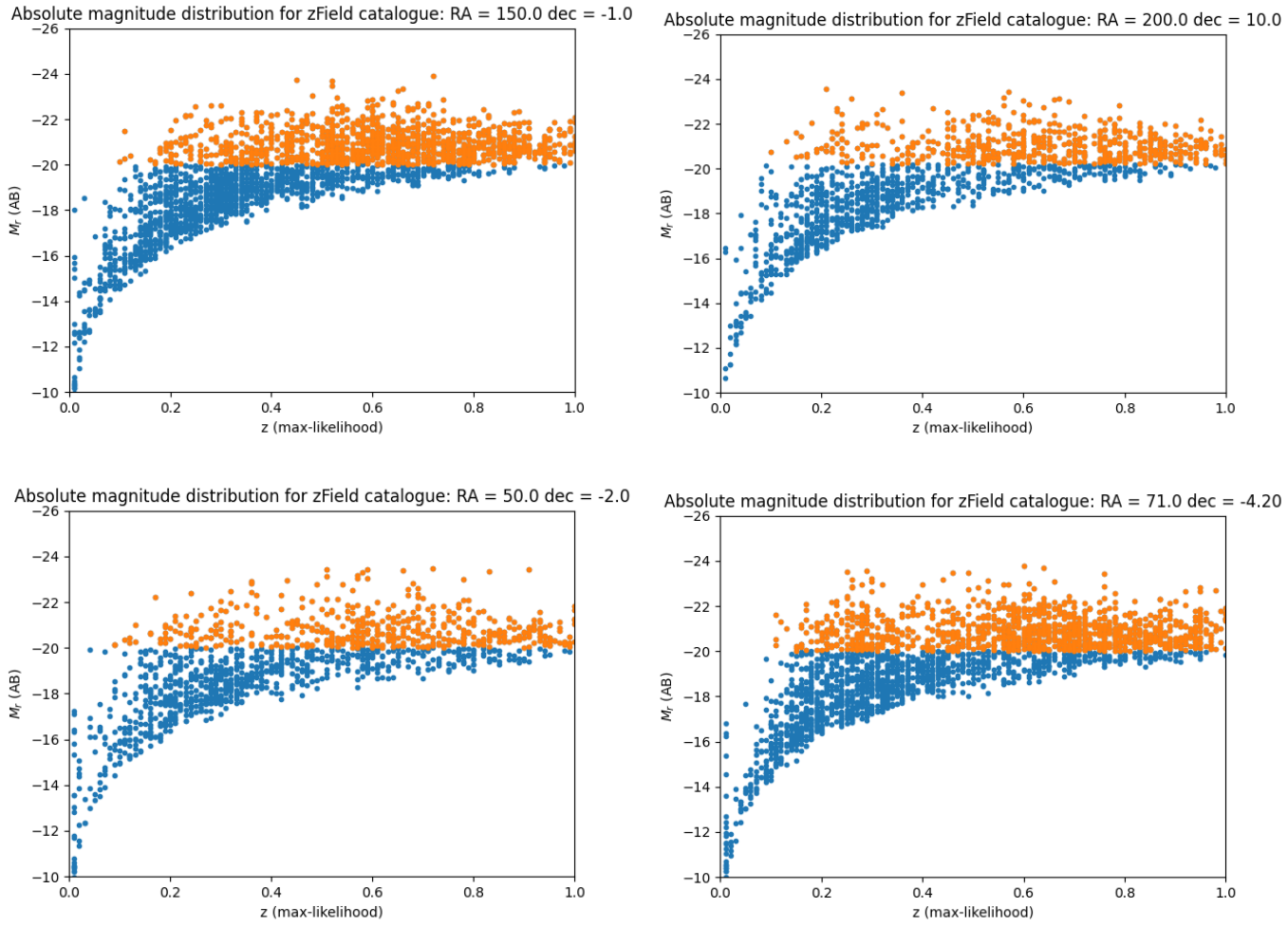

Figure 2.2.4: Plots of absolute magnitude versus the maximum-likelihood photo-z from four arbitrarily selected DECaLS field catalogues. As shown by the orange points, a volume-limited sample reaching to $z = 1$ can be constructed by adopting an absolute magnitude limit of -20. This limit will be used to calculate our richness estimates.

The N_{c0} term represents the sum of all the individual cluster richness estimates, and is given by the following equation,

$$N_{c0} = \sum_i N_{i0}. \tag{2.3}$$

The errors in the composite LF (N_{cj}) were calculated using the formula,

$$\delta N_{cj} = \frac{N_{c0}}{m_j} \left[\sum_i \left(\frac{\delta N_{ij}}{N_{i0}} \right)^2 \right]^{\frac{1}{2}}, \tag{2.4}$$

where the errors in N_{ij} were assumed to be Poissonian, i.e. $\sqrt{N_{ij}}$. Note, this is likely to be an underestimate of the true uncertainty since it does not account for any additional scatter that will be caused by the use of photometric redshifts.

These methods were adopted into our `zLF` code. We used the University of KwaZulu-Natal's high-performance computing facility, Hippo [4], to run the `zLF` algorithm on the DR5 clusters. The results of our LF construction are described in the next chapter.

[4] https://astro.ukzn.ac.za/~hippo/

Chapter 3

Results

In this chapter, we present the results of our composite LF measurements. We discuss fitting the Schechter function model to our composite LFs and obtain the relevant model parameters m^* and α (see Section 1.5). We present the Schechter-fitted LFs for both full redshift binned and mass sub-sample LFs. We also determine the goodness-of-fit of our data to the model.

3.1 Schechter function fitting

The LF construction resulted in 12 stacked LFs, and 12 low-mass and high-mass subset LFs. We present a few of our unfitted composite LFs for the total redshift binned sample, together with our mass subset LFs, in figure 3.1.1. In order to get the desired information from these LFs (e.g., characteristic magnitude and faint-end slope), we need to fit an appropriate model to our data. As mentioned previously (see Section 1.5), the Schechter function is a suitable model to use.

Using the form of equation 1.1, we fitted a single Schechter function, for two parameters, to our LFs. The normalization parameter, ϕ^*, was fixed such that the value of the integral of the fitted function was equal to the total number of galaxies in the composite LF within the same magnitude range (e.g., Hilton et al., 2005). The two function parameters, m^* and α, were estimated using a χ^2 minimization technique. The χ^2 statistic describes the

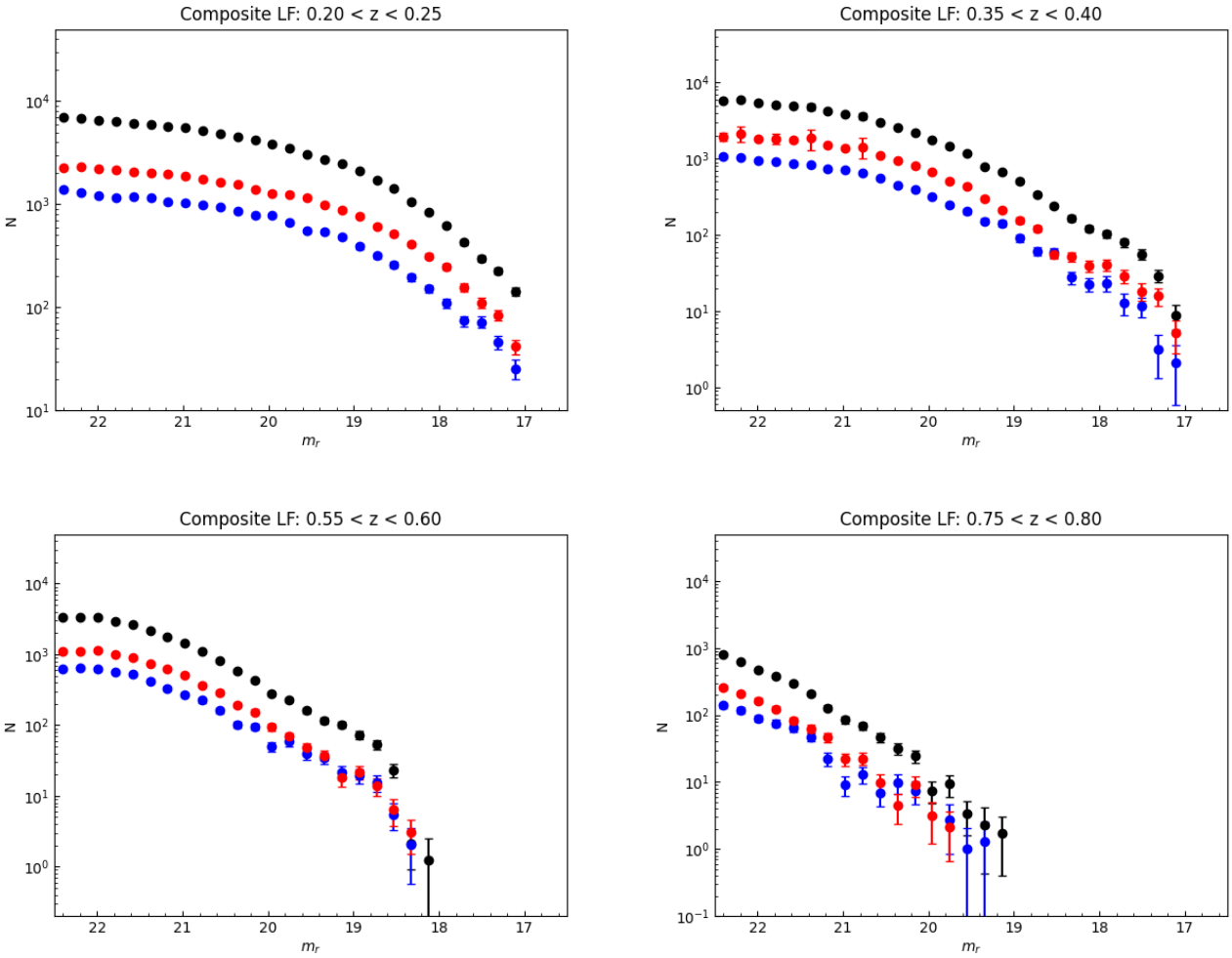

Figure 3.1.1: A few of the unfitted total, low-mass, and high-mass composite cluster LFs constructed in the 12 redshift bins. The low-mass LF is represented by blue data points, while the high-mass LF is represented by red data points. Uncertainties with the data points are estimated using Poisson statistics.

goodness-of-fit of the data to the model. This is represented in the form,

$$\chi^2 = \sum_i \frac{(N_i - N_i^e)^2}{\sigma_i^2}, \tag{3.1}$$

where N_i is the total galaxy counts in the ith bin of the observed LF, N_i^e is the expected number of counts from the model LF (i.e., given by the Schechter function), and σ_i is the uncertainty of the galaxy counts in the ith data bin, which are Poisson errors in our case. The relative probability (or likelihood) of randomly drawing a specific sample of data (I) given a model (θ) is related to the χ^2 of the data given the model,

$$\mathscr{L}(I|\theta) \propto e^{-\chi^2/2}. \tag{3.2}$$

The bigger the χ^2 value is, the smaller the likelihood will be and vice versa. Thus, χ^2 minimization implies likelihood maximization.

The LF fitting procedure was conducted using the `Schechterfits` code we created. We also created a function to return the χ^2 value for our observed LF data given some input model parameters and then adjusted the model parameters to minimize the χ^2 value. This essentially meant creating a grid of initial m^* and α values and finding χ^2 values for the respective combinations of these values, which were then stored. The minimum χ^2 value was found using the maximum likelihood probability. The best-fit m^* and α values were then retrieved from the same grid location as the minimum χ^2 value. We then ran 100 iterations on our 100×100 grid to reduce computing time. A tolerance level of 0.01 (to increase convergence) was set to be the minimum difference between each m^* and α found on each grid iteration. The tolerance level essentially decreased the number of iterations significantly. The period of convergence obviously varied for each composite cluster LF.

Another key piece of information commonly discussed in relation to hypothesis testing, such as χ^2, is the degrees of freedom. Degrees of freedom refers to the maximum number of logically independent values, which are values that have the freedom to vary, in the data sample. This is simply given by the difference between the number of data values or points (N_d) and the number of parameters to fit (N_p). In our case, we used $N - 2$ degrees of

freedom, since ϕ^* is fixed.

An accurate indicator of the goodness of fit is the reduced chi-squared statistic. This is given by the formula,

$$\chi^2_\nu = \frac{\chi^2}{\nu}, \tag{3.3}$$

where ν is the degrees of freedom. If a model is fitted to the data and the resulting chi-square value is $\chi^2_\nu > 1$, it is considered a "bad" fit, whereas if $\chi^2_\nu < 1$, it is considered an "over-fit" (Andrae et al., 2010). A model with $\chi^2_\nu \approx 1$ is considered to be a "good" fit.

The 1σ (68th percentile) uncertainties for m^* and α were measured using Monte-Carlo (MC) simulations. We perform 1000 MC simulations on the LF fitting function, feeding it the observed LF and creating random realisations by drawing random variates for each value in each LF bin by taking into account the value and its uncertainty (and assuming Poisson statistics). Uncertainties in m^* and α were calculated by taking the standard deviation of the two stored lists of m^* and α values, retrieved after the MC simulations. We also found M^* values for the composite LFs, using m^* values and the distance modulus (μ) to the centre of each cluster redshift bin. Due to this direct relationship with m^*, the uncertainty in M^* is the same as those calculated for m^*.

3.2 Redshift-binned results

The Schechter-fitted composite LFs can be found in figures 3.2.1 - 3.2.3. Details of the fit parameters can be found in Table 3.2.1.

Considering the high χ^2 values we retrieved, the single-fitted Schechter model does not appear to be a good fit for our composite LFs. The reduced chi-squared values (χ^2_ν) for $\approx 92\%$ of the redshift bins are much greater than 1 (as shown in Table 3.2.1), implying a "bad fit". The mid-redshift bins (e.g., $\langle z \rangle = 0.425, 0.525$) seem to contribute the highest reduced chi-squared values. This is explained by the relatively small error bars in our plots, which we assumed to be Poisson. Equation 3.1 relates the error bars (σ) to the χ^2 value as

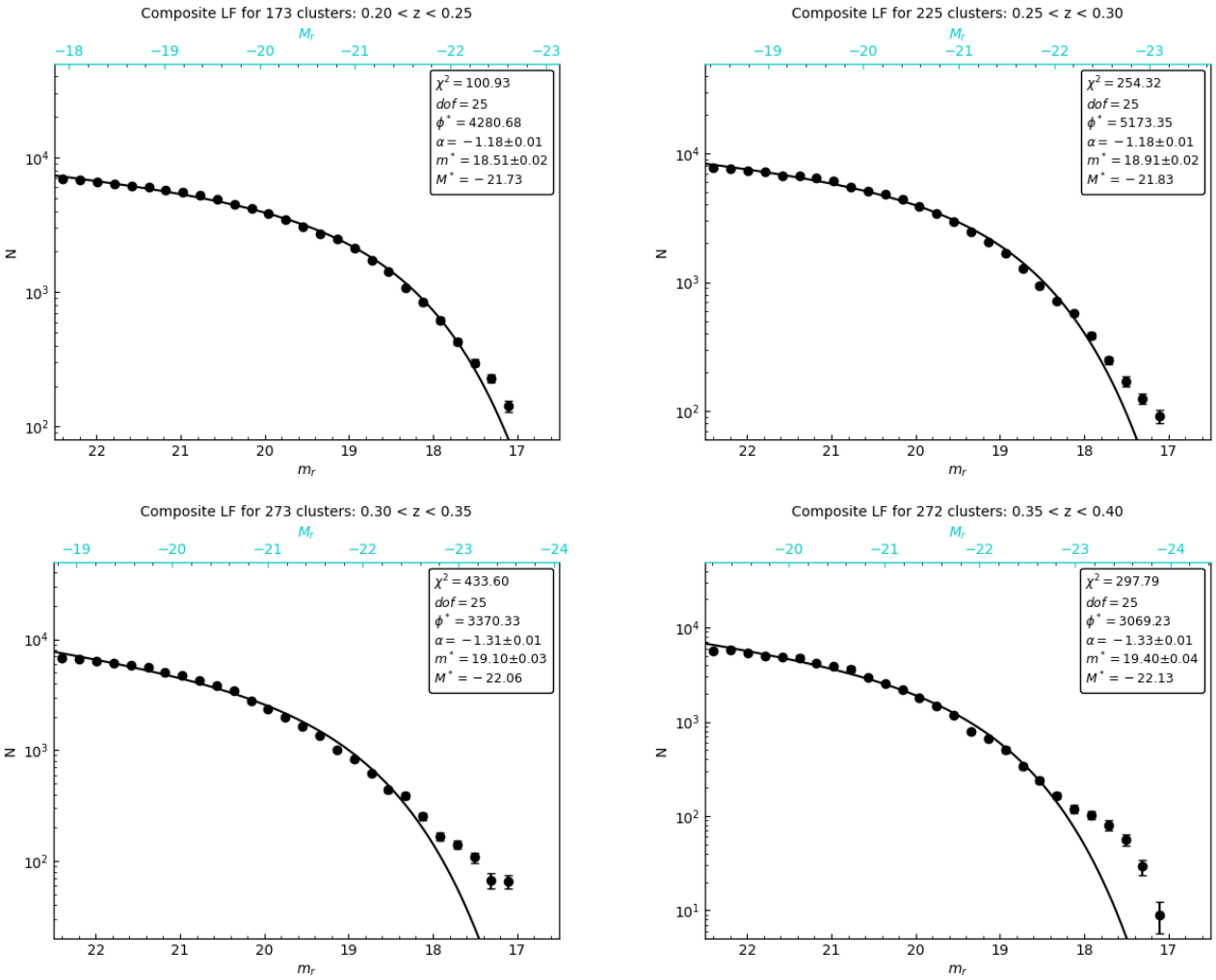

Figure 3.2.1: Schechter fitted composite LFs for redshift bins 1-4 ($0.20 < z < 0.40$). Fitting parameters are included in each plot, including 1σ fitting uncertainties, the minimum χ^2 value, degrees of freedom (dof), and characteristic absolute magnitude (M^*). The absolute magnitude (M_r) axis is shown in light blue.

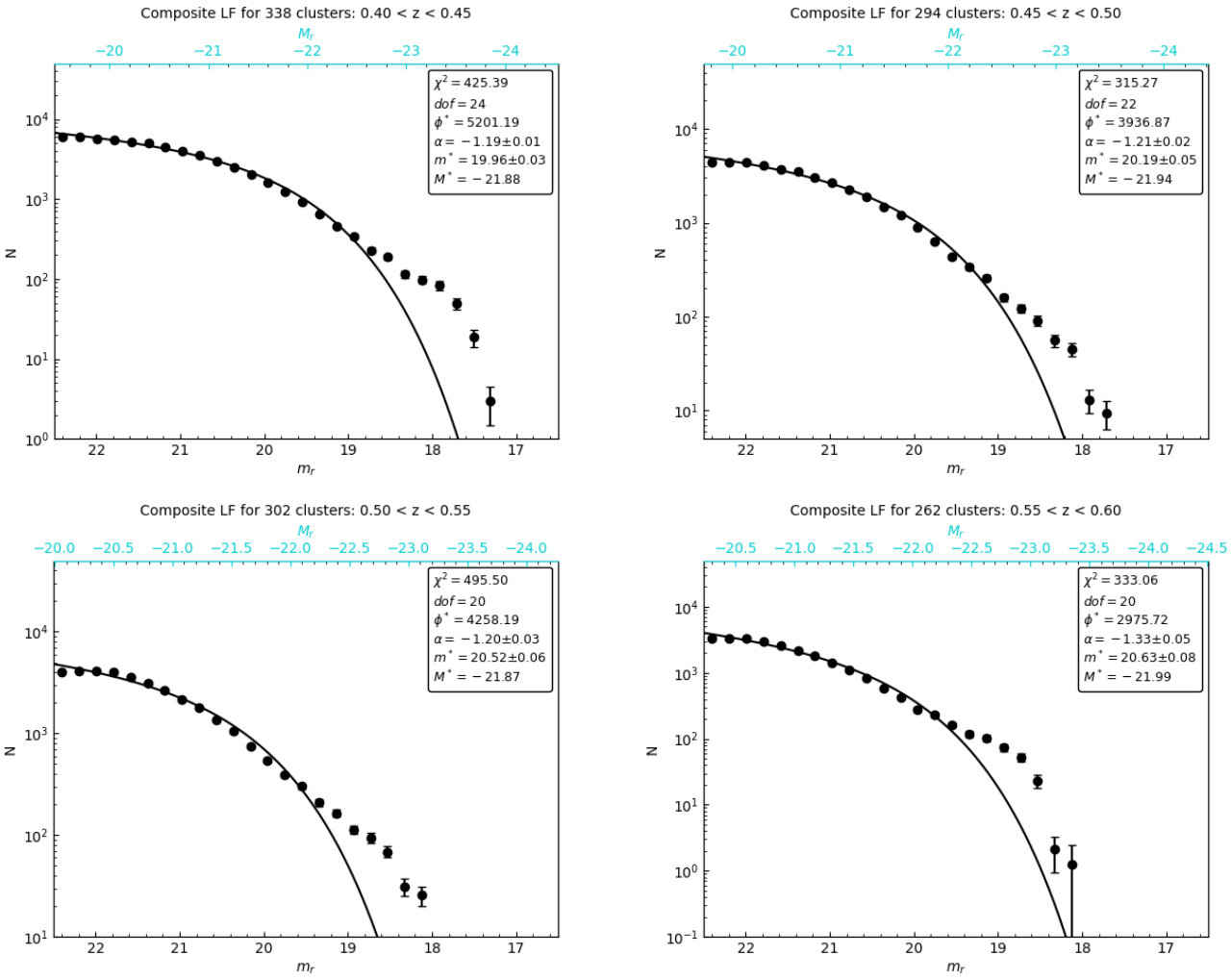

Figure 3.2.2: Schechter fitted composite LFs for redshift bins 4-8 ($0.40 < z < 0.60$). Fitting parameters are included in each plot, including 1σ fitting uncertainties, the minimum χ^2 value, degrees of freedom (dof), and characteristic absolute magnitude (M^*). The absolute magnitude (M_r) axis is shown in light blue.

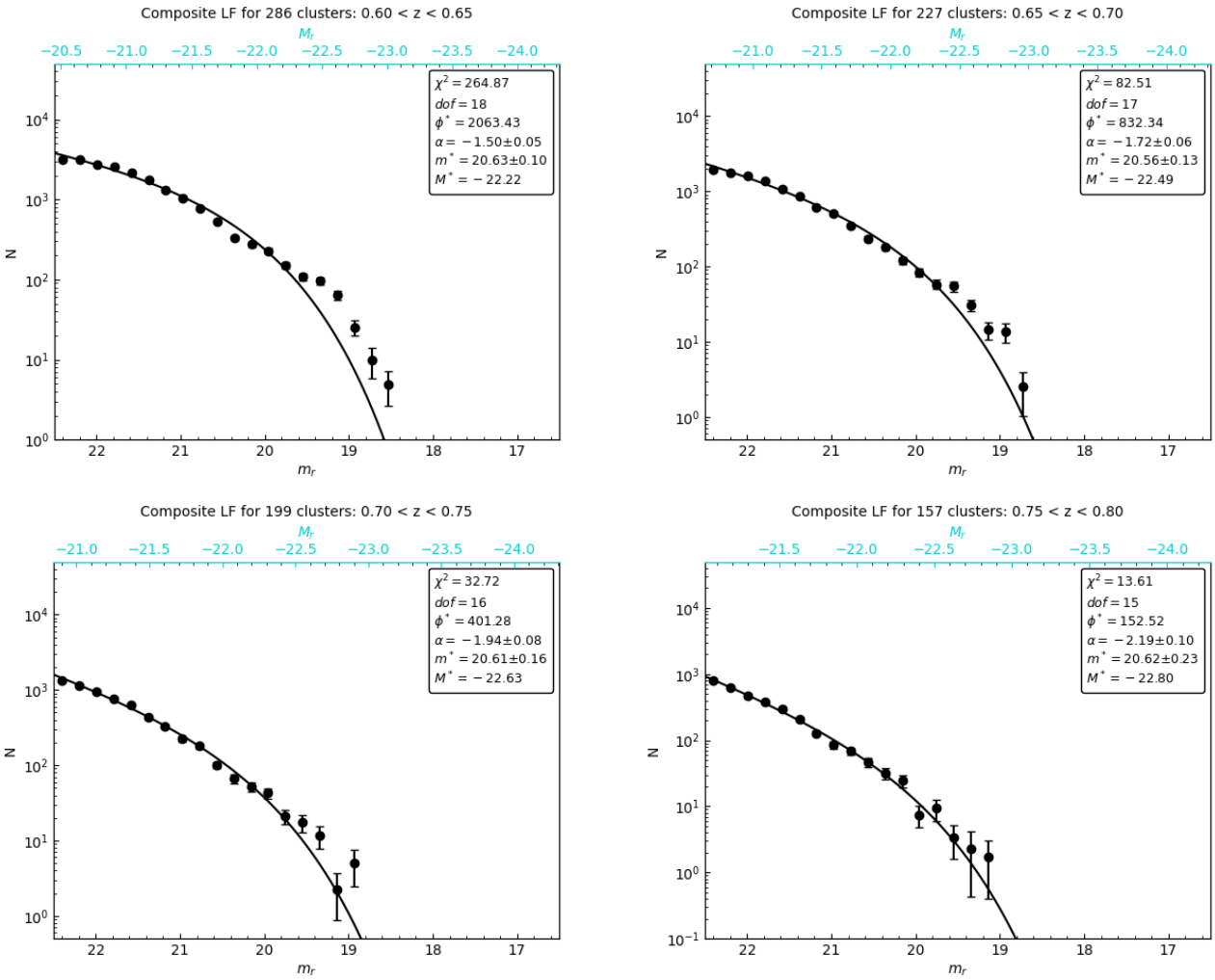

Figure 3.2.3: Schechter fitted composite LFs for redshift bins 8-12 ($0.60 < z < 0.80$). Fitting parameters are included in each plot, including 1σ fitting uncertainties, the minimum χ^2 value, degrees of freedom (dof), and characteristic absolute magnitude (M^*). The absolute magnitude (M_r) axis is shown in light blue.

an inversely proportional relationship. This means that the smaller the error bars on our data are estimated to be, the higher the χ^2 value will be, and, as a result, so will the reduced chi-squared value. Thus, it is highly likely that the Poissonian errors are an underestimate of the true uncertainty. Different k-corrections for different types of galaxies/spectral energy distribution are another source of uncertainty that we have not captured in our error bars. The use of photo-z's also introduces additional uncertainty that we may have not accounted for.

If we consider individual contributions per magnitude bin (see Table 3.2.2), the brighter magnitude bins consist of the highest summed χ^2 values, while the fainter magnitude bins had low values, with the exclusion of the last magnitude bin. This effect is noticeable in our composite LFs as the deviation of the bright-end from the Schechter model. This is especially prominent in the low to mid-redshift bins (e.g., figure 3.2.2). As mentioned in Section 1.5, discrepancies between the observed LF and Schechter model can occur at the bright-end due to the presence of bright cluster members. This noticeable bright-end peak may be better described by a Gaussian distribution (see Section 1.5). This effect is most probably enhanced by the fact that we are able to use narrow magnitude bins ($\Delta m_r = 0.2$), due to the large size of the cluster (and galaxy) sample. The uncertainties in these brighter magnitude bins are much larger, and more pronounced, compared to the fainter end. This is because we expect to find fewer galaxies in the brighter magnitude bins since most of the galaxies in the Universe are faint objects.

Our composite LFs follow a trend of α becoming steeper (or more negative) with redshift. The characteristic magnitude, m^*, also becomes fainter as we move to the higher redshift bins in our sample range, while M^* values become brighter with redshift (see Table 3.2.1). We obtained $\alpha = -1.18 \pm 0.01$; $m^* = 18.51 \pm 0.02$ for our lowest redshift bin: $\langle z \rangle = 0.225$, and $\alpha = -2.19 \pm 0.10$; $m^* = 20.62 \pm 0.23$ for our highest redshift bin: $\langle z \rangle = 0.775$. There is a $\approx 10.1\sigma$ difference between the faint-end slope at $\langle z \rangle = 0.225$ and the slope at $\langle z \rangle = 0.775$. This indicates a strong evolution of α with redshift. There is also evidence for a significant evolution of m^* with redshift (mostly due to varying distance moduli), with a

Composite LF fitting details								
$\langle z \rangle$	$N_{\rm clus}$	m^*	α	M^*	ϕ^*	χ^2	dof	χ^2_ν
0.225	173	18.51 ± 0.02	-1.18 ± 0.01	-21.73 ± 0.02	4280.68	100.93	25	4.04
0.275	225	18.91 ± 0.02	-1.18 ± 0.01	-21.83 ± 0.02	5173.35	254.32	25	10.17
0.325	273	19.10 ± 0.03	-1.31 ± 0.01	-22.06 ± 0.03	3370.33	433.60	25	17.34
0.375	272	19.40 ± 0.04	-1.33 ± 0.01	-22.13 ± 0.04	3069.23	297.79	25	11.91
0.425	338	19.96 ± 0.03	-1.19 ± 0.01	-21.88 ± 0.03	5201.19	425.39	24	17.72
0.475	294	20.19 ± 0.05	-1.21 ± 0.02	-21.94 ± 0.05	3936.87	315.27	22	14.33
0.525	302	20.52 ± 0.06	-1.20 ± 0.03	-21.87 ± 0.06	4258.19	495.50	20	24.78
0.575	262	20.63 ± 0.08	-1.33 ± 0.05	-21.99 ± 0.08	2975.72	333.06	20	16.65
0.625	286	20.63 ± 0.10	-1.50 ± 0.05	-22.22 ± 0.10	2063.43	264.87	18	14.72
0.675	227	20.56 ± 0.13	-1.72 ± 0.06	-22.49 ± 0.13	832.34	82.51	17	4.85
0.725	199	20.61 ± 0.16	-1.94 ± 0.08	-22.63 ± 0.16	401.28	32.72	16	2.05
0.775	157	20.62 ± 0.23	-2.19 ± 0.10	-22.80 ± 0.23	152.52	13.61	15	0.91

Table 3.2.1: Table of Schechter fitted parameters for our redshift-binned stacked LFs. Redshift bins are classified in terms of the median of the redshift bin, $\langle z \rangle$. The errors in M^* were the same measured for m^*. The last column represents the reduced chi-squared (χ^2_ν) values, which indicate poor model fits. This suggests perhaps that our uncertainties are underestimated.

$\approx 9.2\sigma$ difference between the lowest redshift bin and the highest redshift bin. However, this evolution is less significant for M^*, with a $\approx 4.7\sigma$ difference between these bins. We will discuss possible reasons for the evolution we see in Chapter 4. A caveat when fitting Schechter functions over different magnitude ranges is that the fit parameters can vary systematically with the fitting range, even for the same underlying LF. Hence, it may be preferred to fit over a common absolute magnitude range at all redshifts.

3.3 Mass-binned results

As mentioned in Section 2.2.1, low-mass and high-mass subsets were created by selecting the top 25 % and bottom 25 % by cluster mass, for each redshift bin. Our Schechter fitting

Individual χ^2 contributions per redshift bin													
Magnitude bin	$\langle z \rangle =$	0.225	0.275	0.325	0.375	0.425	0.475	0.525	0.575	0.625	0.675	0.725	0.775
17.10		22.75	46.69	48.73	7.07	-	-	-	-	-	-	-	-
17.31		20.19	41.42	28.87	25.36	3.82	-	-	-	-	-	-	-
17.51		2.30	23.60	52.42	40.65	16.27	-	-	-	-	-	-	-
17.71		0.01	10.80	40.29	43.36	39.45	8.71	-	-	-	-	-	-
17.92		0.20	6.32	15.63	36.96	61.58	12.10	-	-	-	-	-	-
18.12		1.89	3.50	10.02	14.37	60.87	33.73	20.90	0.92	-	-	-	-
18.32		7.09	5.41	9.14	3.44	38.34	34.17	25.31	2.31	-	-	-	-
18.53		2.31	15.75	3.91	0.09	41.24	38.60	53.37	18.81	3.51	-	-	-
18.73		2.92	13.88	5.04	2.46	10.66	27.97	58.37	37.52	3.39	0.97	-	-
18.94		0.41	6.10	8.98	0.72	3.06	9.48	44.05	44.30	11.48	7.10	2.68	-
19.14		0.17	9.11	29.46	6.55	2.34	7.39	34.26	39.52	29.44	3.34	0.01	0.76
19.34		3.07	6.90	9.87	38.23	10.53	0.30	9.46	15.79	28.80	6.86	3.00	0.25
19.55		2.16	1.29	13.11	2.43	13.34	14.31	1.44	5.99	7.94	7.58	2.73	0.05
19.75		0.18	0.36	12.51	2.81	14.41	15.97	5.85	0.32	1.99	0.17	0.20	0.98
19.95		0.20	0.26	6.76	1.48	10.57	11.66	19.51	14.29	0.72	0.36	2.19	1.62
20.16		0.99	2.59	1.63	0.59	9.53	5.05	25.85	11.17	8.56	2.67	0.09	1.34
20.36		0.29	3.22	1.79	0.79	2.75	7.85	17.10	22.04	47.73	2.18	3.80	0.07
20.56		3.67	1.53	8.65	5.53	0.28	1.36	18.08	11.35	18.67	8.85	4.84	0.00
20.77		6.68	1.63	9.26	1.87	4.00	0.16	0.99	3.00	5.28	4.02	0.03	0.00
20.97		8.53	13.60	20.29	15.97	2.86	3.86	0.74	0.86	0.51	0.02	2.00	3.00
21.18		1.70	11.58	12.74	8.20	14.61	5.06	2.16	0.46	0.07	1.61	0.01	1.59
21.38		2.46	3.39	9.86	1.14	17.91	10.53	8.82	1.56	10.13	1.38	0.21	0.39
21.58		0.02	0.47	9.71	1.92	3.53	4.20	20.01	16.76	12.94	2.86	3.92	1.90
21.79		0.75	0.08	0.00	0.39	0.76	6.93	33.17	13.80	19.18	9.79	1.48	0.72
21.99		2.08	1.31	4.74	13.40	2.45	3.20	6.59	10.78	1.56	6.84	1.19	0.28
22.19		2.33	8.23	18.07	0.36	1.61	3.29	10.45	2.10	0.01	0.61	0.00	0.03
22.40		5.61	15.28	42.13	21.61	38.62	49.36	79.03	59.40	52.97	15.30	4.35	0.62
Σ		**100.93**	**254.32**	**433.60**	**297.79**	**425.39**	**315.27**	**495.50**	**333.06**	**264.87**	**82.51**	**32.72**	**13.61**

Table 3.2.2: Table representing the individual χ^2 contributions from each magnitude bin per cluster redshift bin. The final row represents the total contributions in each bin.

method was then applied to these subsets. A convenient way to display these sub-samples is to compare them with their respective total sample LF. Comparison plots of the mass-binned LFs and total composite LFs can be found in figures 3.3.1 - 3.3.3. The fitted Schechter parameter values for the mass subsets are provided in Tables 3.3.1 and 3.3.2.

For the low-mass subsets, we obtained α = -1.18 $\pm$ 0.01; m^* = 18.52 $\pm$ 0.05 in our lowest redshift bin ($\langle z \rangle = 0.225$), and α = -2.36 $\pm$ 0.83; m^* = 20.14 $\pm$ 1.82 for our highest redshift bin ($\langle z \rangle = 0.775$). This shows an $\approx 1.4\sigma$ difference in α between the lowest and highest redshift bins. However, due to the large uncertainties in α with redshift, α is not well constrained. There is also weak evidence of the evolution of m^* with redshift, with an $\approx 0.9\sigma$ difference between the lowest and highest redshift bins. This implies a weak evolution of M^* with redshift for low-mass clusters. However, the uncertainty in the final redshift bin is quite large compared to the other bins. There is a very good agreement between the low-mass subset LF and the total redshift binned LF, with a $< 1\sigma$ difference between their m^* and α values in the lowest and highest redshift bins.

For the high-mass subset, we obtained α = -1.15 $\pm$ 0.01; m^* = 18.48 $\pm$ 0.03 for $\langle z \rangle$ = 0.225, and α = -2.05 $\pm$ 0.30; m^* = 21.14 $\pm$ 0.55 for $\langle z \rangle = 0.775$. This is a difference of $\approx 3\sigma$ between α in the lowest and highest redshift bin. This represents a significant evolution of α with redshift for high-mass clusters. Once again, uncertainty for α in the highest redshift bin is relatively high compared to other bins. There is an $\approx 4.8\sigma$ difference in m^*, and an $\approx 0.9\sigma$ difference in M^*, between these two redshift bins. This indicates a weak evolution of M^* with redshift for high-mass clusters. There is a good agreement between the high-mass subset LF and the total composite LF ($< 1\sigma$).

We also observe a $\approx 3\sigma$ difference in α between the low-mass and high-mass subset at $\langle z \rangle = 0.225$. However, these differences are much more noticeable at mid-redshifts - e.g., for $\langle z \rangle = 0.475$, the high-mass subset has a faint-end slope within 3.6σ of the slope derived for the low-mass subset. Differences between derived characteristic magnitudes for both subsets are $< 3\sigma$, implying no significant evolution of m^* with redshift between subsets.

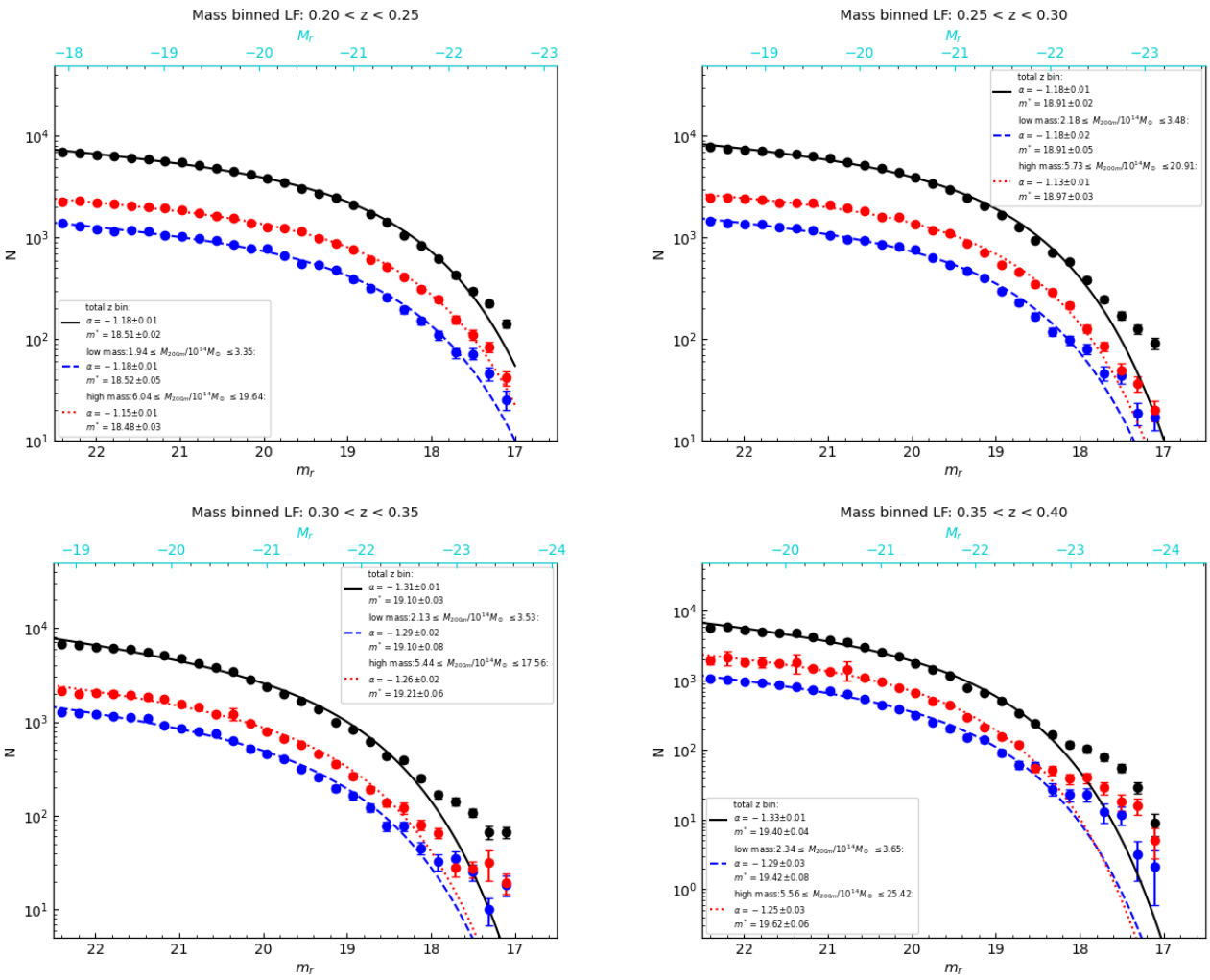

Figure 3.3.1: Comparison of mass-binned composite LFs and total composite LF for redshift bins 1-4 ($0.20 < z < 0.40$). The low-mass subset is represented by blue data points and fitted with a single Schechter function represented by a dashed blue line. The high-mass subset is represented by red data points and fitted with a single Schechter function represented by a dotted red line. Fitting parameters are shown in the plot legend. The absolute magnitude (M_r) axis is shown in light blue.

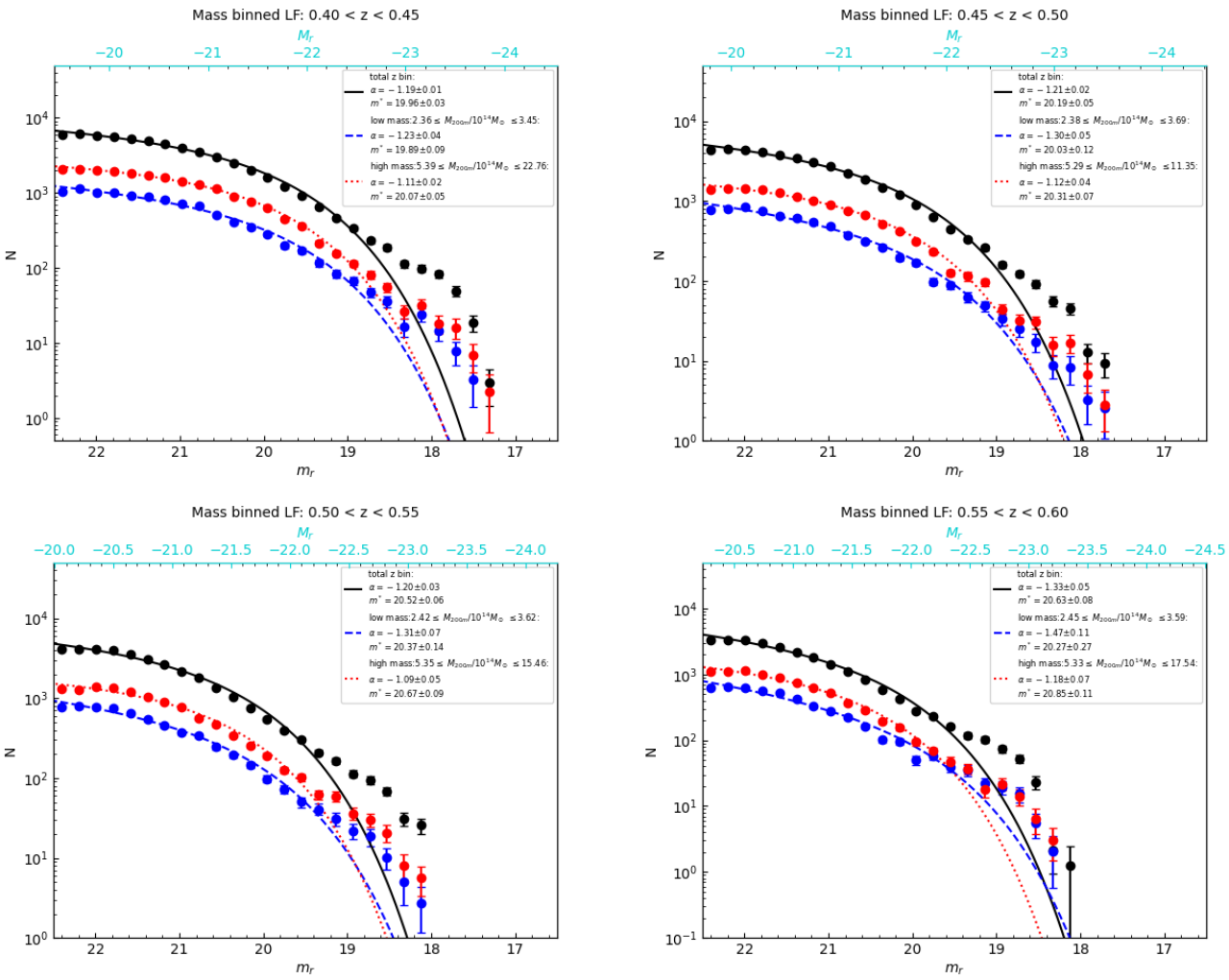

Figure 3.3.2: Comparison of mass-binned composite LFs and total composite LF for redshift bins 4-8 ($0.40 < z < 0.60$). The low-mass subset is represented by blue data points and fitted with a single Schechter function represented by a dashed blue line. The high-mass subset is represented by red data points and fitted with a single Schechter function represented by a dotted red line. Fitting parameters are shown in the plot legend. The absolute magnitude (M_r) axis is shown in light blue.

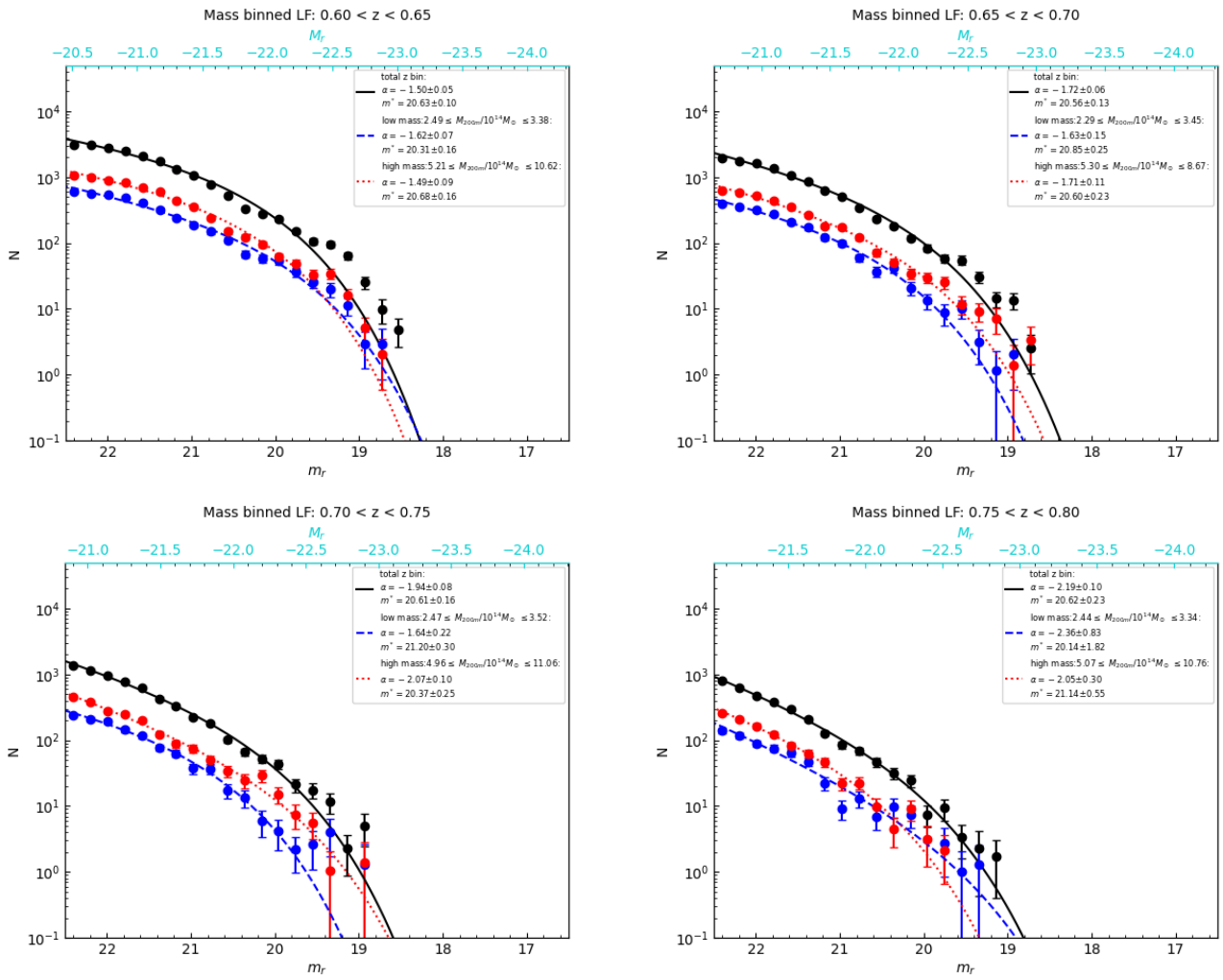

Figure 3.3.3: Comparison of mass-binned composite LFs and total composite LF for redshift bins 8-12 ($0.60 < z < 0.80$). The low-mass subset is represented by blue data points and fitted with a single Schechter function represented by a dashed blue line. The high-mass subset is represented by red data points and fitted with a single Schechter function represented by a dotted red line. Fitting parameters are shown in the plot legend. The absolute magnitude (M_r) axis is shown in light blue.

Low-mass composite LF fitting details								
$\langle z \rangle$	$N_{\rm clus}$	m^*	α	M^*	ϕ^*	χ^2	dof	χ^2_ν
0.225	47	18.52 ± 0.05	-1.18 ± 0.01	-21.73 ± 0.05	805.06	39.93	25	1.60
0.275	60	18.91 ± 0.05	-1.18 ± 0.02	-21.83 ± 0.05	953.56	67.35	25	2.69
0.325	72	19.10 ± 0.08	-1.29 ± 0.02	-22.06 ± 0.08	650.28	108.57	25	4.34
0.375	70	19.42 ± 0.08	-1.29 ± 0.03	-22.10 ± 0.08	594.08	78.39	25	3.14
0.425	89	19.89 ± 0.09	-1.23 ± 0.04	-21.95 ± 0.09	846.18	118.06	23	5.13
0.475	75	20.03 ± 0.12	-1.30 ± 0.05	-22.10 ± 0.12	576.14	83.64	22	3.80
0.525	78	20.37 ± 0.14	-1.31 ± 0.07	-22.02 ± 0.14	633.03	89.28	20	4.46
0.575	66	20.27 ± 0.27	-1.47 ± 0.11	-22.36 ± 0.27	368.97	105.62	19	5.56
0.625	73	20.31 ± 0.16	-1.62 ± 0.07	-22.54 ± 0.16	256.84	48.22	17	2.84
0.675	58	20.85 ± 0.25	-1.63 ± 0.15	-22.20 ± 0.25	241.69	23.88	16	1.49
0.725	50	21.20 ± 0.30	-1.64 ± 0.22	-22.04 ± 0.30	193.37	12.41	15	0.83
0.775	40	20.14 ± 1.82	-2.36 ± 0.83	-23.28 ± 1.82	11.65	25.93	13	1.99

Table 3.3.1: Table of Schechter fitted parameters for our low-mass binned composite LFs, for each redshift bin. Redshift bins are classified in terms of the median of the redshift bin, $\langle z \rangle$. The errors in M^* were the same as measured for m^*. The last column represents the reduced chi-squared (χ^2_ν) values.

The overall reduced chi-squared values for both subsets are considerably lower (≈ 1) than those obtained for the total redshift-binned LFs. This is mainly since each mass subset contains fewer clusters, hence fewer galaxies, than the full redshift bin. Similar to the redshift-binned LFs, the main contributors to high χ^2_ν values came from the mid-redshift bins (see Tables 3.3.1 and 3.3.2).

Through visual inspection of figures 3.3.1 - 3.3.3, we observe that the bright-end mismatches are also distinguishable in both mass subsets and are consistent with the full sample LFs. Once again, the bright-end follows a Gaussian-like distribution for both subsets, while the faint-end follows a steep power-law function. The deviations from the Schechter model are marginally prolific in the high-mass sub-samples, indicating that high-mass clusters contribute more towards this fluctuation in luminosity at the bright-end. These results will be discussed further in the next chapter.

High-mass composite LF fitting details								
$\langle z \rangle$	$N_{\rm clus}$	m^*	α	M^*	ϕ^*	χ^2	dof	χ^2_ν
0.225	37	18.48 ± 0.03	-1.15 ± 0.01	-21.76 ± 0.03	1518.35	27.61	25	1.10
0.275	52	18.97 ± 0.03	-1.13 ± 0.01	-21.77 ± 0.03	1971.37	117.44	25	4.70
0.325	62	19.21 ± 0.06	-1.26 ± 0.02	-21.95 ± 0.06	1263.79	150.73	25	6.03
0.375	65	19.62 ± 0.06	-1.25 ± 0.03	-21.90 ± 0.06	1426.32	135.58	25	5.42
0.425	77	20.07 ± 0.05	-1.11 ± 0.02	-21.77 ± 0.05	2151.53	118.01	24	4.92
0.475	71	20.31 ± 0.07	-1.12 ± 0.04	-21.82 ± 0.07	1544.53	118.68	22	5.39
0.525	73	20.67 ± 0.09	-1.09 ± 0.05	-21.72 ± 0.09	1711.12	192.94	20	9.65
0.575	62	20.85 ± 0.11	-1.18 ± 0.07	-21.78 ± 0.11	1328.52	110.61	19	5.82
0.625	65	20.68 ± 0.16	-1.49 ± 0.09	-22.17 ± 0.16	715.51	83.18	17	4.89
0.675	54	20.60 ± 0.23	-1.71 ± 0.11	-22.45 ± 0.23	281.91	44.47	17	2.62
0.725	46	20.37 ± 0.25	-2.07 ± 0.10	-22.87 ± 0.25	79.99	16.51	15	1.10
0.775	37	21.14 ± 0.55	-2.05 ± 0.30	-22.28 ± 0.55	118.20	10.14	12	0.85

Table 3.3.2: Table of Schechter fitted parameters for our high-mass binned composite LFs, for each redshift bin. Redshift bins are classified in terms of the median of the redshift bin, $\langle z \rangle$. The errors in M^* were the same as measured for m^*. The last column represents the reduced chi-squared (χ^2_ν) values.

Chapter 4

Discussion

In this chapter, we discuss the results of our fitted redshift binned composite LFs and mass binned LFs, making comparisons with previous studies. We discuss the evolution of both m^* and α with redshift. Lastly, we discuss possible improvements that could be made to our work.

4.1 Interpretation of the results

4.1.1 Stacked LFs

We established in Section 3.2 that our redshift-binned composite LFs revealed a trend in the steepness of the faint-end slope with redshift. This is easily visible in a comparison plot of all our redshift binned composite LFs in figure 4.1.1. In particular, we found very steep faint-end slopes in the higher redshift bins, specifically at $\langle z \rangle = 0.775$. These slopes appear to be much steeper than α values obtained in previous studies (e.g., Puddu et al., 2021). The LF of early-type or red galaxies has been observed to have a flatter α than that of late-type or blue galaxies (Muzzin et al., 2007). As discussed in Section 1.5, this idea is further illustrated by the fact that steeper slopes and fainter characteristic magnitudes have been measured in bluer rest-frame passbands. This means that we could be moving into the u or g-band range, resulting in the extreme steepness we observe. Another explanation could be

that we perhaps have an abundance of blue galaxies in our cluster sample contributing to the stacked LFs. Of course, this needs to be verified with the application of a colour-cut to our study.

Galaxy population and the LF also vary with the distance to the cluster centre (Dressler, 1978; Hansen et al., 2005; Barkhouse et al., 2007), and the value of α is steeper in the outer region than that in the central region (Boué et al., 2008; De Filippis et al., 2011). This is consistent with CDM models that predict the most massive galaxies to lie at the cluster cores. For example, Martinet et al. (2015) found more blue galaxies in cluster outskirts than in the core. This larger number of blue or late-type galaxies in the outskirts could be explained by infalls from the field. Few cases of LFs based on deep spectroscopy have produced shallower slopes (e.g., Rines & Geller, 2008), suggesting that the field contamination might be the cause of the observed steep LFs based on photometry only.

We also observed that the characteristic absolute magnitude, M^*, becomes brighter with redshift (see Table 3.2.1). We expect M^* values to become brighter with redshift due to stellar population evolution effects. The luminosity function of galaxies in rich clusters also has a brighter M^* and a steeper α than in poor clusters (e.g., Lin et al., 2004; Hansen et al., 2005). This evidence suggests that our sample consists largely of rich clusters.

The advantage of narrow binning, which is enabled by our very large cluster (and galaxy) sample, allows us to track minor LF trends that would otherwise be averaged out if we used wider bins. Such a trend is the peak (or Gaussian distribution) observed at the bright-end in our composite LFs. As mentioned before (see Section 1.5), the source of this luminosity contribution could be from over-luminous cluster members, such as BCGs/cD galaxies. The luminosity distribution of a sample of BCGs follows a Gaussian function (Hansen et al., 2005; De Filippis et al., 2011). This deviation in luminosity distribution is mainly due to the fact that BCGs or cD galaxies are not drawn from the general cluster galaxy population and have resulted from different formation processes. Hence, many studies have chosen either to exclude them or to treat them differently (e.g., Goto et al., 2002; Hansen et al., 2009; Wen & Han, 2015). The construction of our composite LFs did not include a radial cut to exclude

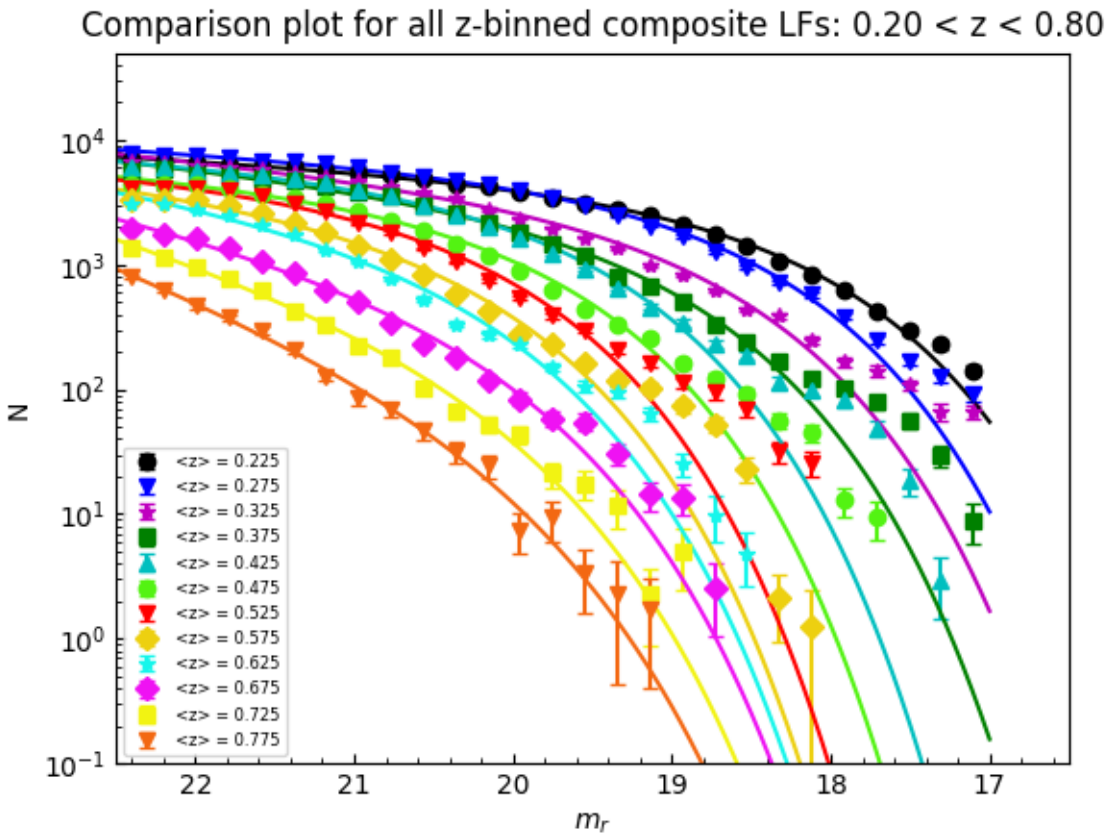

Figure 4.1.1: A comparison of all redshift-binned composite LFs, fitted with a single Schechter function. The median of each redshift bin is represented by $\langle z \rangle$.

these sources from our data. This could be checked in future work.

4.1.2 Mass-binned LFs

The results presented in Section 3.3 indicate no remarkable difference between the properties of the general LF and the LF of the mass subsets, with a $< 1\sigma$ difference between the characteristic magnitudes and faint-end slopes. This is a key result and indicates there is no dependence in α or m^* with cluster mass. We generally observed minor deviations in the mass-binned samples compared to the redshift-binned stacked LFs. While the faint-end slopes for the low-mass subsets are within $\approx 1\sigma$ of the full redshift-binned LF for $z < 0.45$, the faint-end slopes of high-mass subsets are flatter for the low redshift bins. The converse effect is true for the high redshift bins ($0.60 < z < 0.75$), where the faint-end for the high-mass subsets is much steeper than the faint-end of the low-mass subsets, except for the last redshift bin. The low-mass subsets seem to be in better agreement with the full sample LFs than the high-mass subsets. This implies that low-mass galaxy clusters tend to follow a more uniform LF trend than high-mass clusters.

We also obtained a considerably flatter faint-end slope for the high-mass subset than the slope obtained for low-mass subsets. According to previous studies (e.g., Goto et al., 2002; Muzzin et al., 2007) this implies a higher abundance of early-type galaxies (brighter galaxies) in the high-mass clusters, compared to the low-mass clusters, in our sample.

Next, we aim to compare our characteristic magnitudes with results from previous literature and track their evolution with redshift.

4.2 m^* vs z

One way to track galaxy evolution is to consider the trend in m^* values with redshift. The shape of m^* evolution with redshift is compatible with the BC03 (see Section 2.2.3) stellar population evolutionary model with a decaying ($\tau = 0.1$ Gyr) starburst at formation redshifts $z_f = 2$ and $z_f = 5$ (see figure 4.2.1). This allows us to model all types of galaxies since their

colours are easily reproduced with the $\tau = 0.1$ Gyr single burst of star formation at high-z passively evolving model. We can also compare our values to previous ones obtained from field (Montero-Dorta & Prada, 2009; Loveday et al., 2011) and cluster studies (Popesso et al., 2006; Hansen et al., 2009; Zhang et al., 2019; and Puddu et al., 2021). The evolutionary plot of m^* with redshift can be found in figure 4.2.1. We have tabulated our results and previous results in Table 4.2.1.

By visual inspection (see figure 4.2.1), our characteristic magnitudes for the general sample and mass subsets follow a tight correlation with the evolutionary tracks at $z_f = 2.0$ and $z_f = 5.0$ up to $z = 0.60$. For $z > 0.60$, our m^* values deviate from the expected evolutionary trend. For the general sample of clusters, our m^* values appear to be significantly and consistently brighter than predicted at higher redshifts ($z > 0.50$). This trend is also apparent in the high-mass subset m^*'s.

All characteristic magnitudes from the literature were converted to r-band magnitudes, by assuming the BC03 evolutionary model, for comparison (see Table 4.1.1). Comparing our characteristic magnitudes with the cluster LF study of Popesso et al. (2006) is difficult since their study only covered up to a redshift of $z = 0.10$. However, their results could provide us with clues on the behaviour of the cluster LF at low redshift. In particular, Popesso et al. (2006) obtained a very bright characteristic absolute magnitude of M^* = -21.71 $\pm$ 0.52 for late-type galaxies (LTGs) in their sample, which is a $< 1\sigma$ difference (or 0.02 mag. fainter) to our M^* value in our lowest redshift bin. Our characteristic magnitude measured at $\langle z \rangle$ = 0.375 is also in good agreement ($\approx 2\sigma$) with the m^* measured at $z = 0.40$ from the large SDSS cluster study by Hansen et al. (2009). They measured a characteristic magnitude of $m^* = 19.48$, which is only 0.08 mag. fainter than our m^* at a redshift of $\langle z \rangle = 0.375$.

Our m^* at $\langle z \rangle = 0.225$ is in good agreement ($\approx 1.8\sigma$) with the low-redshift ($z = 0.25$) m^* from the cluster study of Zhang et al. (2019). This study focused on measuring RSLFs in two redshift bins (see Section 1.5). Their higher-redshift bin m^* is also consistent with our characteristic magnitude derived at $\langle z \rangle = 0.475$, with a $\approx 1.2\sigma$ difference.

Puddu et al. (2021) followed a similar method used in our study, by measuring the r-

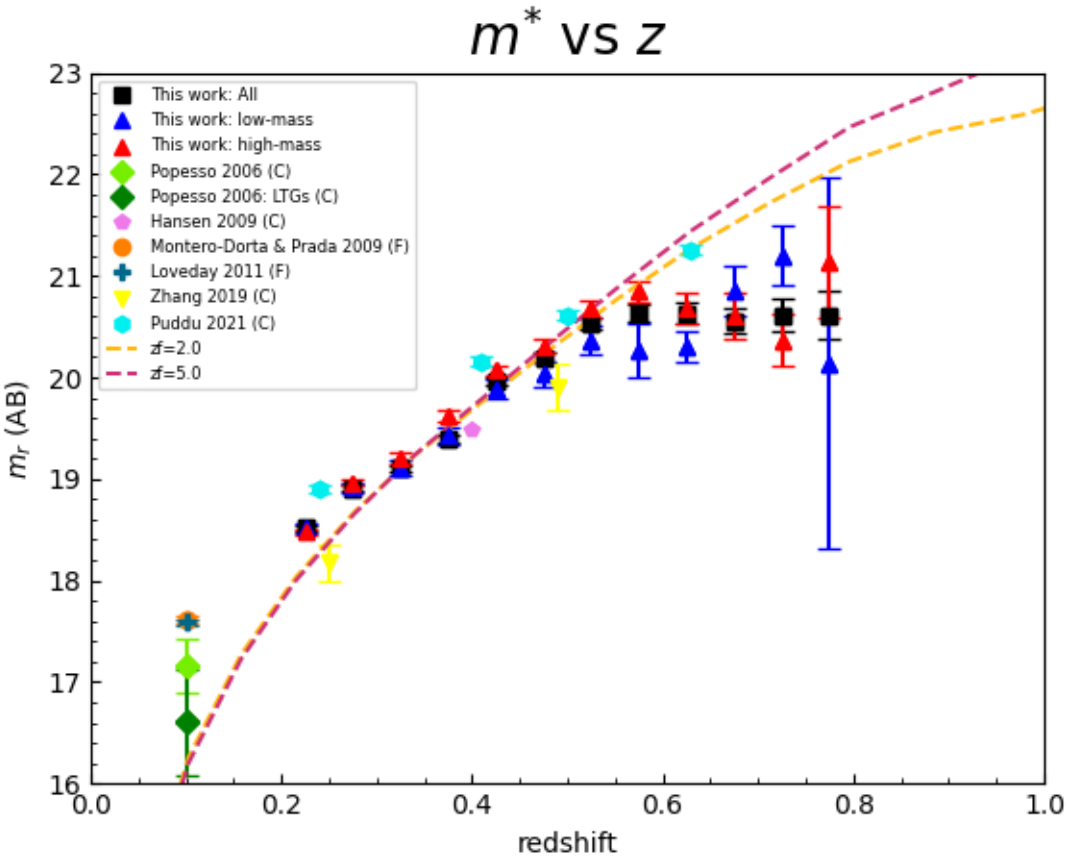

Figure 4.2.1: A plot showing the evolution of m^* with redshift (z), for our full sample of clusters (*All*), and our mass sub-samples (*low-mass* and *high-mass*) shown as black squares, and red and blue triangles respectively. A BC03 solar metallicity, $\tau = 0.1$ Gyr burst model with formation redshifts $z_f = 2$ and $z_f = 5$ are shown as orange and maroon dotted lines respectively. m^* values derived by Popesso et al. (2006), Hansen et al. (2009), Montero-Dorta & Prada (2009), Loveday et al. (2011), Zhang et al. (2019), and Puddu et al. (2021) are shown in green, magenta, orange, teal, yellow, and cyan respectively. The letter 'C' represents cluster study, while 'F' represents field study.

band LFs for $\approx$ 4000 clusters detected by the Adaptive Matched Identifier of Clustered Objects (AMICO; Bellagamba et al., 2018) algorithm and binned by redshift. AMICO is an algorithm for the detection of galaxy clusters in photometric surveys where the data set is affected by a noisy background (Giocoli et al., 2021). Our absolute characteristic magnitudes are overall brighter than the ones obtained by Puddu et al. (2021). By visual inspection (see figure 4.2.1), the m^*'s measured by Puddu et al. (2021) follow a consistent evolutionary trend with redshift. Comparing individual redshift bins, we found a correlation ($\approx 1.5\sigma$ difference) between our m^* value for redshift $\langle z \rangle = 0.525$ and their m^* value measured at $z = 0.50$.

Considering field studies such as Montero-Dorta & Prada (2009) and Loveday et al. (2011), our characteristic magnitudes m^* were much fainter to m^*'s derived in these studies. However, these values were derived for LFs centred on a redshift of $z = 0.10$. Even our lowest redshift bin, which is centred on redshift $z = 0.225$, is 0.9 mag. fainter than the m^*'s measured by Montero-Dorta & Prada (2009) and Loveday et al. (2011). The field LFs measured by Montero-Dorta & Prada (2009) and Loveday et al. (2011) are in very close agreement with each other, with a $< 1\sigma$ difference between parameters. Their apparent characteristic magnitudes show extreme deviations from our low redshift m^*'s. Our M^*'s at low-redshift are significantly brighter (≈ 1 mag.) than the M^*'s from these field studies. This is consistent with the hypothesis that the cluster LF is different from the field LF (e.g., Goto et al., 2002; De Propris et al., 2003). However, we must stress that there is a 0.125 redshift difference between the redshift used in these studies and the lowest redshift used in our study.

A full comparison to previously measured characteristic magnitudes from field and cluster studies can be made using figure 4.2.1 and Table 4.2.1. Our next step is to attempt to track the evolution of the faint-end slope with redshift and make comparisons to previous work.

LF comparison to previous studies					
Author/s	z	N_{clus}/N_{gal}	m^*	α	M^*
This work	0.225	173 (C)	18.51 ± 0.02	-1.18 ± 0.01	-21.73 ± 0.02
	0.275	225 (C)	18.91 ± 0.02	-1.18 ± 0.01	-21.83 ± 0.02
	0.325	273 (C)	19.10 ± 0.03	-1.31 ± 0.01	-22.06 ± 0.03
	0.375	272 (C)	19.40 ± 0.04	-1.33 ± 0.01	-22.13 ± 0.04
	0.425	338 (C)	19.96 ± 0.03	-1.19 ± 0.01	-21.88 ± 0.03
	0.475	294 (C)	20.19 ± 0.05	-1.21 ± 0.02	-21.94 ± 0.05
	0.525	302 (C)	20.52 ± 0.06	-1.20 ± 0.03	-21.87 ± 0.06
	0.575	262 (C)	20.63 ± 0.08	-1.33 ± 0.05	-21.99 ± 0.08
	0.625	286 (C)	20.63 ± 0.10	-1.50 ± 0.05	-22.22 ± 0.10
	0.675	227 (C)	20.56 ± 0.13	-1.72 ± 0.06	-22.49 ± 0.13
	0.725	199 (C)	20.61 ± 0.16	-1.94 ± 0.08	-22.63 ± 0.16
	0.775	157 (C)	20.62 ± 0.23	-2.19 ± 0.10	-22.80 ± 0.23
Popesso et al. (2006) - S+E	0.10	69 (C)	17.16 ± 0.26	-1.26 ± 0.12	-21.16 ± 0.26
LTGs			16.61 ± 0.52	-1.87 ± 0.04	-21.71 ± 0.52
Hansen et al. (2009)	0.40	165597 (C)	19.48	-0.28 ± 0.06	-22.21
Montero-Dorta & Prada (2009)	0.10	437565 (G)	17.61 ± 0.04	-1.26 ± 0.02	-20.71 ± 0.04
Loveday et al. (2011)	0.10	12860 (G)	17.59 ± 0.03	-1.26 ± 0.02	-20.73 ± 0.03
Zhang et al. (2019)	0.25	64 (C)	18.18 ± 0.18	-0.80 ± 0.12	-22.32 ± 0.18
	0.49	27 (C)	19.91 ± 0.23	-0.55 ± 0.18	-22.30 ± 0.23
Puddu et al. (2021)	0.24	755 (C)	18.90 ± 0.03	-1.04 ± 0.03	-21.50 ± 0.03
	0.41	1182 (C)	20.16 ± 0.04	-0.92 ± 0.05	-21.59 ± 0.04
	0.50	939 (C)	20.61 ± 0.05	-0.87 ± 0.07	-21.65 ± 0.05
	0.63	1222 (C)	21.26 ± 0.05	-0.63 ± 0.11	-21.61 ± 0.05

Table 4.2.1: A table displaying the characteristic magnitudes (m^* and M^*) and faint-end slopes (α) from this project and previous field and cluster LF studies. For the Popesso et al. (2006) study, we show both measurements for their Schechter+Exponential (S+E) fit and for Late-Type Galaxies (LTGs). The letter 'C' represents clusters and 'G' represents galaxies.

4.3 α vs z

The evolution of the faint-end of the composite cluster LF can provide key information about the abundance of faint galaxies, at different redshifts. To track this evolution with redshift, we compared our faint-end slopes for our full cluster stacked LFs and mass subsets, with slopes gathered from previous studies (see figure 4.3.1). For consistency, we use the same studies aforementioned in Section 4.2.1.

We find large uncertainties for our faint-end slopes in our high redshift bins ($z > 0.625$) - e.g., α = -2.36 $\pm$ 0.83 for low-mass composite LF at $\langle z \rangle = 0.775$. This implies that α is unconstrained at high redshift in our sample, most likely due to the depth of our photometric data from DECaLS. Past work on cluster LFs that encountered a similar issue decided to assume a value for α and fix it as a function of redshift (e.g., Muzzin et al., 2008; Mancone et al., 2010). However, fixing α has been a potential source of systematic uncertainty, as the strong coupling between M^* or m^* and α means that if α is improperly held fixed then the fitted values of m^* or M^* will also be incorrect (Mancone et al., 2012). This is important for the evolution of the characteristic magnitude because if α is evolving but assumed to be fixed then this false assumption can create spurious evolution in M^* or m^*.

The α value we measure for the full low-redshift ($\langle z \rangle = 0.225$) sample is in good agreement ($\approx 0.7\sigma$ difference) with the value retrieved from the S+E cluster sample from Popesso et al. (2006), despite their small cluster sample and lower redshift bin ($z = 0.10$). Their value obtained for LTGs is much steeper at $z = 0.10$ compared to any of our values near this redshift. We can attribute this to the mix of spectral types in our cluster samples. However, the results from Popesso et al. (2006) are a good indicator for us, in terms of the very steep faint-end slopes we encounter.

The faint-end slope of α = -0.28 $\pm$ 0.06 from Hansen et al. (2009), derived at $z = 0.40$, is considerably flatter ($\approx 15.2\sigma$ difference) compared to our slope of α = -1.19 $\pm$ 0.01 measured at redshift $\langle z \rangle = 0.425$. This flatness in α is also consistent with the cluster studies performed by Zhang et al. (2019) and Puddu et al. (2021). There is a significant difference, $\approx 3.2\sigma$ and $\approx 3.7\sigma$, between the faint-end slopes from Zhang et al. (2019) and our α's measured at $\langle z \rangle$

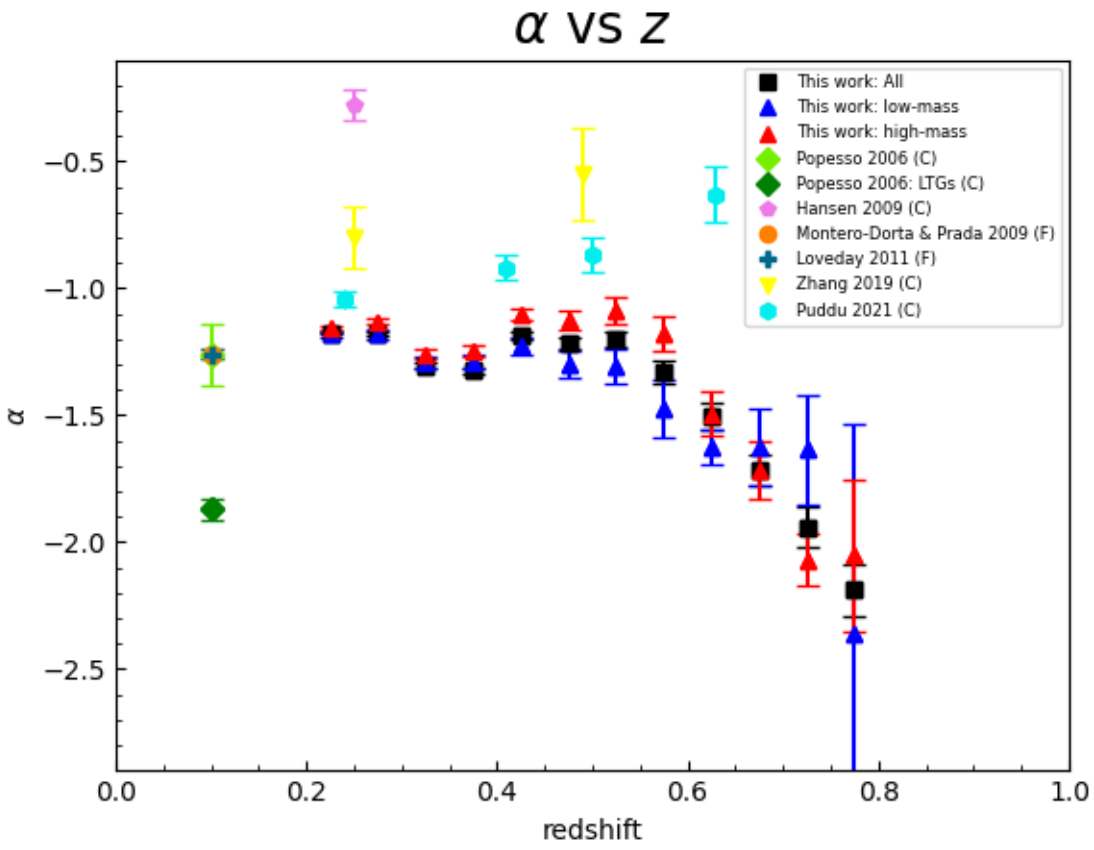

Figure 4.3.1: A plot showing the evolution of α with redshift (z), for our full sample of clusters (*All*), and our mass subsamples (*low-mass* and *high-mass*) shown as black squares, and red and blue triangles respectively. α values derived by Popesso et al. (2006), Hansen et al. (2009), Montero-Dorta & Prada (2009), Loveday et al. (2011), Zhang et al. (2019), and Puddu et al. (2021) are shown in green, magenta, orange, teal, yellow, and cyan respectively. The letter 'C' represents cluster study, while 'F' represents field study.

= 0.225 and $\langle z \rangle$ = 0.475, respectively. The flatter slopes measured by Zhang et al. (2019) can possibly be attributed to the fact that they measured RSLFs, and as we have already established, the LF of red galaxies have flatter faint-end slopes (Muzzin et al., 2007). The differences between the slopes from Puddu et al. (2021) and ours are significant and well beyond 3σ. Additionally, their α's become flatter with redshift, contrary to the trend we observe in our results. This is particularly interesting since their study covered a similar redshift interval as ours, and also consisted of a large number of clusters per bin. Both Zhang et al. (2019) and Puddu et al. (2021) applied colour cuts to their galaxy samples and considered the red and blue galaxy populations. This pattern of increasing steepness in our faint-end slopes could be attributed to the inclusion of the diversity of galaxy populations in our data sample. We have already discussed the possible explanations for our steep faint-end slopes in Section 4.1.1.

Considering our two field LF studies we included, Montero-Dorta & Prada (2009) and Loveday et al. (2011), who both obtained a faint-end slope of α = -1.26 $\pm$ 0.02 at z = 0.10. This value is $\approx 4\sigma$ steeper than our lowest redshift bin slope of -1.18 $\pm$ 0.01. This significant difference is consistent with the result that the cluster LF has a flatter faint-end slope than the field LF (see Section 1.5). This is especially noticeable for the redder passbands (i.e., r, i, and z) while the slope of the cluster LF systematically flattens from the u passband to the z band (Goto et al., 2002). However, further comparisons could be made with field studies at higher redshift.

4.4 Possible improvements

One clear call for improvement comes from our model fitting of the LFs. We used a single Schechter function to describe our stacked LFs. However, some galaxy populations and clusters cannot be constrained by just a single Schechter function. For example, the LFs of some individual merging clusters are better described by a double Schechter function (e.g., Yang et al., 2004). Some studies have also implemented a double Schechter fit (e.g., Popesso et al., 2006) to constrain the upturn of very faint counts that can exist for dwarf galaxies at

fainter magnitudes than the usual LF flat faint-end (Martinet et al., 2015). Other studies have instead fitted a Gaussian to the bright-end and a Schechter function to the faint-end (e.g., Biviano et al., 1994; Stott et al., 2007). This method accounts for the excess of very bright galaxies observed in some clusters. As mentioned in Section 4.1.1, a Gaussian function would be a useful tool to constrain the bright-end of our LFs. These methods could have been adopted in our study but would require a fainter completeness limit due to the large number of data points in our LFs.

We have already mentioned the effect of BCGs on the bright-end of the LF (see Section 4.1.1). The Gaussian-like luminosity distribution produced by these over-luminous cluster members results in a poor fit of the Schechter model to the cluster LF. Since BCGs or cD galaxies are usually found in cluster cores, the implementation of a radial cut to exclude them has been an efficient method (e.g., Hansen et al., 2009; Wen & Han, 2015). While it should be relatively simple to implement and test the effect of a radial cut, we consider it to be beyond the scope of this Master's thesis.

An evident omission from our LF study is the implementation of a colour-cut for galaxy populations. With colour-selected populations, we can analyse the variations of the galaxy types within clusters. Typically, blue and red galaxies are selected in a colour-magnitude diagram in which field galaxies have been already subtracted (Martinet et al., 2015). In this thesis, we have chosen not to classify cluster galaxies by colour or spectral type, and have instead analysed the general LF behaviour for a mixed cluster population. Perhaps the inclusion of a colour-cut could help us differentiate between the LF evolution of each population.

The results from Chapter 3 are difficult to interpret in part because the form of the luminosity function is complex and its evolution is uncertain. A simpler approach, which is based on only galaxy counts, to quantify the relative evolution of the numbers of bright and faint galaxies is to use the ratio of the number of dwarfs to giants along the red sequence - DGR (see Section 1.2). The variation of this quantity with distance from the cluster centre, density and cluster richness have been previously studied in detail (Dahlén et al., 2004; Goto

et al., 2005). The boundary between giants and dwarfs is arbitrary and is usually defined as the magnitude where the faint-end Schechter function begins to dominate over the bright-end Gaussian (Goto et al., 2005). Hence, this method is only helpful in interpreting the faint-end.

Chapter 5

Conclusion

The galaxy luminosity function (LF) is a powerful observational test for theories of galaxy formation and evolution within clusters. In our attempt to understand galaxy evolution, we presented a traditional approach (Colless, 1989) to measuring the cluster LF. In order to do this, we examined the galaxy population of 3008 SZ-selected clusters drawn from the ACT DR5 sample by measuring their composite r-band LFs from $0.20 < z < 0.80$ using optical data from DECaLS DR9. This type of study has been done previously, but not on this specific cluster sample over this chunk of cosmic time. In Chapter 2, we provided a detailed description of the data used and our LF construction method.

An overview of our method is as follows:

- Rather than presenting individual cluster LFs, we derived composite or stacked LFs which makes it more feasible to identify differences hidden by small number statistics in individual cases (De Propris et al., 2003). Due to our large redshift range, we were able to bin clusters into 12 narrow redshift bins of width 0.05 (see Table 2.2.1). We also selected mass bins within each redshift bin, selecting the top and bottom 25 % of clusters by mass (see Table 2.2.2). We implemented apparent magnitude binning, adopting a bin width of 0.2 mag. for the range: $17.0 < m_r < 24.5$. We k-corrected galaxy r-band magnitudes to the median redshift of each cluster bin, using the BC03 (Bruzual & Charlot, 2003) stellar population model.

- We chose to utilize the full galaxy $p(z)$ distributions in estimating photometric redshifts, which is more accurate. Cluster membership was assigned probabilistically, by integrating over the weighted sum of the $p(z)$ distributions between ± 0.1 in redshift around each cluster redshift. To negate completeness corrections, we adopted a brighter magnitude limit of ≈ 22.5.

- The final construction of our stacked LFs utilized a common method given by Colless (1989). This method required a richness weighting to account for the fact that richer clusters consist of more galaxies than poorer clusters and, hence, tend to dominate the composite LF. This required two steps. Firstly, using a richness-radius scaling relation (Andreon & Hurn, 2010), we selected cluster members within $R_{200\mathrm{m}}$. Secondly, we defined an absolute magnitude limit of ≈ -20 mag. by constructing a volume-limited sample using absolute magnitude distributions (see figure 2.2.4) generated from DECaLS field catalogues. Once a richness weighting was established, we stacked LFs per redshift bin and estimated errorbars using Poisson statistics.

- We fitted a single Schecter function, for α and m^*, to our LFs. The normalization parameter (ϕ^*) was fixed such that the value of the integral of the fitted function was equal to the total number of galaxies in the composite LF within the same magnitude range. m^* and α were estimated using χ^2 minimization technique. 1σ uncertainties for these parameters were measured using 1000 Monte-Carlo (MC) simulations.

Our results are presented and discussed in Chapters 3 and 4 respectively. These results indicate that a single Schechter function is a poor fit to our composite LFs, with $\chi^2_\nu > 1$ for most redshift bins (see Table 3.2.1). A logical explanation for this is that the Poisson errors are an underestimate of the true uncertainty in our data, possibly owing to the use of photometric redshifts or different k-corrections for different types of galaxies that have not been captured in our error bars. Individual χ^2 contributions (see Table 3.2.2), as well as visual inspection of our composite LFs, revealed a deviation of the bright-end from the Schechter model. We deduced that this is the Gaussian-like distribution produced by BCGs

that characterizes the bright-end (Binggeli et al., 1988; Dressler et al., 1999; Adami et al., 2000; Rakos et al., 2000). Many previous cluster LF studies have chosen to exclude these objects by adopting a radial cut.

For our total redshift binned LFs, we discovered a characteristic magnitude of $m^* = 18.51 \pm 0.02$ and faint-end slope of α = -1.18 $\pm$ 0.01 in our lowest redshift bin ($\langle z \rangle = 0.225$). We found $m^* = 20.62 \pm 0.23$ and α = -2.19 $\pm$ 0.10 in our highest redshift bin ($\langle z \rangle = 0.775$). This shows significant evidence ($> 8\sigma$) for the evolution of both α and m^* with redshift.

For the low-mass subset, we obtained best-fit parameters of (m^*, α) = (18.52 $\pm$ 0.05, -1.18 $\pm$ 0.01) at $\langle z \rangle = 0.225$, and ($m^*$, α) = (20.14 $\pm$ 1.82, -2.36 $\pm$ 0.83) at $\langle z \rangle = 0.775$. For the high-mass subset, we found best-fit parameters of (m^*, α) = (18.48 $\pm$ 0.03, -1.15 $\pm$ 0.01) at $\langle z \rangle = 0.225$, and ($m^*$, α) = (21.14 $\pm$ 0.55, -2.05 $\pm$ 0.30) at $\langle z \rangle = 0.775$. There is evidence of weak ($< 2\sigma$) evolution of α and m^* with redshift, for low-mass subsets, while high-mass subset LFs indicate strong evidence ($> 3\sigma$) for the evolution of m^* and α with redshift. Our mass-binned LFs reveal a strong correlation ($< 1\sigma$) with the total stacked LFs, with the low-mass subsets in slightly better agreement. This key result implies no dependence in α or m^* with cluster mass.

Our total stacked LFs reveal an expected trend of m^* becoming fainter with redshift, while M^* becomes brighter with redshift. We expected M^* values to become brighter with redshift due to stellar population effects. We found that the shape of our m^* evolution with redshift (see figure 4.2.1) is compatible with a BC03 (Bruzual & Charlot, 2003) stellar population model up to $\langle z \rangle = 0.60$. For $z > 0.60$, we observed significantly brighter m^*'s than predicted for formation redshifts $z_f = 2$ and $z_f = 5$.

The evolution of the faint-end slope with redshift reveals a trend in steepness (see figures 4.1.1 and 4.3.1). This steepness appears to be more significant than observed in previous literature (e.g., Puddu et al., 2021). We deduced that this steepness in α could mean we are moving into the u or g-band range since bluer passbands tend to have steeper slopes than redder bands such as the r-band (Goto et al., 2002; Muzzin et al., 2007). The combined result of brighter M^*'s and steeper α's also suggests that our sample consists largely of rich

clusters (e.g., Hansen et al., 2005).

An important result from the mass subset LFs was that we achieved considerably flatter faint-end slopes for high-mass subsets compared to low-mass subsets. The high-mass clusters are more likely to have a higher fraction of early-type galaxies, for which previous measurements show that α is flatter. The large uncertainties pointed out in α, especially in the high redshift bins of our mass subsets, implies that α was poorly constrained at high redshift ($z > 0.625$) probably due to the depth of our photometric data from DECaLS. We could have assumed a fixed value for α but this has proved to be a source of systematic uncertainty, and a false assumption could lead to spurious evolution in M^* or m^* (Mancone et al., 2012).

Comparing our work to previous cluster and field studies, we found that our LFs are in better agreement with previous cluster studies, such as Popesso et al. (2006) and Zhang et al. (2019), than field studies (see Table 3.2.1). However, our trend in faint-end steepness disagrees with the large cluster study by Puddu et al. (2021). The field LFs presented by Montero-Dorta & Prada (2009) and Loveday et al. (2011) showed large deviations in m^* and α compared to our composite cluster LFs. This is consistent with the hypothesis that cluster LF is different than the field LF, which is especially noticeable for the redder passbands (Goto et al., 2002; De Propris et al., 2003). However, further comparisons should be made with more field studies at higher redshifts.

We suggested a number of possible improvements to the analysis presented in the thesis in Section 4.4. While some of these should be fairly straightforward to implement, due to time constraints we were unable to include them in this project. They may be investigated in future work. Despite this, we still have provided valuable insight into the galaxy evolution within the ACT DR5 cluster environment. This is certainly the biggest sample of SZ-selected clusters for which the galaxy LF has been investigated to date.

Bibliography

Abazajian, K. N., Adelman-McCarthy, J. K., Agüeros, M. A., Allam, S. S., Prieto, C. A., An, D., Anderson, K. S. J., Anderson, S. F., Annis, J., Bahcall, N. A., Bailer-Jones, C. A. L., Barentine, J. C., Bassett, B. A., Becker, A. C., Beers, T. C., Bell, E. F., Belokurov, V., Berlind, A. A., Berman, E. F., Bernardi, M., Bickerton, S. J., Bizyaev, D., Blakeslee, J. P., Blanton, M. R., Bochanski, J. J., Boroski, W. N., Brewington, H. J., Brinchmann, J., Brinkmann, J., Brunner, R. J., Budavári, T., Carey, L. N., Carliles, S., Carr, M. A., Castander, F. J., Cinabro, D., Connolly, A. J., Csabai, I., Cunha, C. E., Czarapata, P. C., Davenport, J. R. A., de Haas, E., Dilday, B., Doi, M., Eisenstein, D. J., Evans, M. L., Evans, N. W., Fan, X., Friedman, S. D., Frieman, J. A., Fukugita, M., Gänsicke, B. T., Gates, E., Gillespie, B., Gilmore, G., Gonzalez, B., Gonzalez, C. F., Grebel, E. K., Gunn, J. E., György, Z., Hall, P. B., Harding, P., Harris, F. H., Harvanek, M., Hawley, S. L., Hayes, J. J. E., Heckman, T. M., Hendry, J. S., Hennessy, G. S., Hindsley, R. B., Hoblitt, J., Hogan, C. J., Hogg, D. W., Holtzman, J. A., Hyde, J. B., ichi Ichikawa, S., Ichikawa, T., Im, M., Ivezić, Ž., Jester, S., Jiang, L., Johnson, J. A., Jorgensen, A. M., Jurić, M., Kent, S. M., Kessler, R., Kleinman, S. J., Knapp, G. R., Konishi, K., Kron, R. G., Krzesinski, J., Kuropatkin, N., Lampeitl, H., Lebedeva, S., Lee, M. G., Lee, Y. S., Leger, R. F., Lépine, S., Li, N., Lima, M., Lin, H., Long, D. C., Loomis, C. P., Loveday, J., Lupton, R. H., Magnier, E., Malanushenko, O., Malanushenko, V., Mandelbaum, R., Margon, B., Marriner, J. P., Martínez-Delgado, D., Matsubara, T., McGehee, P. M., McKay, T. A., Meiksin, A., Morrison, H. L., Mullally, F., Munn, J. A., Murphy, T., Nash, T., Nebot, A., Neilsen, E. H., Newberg, H. J., Newman, P. R., Nichol, R. C., Nicinski, T.,

Nieto-Santisteban, M., Nitta, A., Okamura, S., Oravetz, D. J., Ostriker, J. P., Owen, R., Padmanabhan, N., Pan, K., Park, C., Pauls, G., Peoples, J., Percival, W. J., Pier, J. R., Pope, A. C., Pourbaix, D., Price, P. A., Purger, N., Quinn, T., Raddick, M. J., Fiorentin, P. R., Richards, G. T., Richmond, M. W., Riess, A. G., Rix, H.-W., Rockosi, C. M., Sako, M., Schlegel, D. J., Schneider, D. P., Scholz, R.-D., Schreiber, M. R., Schwope, A. D., Seljak, U., Sesar, B., Sheldon, E., Shimasaku, K., Sibley, V. C., Simmons, A. E., Sivarani, T., Smith, J. A., Smith, M. C., Smolčić, V., Snedden, S. A., Stebbins, A., Steinmetz, M., Stoughton, C., Strauss, M. A., SubbaRao, M., Suto, Y., Szalay, A. S., Szapudi, I., Szkody, P., Tanaka, M., Tegmark, M., Teodoro, L. F. A., Thakar, A. R., Tremonti, C. A., Tucker, D. L., Uomoto, A., Berk, D. E. V., Vandenberg, J., Vidrih, S., Vogeley, M. S., Voges, W., Vogt, N. P., Wadadekar, Y., Watters, S., Weinberg, D. H., West, A. A., White, S. D. M., Wilhite, B. C., Wonders, A. C., Yanny, B., Yocum, D. R., York, D. G., Zehavi, I., Zibetti, S., & Zucker, D. B. (2009). THE SEVENTH DATA RELEASE OF THE SLOAN DIGITAL SKY SURVEY. *The Astrophysical Journal Supplement Series*, 182(2), 543–558.

Abbott, B. P., Abbott, R., Abbott, T. D., Acernese, F., Ackley, K., Adams, C., Adams, T., Addesso, P., Adhikari, R. X., Adya, V. B., Affeldt, C., Afrough, M., Agarwal, B., Agathos, M., Agatsuma, K., Aggarwal, N., Aguiar, O. D., Aiello, L., Ain, A., Ajith, P., Allen, B., Allen, G., Allocca, A., Altin, P. A., Amato, A., Ananyeva, A., Anderson, S. B., Anderson, W. G., Angelova, S. V., Antier, S., Appert, S., Arai, K., Araya, M. C., Areeda, J. S., Arnaud, N., Arun, K. G., Ascenzi, S., Ashton, G., Ast, M., Aston, S. M., Astone, P., Atallah, D. V., Aufmuth, P., Aulbert, C., Aultoneal, K., Austin, C., Avila-Alvarez, A., Babak, S., Bacon, P., Bader, M. K. M., Bae, S., Baker, P. T., Baldaccini, F., Ballardin, G., Ballmer, S. W., Banagiri, S., Barayoga, J. C., Barclay, S. E., Barish, B. C., Barker, D., Barkett, K., Barone, F., Barr, B., Barsotti, L., Barsuglia, M., Barta, D., Bartlett, J., Bartos, I., Bassiri, R., Basti, A., Batch, J. C., Bawaj, M., Bayley, J. C., Bazzan, M., Bécsy, B., Beer, C., Bejger, M., Belahcene, I., Bell, A. S., Berger, B. K., Bergmann, G., Bero, J. J., Berry, C. P. L., Bersanetti, D., Bertolini, A., Betzwieser, J., Bhagwat, S., Bhandare, R., Bilenko, I. A., Billingsley, G., Billman, C. R., Birch, J., Birney, R., Birnholtz, O., Biscans,

S., Biscoveanu, S., Bisht, A., Bitossi, M., Biwer, C., Bizouard, M. A., Blackburn, J. K., Blackman, J., Blair, C. D., Blair, D. G., Blair, R. M., Bloemen, S., Bock, O., Bode, N., Boer, M., Bogaert, G., Bohe, A., Bondu, F., Bonilla, E., Bonnand, R., Boom, B. A., Bork, R., Boschi, V., Bose, S., Bossie, K., Bouffanais, Y., Bozzi, A., Bradaschia, C., Brady, P. R., Branchesi, M., Brau, J. E., Briant, T., Brillet, A., Brinkmann, M., Brisson, V., Brockill, P., Broida, J. E., Brooks, A. F., Brown, D. A., Brown, D. D., Brunett, S., Buchanan, C. C., Buikema, A., Bulik, T., Bulten, H. J., Buonanno, A., Buskulic, D., Buy, C., Byer, R. L., Cabero, M., Cadonati, L., Cagnoli, G., Cahillane, C., Bustillo, J. C., Callister, T. A., Calloni, E., Camp, J. B., Canepa, M., Canizares, P., Cannon, K. C., Cao, H., Cao, J., Capano, C. D., Capocasa, E., Carbognani, F., Caride, S., Carney, M. F., Diaz, J. C., Casentini, C., Caudill, S., Cavaglià, M., Cavalier, F., Cavalieri, R., Cella, G., Cepeda, C. B., Cerdá-Durán, P., Cerretani, G., Cesarini, E., Chamberlin, S. J., Chan, M., Chao, S., Charlton, P., Chase, E., Chassande-Mottin, E., Chatterjee, D., Chatziioannou, K., Cheeseboro, B. D., Chen, H. Y., Chen, X., Chen, Y., Cheng, H. P., Chia, H., Chincarini, A., Chiummo, A., Chmiel, T., Cho, H. S., Cho, M., Chow, J. H., Christensen, N., Chu, Q., Chua, A. J. K., Chua, S., Chung, A. K. W., Chung, S., Ciani, G., Ciolfi, R., Cirelli, C. E., Cirone, A., Clara, F., Clark, J. A., Clearwater, P., Cleva, F., Cocchieri, C., Coccia, E., Cohadon, P. F., Cohen, D., Colla, A., Collette, C. G., Cominsky, L. R., Constancio, M., Conti, L., Cooper, S. J., Corban, P., Corbitt, T. R., Cordero-Carrión, I., Corley, K. R., Cornish, N., Corsi, A., Cortese, S., Costa, C. A., Coughlin, M. W., Coughlin, S. B., Coulon, J. P., Countryman, S. T., Couvares, P., Covas, P. B., Cowan, E. E., Coward, D. M., Cowart, M. J., Coyne, D. C., Coyne, R., Creighton, J. D. E., Creighton, T. D., Cripe, J., Crowder, S. G., Cullen, T. J., Cumming, A., Cunningham, L., Cuoco, E., Dal Canton, T., Dálya, G., Danilishin, S. L., D'Antonio, S., Danzmann, K., Dasgupta, A., da Silva Costa, C. F., Datrier, L. E. H., Dattilo, V., Dave, I., Davier, M., Davis, D., Daw, E. J., Day, B., de, S., Debra, D., Degallaix, J., de Laurentis, M., Deléglise, S., Del Pozzo, W., Demos, N., Denker, T., Dent, T., de Pietri, R., Dergachev, V., De Rosa, R., Derosa, R. T., de Rossi, C., Desalvo, R., de Varona, O., Devenson, J., Dhurandhar, S., Díaz, M. C., di Fiore, L., di

Giovanni, M., di Girolamo, T., di Lieto, A., di Pace, S., di Palma, I., di Renzo, F., Doctor, Z., Dolique, V., Donovan, F., Dooley, K. L., Doravari, S., Dorrington, I., Douglas, R., Dovale Álvarez, M., Downes, T. P., Drago, M., Dreissigacker, C., Driggers, J. C., Du, Z., Ducrot, M., Dupej, P., Dwyer, S. E., Edo, T. B., Edwards, M. C., Effler, A., Eggenstein, H. B., Ehrens, P., Eichholz, J., Eikenberry, S. S., Eisenstein, R. A., Essick, R. C., Estevez, D., Etienne, Z. B., Etzel, T., Evans, M., Evans, T. M., Factourovich, M., Fafone, V., Fair, H., Fairhurst, S., Fan, X., Farinon, S., Farr, B., Farr, W. M., Fauchon-Jones, E. J., Favata, M., Fays, M., Fee, C., Fehrmann, H., Feicht, J., Fejer, M. M., Fernandez-Galiana, A., Ferrante, I., Ferreira, E. C., Ferrini, F., Fidecaro, F., Finstad, D., Fiori, I., Fiorucci, D., Fishbach, M., Fisher, R. P., Fitz-Axen, M., Flaminio, R., Fletcher, M., Fong, H., Font, J. A., Forsyth, P. W. F., Forsyth, S. S., Fournier, J. D., Frasca, S., Frasconi, F., Frei, Z., Freise, A., Frey, R., Frey, V., Fries, E. M., Fritschel, P., Frolov, V. V., Fulda, P., Fyffe, M., Gabbard, H., Gadre, B. U., Gaebel, S. M., Gair, J. R., Gammaitoni, L., Ganija, M. R., Gaonkar, S. G., Garcia-Quiros, C., Garufi, F., Gateley, B., Gaudio, S., Gaur, G., Gayathri, V., Gehrels, N., Gemme, G., Genin, E., Gennai, A., George, D., George, J., Gergely, L., Germain, V., Ghonge, S., Ghosh, A., Ghosh, A., Ghosh, S., Giaime, J. A., Giardina, K. D., Giazotto, A., Gill, K., Glover, L., Goetz, E., Goetz, R., Gomes, S., Goncharov, B., González, G., Castro, J. M. G., Gopakumar, A., Gorodetsky, M. L., Gossan, S. E., Gosselin, M., Gouaty, R., Grado, A., Graef, C., Granata, M., Grant, A., Gras, S., Gray, C., Greco, G., Green, A. C., Gretarsson, E. M., Groot, P., Grote, H., Grunewald, S., Gruning, P., Guidi, G. M., Guo, X., Gupta, A., Gupta, M. K., Gushwa, K. E., Gustafson, E. K., Gustafson, R., Halim, O., Hall, B. R., Hall, E. D., Hamilton, E. Z., Hammond, G., Haney, M., Hanke, M. M., Hanks, J., Hanna, C., Hannam, M. D., Hannuksela, O. A., Hanson, J., Hardwick, T., Harms, J., Harry, G. M., Harry, I. W., Hart, M. J., Haster, C. J., Haughian, K., Healy, J., Heidmann, A., Heintze, M. C., Heitmann, H., Hello, P., Hemming, G., Hendry, M., Heng, I. S., Hennig, J., Heptonstall, A. W., Heurs, M., Hild, S., Hinderer, T., Hoak, D., Hofman, D., Holt, K., Holz, D. E., Hopkins, P., Horst, C., Hough, J., Houston, E. A., Howell, E. J., Hreibi, A., Hu, Y. M., Huerta, E. A., Huet,

D., Hughey, B., Husa, S., Huttner, S. H., Huynh-Dinh, T., Indik, N., Inta, R., Intini, G., Isa, H. N., Isac, J. M., Isi, M., Iyer, B. R., Izumi, K., Jacqmin, T., Jani, K., Jaranowski, P., Jawahar, S., Jiménez-Forteza, F., Johnson, W. W., Jones, D. I., Jones, R., Jonker, R. J. G., Ju, L., Junker, J., Kalaghatgi, C. V., Kalogera, V., Kamai, B., Kandhasamy, S., Kang, G., Kanner, J. B., Kapadia, S. J., Karki, S., Karvinen, K. S., Kasprzack, M., Katolik, M., Katsavounidis, E., Katzman, W., Kaufer, S., Kawabe, K., Kéfélian, F., Keitel, D., Kemball, A. J., Kennedy, R., Kent, C., Key, J. S., Khalili, F. Y., Khan, I., Khan, S., Khan, Z., Khazanov, E. A., Kijbunchoo, N., Kim, C., Kim, J. C., Kim, K., Kim, W., Kim, W. S., Kim, Y. M., Kimbrell, S. J., King, E. J., King, P. J., Kinley-Hanlon, M., Kirchhoff, R., Kissel, J. S., Kleybolte, L., Klimenko, S., Knowles, T. D., Koch, P., Koehlenbeck, S. M., Koley, S., Kondrashov, V., Kontos, A., Korobko, M., Korth, W. Z., Kowalska, I., Kozak, D. B., Krämer, C., Kringel, V., Krishnan, B., Królak, A., Kuehn, G., Kumar, P., Kumar, R., Kumar, S., Kuo, L., Kutynia, A., Kwang, S., Lackey, B. D., Lai, K. H., Landry, M., Lang, R. N., Lange, J., Lantz, B., Lanza, R. K., Lartaux-Vollard, A., Lasky, P. D., Laxen, M., Lazzarini, A., Lazzaro, C., Leaci, P., Leavey, S., Lee, C. H., Lee, H. K., Lee, H. M., Lee, H. W., Lee, K., Lehmann, J., Lenon, A., Leonardi, M., Leroy, N., Letendre, N., Levin, Y., Li, T. G. F., Linker, S. D., Littenberg, T. B., Liu, J., Liu, X., Lo, R. K. L., Lockerbie, N. A., London, L. T., Lord, J. E., Lorenzini, M., Loriette, V., Lormand, M., Losurdo, G., Lough, J. D., Lousto, C. O., Lovelace, G., Lück, H., Lumaca, D., Lundgren, A. P., Lynch, R., Ma, Y., Macas, R., Macfoy, S., Machenschalk, B., Macinnis, M., MacLeod, D. M., Hernandez, I. M., Magaña-Sandoval, F., Zertuche, L. M., Magee, R. M., Majorana, E., Maksimovic, I., Man, N., Mandic, V., Mangano, V., Mansell, G. L., Manske, M., Mantovani, M., Marchesoni, F., Marion, F., Márka, S., Márka, Z., Markakis, C., Markosyan, A. S., Markowitz, A., Maros, E., Marquina, A., Martelli, F., Martellini, L., Martin, I. W., Martin, R. M., Martynov, D. V., Mason, K., Massera, E., Masserot, A., Massinger, T. J., Masso-Reid, M., Mastrogiovanni, S., Matas, A., Matichard, F., Matone, L., Mavalvala, N., Mazumder, N., McCarthy, R., McClelland, D. E., McCormick, S., McCuller, L., McGuire, S. C., McIntyre, G., McIver, J., McManus,

D. J., McNeill, L., McRae, T., McWilliams, S. T., Meacher, D., Meadors, G. D., Mehmet, M., Meidam, J., Mejuto-Villa, E., Melatos, A., Mendell, G., Mercer, R. A., Merilh, E. L., Merzougui, M., Meshkov, S., Messenger, C., Messick, C., Metzdorff, R., Meyers, P. M., Miao, H., Michel, C., Middleton, H., Mikhailov, E. E., Milano, L., Miller, A. L., Miller, B. B., Miller, J., Millhouse, M., Milovich-Goff, M. C., Minazzoli, O., Minenkov, Y., Ming, J., Mishra, C., Mitra, S., Mitrofanov, V. P., Mitselmakher, G., Mittleman, R., Moffa, D., Moggi, A., Mogushi, K., Mohan, M., Mohapatra, S. R. P., Montani, M., Moore, C. J., Moraru, D., Moreno, G., Morriss, S. R., Mours, B., Mow-Lowry, C. M., Mueller, G., Muir, A. W., Mukherjee, A., Mukherjee, D., Mukherjee, S., Mukund, N., Mullavey, A., Munch, J., Muñiz, E. A., Muratore, M., Murray, P. G., Napier, K., Nardecchia, I., Naticchioni, L., Nayak, R. K., Neilson, J., Nelemans, G., Nelson, T. J. N., Nery, M., Neunzert, A., Nevin, L., Newport, J. M., Newton, G., Ng, K. K. Y., Nguyen, T. T., Nichols, D., Nielsen, A. B., Nissanke, S., Nitz, A., Noack, A., Nocera, F., Nolting, D., North, C., Nuttall, L. K., Oberling, J., O'Dea, G. D., Ogin, G. H., Oh, J. J., Oh, S. H., Ohme, F., Okada, M. A., Oliver, M., Oppermann, P., Oram, R. J., O'Reilly, B., Ormiston, R., Ortega, L. F., O'Shaughnessy, R., Ossokine, S., Ottaway, D. J., Overmier, H., Owen, B. J., Pace, A. E., Page, J., Page, M. A., Pai, A., Pai, S. A., Palamos, J. R., Palashov, O., Palomba, C., Pal-Singh, A., Pan, H., Pan, H.-W., Pang, B., Pang, P. T. H., Pankow, C., Pannarale, F., Pant, B. C., Paoletti, F., Paoli, A., Papa, M. A., Parida, A., Parker, W., Pascucci, D., Pasqualetti, A., Passaquieti, R., Passuello, D., Patil, M., Patricelli, B., Pearlstone, B. L., Pedraza, M., Pedurand, R., Pekowsky, L., Pele, A., Penn, S., Perez, C. J., Perreca, A., Perri, L. M., Pfeiffer, H. P., Phelps, M., Piccinni, O. J., Pichot, M., Piergiovanni, F., Pierro, V., Pillant, G., Pinard, L., Pinto, I. M., Pirello, M., Pitkin, M., Poe, M., Poggiani, R., Popolizio, P., Porter, E. K., Post, A., Powell, J., Prasad, J., Pratt, J. W. W., Pratten, G., Predoi, V., Prestegard, T., Prijatelj, M., Principe, M., Privitera, S., Prodi, G. A., Prokhorov, L. G., Puncken, O., Punturo, M., Puppo, P., Pürrer, M., Qi, H., Quetschke, V., Quintero, E. A., Quitzow-James, R., Raab, F. J., Rabeling, D. S., Radkins, H., Raffai, P., Raja, S., Rajan, C., Rajbhandari, B., Rakhmanov, M., Ramirez, K. E., Ramos-Buades,

A., Rapagnani, P., Raymond, V., Razzano, M., Read, J., Regimbau, T., Rei, L., Reid, S., Reitze, D. H., Ren, W., Reyes, S. D., Ricci, F., Ricker, P. M., Rieger, S., Riles, K., Rizzo, M., Robertson, N. A., Robie, R., Robinet, F., Rocchi, A., Rolland, L., Rollins, J. G., Roma, V. J., Romano, J. D., Romano, R., Romel, C. L., Romie, J. H., Rosińska, D., Ross, M. P., Rowan, S., Rüdiger, A., Ruggi, P., Rutins, G., Ryan, K., Sachdev, S., Sadecki, T., Sadeghian, L., Sakellariadou, M., Salconi, L., Saleem, M., Salemi, F., Samajdar, A., Sammut, L., Sampson, L. M., Sanchez, E. J., Sanchez, L. E., Sanchis-Gual, N., Sandberg, V., Sanders, J. R., Sassolas, B., Sathyaprakash, B. S., Saulson, P. R., Sauter, O., Savage, R. L., Sawadsky, A., Schale, P., Scheel, M., Scheuer, J., Schmidt, J., Schmidt, P., Schnabel, R., Schofield, R. M. S., Schönbeck, A., Schreiber, E., Schuette, D., Schulte, B. W., Schutz, B. F., Schwalbe, S. G., Scott, J., Scott, S. M., Seidel, E., Sellers, D., Sengupta, A. S., Sentenac, D., Sequino, V., Sergeev, A., Shaddock, D. A., Shaffer, T. J., Shah, A. A., Shahriar, M. S., Shaner, M. B., Shao, L., Shapiro, B., Shawhan, P., Sheperd, A., Shoemaker, D. H., Shoemaker, D. M., Siellez, K., Siemens, X., Sieniawska, M., Sigg, D., Silva, A. D., Singer, L. P., Singh, A., Singhal, A., Sintes, A. M., Slagmolen, B. J. J., Smith, B., Smith, J. R., Smith, R. J. E., Somala, S., Son, E. J., Sonnenberg, J. A., Sorazu, B., Sorrentino, F., Souradeep, T., Spencer, A. P., Srivastava, A. K., Staats, K., Staley, A., Steer, D., Steinke, M., Steinlechner, J., Steinlechner, S., Steinmeyer, D., Stevenson, S. P., Stone, R., Stops, D. J., Strain, K. A., Stratta, G., Strigin, S. E., Strunk, A., Sturani, R., Stuver, A. L., Summerscales, T. Z., Sun, L., Sunil, S., Suresh, J., Sutton, P. J., Swinkels, B. L., Szczepańczyk, M. J., Tacca, M., Tait, S. C., Talbot, C., Talukder, D., Tanner, D. B., Tápai, M., Taracchini, A., Tasson, J. D., Taylor, J. A., Taylor, R., Tewari, S. V., Theeg, T., Thies, F., Thomas, E. G., Thomas, M., Thomas, P., Thorne, K. A., Thrane, E., Tiwari, S., Tiwari, V., Tokmakov, K. V., Toland, K., Tonelli, M., Tornasi, Z., Torres-Forné, A., Torrie, C. I., Töyrä, D., Travasso, F., Traylor, G., Trinastic, J., Tringali, M. C., Trozzo, L., Tsang, K. W., Tse, M., Tso, R., Tsukada, L., Tsuna, D., Tuyenbayev, D., Ueno, K., Ugolini, D., Unnikrishnan, C. S., Urban, A. L., Usman, S. A., Vahlbruch, H., Vajente, G., Valdes, G., van Bakel, N., van Beuzekom, M., van den Brand,

J. F. J., van den Broeck, C., Vander-Hyde, D. C., van der Schaaf, L., van Heijningen, J. V., van Veggel, A. A., Vardaro, M., Varma, V., Vass, S., Vasúth, M., Vecchio, A., Vedovato, G., Veitch, J., Veitch, P. J., Venkateswara, K., Venugopalan, G., Verkindt, D., Vetrano, F., Viceré, A., Viets, A. D., Vinciguerra, S., Vine, D. J., Vinet, J. Y., Vitale, S., Vo, T., Vocca, H., Vorvick, C., Vyatchanin, S. P., Wade, A. R., Wade, L. E., Wade, M., Walet, R., Walker, M., Wallace, L., Walsh, S., Wang, G., Wang, H., Wang, J. Z., Wang, W. H., Wang, Y. F., Ward, R. L., Warner, J., Was, M., Watchi, J., Weaver, B., Wei, L. W., Weinert, M., Weinstein, A. J., Weiss, R., Wen, L., Wessel, E. K., Weßels, P., Westerweck, J., Westphal, T., Wette, K., Whelan, J. T., Whitcomb, S. E., Whiting, B. F., Whittle, C., Wilken, D., Williams, D., Williams, R. D., Williamson, A. R., Willis, J. L., Willke, B., Wimmer, M. H., Winkler, W., Wipf, C. C., Wittel, H., Woan, G., Woehler, J., Wofford, J., Wong, K. W. K., Worden, J., Wright, J. L., Wu, D. S., Wysocki, D. M., Xiao, S., Yamamoto, H., Yancey, C. C., Yang, L., Yap, M. J., Yazback, M., Yu, H., Yu, H., Yvert, M., Zadrożny, A., Zanolin, M., Zelenova, T., Zendri, J. P., Zevin, M., Zhang, L., Zhang, M., Zhang, T., Zhang, Y. H., Zhao, C., Zhou, M., Zhou, Z., Zhu, S. J., Zhu, X. J., Zimmerman, A. B., Zucker, M. E., Zweizig, J., Foley, R. J., Coulter, D. A., Drout, M. R., Kasen, D., Kilpatrick, C. D., Madore, B. F., Murguia-Berthier, A., Pan, Y. C., Piro, A. L., Prochaska, J. X., Ramirez-Ruiz, E., Rest, A., Rojas-Bravo, C., Shappee, B. J., Siebert, M. R., Simon, J. D., Ulloa, N., Annis, J., Soares-Santos, M., Brout, D., Scolnic, D., Diehl, H. T., Frieman, J., Berger, E., Alexander, K. D., Allam, S., Balbinot, E., Blanchard, P., Butler, R. E., Chornock, R., Cook, E. R., Cowperthwaite, P., Drlica-Wagner, A., Drout, M. R., Durret, F., Eftekhari, T., Finley, D. A., Fong, W., Fryer, C. L., García-Bellido, J., Gill, M. S. S., Gruendl, R. A., Hanna, C., Hartley, W., Herner, K., Huterer, D., Kasen, D., Kessler, R., Li, T. S., Lin, H., Lopes, P. A. A., Lourenço, A. C. C., Margutti, R., Marriner, J., Marshall, J. L., Matheson, T., Medina, G. E., Metzger, B. D., Muñoz, R. R., Muir, J., Nicholl, M., Nugent, P., Palmese, A., Paz-Chinchón, F., Quataert, E., Sako, M., Sauseda, M., Schlegel, D. J., Secco, L. F., Smith, N., Sobreira, F., Stebbins, A., Villar, V. A., Vivas, A. K., Wester, W., Williams, P. K. G., Yanny, B., Zenteno, A.,

Abbott, T. M. C., Abdalla, F. B., Bechtol, K., Benoit-Lévy, A., Bertin, E., Bridle, S. L., Brooks, D., Buckley-Geer, E., Burke, D. L., Rosell, A. C., Kind, M. C., Carretero, J., Castander, F. J., Cunha, C. E., D'Andrea, C. B., da Costa, L. N., Davis, C., Depoy, D. L., Desai, S., Dietrich, J. P., Estrada, J., Fernandez, E., Flaugher, B., Fosalba, P., Gaztanaga, E., Gerdes, D. W., Giannantonio, T., Goldstein, D. A., Gruen, D., Gutierrez, G., Hartley, W. G., Honscheid, K., Jain, B., James, D. J., Jeltema, T., Johnson, M. W. G., Kent, S., Krause, E., Kron, R., Kuehn, K., Kuhlmann, S., Kuropatkin, N., Lahav, O., Lima, M., Maia, M. A. G., March, M., Miller, C. J., Miquel, R., Neilsen, E., Nord, B., Ogando, R. L. C., Plazas, A. A., Romer, A. K., Roodman, A., Rykoff, E. S., Sanchez, E., Scarpine, V., Schubnell, M., Sevilla-Noarbe, I., Smith, M., Smith, R. C., Suchyta, E., Tarle, G., Thomas, D., Thomas, R. C., Troxel, M. A., Tucker, D. L., Vikram, V., Walker, A. R., Weller, J., Zhang, Y., Haislip, J. B., Kouprianov, V. V., Reichart, D. E., Tartaglia, L., Sand, D. J., Valenti, S., Yang, S., Arcavi, I., Hosseinzadeh, G., Howell, D. A., McCully, C., Poznanski, D., Vasylyev, S., Tanvir, N. R., Levan, A. J., Hjorth, J., Cano, Z., Copperwheat, C., de Ugarte-Postigo, A., Evans, P. A., Fynbo, J. P. U., González-Fernández, C., Greiner, J., Irwin, M., Lyman, J., Mandel, I., McMahon, R., Milvang-Jensen, B., O'Brien, P., Osborne, J. P., Perley, D. A., Pian, E., Palazzi, E., Rol, E., Rosetti, S., Rosswog, S., Rowlinson, A., Schulze, S., Steeghs, D. T. H., Thöne, C. C., Ulaczyk, K., Watson, D., Wiersema, K., Lipunov, V. M., Gorbovskoy, E., Kornilov, V. G., Tyurina, N., Balanutsa, P., Vlasenko, D., Gorbunov, I., Podesta, R., Levato, H., Saffe, C., Buckley, D. A. H., Budnev, N. M., Gress, O., Yurkov, V., Rebolo, R., & Serra-Ricart, M. (2017). A gravitational-wave standard siren measurement of the Hubble constant. *Nature*, 551(7678), 85–88.

Abbott, T. M. C., Adamó w, M., Aguena, M., Allam, S., Amon, A., Annis, J., Avila, S., Bacon, D., Banerji, M., Bechtol, K., Becker, M. R., Bernstein, G. M., Bertin, E., Bhargava, S., Bridle, S. L., Brooks, D., Burke, D. L., Rosell, A. C., Kind, M. C., Carretero, J., Castander, F. J., Cawthon, R., Chang, C., Choi, A., Conselice, C., Costanzi, M., Crocce, M., da Costa, L. N., Davis, T. M., Vicente, J. D., DeRose, J., Desai, S., Diehl, H. T.,

Dietrich, J. P., Drlica-Wagner, A., Eckert, K., Elvin-Poole, J., Everett, S., Evrard, A. E., Ferrero, I., Ferté, A., Flaugher, B., Fosalba, P., Friedel, D., Frieman, J., García-Bellido, J., Gaztanaga, E., Gelman, L., Gerdes, D. W., Giannantonio, T., Gill, M. S. S., Gruen, D., Gruendl, R. A., Gschwend, J., Gutierrez, G., Hartley, W. G., Hinton, S. R., Hollowood, D. L., Honscheid, K., Huterer, D., James, D. J., Jeltema, T., Johnson, M. D., Kent, S., Kron, R., Kuehn, K., Kuropatkin, N., Lahav, O., Li, T. S., Lidman, C., Lin, H., MacCrann, N., Maia, M. A. G., Manning, T. A., Maloney, J. D., March, M., Marshall, J. L., Martini, P., Melchior, P., Menanteau, F., Miquel, R., Morgan, R., Myles, J., Neilsen, E., Ogando, R. L. C., Palmese, A., Paz-Chinchón, F., Petravick, D., Pieres, A., Plazas, A. A., Pond, C., Rodriguez-Monroy, M., Romer, A. K., Roodman, A., Rykoff, E. S., Sako, M., Sanchez, E., Santiago, B., Scarpine, V., Serrano, S., Sevilla-Noarbe, I., Smith, J. A., Smith, M., Soares-Santos, M., Suchyta, E., Swanson, M. E. C., Tarle, G., Thomas, D., To, C., Tremblay, P. E., Troxel, M. A., Tucker, D. L., Turner, D. J., Varga, T. N., Walker, A. R., Wechsler, R. H., Weller, J., Wester, W., Wilkinson, R. D., Yanny, B., Zhang, Y., Nikutta, R., Fitzpatrick, M., Jacques, A., Scott, A., Olsen, K., Huang, L., Herrera, D., Juneau, S., Nidever, D., Weaver, B. A., Adean, C., Correia, V., de Freitas, M., Freitas, F. N., Singulani, C., & Vila-Verde, G. (2021). The Dark Energy Survey Data Release 2. *The Astrophysical Journal Supplement Series*, 255(2), 20.

Abdurro'uf, Accetta, K., Aerts, C., Aguirre, V. S., Ahumada, R., Ajgaonkar, N., Ak, N. F., Alam, S., Prieto, C. A., Almeida, A., Anders, F., Anderson, S. F., Andrews, B. H., Anguiano, B., Aquino-Ortíz, E., Aragón-Salamanca, A., Argudo-Fernández, M., Ata, M., Aubert, M., Avila-Reese, V., Badenes, C., Barbá, R. H., Barger, K., Barrera-Ballesteros, J. K., Beaton, R. L., Beers, T. C., Belfiore, F., Bender, C. F., Bernardi, M., Bershady, M. A., Beutler, F., Bidin, C. M., Bird, J. C., Bizyaev, D., Blanc, G. A., Blanton, M. R., Boardman, N. F., Bolton, A. S., Boquien, M., Borissova, J., Bovy, J., Brandt, W. N., Brown, J., Brownstein, J. R., Brusa, M., Buchner, J., Bundy, K., Burchett, J. N., Bureau, M., Burgasser, A., Cabang, T. K., Campbell, S., Cappellari, M., Carlberg, J. K., Wanderley, F. C., Carrera, R., Cash, J., Chen, Y.-P., Chen, W.-H., Cherinka, B., Chiappini,

C., Choi, P. D., Chojnowski, S. D., Chung, H., Clerc, N., Cohen, R. E., Comerford, J. M., Comparat, J., da Costa, L., Covey, K., Crane, J. D., Cruz-Gonzalez, I., Culhane, C., Cunha, K., Dai, Y. S., Damke, G., Darling, J., Jr., J. W. D., Davies, R., Dawson, K., Lee, N. D., Diamond-Stanic, A. M., Cano-Díaz, M., Sánchez, H. D., Donor, J., Duckworth, C., Dwelly, T., Eisenstein, D. J., Elsworth, Y. P., Emsellem, E., Eracleous, M., Escoffier, S., Fan, X., Farr, E., Feng, S., Fernández-Trincado, J. G., Feuillet, D., Filipp, A., Fillingham, S. P., Frinchaboy, P. M., Fromenteau, S., Galbany, L., García, R. A., García-Hernández, D. A., Ge, J., Geisler, D., Gelfand, J., Géron, T., Gibson, B. J., Goddy, J., Godoy-Rivera, D., Grabowski, K., Green, P. J., Greener, M., Grier, C. J., Griffith, E., Guo, H., Guy, J., Hadjara, M., Harding, P., Hasselquist, S., Hayes, C. R., Hearty, F., Hernández, J., Hill, L., Hogg, D. W., Holtzman, J. A., Horta, D., Hsieh, B.-C., Hsu, C.-H., Hsu, Y.-H., Huber, D., Huertas-Company, M., Hutchinson, B., Hwang, H. S., Ibarra-Medel, H. J., Chitham, J. I., Ilha, G. S., Imig, J., Jaekle, W., Jayasinghe, T., Ji, X., Johnson, J. A., Jones, A., Jönsson, H., Katkov, I., Khalatyan, D. A., Kinemuchi, K., Kisku, S., Knapen, J. H., Kneib, J.-P., Kollmeier, J. A., Kong, M., Kounkel, M., Kreckel, K., Krishnarao, D., Lacerna, I., Lane, R. R., Langgin, R., Lavender, R., Law, D. R., Lazarz, D., Leung, H. W., Leung, H.-H., Lewis, H. M., Li, C., Li, R., Lian, J., Liang, F.-H., Lin, L., Lin, Y.-T., Lin, S., Lintott, C., Long, D., Longa-Peña, P., López-Cobá, C., Lu, S., Lundgren, B. F., Luo, Y., Mackereth, J. T., de la Macorra, A., Mahadevan, S., Majewski, S. R., Manchado, A., Mandeville, T., Maraston, C., Margalef-Bentabol, B., Masseron, T., Masters, K. L., Mathur, S., McDermid, R. M., Mckay, M., Merloni, A., Merrifield, M., Meszaros, S., Miglio, A., Mille, F. D., Minniti, D., Minsley, R., Monachesi, A., Moon, J., Mosser, B., Mulchaey, J., Muna, D., Muñoz, R. R., Myers, A. D., Myers, N., Nadathur, S., Nair, P., Nandra, K., Neumann, J., Newman, J. A., Nidever, D. L., Nikakhtar, F., Nitschelm, C., O'Connell, J. E., Garma-Oehmichen, L., de Oliveira, G. L. S., Olney, R., Oravetz, D., Ortigoza-Urdaneta, M., Osorio, Y., Otter, J., Pace, Z. J., Padilla, N., Pan, K., Pan, H.-A., Parikh, T., Parker, J., Peirani, S., Ramírez, K. P., Penny, S., Percival, W. J., Perez-Fournon, I., Pinsonneault, M., Poidevin, F., Poovelil, V. J., Price-Whelan, A. M.,

de Andrade Queiroz, A. B., Raddick, M. J., Ray, A., Rembold, S. B., Riddle, N., Riffel, R. A., Riffel, R., Rix, H.-W., Robin, A. C., Rodríguez-Puebla, A., Roman-Lopes, A., Román-Zúñiga, C., Rose, B., Ross, A. J., Rossi, G., Rubin, K. H. R., Salvato, M., Sánchez, S. F., Sánchez-Gallego, J. R., Sanderson, R., Rojas, F. A. S., Sarceno, E., Sarmiento, R., Sayres, C., Sazonova, E., Schaefer, A. L., Schiavon, R., Schlegel, D. J., Schneider, D. P., Schultheis, M., Schwope, A., Serenelli, A., Serna, J., Shao, Z., Shapiro, G., Sharma, A., Shen, Y., Shetrone, M., Shu, Y., Simon, J. D., Skrutskie, M. F., Smethurst, R., Smith, V., Sobeck, J., Spoo, T., Sprague, D., Stark, D. V., Stassun, K. G., Steinmetz, M., Stello, D., Stone-Martinez, A., Storchi-Bergmann, T., Stringfellow, G. S., Stutz, A., Su, Y.-C., Taghizadeh-Popp, M., Talbot, M. S., Tayar, J., Telles, E., Teske, J., Thakar, A., Theissen, C., Tkachenko, A., Thomas, D., Tojeiro, R., Toledo, H. H., Troup, N. W., Trump, J. R., Trussler, J., Turner, J., Tuttle, S., Unda-Sanzana, E., Vázquez-Mata, J. A., Valentini, M., Valenzuela, O., Vargas-González, J., Vargas-Magaña, M., Alfaro, P. V., Villanova, S., Vincenzo, F., Wake, D., Warfield, J. T., Washington, J. D., Weaver, B. A., Weijmans, A.-M., Weinberg, D. H., Weiss, A., Westfall, K. B., Wild, V., Wilde, M. C., Wilson, J. C., Wilson, R. F., Wilson, M., Wolf, J., Wood-Vasey, W. M., Yan, R., Zamora, O., Zasowski, G., Zhang, K., Zhao, C., Zheng, Z., Zheng, Z., & Zhu, K. (2022). The Seventeenth Data Release of the Sloan Digital Sky Surveys: Complete Release of MaNGA, MaStar, and APOGEE-2 Data. *The Astrophysical Journal Supplement Series*, 259(2), 35.

Abell, G. O. (1958). The Distribution of Rich Clusters of Galaxies. *Astrophysical Journal Supplement*, 3, 211.

Adami, C., Ulmer, M. P., Romer, A. K., Nichol, R. C., Holden, B. P., & Pildis, R. A. (2000). The Bright SHARC Survey: The Selection Function and Its Impact on the Cluster X-Ray Luminosity Function. *The Astrophysical Journal Supplement Series*, 131(2), 391.

Aguerri, J. A. L., Méndez-Abreu, J., & Corsini, E. M. (2009). The population of barred galaxies in the local universe. I. Detection and characterisation of bars. *Astronomy & Astrophysics*, 495(2), 491–504.

Agulli, I., Aguerri, J. A. L., Sánchez-Janssen, R., Barrena, R., Diaferio, A., Serra, A. L., & Méndez-Abreu, J. (2014). Deep spectroscopic luminosity function of Abell 85: no evidence for a steep upturn of the faint-end slope. *Monthly Notices of the Royal Astronomical Society: Letters*, 444(1), L34–L38.

Aihara, H., Arimoto, N., Armstrong, R., Arnouts, S., Bahcall, N. A., Bickerton, S., Bosch, J., Bundy, K., Capak, P. L., Chan, J. H. H., Chiba, M., Coupon, J., Egami, E., Enoki, M., Finet, F., Fujimori, H., Fujimoto, S., Furusawa, H., Furusawa, J., Goto, T., Goulding, A., Greco, J. P., Greene, J. E., Gunn, J. E., Hamana, T., Harikane, Y., Hashimoto, Y., Hattori, T., Hayashi, M., Hayashi, Y., Hełminiak, K. G., Higuchi, R., Hikage, C., Ho, P. T. P., Hsieh, B.-C., Huang, K., Huang, S., Ikeda, H., Imanishi, M., Inoue, A. K., Iwasawa, K., Iwata, I., Jaelani, A. T., Jian, H.-Y., Kamata, Y., Karoji, H., Kashikawa, N., Katayama, N., Kawanomoto, S., Kayo, I., Koda, J., Koike, M., Kojima, T., Komiyama, Y., Konno, A., Koshida, S., Koyama, Y., Kusakabe, H., Leauthaud, A., Lee, C.-H., Lin, L., Lin, Y.-T., Lupton, R. H., Mandelbaum, R., Matsuoka, Y., Medezinski, E., Mineo, S., Miyama, S., Miyatake, H., Miyazaki, S., Momose, R., More, A., More, S., Moritani, Y., Moriya, T. J., Morokuma, T., Mukae, S., Murata, R., Murayama, H., Nagao, T., Nakata, F., Niida, M., Niikura, H., Nishizawa, A. J., Obuchi, Y., Oguri, M., Oishi, Y., Okabe, N., Okamoto, S., Okura, Y., Ono, Y., Onodera, M., Onoue, M., Osato, K., Ouchi, M., Price, P. A., Pyo, T.-S., Sako, M., Sawicki, M., Shibuya, T., Shimasaku, K., Shimono, A., Shirasaki, M., Silverman, J. D., Simet, M., Speagle, J., Spergel, D. N., Strauss, M. A., Sugahara, Y., Sugiyama, N., Suto, Y., Suyu, S. H., Suzuki, N., Tait, P. J., Takada, M., Takata, T., Tamura, N., Tanaka, M. M., Tanaka, M., Tanaka, M., Tanaka, Y., Terai, T., Terashima, Y., Toba, Y., Tominaga, N., Toshikawa, J., Turner, E. L., Uchida, T., Uchiyama, H., Umetsu, K., Uraguchi, F., Urata, Y., Usuda, T., Utsumi, Y., Wang, S.-Y., Wang, W.-H., Wong, K. C., Yabe, K., Yamada, Y., Yamanoi, H., Yasuda, N., Yeh, S., Yonehara, A., & Yuma, S. (2017). The Hyper Suprime-Cam SSP Survey: Overview and survey design. *Publications of the Astronomical Society of Japan*, 70(SP1). S4.

Aiola, S., Calabrese, E., Maurin, L., Naess, S., Schmitt, B. L., Abitbol, M. H., Addison,

G. E., Ade, P. A. R., Alonso, D., Amiri, M., Amodeo, S., Angile, E., Austermann, J. E., Baildon, T., Battaglia, N., Beall, J. A., Bean, R., Becker, D. T., Bond, J. R., Bruno, S. M., Calafut, V., Campusano, L. E., Carrero, F., Chesmore, G. E., Cho, H.-m., Choi, S. K., Clark, S. E., Cothard, N. F., Crichton, D., Crowley, K. T., Darwish, O., Datta, R., Denison, E. V., Devlin, M. J., Duell, C. J., Duff, S. M., Duivenvoorden, A. J., Dunkley, J., Dünner, R., Essinger-Hileman, T., Fankhanel, M., Ferraro, S., Fox, A. E., Fuzia, B., Gallardo, P. A., Gluscevic, V., Golec, J. E., Grace, E., Gralla, M., Guan, Y., Hall, K., Halpern, M., Han, D., Hargrave, P., Hasselfield, M., Helton, J. M., Henderson, S., Hensley, B., Hill, J. C., Hilton, G. C., Hilton, M., Hincks, A. D., Hložek, R., Ho, S.-P. P., Hubmayr, J., Huffenberger, K. M., Hughes, J. P., Infante, L., Irwin, K., Jackson, R., Klein, J., Knowles, K., Koopman, B., Kosowsky, A., Lakey, V., Li, D., Li, Y., Li, Z., Lokken, M., Louis, T., Lungu, M., MacInnis, A., Madhavacheril, M., Maldonado, F., Mallaby-Kay, M., Marsden, D., McMahon, J., Menanteau, F., Moodley, K., Morton, T., Namikawa, T., Nati, F., Newburgh, L., Nibarger, J. P., Nicola, A., Niemack, M. D., Nolta, M. R., Orlowski-Sherer, J., Page, L. A., Pappas, C. G., Partridge, B., Phakathi, P., Pisano, G., Prince, H., Puddu, R., Qu, F. J., Rivera, J., Robertson, N., Rojas, F., Salatino, M., Schaan, E., Schillaci, A., Sehgal, N., Sherwin, B. D., Sierra, C., Sievers, J., Sifon, C., Sikhosana, P., Simon, S., Spergel, D. N., Staggs, S. T., Stevens, J., Storer, E., Sunder, D. D., Switzer, E. R., Thorne, B., Thornton, R., Trac, H., Treu, J., Tucker, C., Vale, L. R., Van Engelen, A., Van Lanen, J., Vavagiakis, E. M., Wagoner, K., Wang, Y., Ward, J. T., Wollack, E. J., Xu, Z., Zago, F., & Zhu, N. (2020). The Atacama Cosmology Telescope: DR4 maps and cosmological parameters. *Journal of Cosmology and Astroparticle Physics*, 2020(12), 047.

Alam, S., Albareti, F. D., Prieto, C. A., Anders, F., Anderson, S. F., Anderton, T., Andrews, B. H., Armengaud, E., Aubourg, É., Bailey, S., Basu, S., Bautista, J. E., Beaton, R. L., Beers, T. C., Bender, C. F., Berlind, A. A., Beutler, F., Bhardwaj, V., Bird, J. C., Bizyaev, D., Blake, C. H., Blanton, M. R., Blomqvist, M., Bochanski, J. J., Bolton, A. S., Bovy, J., Bradley, A. S., Brandt, W. N., Brauer, D. E., Brinkmann, J., Brown, P. J., Brownstein,

J. R., Burden, A., Burtin, E., Busca, N. G., Cai, Z., Capozzi, D., Rosell, A. C., Carr, M. A., Carrera, R., Chambers, K. C., Chaplin, W. J., Chen, Y.-C., Chiappini, C., Chojnowski, S. D., Chuang, C.-H., Clerc, N., Comparat, J., Covey, K., Croft, R. A. C., Cuesta, A. J., Cunha, K., da Costa, L. N., Rio, N. D., Davenport, J. R. A., Dawson, K. S., Lee, N. D., Delubac, T., Deshpande, R., Dhital, S., Dutra-Ferreira, L., Dwelly, T., Ealet, A., Ebelke, G. L., Edmondson, E. M., Eisenstein, D. J., Ellsworth, T., Elsworth, Y., Epstein, C. R., Eracleous, M., Escoffier, S., Esposito, M., Evans, M. L., Fan, X., Fernández-Alvar, E., Feuillet, D., Ak, N. F., Finley, H., Finoguenov, A., Flaherty, K., Fleming, S. W., Font-Ribera, A., Foster, J., Frinchaboy, P. M., Galbraith-Frew, J. G., García, R. A., García-Hernández, D. A., Pérez, A. E. G., Gaulme, P., Ge, J., Génova-Santos, R., Georgakakis, A., Ghezzi, L., Gillespie, B. A., Girardi, L., Goddard, D., Gontcho, S. G. A., Hernández, J. I. G., Grebel, E. K., Green, P. J., Grieb, J. N., Grieves, N., Gunn, J. E., Guo, H., Harding, P., Hasselquist, S., Hawley, S. L., Hayden, M., Hearty, F. R., Hekker, S., Ho, S., Hogg, D. W., Holley-Bockelmann, K., Holtzman, J. A., Honscheid, K., Huber, D., Huehnerhoff, J., Ivans, I. I., Jiang, L., Johnson, J. A., Kinemuchi, K., Kirkby, D., Kitaura, F., Klaene, M. A., Knapp, G. R., Kneib, J.-P., Koenig, X. P., Lam, C. R., Lan, T.-W., Lang, D., Laurent, P., Goff, J.-M. L., Leauthaud, A., Lee, K.-G., Lee, Y. S., Licquia, T. C., Liu, J., Long, D. C., López-Corredoira, M., Lorenzo-Oliveira, D., Lucatello, S., Lundgren, B., Lupton, R. H., III, C. E. M., Mahadevan, S., Maia, M. A. G., Majewski, S. R., Malanushenko, E., Malanushenko, V., Manchado, A., Manera, M., Mao, Q., Maraston, C., Marchwinski, R. C., Margala, D., Martell, S. L., Martig, M., Masters, K. L., Mathur, S., McBride, C. K., McGehee, P. M., McGreer, I. D., McMahon, R. G., Ménard, B., Menzel, M.-L., Merloni, A., Mészáros, S., Miller, A. A., Miralda-Escudé, J., Miyatake, H., Montero-Dorta, A. D., More, S., Morganson, E., Morice-Atkinson, X., Morrison, H. L., Mosser, B., Muna, D., Myers, A. D., Nandra, K., Newman, J. A., Neyrinck, M., Nguyen, D. C., Nichol, R. C., Nidever, D. L., Noterdaeme, P., Nuza, S. E., O'Connell, J. E., O'Connell, R. W., O'Connell, R., Ogando, R. L. C., Olmstead, M. D., Oravetz, A. E., Oravetz, D. J., Osumi, K., Owen, R., Padgett, D. L., Padmanabhan, N., Paegert, M.,

Palanque-Delabrouille, N., Pan, K., Parejko, J. K., Pâris, I., Park, C., Pattarakijwanich, P., Pellejero-Ibanez, M., Pepper, J., Percival, W. J., Pérez-Fournon, I., Pe´rez-Ra`fols, I., Petitjean, P., Pieri, M. M., Pinsonneault, M. H., de Mello, G. F. P., Prada, F., Prakash, A., Price-Whelan, A. M., Protopapas, P., Raddick, M. J., Rahman, M., Reid, B. A., Rich, J., Rix, H.-W., Robin, A. C., Rockosi, C. M., Rodrigues, T. S., Rodríguez-Torres, S., Roe, N. A., Ross, A. J., Ross, N. P., Rossi, G., Ruan, J. J., Rubiño-Martín, J. A., Rykoff, E. S., Salazar-Albornoz, S., Salvato, M., Samushia, L., Sánchez, A. G., Santiago, B., Sayres, C., Schiavon, R. P., Schlegel, D. J., Schmidt, S. J., Schneider, D. P., Schultheis, M., Schwope, A. D., Scóccola, C. G., Scott, C., Sellgren, K., Seo, H.-J., Serenelli, A., Shane, N., Shen, Y., Shetrone, M., Shu, Y., Aguirre, V. S., Sivarani, T., Skrutskie, M. F., Slosar, A., Smith, V. V., Sobreira, F., Souto, D., Stassun, K. G., Steinmetz, M., Stello, D., Strauss, M. A., Streblyanska, A., Suzuki, N., Swanson, M. E. C., Tan, J. C., Tayar, J., Terrien, R. C., Thakar, A. R., Thomas, D., Thomas, N., Thompson, B. A., Tinker, J. L., Tojeiro, R., Troup, N. W., Vargas-Magaña, M., Vazquez, J. A., Verde, L., Viel, M., Vogt, N. P., Wake, D. A., Wang, J., Weaver, B. A., Weinberg, D. H., Weiner, B. J., White, M., Wilson, J. C., Wisniewski, J. P., Wood-Vasey, W. M., Ye`che, C., York, D. G., Zakamska, N. L., Zamora, O., Zasowski, G., Zehavi, I., Zhao, G.-B., Zheng, Z., (), X. Z., (), Z. Z., (), H. Z., & Zhu, G. (2015). THE ELEVENTH AND TWELFTH DATA RELEASES OF THE SLOAN DIGITAL SKY SURVEY: FINAL DATA FROM SDSS-III. *The Astrophysical Journal Supplement Series*, 219(1), 12.

Alam, S., Ho, S., & Silvestri, A. (2016). Testing deviations from ΛCDM with growth rate measurements from six large-scale structure surveys at z = 0.06–1. *Monthly Notices of the Royal Astronomical Society*, 456(4), 3743–3756.

Alpher, R. A. & Herman, R. C. (1948). On the Relative Abundance of the Elements. *Phys. Rev.*, 74, 1737–1742.

Anderson, R. (2015). *The Cosmic Compendium: The Big Bang & the Early Universe*. Lulu Enterprises Incorporated.

Andrae, R., Schulze-Hartung, T., & Melchior, P. (2010). Dos and don'ts of reduced chi-squared. *arXiv preprint arXiv:1012.3754*.

Andreon, S. & Hurn, M. A. (2010). The scaling relation between richness and mass of galaxy clusters: a Bayesian approach. *Monthly Notices of the Royal Astronomical Society*, 404(4), 1922–1937.

Arnaud, M., Pratt, G. W., Piffaretti, R., Böhringer, H., Croston, J. H., & Pointecouteau, E. (2010). The universal galaxy cluster pressure profile from a representative sample of nearby systems (REXCESS) and the Y_{SZ} - M_{500} relation. *Astronomy & Astrophysics*, 517, A92.

Astier, P., Guy, J., Regnault, N., Pain, R., Aubourg, E., Balam, D., Basa, S., Carlberg, R. G., Fabbro, S., Fouchez, D., Hook, I. M., Howell, D. A., Lafoux, H., Neill, J. D., Palanque-Delabrouille, N., Perrett, K., Pritchet, C. J., Rich, J., Sullivan, M., Taillet, R., Aldering, G., Antilogus, P., Arsenijevic, V., Balland, C., Baumont, S., Bronder, J., Courtois, H., Ellis, R. S., Filiol, M., Gonçalves, A. C., Goobar, A., Guide, D., Hardin, D., Lusset, V., Lidman, C., McMahon, R., Mouchet, M., Mourao, A., Perlmutter, S., Ripoche, P., Tao, C., & Walton, N. (2006). The Supernova Legacy Survey: measurement of Ω_M, Ω_Λ and w from the first year data set. *Astronomy & Astrophysics*, 447(1), 31–48.

Babyk, I., Melnyk, O., & Elyiv, A. (2012). The distribution of dark matter and intracluster gas in galaxy clusters. *Advances in Astronomy and Space Physics*, 2, 56–59.

Bahcall, N. A. (1977). Clusters of Galaxies. *Annual Review of Astronomy and Astrophysics*, 15(1), 505–540.

Bahé , Y. M., McCarthy, I. G., Balogh, M. L., & Font, A. S. (2013). Why does the environmental influence on group and cluster galaxies extend beyond the virial radius? *Monthly Notices of the Royal Astronomical Society*, 430(4), 3017–3031.

Bahé, Y. M., McCarthy, I. G., Crain, R. A., & Theuns, T. (2012). The competition between

confinement and ram pressure and its implications for galaxies in groups and clusters. *Monthly Notices of the Royal Astronomical Society*, 424(2), 1179–1186.

Bai, L., Rieke, G. H., Rieke, M. J., Hinz, J. L., Kelly, D. M., & Blaylock, M. (2006). Infrared luminosity function of the Coma cluster. *The Astrophysical Journal*, 639(2), 827.

Barkhouse, W. A., Green, P. J., Vikhlinin, A., Kim, D. W., Perley, D., Cameron, R., Silverman, J., Mossman, A., Burenin, R., Jannuzi, B. T., Kim, M., Smith, M. G., Smith, R. C., Tananbaum, H., & Wilkes, B. J. (2006). ChaMP Serendipitous Galaxy Cluster Survey. *The Astrophysical Journal*, 645(2), 955–976.

Barkhouse, W. A., Yee, H. K. C., & López-Cruz, O. (2007). The Luminosity Function of Low-Redshift Abell Galaxy Clusters. *The Astrophysical Journal*, 671(2), 1471.

Baron, D., Netzer, H., Davies, R. I., & Xavier Prochaska, J. (2020). Multiphase outflows in post-starburst E+A galaxies - II. A direct connection between the neutral and ionized outflow phases. *Monthly Notices of the Royal Astronomical Society*, 494(4), 5396–5420.

Bartelmann, M. & Schneider, P. (2001). Weak gravitational lensing. *Physics Reports*, 340(4-5), 291–472.

Baum, W. A. (1959). The Hertzsprung-Russell diagrams of old stellar Populations. In J. L. Greenstein (Ed.), *The Hertzsprung-Russell Diagram*, volume 10 (pp.$\tilde{2}$3).

Bautz, L. P. & Morgan, W. W. (1970). On the Classification of the Forms of Clusters of Galaxies. *The Astrophysical Journal*, 162, L149.

Begeman, K. G. (1987). *HI rotation curves of spiral galaxies.* PhD thesis, University of Groningen, Kapteyn Astronomical Institute.

Bell, E. F., McIntosh, D. H., Katz, N., & Weinberg, M. D. (2003). The Optical and Near-Infrared Properties of Galaxies. I. Luminosity and Stellar Mass Functions. *The Astrophysical Journal Supplement Series*, 149(2), 289–312.

Bellagamba, F., Roncarelli, M., Maturi, M., & Moscardini, L. (2018). AMICO: optimized detection of galaxy clusters in photometric surveys. *Monthly Notices of the Royal Astronomical Society*, 473(4), 5221–5236.

Benítez, N. (2000). Bayesian Photometric Redshift Estimation. *The Astrophysical Journal*, 536(2), 571–583.

Bennett, C. L., Hill, R. S., Hinshaw, G., Nolta, M. R., Odegard, N., Page, L., Spergel, D. N., Weiland, J. L., Wright, E. L., Halpern, M., Jarosik, N., Kogut, A., Limon, M., Meyer, S. S., Tucker, G. S., & Wollack, E. (2003). First-Year Wilkinson Microwave Anisotropy Probe (WMAP) Observations: Foreground Emission. *The Astrophysical Journal Supplement Series*, 148(1), 97–117.

Bennett, C. L., Larson, D., Weiland, J. L., Jarosik, N., Hinshaw, G., Odegard, N., Smith, K. M., Hill, R. S., Gold, B., Halpern, M., Komatsu, E., Nolta, M. R., Page, L., Spergel, D. N., Wollack, E., Dunkley, J., Kogut, A., Limon, M., Meyer, S. S., Tucker, G. S., & Wright, E. L. (2013). NINE-YEAR WILKINSON MICROWAVE ANISOTROPY PROBE (WMAP) OBSERVATIONS: FINAL MAPS AND RESULTS. *The Astrophysical Journal Supplement Series*, 208(2), 20.

Benson, A. J. & Bower, R. (2011). Accretion shocks and cold filaments in galaxy formation. *Monthly Notices of the Royal Astronomical Society*, 410(4), 2653–2661.

Benson, A. J., Bower, R. G., Frenk, C. S., Lacey, C. G., Baugh, C. M., & Cole, S. (2003). What Shapes the Luminosity Function of Galaxies? *The Astrophysical Journal*, 599(1), 38.

Berrier, J. C., Stewart, K. R., Bullock, J. S., Purcell, C. W., Barton, E. J., & Wechsler, R. H. (2008). THE ASSEMBLY OF GALAXY CLUSTERS. *The Astrophysical Journal*, 690(2), 1292–1302.

Best, P. N., von der Linden, A., Kauffmann, G., Heckman, T. M., & Kaiser, C. R. (2007). On the prevalence of radio-loud active galactic nuclei in brightest cluster galaxies: implications

for AGN heating of cooling flows. *Monthly Notices of the Royal Astronomical Society*, 379(3), 894–908.

Binggeli, B., Sandage, A., & Tammann, G. A. (1988). The luminosity function of galaxies. *Annual review of astronomy and astrophysics*, 26, 509–560.

Binney, J. & Tremaine, S. (1987). *Galactic dynamics*.

Binney, J. & Tremaine, S. (2011). *Galactic dynamics*, volume 20. Princeton university press.

Birkinshaw, M., Gull, S., & Northover, K. (1978a). Measurements of the gas contents of clusters of galaxies by observations of the background radiation at 10.6 GHz. *Monthly Notices of the Royal Astronomical Society*, 185(2), 245–262.

Birkinshaw, M., Gull, S., & Northover, K. (1978b). Extent of hot intergalactic gas in the cluster Abell 2218. *Nature*, 275(5675), 40–41.

Birnboim, Y. & Dekel, A. (2003). Virial shocks in galactic haloes? *Monthly Notices of the Royal Astronomical Society*, 345(1), 349–364.

Biviano, A., Durret, F., Gerbal, D., Fèvre, O. L., Lobo, C., Mazure, A., & Slezak, E. (1994). On the galaxy luminosity function in the central regions of the Coma cluster. *arXiv preprint astro-ph/9411025*.

Biviano, A. & Salucci, P. (2006). The radial profiles of the different mass components in galaxy clusters. *Astronomy & Astrophysics*, 452(1), 75–81.

Blanton, M. R., Lupton, R. H., Schlegel, D. J., Strauss, M. A., Brinkmann, J., Fukugita, M., & Loveday, J. (2005). The properties and luminosity function of extremely low luminosity galaxies. *The Astrophysical Journal*, 631(1), 208.

Bleem, L. E., Stalder, B., de Haan, T., Aird, K. A., Allen, S. W., Applegate, D. E., Ashby, M. L. N., Bautz, M., Bayliss, M., Benson, B. A., & et al. (2015). GALAXY CLUSTERS DISCOVERED VIA THE SUNYAEV-ZEL'DOVICH EFFECT IN THE 2500-SQUARE-DEGREE SPT-SZ SURVEY. *The Astrophysical Journal Supplement Series*, 216(2), 27.

Böhringer, H., Guzzo, L., Collins, C., Neumann, D., Schindler, S., Schuecker, P., Cruddace, R., De Grandi, S., Chincarini, G., Edge, A., et al. (1998). Probing the cosmic large-scale structure with the REFLEX Cluster Survey: profile of an ESO key programme. *arXiv preprint astro-ph/9809382*.

Böhringer, H., Voges, W., Huchra, J. P., McLean, B., Giacconi, R., Rosati, P., Burg, R., Mader, J., Schuecker, P., Simiç, D., Komossa, S., Reiprich, T. H., Retzlaff, J., & Trümper, J. (2000). The Northern ROSAT All-Sky (NORAS) Galaxy Cluster Survey. I. X-Ray Properties of Clusters Detected as Extended X-Ray Sources. *The Astrophysical Journal Supplement Series*, 129(2), 435–474.

Böhringer, H. & Werner, N. (2010). X-ray spectroscopy of galaxy clusters: studying astrophysical processes in the largest celestial laboratories. *The Astronomy and Astrophysics Review*, 18, 127–196.

Boldt, E., McDonald, F. B., Riegler, G., & Serlemitsos, P. (1966). Extended source of energetic cosmic X rays. *Physical Review Letters*, 17(8), 447.

Boselli, A. & Gavazzi, G. (2014). On the origin of the faint-end of the red sequence in high-density environments. *The Astronomy and Astrophysics Review*, 22(1).

Bouchet, F. R. (2009). The Planck Satellite: Status & Perspectives. *arXiv e-prints*, (pp. arXiv:0911.3101).

Boué, G., Adami, C., Durret, F., Mamon, G., & Cayatte, V. (2008). The galaxy luminosity function of the Abell 496 cluster and its spatial variations. *Astronomy & Astrophysics*, 479(2), 335–346.

Bower, R. G., Benson, A. J., Malbon, R., Helly, J. C., Frenk, C. S., Baugh, C. M., Cole, S., & Lacey, C. G. (2006). Breaking the hierarchy of galaxy formation. *Monthly Notices of the Royal Astronomical Society*, 370(2), 645–655.

Boyce, P. J., Phillipps, S., Jones, J. B., Driver, S. P., Smith, R. M., & Couch, W. J. (2001). The nature of the dwarf population in Abell 868. *Monthly Notices of the Royal Astronomical Society*, 328(1), 277–282.

Boylan-Kolchin, M., Ma, C.-P., & Quataert, E. (2008). Dynamical friction and galaxy merging time-scales. *Monthly Notices of the Royal Astronomical Society*, 383(1), 93–101.

Brammer, G. B., van Dokkum, P. G., & Coppi, P. (2008). EAZY: A Fast, Public Photometric Redshift Code. *The Astrophysical Journal*, 686(2), 1503–1513.

Brammer, G. B., Whitaker, K. E., van Dokkum, P. G., Marchesini, D., Labbé, I., Franx, M., Kriek, M., Quadri, R. F., Illingworth, G., Lee, K. S., Muzzin, A., & Rudnick, G. (2009). The Dead Sequence: A Clear Bimodality in Galaxy Colors from z = 0 to z = 2.5. *The Astrophysical Journal*, 706(1), L173–L177.

Bridges, T., Gebhardt, K., Sharples, R., Faifer, F. R., Forte, J. C., Beasley, M. A., Zepf, S. E., Forbes, D. A., Hanes, D. A., & Pierce, M. (2006). The globular cluster kinematics and galaxy dark matter content of NGC 4649 (M60). *Monthly Notices of the Royal Astronomical Society*, 373(1), 157–166.

Brighenti, F. & Mathews, W. G. (2002). Confrontation of Intracluster and Interstellar Gas in Cluster-centered Elliptical Galaxies: M87 in Virgo and NGC 4874 in Coma. *The Astrophysical Journal*, 567(1), 130–143.

Brook, C. B. & Shankar, F. (2015). A matter of measurement: rotation velocities and the velocity function of dwarf galaxies. *Monthly Notices of the Royal Astronomical Society*, 455(4), 3841–3847.

Brunner, R. & Lubin, L. (2000). A probabilistic quantification of galaxy cluster membership. *The Astronomical Journal*, 120(6), 2851.

Bruzual, G. & Charlot, S. (2003). Stellar population synthesis at the resolution of 2003. *Monthly Notices of the Royal Astronomical Society*, 344(4), 1000–1028.

Burenin, R. A., Vikhlinin, A., Hornstrup, A., Ebeling, H., Quintana, H., & Mescheryakov, A. (2007). The 400 Square Degree ROSAT PSPC Galaxy Cluster Survey: Catalog and Statistical Calibration. *The Astrophysical Journal Supplement Series*, 172(2), 561–582.

Buta, R. & Combes, F. (1996). Galactic Rings. *Fundamentals of Cosmic Physics*, 17, 95–281.

Butcher, H. & Oemler, A., J. (1978a). The evolution of galaxies in clusters. I. ISIT photometry of Cl 0024+1654 and 3C 295. *The Astrophysical Journal*, 219, 18–30.

Butcher, H. & Oemler, A., J. (1978b). The evolution of galaxies in clusters. II. The galaxy content of nearby clusters. *The Astrophysical Journal*, 226, 559–565.

Caminha, G. B., Suyu, S. H., Mercurio, A., Brammer, G., Bergamini, P., Acebron, A., & Vanzella, E. (2022). First JWST observations of a gravitational lens. mass model from new multiple images with near-infrared observations of SMACS˜j0723.3-7327. *Astronomy & Astrophysics*.

Carlstrom, J. E., Ade, P. A. R., Aird, K. A., Benson, B. A., Bleem, L. E., Busetti, S., Chang, C. L., Chauvin, E., Cho, H.-M., Crawford, T. M., Crites, A. T., Dobbs, M. A., Halverson, N. W., Heimsath, S., Holzapfel, W. L., Hrubes, J. D., Joy, M., Keisler, R., Lanting, T. M., Lee, A. T., Leitch, E. M., Leong, J., Lu, W., Lueker, M., Luong-Van, D., McMahon, J. J., Mehl, J., Meyer, S. S., Mohr, J. J., Montroy, T. E., Padin, S., Plagge, T., Pryke, C., Ruhl, J. E., Schaffer, K. K., Schwan, D., Shirokoff, E., Spieler, H. G., Staniszewski, Z., Stark, A. A., Tucker, C., Vanderlinde, K., Vieira, J. D., & Williamson, R. (2011). The 10 meter south pole telescope. *Publications of the Astronomical Society of the Pacific*, 123(903), 568.

Ceverino, D. & Klypin, A. (2009). The Role of Stellar Feedback in the Formation of Galaxies. *The Astrophysical Journal*, 695(1), 292–309.

Chadayammuri, U., Tremmel, M., Nagai, D., Babul, A., & Quinn, T. (2021). Fountains and storms: the effects of AGN feedback and mergers on the evolution of the intraclus-

ter medium in the ROMULUSC simulation. *Monthly Notices of the Royal Astronomical Society*, 504(3), 3922–3937.

Chester, C. & Roberts, M. S. (1964). Properties of Galaxies: color-magnitude diagram. *Astronomical Journal*, 69, 635.

Cheung, E., Athanassoula, E., Masters, K. L., Nichol, R. C., Bosma, A., Bell, E. F., Faber, S. M., Koo, D. C., Lintott, C., Melvin, T., Schawinski, K., Skibba, R. A., & Willett, K. W. (2013). GALAXY ZOO: OBSERVING SECULAR EVOLUTION THROUGH BARS. *The Astrophysical Journal*, 779(2), 162.

Chiosi, C. (1967). On the colour magnitude diagram of galaxies. *Memorie della Societa Astronomica Italiana*, 38, 3.

Choi, S. K., Hasselfield, M., Ho, S.-P. P., Koopman, B., Lungu, M., Abitbol, M. H., Addison, G. E., Ade, P. A. R., Aiola, S., Alonso, D., Amiri, M., Amodeo, S., Angile, E., Austermann, J. E., Baildon, T., Battaglia, N., Beall, J. A., Bean, R., Becker, D. T., Bond, J. R., Bruno, S. M., Calabrese, E., Calafut, V., Campusano, L. E., Carrero, F., Chesmore, G. E., mei Cho, H., Clark, S. E., Cothard, N. F., Crichton, D., Crowley, K. T., Darwish, O., Datta, R., Denison, E. V., Devlin, M. J., Duell, C. J., Duff, S. M., Duivenvoorden, A. J., Dunkley, J., Dünner, R., Essinger-Hileman, T., Fankhanel, M., Ferraro, S., Fox, A. E., Fuzia, B., Gallardo, P. A., Gluscevic, V., Golec, J. E., Grace, E., Gralla, M., Guan, Y., Hall, K., Halpern, M., Han, D., Hargrave, P., Henderson, S., Hensley, B., Hill, J. C., Hilton, G. C., Hilton, M., Hincks, A. D., Hložek, R., Hubmayr, J., Huffenberger, K. M., Hughes, J. P., Infante, L., Irwin, K., Jackson, R., Klein, J., Knowles, K., Kosowsky, A., Lakey, V., Li, D., Li, Y., Li, Z., Lokken, M., Louis, T., MacInnis, A., Madhavacheril, M., Maldonado, F., Mallaby-Kay, M., Marsden, D., Maurin, L., McMahon, J., Menanteau, F., Moodley, K., Morton, T., Naess, S., Namikawa, T., Nati, F., Newburgh, L., Nibarger, J. P., Nicola, A., Niemack, M. D., Nolta, M. R., Orlowski-Sherer, J., Page, L. A., Pappas, C. G., Partridge, B., Phakathi, P., Prince, H., Puddu, R., Qu, F. J., Rivera, J., Robertson, N., Rojas, F., Salatino, M., Schaan, E., Schillaci, A., Schmitt, B. L., Sehgal, N., Sherwin, B. D., Sierra,

C., Sievers, J., Sifon, C., Sikhosana, P., Simon, S., Spergel, D. N., Staggs, S. T., Stevens, J., Storer, E., Sunder, D. D., Switzer, E. R., Thorne, B., Thornton, R., Trac, H., Treu, J., Tucker, C., Vale, L. R., Engelen, A. V., Lanen, J. V., Vavagiakis, E. M., Wagoner, K., Wang, Y., Ward, J. T., Wollack, E. J., Xu, Z., Zago, F., & Zhu, N. (2020). The Atacama Cosmology Telescope: a measurement of the Cosmic Microwave Background power spectra at 98 and 150 GHz. *Journal of Cosmology and Astroparticle Physics*, 2020(12), 045.

Cicone, C., Maiolino, R., Sturm, E., Graciá-Carpio, J., Feruglio, C., Neri, R., Aalto, S., Davies, R., Fiore, F., Fischer, J., García-Burillo, S., González-Alfonso, E., Hailey-Dunsheath, S., Piconcelli, E., & Veilleux, S. (2014). Massive molecular outflows and evidence for AGN feedback from CO observations. *Astronomy & Astrophysics*, 562, A21.

Cielo, S., Bieri, R., Volonteri, M., Wagner, A. Y., & Dubois, Y. (2018). AGN feedback compared: jets versus radiation. *Monthly Notices of the Royal Astronomical Society*, 477(1), 1336–1355.

Coe, D., Benítez, N., Broadhurst, T., & Moustakas, L. A. (2010). A High-resolution Mass Map of Galaxy Cluster Substructure: LensPerfect Analysis of A1689. *The Astrophysical Journal*, 723(2), 1678–1702.

Colless, M. (1989). The dynamics of rich clusters – II. Luminosity functions. *Monthly Notices of the Royal Astronomical Society*, 237(3), 799–826.

Conselice, C. J., Wilkinson, A., Duncan, K., & Mortlock, A. (2016). The Evolution of Galaxy Number Density at $z < 8$ and Its Implications. *The Astrophysical Journal*, 830(2), 83.

Cortese, L., Gavazzi, G., Boselli, A., Iglesias-Paramo, J., Donas, J., & Milliard, B. (2003). The UV luminosity function of nearby clusters of galaxies. *Astronomy & Astrophysics*, 410(2), L25–L28.

Cutri, R. M. & et al. (2012). VizieR Online Data Catalog: WISE All-Sky Data Release (Cutri+ 2012). *VizieR Online Data Catalog*, (pp. II/311).

Da Costa, G. S., Rejkuba, M., Jerjen, H., & Grebel, E. K. (2010). Ancient Stars Beyond the Local Group: RR Lyrae Variables and Blue Horizontal Branch Stars in Sculptor Group Dwarf Galaxies. *The Astrophysical Journal Letters*, 708(2), L121–L125.

Dahlén, T., Fransson, C., Östlin, G., & Näslund, M. (2004). The galaxy population of intermediate-redshift clusters. *Monthly Notices of the Royal Astronomical Society*, 350(1), 253–266.

Dalton, G., Efstathiou, G., Maddox, S., & Sutherland, W. (1992). Spatial correlations in a redshift survey of APM galaxy clusters. *The Astrophysical Journal*, 390, L1–L4.

Dark Energy Survey Collaboration, Abbott, T., Abdalla, F. B., Aleksić, J., Allam, S., Amara, A., Bacon, D., Balbinot, E., Banerji, M., Bechtol, K., Benoit-Lévy, A., Bernstein, G. M., Bertin, E., Blazek, J., Bonnett, C., Bridle, S., Brooks, D., Brunner, R. J., Buckley-Geer, E., Burke, D. L., Caminha, G. B., Capozzi, D., Carlsen, J., Carnero-Rosell, A., Carollo, M., Carrasco-Kind, M., Carretero, J., Castander, F. J., Clerkin, L., Collett, T., Conselice, C., Crocce, M., Cunha, C. E., D'Andrea, C. B., da Costa, L. N., Davis, T. M., Desai, S., Diehl, H. T., Dietrich, J. P., Dodelson, S., Doel, P., Drlica-Wagner, A., Estrada, J., Etherington, J., Evrard, A. E., Fabbri, J., Finley, D. A., Flaugher, B., Foley, R. J., Fosalba, P., Frieman, J., García-Bellido, J., Gaztanaga, E., Gerdes, D. W., Giannantonio, T., Goldstein, D. A., Gruen, D., Gruendl, R. A., Guarnieri, P., Gutierrez, G., Hartley, W., Honscheid, K., Jain, B., James, D. J., Jeltema, T., Jouvel, S., Kessler, R., King, A., Kirk, D., Kron, R., Kuehn, K., Kuropatkin, N., Lahav, O., Li, T. S., Lima, M., Lin, H., Maia, M. A. G., Makler, M., Manera, M., Maraston, C., Marshall, J. L., Martini, P., McMahon, R. G., Melchior, P., Merson, A., Miller, C. J., Miquel, R., Mohr, J. J., Morice-Atkinson, X., Naidoo, K., Neilsen, E., Nichol, R. C., Nord, B., Ogando, R., Ostrovski, F., Palmese, A., Papadopoulos, A., Peiris, H. V., Peoples, J., Percival, W. J., Plazas, A. A., Reed, S. L., Refregier, A., Romer, A. K., Roodman, A., Ross, A., Rozo, E., Rykoff, E. S., Sadeh, I., Sako, M., Sánchez, C., Sanchez, E., Santiago, B., Scarpine, V., Schubnell, M., Sevilla-Noarbe, I., Sheldon, E., Smith, M., Smith, R. C., Soares-Santos, M., Sobreira, F.,

Soumagnac, M., Suchyta, E., Sullivan, M., Swanson, M., Tarle, G., Thaler, J., Thomas, D., Thomas, R. C., Tucker, D., Vieira, J. D., Vikram, V., Walker, A. R., Wechsler, R. H., Weller, J., Wester, W., Whiteway, L., Wilcox, H., Yanny, B., Zhang, Y., & Zuntz, J. (2016). The Dark Energy Survey: more than dark energy - an overview. *Monthly Notices of the Royal Astronomical Society*, 460(2), 1270–1299.

Dayal, P. & Ferrara, A. (2018). Early galaxy formation and its large-scale effects. *Proceedings of the International Astronomical Union*, 780, 1–64.

De Filippis, E., Paolillo, M., Longo, G., La Barbera, F., de Carvalho, R., & Gal, R. (2011). The luminosity function of the NoSOCS galaxy cluster sample. *Monthly Notices of the Royal Astronomical Society*, 414(3), 2771–2784.

De Grandi, S., Böhringer, H., Guzzo, L., Molendi, S., Chincarini, G., Collins, C., Cruddace, R., Neumann, D., Schindler, S., Schuecker, P., et al. (1999). A flux-limited sample of bright clusters of galaxies from the southern part of the ROSAT All-Sky Survey: The Catalog and LOG N-LOG S. *The Astrophysical Journal*, 514(1), 148.

De Jong, J. T. A., Verdoes Kleijn, G. A., Kuijken, K. H., & Valentijn, E. A. (2013). The Kilo-Degree Survey. *Experimental Astronomy*, 35(1-2), 25–44.

De Propris, R., Colless, M., Driver, S. P., Couch, W., Peacock, J. A., Baldry, I. K., Baugh, C. M., Bland-Hawthorn, J., Bridges, T., Cannon, R., Cole, S., Collins, C., Cross, N., Dalton, G. B., Efstathiou, G., Ellis, R. S., Frenk, C. S., Glazebrook, K., Hawkins, E., Jackson, C., Lahav, O., Lewis, I., Lumsden, S., Maddox, S., Madgwick, D. S., Norberg, P., Percival, W., Peterson, B., Sutherland, W., & Taylor, K. (2003). The 2dF Galaxy Redshift Survey: the luminosity function of cluster galaxies. *Monthly Notices of the Royal Astronomical Society*, 342(3), 725–737.

De Propris, R., Eisenhardt, P. R., Stanford, S. A., & Dickinson, M. (1998). The infrared luminosity function of galaxies in the Coma cluster. *The Astrophysical Journal*, 503(1), L45.

De Propris, R., Stanford, S., Eisenhardt, P. R., Dickinson, M., & Elston, R. (1999). The K-Band Luminosity Function in Galaxy Clusters to z. *The Astronomical Journal*, 118(2), 719.

De Vaucouleurs, G. (1948). Recherches sur les Nebuleuses Extragalactiques. *Annales d'Astrophysique*, 11, 247.

De Vaucouleurs, G. (1953). On the Distribution of Mass and Luminosity in Elliptical Galaxies. *Monthly Notices of the Royal Astronomical Society*, 113(2), 134–161.

De Vaucouleurs, G. (1958). Photoelectric photometry of the Andromeda Nebula in the UBV system. *Astrophysical Journal*, 128, 465.

De Vaucouleurs, G. (1959a). Classification and Morphology of External Galaxies. *Handbuch der Physik*, 53, 275.

De Vaucouleurs, G. (1959b). General Physical Properties of External Galaxies. *Handbuch der Physik*, 53, 311.

Dey, A., Schlegel, D. J., Lang, D., Blum, R., Burleigh, K., Fan, X., Findlay, J. R., Finkbeiner, D., Herrera, D., Juneau, S., Landriau, M., Levi, M., McGreer, I., Meisner, A., Myers, A. D., Moustakas, J., Nugent, P., Patej, A., Schlafly, E. F., Walker, A. R., Valdes, F., Weaver, B. A., Yèche, C., Zou, H., Zhou, X., Abareshi, B., Abbott, T. M. C., Abolfathi, B., Aguilera, C., Alam, S., Allen, L., Alvarez, A., Annis, J., Ansarinejad, B., Aubert, M., Beechert, J., Bell, E. F., BenZvi, S. Y., Beutler, F., Bielby, R. M., Bolton, A. S., Briceño, C., Buckley-Geer, E. J., Butler, K., Calamida, A., Carlberg, R. G., Carter, P., Casas, R., Castander, F. J., Choi, Y., Comparat, J., Cukanovaite, E., Delubac, T., DeVries, K., Dey, S., Dhungana, G., Dickinson, M., Ding, Z., Donaldson, J. B., Duan, Y., Duckworth, C. J., Eftekharzadeh, S., Eisenstein, D. J., Etourneau, T., Fagrelius, P. A., Farihi, J., Fitzpatrick, M., Font-Ribera, A., Fulmer, L., Gänsicke, B. T., Gaztanaga, E., George, K., Gerdes, D. W., Gontcho, S. G. A., Gorgoni, C., Green, G., Guy, J., Harmer, D., Hernandez, M., Honscheid, K., Huang, L. W., James, D. J., Jannuzi, B. T., Jiang, L.,

Joyce, R., Karcher, A., Karkar, S., Kehoe, R., Jean-Paul, K., Kueter-Young, A., Lan, T.-W., Lauer, T. R., Guillou, L. L., Suu, A. L. V., Lee, J. H., Lesser, M., Levasseur, L. P., Li, T. S., Mann, J. L., Marshall, R., Martínez-Vázquez, C. E., Martini, P., du Mas des Bourboux, H., McManus, S., Meier, T. G., Ménard, B., Metcalfe, N., Muñoz-Gutiérrez, A., Najita, J., Napier, K., Narayan, G., Newman, J. A., Nie, J., Nord, B., Norman, D. J., Olsen, K. A. G., Paat, A., Palanque-Delabrouille, N., Peng, X., Poppett, C. L., Poremba, M. R., Prakash, A., Rabinowitz, D., Raichoor, A., Rezaie, M., Robertson, A. N., Roe, N. A., Ross, A. J., Ross, N. P., Rudnick, G., Safonova, S., Saha, A., Sánchez, F. J., Savary, E., Schweiker, H., Scott, A., Seo, H.-J., Shan, H., Silva, D. R., Slepian, Z., Soto, C., Sprayberry, D., Staten, R., Stillman, C. M., Stupak, R. J., Summers, D. L., Tie, S. S., Tirado, H., Vargas-Magaña, M., Vivas, A. K., Wechsler, R. H., Williams, D., Yang, J., Yang, Q., Yapici, T., Zaritsky, D., Zenteno, A., Zhang, K., Zhang, T., Zhou, R., & Zhou, Z. (2019). Overview of the DESI Legacy Imaging Surveys. *The Astronomical Journal*, 157(5), 168.

Dhawan, S., Jha, S. W., & Leibundgut, B. (2018). Measuring the Hubble constant with Type Ia supernovae as near-infrared standard candles. *Astronomy & Astrophysics*, 609, A72.

Díaz-Sánchez, Anastasio, A. A. A. (2021). Searching for Massive Galaxy Clusters at z 1 with WISE+VISTA+SDSS Catalogues CARTAGO Algorithm. In *Galaxy Cluster Formation II* (pp.3̃1).

Dicke, R. H. (1946). The Measurement of Thermal Radiation at Microwave Frequencies. *Review of Scientific Instruments*, 17(7), 268–275.

Dicke, R. H., Peebles, P. J. E., Roll, P. G., & Wilkinson, D. T. (1965). Cosmic Black-Body Radiation. , 142, 414–419.

Dressler, A. (1978). A comprehensive study of 12 very rich clusters of galaxies. I. Photometric technique and analysis of the luminosity function. *The Astrophysical Journal*, 223, 765–787.

Dressler, A. (1980). Galaxy morphology in rich clusters: implications for the formation and evolution of galaxies. *Astrophysical Journal*, 236, 351–365.

Dressler, A. & Gunn, J. E. (1983). Spectroscopy of galaxies in distant clusters. II. The population of the 3C 295 cluster. *The Astrophysical Journal*, 270, 7–19.

Dressler, A., Oemler, Augustus, J., Couch, W. J., Smail, I., Ellis, R. S., Barger, A., Butcher, H., Poggianti, B. M., & Sharples, R. M. (1997). Evolution since z = 0.5 of the Morphology-Density Relation for Clusters of Galaxies. *The Astrophysical Journal*, 490(2), 577–591.

Dressler, A., Smail, I., Poggianti, B. M., Butcher, H., Couch, W. J., Ellis, R. S., & Oemler Jr, A. (1999). A spectroscopic catalog of 10 distant rich clusters of galaxies. *The Astrophysical Journal Supplement Series*, 122(1), 51.

Eales, S. A., Baes, M., Bourne, N., Bremer, M., Brown, M. J. I., Clark, C., Clements, D., de Vis, P., Driver, S., Dunne, L., Dye, S., Furlanetto, C., Holwerda, B., Ivison, R. J., Kelvin, L. S., Lara-Lopez, M., Leeuw, L., Loveday, J., Maddox, S., Michałowski, M. J., Phillipps, S., Robotham, A., Smith, D., Smith, M., Valiante, E., van der Werf, P., & Wright, A. (2018). The causes of the red sequence, the blue cloud, the green valley, and the green mountain. *Monthly Notices of the Royal Astronomical Society*, 481(1), 1183–1194.

Ebeling, H., Edge, A. C., Bohringer, H., Allen, S. W., Crawford, C. S., Fabian, A. C., Voges, W., & Huchra, J. P. (1998). The ROSAT Brightest Cluster Sample - I. The compilation of the sample and the cluster log N-log S distribution. *Monthly Notices of the Royal Astronomical Society*, 301(4), 881–914.

Ebeling, H., Edge, A. C., & Henry, J. P. (2001). MACS: A Quest for the Most Massive Galaxy Clusters in the Universe. *The Astrophysical Journal*, 553(2), 668–676.

Eisenstein, D. J., Weinberg, D. H., Agol, E., Aihara, H., Allende Prieto, C., Anderson, S. F., Arns, J. A., Aubourg, É., Bailey, S., Balbinot, E., Barkhouser, R., Beers, T. C., Berlind, A. A., Bickerton, S. J., Bizyaev, D., Blanton, M. R., Bochanski, J. J., Bolton, A. S.,

Bosman, C. T., Bovy, J., Brandt, W. N., Breslauer, B., Brewington, H. J., Brinkmann, J., Brown, P. J., Brownstein, J. R., Burger, D., Busca, N. G., Campbell, H., Cargile, P. A., Carithers, W. C., Carlberg, J. K., Carr, M. A., Chang, L., Chen, Y., Chiappini, C., Comparat, J., Connolly, N., Cortes, M., Croft, R. A. C., Cunha, K., da Costa, L. N., Davenport, J. R. A., Dawson, K., De Lee, N., Porto de Mello, G. F., de Simoni, F., Dean, J., Dhital, S., Ealet, A., Ebelke, G. L., Edmondson, E. M., Eiting, J. M., Escoffier, S., Esposito, M., Evans, M. L., Fan, X., Femenía Castellá, B., Dutra Ferreira, L., Fitzgerald, G., Fleming, S. W., Font-Ribera, A., Ford, E. B., Frinchaboy, P. M., García Pérez, A. E., Gaudi, B. S., Ge, J., Ghezzi, L., Gillespie, B. A., Gilmore, G., Girardi, L., Gott, J. R., Gould, A., Grebel, E. K., Gunn, J. E., Hamilton, J.-C., Harding, P., Harris, D. W., Hawley, S. L., Hearty, F. R., Hennawi, J. F., González Hernández, J. I., Ho, S., Hogg, D. W., Holtzman, J. A., Honscheid, K., Inada, N., Ivans, I. I., Jiang, L., Jiang, P., Johnson, J. A., Jordan, C., Jordan, W. P., Kauffmann, G., Kazin, E., Kirkby, D., Klaene, M. A., Knapp, G. R., Kneib, J.-P., Kochanek, C. S., Koesterke, L., Kollmeier, J. A., Kron, R. G., Lampeitl, H., Lang, D., Lawler, J. E., Le Goff, J.-M., Lee, B. L., Lee, Y. S., Leisenring, J. M., Lin, Y.-T., Liu, J., Long, D. C., Loomis, C. P., Lucatello, S., Lundgren, B., Lupton, R. H., Ma, B., Ma, Z., MacDonald, N., Mack, C., Mahadevan, S., Maia, M. A. G., Majewski, S. R., Makler, M., Malanushenko, E., Malanushenko, V., Mandelbaum, R., Maraston, C., Margala, D., Maseman, P., Masters, K. L., McBride, C. K., McDonald, P., McGreer, I. D., McMahon, R. G., Mena Requejo, O., Ménard, B., Miralda-Escudé, J., Morrison, H. L., Mullally, F., Muna, D., Murayama, H., Myers, A. D., Naugle, T., Neto, A. F., Nguyen, D. C., Nichol, R. C., Nidever, D. L., O'Connell, R. W., Ogando, R. L. C., Olmstead, M. D., Oravetz, D. J., Padmanabhan, N., Paegert, M., Palanque-Delabrouille, N., Pan, K., Pandey, P., Parejko, J. K., Pâris, I., Pellegrini, P., Pepper, J., Percival, W. J., Petitjean, P., Pfaffenberger, R., Pforr, J., Phleps, S., Pichon, C., Pieri, M. M., Prada, F., Price-Whelan, A. M., Raddick, M. J., Ramos, B. H. F., Reid, I. N., Reyle, C., Rich, J., Richards, G. T., Rieke, G. H., Rieke, M. J., Rix, H.-W., Robin, A. C., Rocha-Pinto, H. J., Rockosi, C. M., Roe, N. A., Rollinde, E., Ross, A. J., Ross, N. P., Rossetto, B., Sánchez,

A. G., Santiago, B., Sayres, C., Schiavon, R., Schlegel, D. J., Schlesinger, K. J., Schmidt, S. J., Schneider, D. P., Sellgren, K., Shelden, A., Sheldon, E., Shetrone, M., Shu, Y., Silverman, J. D., Simmerer, J., Simmons, A. E., Sivarani, T., Skrutskie, M. F., Slosar, A., Smee, S., Smith, V. V., Snedden, S. A., Stassun, K. G., Steele, O., Steinmetz, M., Stockett, M. H., Stollberg, T., Strauss, M. A., Szalay, A. S., Tanaka, M., Thakar, A. R., Thomas, D., Tinker, J. L., Tofflemire, B. M., Tojeiro, R., Tremonti, C. A., Vargas Magaña, M., Verde, L., Vogt, N. P., Wake, D. A., Wan, X., Wang, J., Weaver, B. A., White, M., White, S. D. M., Wilson, J. C., Wisniewski, J. P., Wood-Vasey, W. M., Yanny, B., Yasuda, N., Yèche, C., York, D. G., Young, E., Zasowski, G., Zehavi, I., & Zhao, B. (2011). SDSS-III: Massive Spectroscopic Surveys of the Distant Universe, the Milky Way, and Extra-Solar Planetary Systems. *The Astronomical Journal*, 142(3), 72.

Ellison, S. L., Wilkinson, S., Woo, J., Leung, H.-H., Wild, V., Bickley, R. W., Patton, D. R., Quai, S., & Gwyn, S. (2022). Galaxy mergers can rapidly shut down star formation. *Monthly Notices of the Royal Astronomical Society: Letters*, 517(1), L92–L96.

Elmegreen, B. G. & Scalo, J. (2004). Interstellar Turbulence I: Observations and Processes. *Annu. Rev. Astron. Astrophys.*, 42(1), 211–273.

Emerick, A., Bryan, G. L., & Mac Low, M.-M. (2018). Stellar Radiation Is Critical for Regulating Star Formation and Driving Outflows in Low-mass Dwarf Galaxies. *The Astrophysical Journal Letters*, 865(2), L22.

Emsellem, E., Cappellari, M., Krajnović, D., Alatalo, K., Blitz, L., Bois, M., Bournaud, F., Bureau, M., Davies, R. L., Davis, T. A., de Zeeuw, P. T., Khochfar, S., Kuntschner, H., Lablanche, P.-Y., McDermid, R. M., Morganti, R., Naab, T., Oosterloo, T., Sarzi, M., Scott, N., Serra, P., van de Ven, G., Weijmans, A.-M., & Young, L. M. (2011). The ATLAS^{3D} project - III. A census of the stellar angular momentum within the effective radius of early-type galaxies: unveiling the distribution of fast and slow rotators. *Monthly Notices of the Royal Astronomical Society*, 414(2), 888–912.

Emsellem, E., Cappellari, M., Krajnović, D., van de Ven, G., Bacon, R., Bureau, M., Davies, R. L., de Zeeuw, P. T., Falcón-Barroso, J., Kuntschner, H., McDermid, R., Peletier, R. F., & Sarzi, M. (2007). The SAURON project - IX. A kinematic classification for early-type galaxies. *Monthly Notices of the Royal Astronomical Society*, 379(2), 401–417.

Fabian, A. C. (2012). Observational Evidence of Active Galactic Nuclei Feedback. *Annual Review of Astronomy and Astrophysics*, 50, 455–489.

Farhang, M., Bond, J. R., & Chluba, J. (2012). SEMI-BLIND EIGEN ANALYSES OF RECOMBINATION HISTORIES USING COSMIC MICROWAVE BACKGROUND DATA. *The Astrophysical Journal*, 752(2), 88.

Felten, J. E., Gould, R. J., Stein, W. A., & Woolf, N. J. (1966). X-Rays from the Coma Cluster of Galaxies. *The Astrophysical Journal*, 146, 955–958.

Fixsen, D. J. (2009). THE TEMPERATURE OF THE COSMIC MICROWAVE BACKGROUND. *The Astrophysical Journal*, 707(2), 916.

Flaugher, B., Diehl, H. T., Honscheid, K., Abbott, T. M. C., Alvarez, O., Angstadt, R., Annis, J. T., Antonik, M., Ballester, O., Beaufore, L., & et al. (2015). THE DARK ENERGY CAMERA. *The Astronomical Journal*, 150(5), 150.

Fowler, J. W., Niemack, M. D., Dicker, S. R., Aboobaker, A. M., Ade, P. A. R., Battistelli, E. S., Devlin, M. J., Fisher, R. P., Halpern, M., Hargrave, P. C., Hincks, A. D., Kaul, M., Klein, J., Lau, J. M., Limon, M., Marriage, T. A., Mauskopf, P. D., Page, L., Staggs, S. T., Swetz, D. S., Switzer, E. R., Thornton, R. J., & Tucker, C. E. (2007). Optical design of the Atacama Cosmology Telescope and the Millimeter Bolometric Array Camera. *Applied Optics IP*, 46(17), 3444–3454.

Freedman, W. L., Burns, C. R., Phillips, M. M., Wyatt, P., Persson, S. E., Madore, B. F., Contreras, C., Folatelli, G., Gonzalez, E. S., Hamuy, M., Hsiao, E., Kelson, D. D., Morrell, N., Murphy, D. C., Roth, M., Stritzinger, M., Sturch, L., Suntzeff, N. B., Astier, P.,

Balland, C., Bassett, B., Boldt, L., Carlberg, R. G., Conley, A. J., Frieman, J. A., Garnavich, P. M., Guy, J., Hardin, D., Howell, D. A., Kessler, R., Lampeitl, H., Marriner, J., Pain, R., Perrett, K., Regnault, N., Riess, A. G., Sako, M., Schneider, D. P., Sullivan, M., & Wood-Vasey, M. (2009). THE CARNEGIE SUPERNOVA PROJECT: FIRST NEAR-INFRARED HUBBLE DIAGRAM TO z $\sim$ 0.7*. *The Astrophysical Journal*, 704(2), 1036.

Freedman, W. L., Madore, B. F., Gibson, B. K., Ferrarese, L., Kelson, D. D., Sakai, S., Mould, J. R., Kennicutt, Robert C., J., Ford, H. C., Graham, J. A., Huchra, J. P., Hughes, S. M. G., Illingworth, G. D., Macri, L. M., & Stetson, P. B. (2001). Final Results from the Hubble Space Telescope Key Project to Measure the Hubble Constant. *The Astrophysical Journal*, 553(1), 47–72.

Frenk, C. S., White, S. D. M., Efstathiou, G., & Davis, M. (1990). Galaxy Clusters and the Amplitude of Primordial Fluctuations. *The Astrophysical Journal*, 351, 10.

Friedman, H. (1979). A Survey of the X-Ray Sky with HEAO A-1. *Proceedings of the Royal Society of London Series A*, 366(1726), 423–434.

Friedmann, A. (1924). Über die möglichkeit einer Welt mit konstanter negativer Krümmung des Raumes. *Zeitschrift für Physik*, 21(1), 326–332.

Gamow, G. (1948). The Evolution of the Universe. *Nature*, 162(4122), 680–682.

Gawiser, E. & Silk, J. (2000). The cosmic microwave background radiation. *Physics Reports*, 333-334, 245–267.

George, K., Poggianti, B. M., Bellhouse, C., Radovich, M., Fritz, J., Paladino, R., Bettoni, D., Jaffé, Y., Moretti, A., Gullieuszik, M., Vulcani, B., Fasano, G., Stalin, C. S., Subramaniam, A., & Tandon, S. N. (2019). GASP XVIII: star formation quenching due to AGN feedback in the central region of a jellyfish galaxy. *Monthly Notices of the Royal Astronomical Society*, 487(3), 3102–3111.

Gilbank, D. G., Gladders, M. D., Yee, H. K. C., & Hsieh, B. C. (2011). THE RED-SEQUENCE CLUSTER SURVEY-2 (RCS-2): SURVEY DETAILS AND PHOTOMETRIC CATALOG CONSTRUCTION. *The Astronomical Journal*, 141(3), 94.

Giocoli, C., Marulli, F., Moscardini, L., Sereno, M., Veropalumbo, A., Gigante, L., Maturi, M., Radovich, M., Bellagamba, F., Roncarelli, M., Bardelli, S., Contarini, S., Covone, G., Harnois-Dé raps, J., Ingoglia, L., Lesci, G. F., Nanni, L., & Puddu, E. (2021). AMICO galaxy clusters in KiDS-DR3. *Astronomy & Astrophysics*, 653, A19.

Gioia, I., Maccacaro, T., Schild, R., Wolter, A., Stocke, J., Morris, S., & Henry, J. (1990). The Einstein Observatory Extended Medium-Sensitivity Survey. I-X-ray data and analysis. *The Astrophysical Journal Supplement Series*, 72, 567–619.

Gioia, I. M. (2000). Cluster Surveys. In F. Durret & D. Gerbal (Eds.), *Constructing the Universe with Clusters of Galaxies* (pp. 3.1).

Gnedin, O. Y. (2003). Tidal Effects in Clusters of Galaxies. *The Astrophysical Journal*, 582(1), 141–161.

Gonzalez, A. H., Zaritsky, D., Dalcanton, J. J., & Nelson, A. (2001). The Las Campanas Distant Cluster Survey: The Catalog. *The Astrophysical Journal Supplement Series*, 137(1), 117.

Goto, T., Okamura, S., Mckay, T. A., Bahcall, N. A., Annis, J., Bernardi, M., Brinkmann, J., Gómez, P. L., Hansen, S., Kim, R. S. J., Sekiguchi, M., & Sheth, R. K. (2002). Composite Luminosity Functions Based on the Sloan Digital Sky Survey "Cut and Enhance" Galaxy Cluster Catalog. *Publications of the Astronomical Society of Japan*, 54(4), 515–525.

Goto, T., Postman, M., Cross, N. J., Illingworth, G., Tran, K., Magee, D., Franx, M., Benítez, N., Bouwens, R., Demarco, R., et al. (2005). Luminosity Functions of the Galaxy Cluster MS 1054–0321 at $z = 0.83$ based on ACS Photometry. *The Astrophysical Journal*, 621(1), 188.

Gull, S. F. & Northover, K. J. E. (1976). Detection of hot gas in clusters of galaxies by observation of the microwave background radiation. *Nature*, 263(5578), 572–573.

Gunn, J. E. & Gott, J. Richard, I. (1972). On the Infall of Matter Into Clusters of Galaxies and Some Effects on Their Evolution. *The Astrophysical Journal*, 176, 1.

Guth, A. H. (1981). Inflationary universe: A possible solution to the horizon and flatness problems. *Physical Review D (Particles and Fields)*, 23(2), 347–356.

Gvaramadze, V. V., Kniazev, A. Y., Maryeva, O. V., & Berdnikov, L. N. (2017). Optical spectroscopy of the blue supergiant Sk69°279 and its circumstellar shell with SALT. *Monthly Notices of the Royal Astronomical Society*, 474(1), 1412–1425.

Hand, N., Addison, G. E., Aubourg, E., Battaglia, N., Battistelli, E. S., Bizyaev, D., Bond, J. R., Brewington, H., Brinkmann, J., Brown, B. R., Das, S., Dawson, K. S., Devlin, M. J., Dunkley, J., Dunner, R., Eisenstein, D. J., Fowler, J. W., Gralla, M. B., Hajian, A., Halpern, M., Hilton, M., Hincks, A. D., Hlozek, R., Hughes, J. P., Infante, L., Irwin, K. D., Kosowsky, A., Lin, Y.-T., Malanushenko, E., Malanushenko, V., Marriage, T. A., Marsden, D., Menanteau, F., Moodley, K., Niemack, M. D., Nolta, M. R., Oravetz, D., Page, L. A., Palanque-Delabrouille, N., Pan, K., Reese, E. D., Schlegel, D. J., Schneider, D. P., Sehgal, N., Shelden, A., Sievers, J., Sifón, C., Simmons, A., Snedden, S., Spergel, D. N., Staggs, S. T., Swetz, D. S., Switzer, E. R., Trac, H., Weaver, B. A., Wollack, E. J., Yeche, C., & Zunckel, C. (2012). Evidence of Galaxy Cluster Motions with the Kinematic Sunyaev-Zel'dovich Effect. *Phys. Rev. Lett.*, 109, 041101.

Hansen, C. J., Koch, A., Mashonkina, L., Magg, M., Bergemann, M., Sitnova, T., Gallagher, A. J., Ilyin, I., Caffau, E., Zhang, H. W., Strassmeier, K. G., & Klessen, R. S. (2020). Mono-enriched stars and Galactic chemical evolution. Possible biases in observations and theory. *Astronomy & Astrophysics*, 643, A49.

Hansen, S. M., McKay, T. A., Wechsler, R. H., Annis, J., Sheldon, E. S., & Kimball, A.

(2005). Measurement of Galaxy Cluster Sizes, Radial Profiles, and Luminosity Functions from SDSS Photometric Data. *The Astrophysical Journal*, 633(1), 122.

Hansen, S. M., Sheldon, E. S., Wechsler, R. H., & Koester, B. P. (2009). THE GALAXY CONTENT OF SDSS CLUSTERS AND GROUPS. *The Astrophysical Journal*, 699(2), 1333–1353.

Hao, J., McKay, T. A., Koester, B. P., Rykoff, E. S., Rozo, E., Annis, J., Wechsler, R. H., Evrard, A., Siegel, S. R., Becker, M., & et al. (2010). A GMBCG GALAXY CLUSTER CATALOG OF 55,424 RICH CLUSTERS FROM SDSS DR7. *The Astrophysical Journal Supplement Series*, 191(2), 254–274.

Hasselfield, M., Hilton, M., Marriage, T. A., Addison, G. E., Barrientos, L. F., Battaglia, N., Battistelli, E. S., Bond, J. R., Crichton, D., Das, S., & et al. (2013). The Atacama Cosmology Telescope: Sunyaev-Zel'dovich selected galaxy clusters at 148 GHz from three seasons of data. *Journal of Cosmology and Astroparticle Physics*, 2013(07), 008–008.

Henderson, S. W., Allison, R., Austermann, J., Baildon, T., Battaglia, N., Beall, J. A., Becker, D., Bernardis, F. D., Bond, J. R., Calabrese, E., Choi, S. K., Coughlin, K. P., Crowley, K. T., Datta, R., Devlin, M. J., Duff, S. M., Dunkley, J., Dünner, R., van Engelen, A., Gallardo, P. A., Grace, E., Hasselfield, M., Hills, F., Hilton, G. C., Hincks, A. D., Hloek, R., Ho, S. P., Hubmayr, J., Huffenberger, K., Hughes, J. P., Irwin, K. D., Koopman, B. J., Kosowsky, A. B., Li, D., McMahon, J., Munson, C., Nati, F., Newburgh, L., Niemack, M. D., Niraula, P., Page, L. A., Pappas, C. G., Salatino, M., Schillaci, A., Schmitt, B. L., Sehgal, N., Sherwin, B. D., Sievers, J. L., Simon, S. M., Spergel, D. N., Staggs, S. T., Stevens, J. R., Thornton, R., Lanen, J. V., Vavagiakis, E. M., Ward, J. T., & Wollack, E. J. (2016). Advanced ACTPol cryogenic detector arrays and readout. *Journal of Low Temperature Physics*, 184(3-4), 772–779.

Henry, J. P., Gioia, I. M., Huchra, J. P., Burg, R., McLean, B., Boehringer, H., Bower, R. G., Briel, U. G., Voges, W., MacGillivray, H., & Cruddace, R. G. (1995). Groups of Galaxies in the ROSAT North Ecliptic Pole Survey. *The Astrophysical Journal*, 449, 422.

Herschel, J. F. W. (1864). A General Catalogue of Nebulae and Clusters of Stars. *Philosophical Transactions of the Royal Society of London Series I*, 154, 1–137.

Herschel, W. (1785). On the Construction of the Heavens. *Philosophical Transactions of the Royal Society of London Series I*, 75, 213–266.

Heydon-Dumbleton, N. H., Collins, C. A., & MacGillivray, H. T. (1989). The Edinburgh/-Durham Southern Galaxy Catalogue – II. Image classification and galaxy number counts. *Monthly Notices of the Royal Astronomical Society*, 238(2), 379–406.

Heymans, C., Waerbeke, L. V., Miller, L., Erben, T., Hildebrandt, H., Hoekstra, H., Kitching, T. D., Mellier, Y., Simon, P., Bonnett, C., Coupon, J., Fu, L., Harnois-Dé raps, J., Hudson, M. J., Kilbinger, M., Kuijken, K., Rowe, B., Schrabback, T., Semboloni, E., van Uitert, E., Vafaei, S., & Velander, M. (2012). CFHTLenS: the Canada–France–Hawaii Telescope Lensing Survey. *Monthly Notices of the Royal Astronomical Society*, 427(1), 146–166.

Hilton, M., Collins, C., de Propris, R., Baldry, I. K., Baugh, C. M., Bland-Hawthorn, J., Bridges, T., Cannon, R., Cole, S., Colless, M., Couch, W. J., Dalton, G. B., Driver, S. P., Efstathiou, G., Ellis, R. S., Frenk, C. S., Glazebrook, K., Jackson, C. A., Lahav, O., Lewis, I., Lumsden, S., Maddox, S. J., Madgwick, D., Norberg, P., Peacock, J. A., Peterson, B. A., Sutherland, W., & Taylor, K. (2005). The 2dF Galaxy Redshift Survey: correlation with the ROSAT-ESO flux-limited X-ray galaxy cluster survey. *Monthly Notices of the Royal Astronomical Society*, 363(2), 661–674.

Hilton, M., Hasselfield, M., Sifón, C., Battaglia, N., Aiola, S., Bharadwaj, V., Bond, J. R., Choi, S. K., Crichton, D., Datta, R., Devlin, M. J., Dunkley, J., Dünner, R., Gallardo, P. A., Gralla, M., Hincks, A. D., Ho, S.-P. P., Hubmayr, J., Huffenberger, K. M., Hughes, J. P., Koopman, B. J., Kosowsky, A., Louis, T., Madhavacheril, M. S., Marriage, T. A., Maurin, L., McMahon, J., Miyatake, H., Moodley, K., Næss, S., Nati, F., Newburgh, L., Niemack, M. D., Oguri, M., Page, L. A., Partridge, B., Schmitt, B. L., Sievers, J., Spergel,

D. N., Staggs, S. T., Trac, H., van Engelen, A., Vavagiakis, E. M., & Wollack, E. J. (2018). The Atacama Cosmology Telescope: The Two-season ACTPol Sunyaev–Zel'dovich Effect Selected Cluster Catalog. *The Astrophysical Journal Supplement Series*, 235(1), 20.

Hilton, M., Hasselfield, M., Sifón, C., Baker, A. J., Barrientos, L. F., Battaglia, N., Bond, J. R., Crichton, D., Das, S., Devlin, M. J., Gralla, M., Hajian, A., Hincks, A. D., Hughes, J. P., Infante, L., Irwin, K. D., Kosowsky, A., Lin, Y.-T., Marriage, T. A., Marsden, D., Menanteau, F., Moodley, K., Niemack, M. D., Nolta, M. R., Page, L. A., Reese, E. D., Sievers, J., Spergel, D. N., & Wollack, E. J. (2013). The Atacama Cosmology Telescope: the stellar content of galaxy clusters selected using the Sunyaev–Zel'dovich effect. *Monthly Notices of the Royal Astronomical Society*, 435(4), 3469–3480.

Hilton, M., Sifón, C., Naess, S., Madhavacheril, M., Oguri, M., Rozo, E., Rykoff, E., Abbott, T. M. C., Adhikari, S., Aguena, M., Aiola, S., Allam, S., Amodeo, S., Amon, A., Annis, J., Ansarinejad, B., Aros-Bunster, C., Austermann, J. E., Avila, S., Bacon, D., Battaglia, N., Beall, J. A., Becker, D. T., Bernstein, G. M., Bertin, E., Bhandarkar, T., Bhargava, S., Bond, J. R., Brooks, D., Burke, D. L., Calabrese, E., Carrasco Kind, M., Carretero, J., Choi, S. K., Choi, A., Conselice, C., da Costa, L. N., Costanzi, M., Crichton, D., Crowley, K. T., Dünner, R., Denison, E. V., Devlin, M. J., Dicker, S. R., Diehl, H. T., Dietrich, J. P., Doel, P., Duff, S. M., Duivenvoorden, A. J., Dunkley, J., Everett, S., Ferraro, S., Ferrero, I., Ferté, A., Flaugher, B., Frieman, J., Gallardo, P. A., García-Bellido, J., Gaztanaga, E., Gerdes, D. W., Giles, P., Golec, J. E., Gralla, M. B., Grandis, S., Gruen, D., Gruendl, R. A., Gschwend, J., Gutierrez, G., Han, D., Hartley, W. G., Hasselfield, M., Hill, J. C., Hilton, G. C., Hincks, A. D., Hinton, S. R., Ho, S. P. P., Honscheid, K., Hoyle, B., Hubmayr, J., Huffenberger, K. M., Hughes, J. P., Jaelani, A. T., Jain, B., James, D. J., Jeltema, T., Kent, S., Knowles, K., Koopman, B. J., Kuehn, K., Lahav, O., Lima, M., Lin, Y. T., Lokken, M., Loubser, S. I., MacCrann, N., Maia, M. A. G., Marriage, T. A., Martin, J., McMahon, J., Melchior, P., Menanteau, F., Miquel, R., Miyatake, H., Moodley, K., Morgan, R., Mroczkowski, T., Nati, F., Newburgh, L. B., Niemack, M. D., Nishizawa, A. J., Ogando, R. L. C., Orlowski-Scherer, J., Page, L. A., Palmese, A.,

Partridge, B., Paz-Chinchón, F., Phakathi, P., Plazas, A. A., Robertson, N. C., Romer, A. K., Carnero Rosell, A., Salatino, M., Sanchez, E., Schaan, E., Schillaci, A., Sehgal, N., Serrano, S., Shin, T., Simon, S. M., Smith, M., Soares-Santos, M., Spergel, D. N., Staggs, S. T., Storer, E. R., Suchyta, E., Swanson, M. E. C., Tarle, G., Thomas, D., To, C., Trac, H., Ullom, J. N., Vale, L. R., Van Lanen, J., Vavagiakis, E. M., De Vicente, J., Wilkinson, R. D., Wollack, E. J., Xu, Z., & Zhang, Y. (2021). The Atacama Cosmology Telescope: A Catalog of $>$ 4000 Sunyaev-Zel'dovich Galaxy Clusters. *The Astrophysical Journal Supplement Series*, 253(1), 3.

Hinshaw, G., Larson, D., Komatsu, E., Spergel, D. N., Bennett, C. L., Dunkley, J., Nolta, M. R., Halpern, M., Hill, R. S., Odegard, N., Page, L., Smith, K. M., Weiland, J. L., Gold, B., Jarosik, N., Kogut, A., Limon, M., Meyer, S. S., Tucker, G. S., Wollack, E., & Wright, E. L. (2013). Nine-year Wilkinson Microwave Anisotropy Probe (WMAP) Observations: Cosmological Parameter Results. *The Astrophysical Journal Supplement Series*, 208(2), 19.

Hogg, D. W., Baldry, I. K., Blanton, M. R., & Eisenstein, D. J. (2002). The K correction. *arXiv preprint astro-ph/0210394*.

Hopkins, P. F., Cox, T. J., Hernquist, L., Narayanan, D., Hayward, C. C., & Murray, N. (2013). Star formation in galaxy mergers with realistic models of stellar feedback and the interstellar medium. *Monthly Notices of the Royal Astronomical Society*, 430(3), 1901–1927.

Hopkins, P. F., Kereš, D., Oñorbe, J., Faucher-Giguère, C.-A., Quataert, E., Murray, N., & Bullock, J. S. (2014). Galaxies on FIRE (Feedback In Realistic Environments): stellar feedback explains cosmologically inefficient star formation. *Monthly Notices of the Royal Astronomical Society*, 445(1), 581–603.

Hubble, E. (1929). A Relation between Distance and Radial Velocity among Extra-Galactic Nebulae. *Proceedings of the National Academy of Science*, 15(3), 168–173.

Hubble, E. P. (1925). Cepheids in spiral nebulae. *The Observatory*, 48, 139–142.

Hubble, E. P. (1926). Extragalactic nebulae. *Astrophysical Journal*, 64, 321–369.

Hubble, E. P. (1927). The classification of spiral nebulae. *The Observatory*, 50, 276–281.

Hubble, E. P. (1936). *Realm of the Nebulae*.

Huss, A., Jain, B., & Steinmetz, M. (1999). The formation and evolution of clusters of galaxies in different cosmogonies. *Monthly Notices of the Royal Astronomical Society*, 308(4), 1011–1031.

Jaffé, Y. L., Poggianti, B. M., Moretti, A., Gullieuszik, M., Smith, R., Vulcani, B., Fasano, G., Fritz, J., Tonnesen, S., Bettoni, D., Hau, G., Biviano, A., Bellhouse, C., & McGee, S. (2018). GASP. IX. Jellyfish galaxies in phase-space: an orbital study of intense ram-pressure stripping in clusters. *Monthly Notices of the Royal Astronomical Society*, 476(4), 4753–4764.

Jansen, F., Lumb, D., Altieri, B., Clavel, J., Ehle, M., Erd, C., Gabriel, C., Guainazzi, M., Gondoin, P., Much, R., Munoz, R., Santos, M., Schartel, N., Texier, D., & Vacanti, G. (2001). XMM-Newton observatory. I. The spacecraft and operations. *Astronomy & Astrophysics*, 365, L1–L6.

Johnson, H. L. & Morgan, W. W. (1953). Fundamental stellar photometry for standards of spectral type on the Revised System of the Yerkes Spectral Atlas. *The Astrophysical Journal*, 117, 313.

Jones, K. G. (1991). Messier's nebulae and star clusters. *Pract. Astron. Handb*, 2.

Jones, M. (1995). A Mosaiced Image of the Sunyaev-Zel'dovich Effect and a Value of the Hubble Constant. *Astrophysical Letters and Communications*, 32, 347.

Kaiser, N. (1986). Evolution and clustering of rich clusters. *Monthly Notices of the Royal Astronomical Society*, 222, 323–345.

Katayama, H., Hayashida, K., Takahara, F., & Fujita, Y. (2003). Properties of the brightest cluster galaxy and its host cluster. *The Astrophysical Journal*, 585(2), 687.

Katz, N. & Gunn, J. E. (1991). Dissipational Galaxy Formation. I. Effects of Gasdynamics. *The Astrophysical Journal*, 377, 365.

Kauffmann, G., Huang, M.-L., Moran, S., & Heckman, T. M. (2015). A systematic study of the inner rotation curves of galaxies observed as part of the GASS and COLD GASS surveys. *Monthly Notices of the Royal Astronomical Society*, 451(1), 878–887.

Kawata, D. & Mulchaey, J. S. (2008). Strangulation in Galaxy Groups. *The Astrophysical Journal*, 672(2), L103.

Kennicutt, Robert C., J. (1989). The Star Formation Law in Galactic Disks. *Astrophysical Journal*, 344, 685.

Kereš, D., Katz, N., Weinberg, D. H., & Davé, R. (2005). How do galaxies get their gas? *Monthly Notices of the Royal Astronomical Society*, 363(1), 2–28.

Khedekar, S. & Majumdar, S. (2013). Cosmology with the largest galaxy cluster surveys: going beyond Fisher matrix forecasts. *Journal of Cosmology and Astroparticle Physics*, 2013(02), 030–030.

Kilbinger, M., Fu, L., Heymans, C., Simpson, F., Benjamin, J., Erben, T., Harnois-Dé raps, J., Hoekstra, H., Hildebrandt, H., Kitching, T. D., Mellier, Y., Miller, L., Waerbeke, L. V., Benabed, K., Bonnett, C., Coupon, J., Hudson, M. J., Kuijken, K., Rowe, B., Schrabback, T., Semboloni, E., Vafaei, S., & Velander, M. (2013). CFHTLenS: combined probe cosmological model comparison using 2D weak gravitational lensing. *Monthly Notices of the Royal Astronomical Society*, 430(3), 2200–2220.

Koester, B. P., McKay, T. A., Annis, J., Wechsler, R. H., Evrard, A., Bleem, L., Becker, M., Johnston, D., Sheldon, E., Nichol, R., Miller, C., Scranton, R., Bahcall, N., Barentine, J., Brewington, H., Brinkmann, J., Harvanek, M., Kleinman, S., Krzesinski, J., Long,

D., Nitta, A., Schneider, D. P., Sneddin, S., Voges, W., & York, D. (2007). A MaxBCG Catalog of 13,823 Galaxy Clusters from the Sloan Digital Sky Survey. *The Astrophysical Journal*, 660(1), 239–255.

Kormendy, J., Fisher, D. B., Cornell, M. E., & Bender, R. (2009). Structure and Formation of Elliptical and Spheroidal Galaxies. *The Astrophysical Journal Supplement Series*, 182(1), 216–309.

Kosowsky, A. (2006). The Atacama Cosmology Telescope project: A progress report. *New Astronomy Reviews*, 50(11-12), 969–976.

Krajnović, D., Ural, U., Kuntschner, H., Goudfrooij, P., Wolfe, M., Cappellari, M., Davies, R., de Zeeuw, T. P., Duc, P.-A., Emsellem, E., Karick, A., McDermid, R. M., Mei, S., & Naab, T. (2020). Formation channels of slowly rotating early-type galaxies. *Astronomy & Astrophysics*, 635, A129.

Kravtsov, A. V. & Borgani, S. (2012). Formation of Galaxy Clusters. *Annual Review of Astronomy and Astrophysics*, 50(1), 353–409.

Lan, T.-W., Ménard, B., & Mo, H. (2016). The galaxy luminosity function in groups and clusters: the faint-end upturn and the connection to the field luminosity function. *Monthly Notices of the Royal Astronomical Society*, 459(4), 3998–4019.

Lee, Y. H., Ann, H. B., & Park, M.-G. (2019). Bar Fraction in Early- and Late-type Spirals. *The Astrophysical Journal*, 872(1), 97.

Lemaître, G. (1927). Un Univers homogène de masse constante et de rayon croissant rendant compte de la vitesse radiale des nébuleuses extra-galactiques. *Annales de la Société Scientifique de Bruxelles*, 47, 49–59.

Lin, Y.-T., Mohr, J. J., & Stanford, S. A. (2004). K-band properties of galaxy clusters and groups: Luminosity function, radial distribution, and halo occupation number. *The Astrophysical Journal*, 610(2), 745.

Lin, Y.-T., Ostriker, J. P., & Miller, C. J. (2010). A NEW TEST OF THE STATISTICAL NATURE OF THE BRIGHTEST CLUSTER GALAXIES. *The Astrophysical Journal*, 715(2), 1486.

Lintott, C., Schawinski, K., Bamford, S., Slosar, A., Land, K., Thomas, D., Edmondson, E., Masters, K., Nichol, R. C., Raddick, M. J., Szalay, A., Andreescu, D., Murray, P., & Vandenberg, J. (2011). Galaxy Zoo 1: data release of morphological classifications for nearly 900 000 galaxies. *Monthly Notices of the Royal Astronomical Society*, 410(1), 166–178.

Lintott, C. J., Schawinski, K., Slosar, A., Land, K., Bamford, S., Thomas, D., Raddick, M. J., Nichol, R. C., Szalay, A., Andreescu, D., Murray, P., & Vandenberg, J. (2008). Galaxy Zoo: morphologies derived from visual inspection of galaxies from the Sloan Digital Sky Survey. *Monthly Notices of the Royal Astronomical Society*, 389(3), 1179–1189.

Loh, Y.-S., Rich, R. M., Heinis, S., Scranton, R., Mallery, R. P., Salim, S., Martin, D. C., Wyder, T., Arnouts, S., Barlow, T. A., Forster, K., Friedman, P. G., Morrissey, P., Neff, S. G., Schiminovich, D., Seibert, M., Bianchi, L., Donas, J., Heckman, T. M., Lee, Y.-W., Madore, B. F., Milliard, B., Szalay, A. S., & Welsh, B. Y. (2010). The UV–optical colour dependence of galaxy clustering in the local universe. *Monthly Notices of the Royal Astronomical Society*, 407(1), 55–70.

Loh, Y.-S. & Strauss, M. A. (2006). The bright end of the luminosity function of red sequence galaxies. *Monthly Notices of the Royal Astronomical Society*, 366(2), 373–386.

López-Cruz, O., Yee, H., Brown, J. P., Jones, C., & Forman, W. (1997). Are luminous cD halos formed by the disruption of dwarf galaxies? *The Astrophysical Journal*, 475(2), L97.

Loveday, J., Norberg, P., Baldry, I. K., Driver, S. P., Hopkins, A. M., Peacock, J. A., Bamford, S. P., Liske, J., Bland-Hawthorn, J., Brough, S., Brown, M. J. I., Cameron, E., Conselice, C. J., Croom, S. M., Frenk, C. S., Gunawardhana, M., Hill, D. T., Jones, D. H., Kelvin, L. S., Kuijken, K., Nichol, R. C., Parkinson, H. R., Phillipps, S., Pimbblet,

K. A., Popescu, C. C., Prescott, M., Robotham, A. S. G., Sharp, R. G., Sutherland, W. J., Taylor, E. N., Thomas, D., Tuffs, R. J., van Kampen, E., & Wijesinghe, D. (2011). Galaxy and Mass Assembly (GAMA): *ugriz* galaxy luminosity functions. *Monthly Notices of the Royal Astronomical Society*, 420(2), 1239–1262.

Lucey, J. R. (1983). An assessment of the completeness and correctness of the Abell catalogue. *Monthly Notices of the Royal Astronomical Society*, 204(1), 33–43.

Lumsden, S. L., Nichol, R. C., Collins, C. A., & Guzzo, L. (1992). The Edinburgh-Durham southern galaxy catalogue. IV-The cluster catalogue. *Monthly Notices of the Royal Astronomical Society*, 258, 1–22.

Maddox, S., Efstathiou, G., & Loveday, J. (1988). The APM Galaxy Survey. *Symposium - International Astronomical Union*, 130, 151–160.

Mancone, C. L., Baker, T., Gonzalez, A. H., Ashby, M. L., Stanford, S. A., Brodwin, M., Eisenhardt, P. R., Snyder, G., Stern, D., & Wright, E. L. (2012). The Faint End of the Cluster-galaxy Luminosity Function at High Redshift. *The Astrophysical Journal*, 761(2), 141.

Mancone, C. L., Gonzalez, A. H., Brodwin, M., Stanford, S. A., Eisenhardt, P. R. M., Stern, D., & Jones, C. (2010). The Formation of Massive Cluster Galaxies. *The Astrophysical Journal*, 720(1), 284–298.

Mantz, A., Allen, S. W., Ebeling, H., Rapetti, D., & Drlica-Wagner, A. (2010). The observed growth of massive galaxy clusters – II. X-ray scaling relations. *Monthly Notices of the Royal Astronomical Society*, 406(3), 1773–1795.

Marriage, T. A., Acquaviva, V., Ade, P. A. R., Aguirre, P., Amiri, M., Appel, J. W., Barrientos, L. F., Battistelli, E. S., Bond, J. R., Brown, B., & et al. (2011). THE ATACAMA COSMOLOGY TELESCOPE: SUNYAEV-ZEL'DOVICH-SELECTED GALAXY CLUSTERS AT 148 GHz IN THE 2008 SURVEY. *The Astrophysical Journal*, 737(2), 61.

Martig, M., Bournaud, F., Teyssier, R., & Dekel, A. (2009). Morphological Quenching of Star Formation: Making Early-Type Galaxies Red. *The Astrophysical Journal*, 707(1), 250–267.

Martin, C. L. & Kennicutt, Robert C., J. (2001). Star Formation Thresholds in Galactic Disks. , 555(1), 301–321.

Martin, D. C., Fanson, J., Schiminovich, D., Morrissey, P., Friedman, P. G., Barlow, T. A., Conrow, T., Grange, R., Jelinsky, P. N., Milliard, B., Siegmund, O. H. W., Bianchi, L., Byun, Y.-I., Donas, J., Forster, K., Heckman, T. M., Lee, Y.-W., Madore, B. F., Malina, R. F., Neff, S. G., Rich, R. M., Small, T., Surber, F., Szalay, A. S., Welsh, B., & Wyder, T. K. (2005). The Galaxy Evolution Explorer: A Space Ultraviolet Survey Mission. *The Astrophysical Journal*, 619(1), L1–L6.

Martinet, N., Durret, F., Guennou, L., Adami, C., Biviano, A., Ulmer, M. P., Clowe, D., Halliday, C., Ilbert, O., Márquez, I., et al. (2015). The evolution of the cluster optical galaxy luminosity function between z = 0.4 and 0.9 in the DAFT/FADA survey. *Astronomy & Astrophysics*, 575, A116.

Masters, K. L., Nichol, R. C., Hoyle, B., Lintott, C., Bamford, S. P., Edmondson, E. M., Fortson, L., Keel, W. C., Schawinski, K., Smith, A. M., & Thomas, D. (2011). Galaxy Zoo: bars in disc galaxies. *Monthly Notices of the Royal Astronomical Society*, 411(3), 2026–2034.

Mather, J. C., Cheng, E. S., Eplee, R. E., J., Isaacman, R. B., Meyer, S. S., Shafer, R. A., Weiss, R., Wright, E. L., Bennett, C. L., Boggess, N. W., Dwek, E., Gulkis, S., Hauser, M. G., Janssen, M., Kelsall, T., Lubin, P. M., Moseley, S. H., J., Murdock, T. L., Silverberg, R. F., Smoot, G. F., & Wilkinson, D. T. (1990). A Preliminary Measurement of the Cosmic Microwave Background Spectrum by the Cosmic Background Explorer (COBE) Satellite. *Astrophysical Journal Letters*, 354, L37.

Matzner, C. D. (2002). On the Role of Massive Stars in the Support and Destruction of Giant Molecular Clouds. *The Astrophysical Journal*, 566(1), 302.

Mauskopf, P. D., Ade, P. A., Allen, S., Church, S., Edge, A., Ganga, K., Holzapfel, W., Lange, A., Rownd, B., Philhour, B., et al. (2000). A determination of the Hubble constant using measurements of X-ray emission and the Sunyaev-Zeldovich effect at millimeter wavelengths in the cluster Abell 1835. *The Astrophysical Journal*, 538(2), 505.

McAlpine, S., Bower, R. G., Harrison, C. M., Crain, R. A., Schaller, M., Schaye, J., & Theuns, T. (2017). The link between galaxy and black hole growth in the eagle simulation. *Monthly Notices of the Royal Astronomical Society*, 468(3), 3395–3407.

McCarthy, I. G., Frenk, C. S., Font, A. S., Lacey, C. G., Bower, R. G., Mitchell, N. L., Balogh, M. L., & Theuns, T. (2008). Ram pressure stripping the hot gaseous haloes of galaxies in groups and clusters. *Monthly Notices of the Royal Astronomical Society*, 383(2), 593–605.

Mehrtens, N., Romer, A. K., Hilton, M., Lloyd-Davies, E. J., Miller, C. J., Stanford, S. A., Hosmer, M., Hoyle, B., Collins, C. A., Liddle, A. R., Viana, P. T. P., Nichol, R. C., Stott, J. P., Dubois, E. N., Kay, S. T., Sahlén, M., Young, O., Short, C. J., Christodoulou, L., Watson, W. A., Davidson, M., Harrison, C. D., Baruah, L., Smith, M., Burke, C., Mayers, J. A., Deadman, P.-J., Rooney, P. J., Edmondson, E. M., West, M., Campbell, H. C., Edge, A. C., Mann, R. G., Sabirli, K., Wake, D., Benoist, C., da Costa, L., Maia, M. A. G., & Ogando, R. (2012). The XMM Cluster Survey: optical analysis methodology and the first data release. *Monthly Notices of the Royal Astronomical Society*, 423(2), 1024–1052.

Menanteau, F., Hughes, J. P., Sifón, C., Hilton, M., González, J., Infante, L., Barrientos, L. F., Baker, A. J., Bond, J. R., Das, S., Devlin, M. J., Dunkley, J., Hajian, A., Hincks, A. D., Kosowsky, A., Marsden, D., Marriage, T. A., Moodley, K., Niemack, M. D., Nolta, M. R., Page, L. A., Reese, E. D., Sehgal, N., Sievers, J., Spergel, D. N., Staggs, S. T., &

Wollack, E. (2012). THE ATACAMA COSMOLOGY TELESCOPE: ACT-CL J01024915 "EL GORDO," A MASSIVE MERGING CLUSTER AT REDSHIFT 0.87. *The Astrophysical Journal*, 748(1), 7.

Menci, N. & Fusco-Femiano, R. (1996). Galaxy Velocity Dispersion Profiles from Merging in Clusters. *The Astrophysical Journal*, 472, 46.

Merloni, A., Predehl, P., Becker, W., Böhringer, H., Boller, T., Brunner, H., Brusa, M., Dennerl, K., Freyberg, M., Friedrich, P., Georgakakis, A., Haberl, F., Hasinger, G., Meidinger, N., Mohr, J., Nandra, K., Rau, A., Reiprich, T. H., Robrade, J., Salvato, M., Santangelo, A., Sasaki, M., Schwope, A., Wilms, J., & German eROSITA Consortium, t. (2012). eROSITA Science Book: Mapping the Structure of the Energetic Universe. *arXiv e-prints*, (pp. arXiv:1209.3114).

Merritt, D. (1984). Relaxation and tidal stripping in rich clusters of galaxies. II. Evolution of the luminosity distribution. *Astrophysical Journal*, 276, 26–37.

Minkowski, R. & Abell, G. O. (1963). The Galactic Distribution of Planetary Nebulae. *Publications of the Astronomical Society of the Pacific*, 75(447), 488.

Mo, H., van den Bosch, F. C., & White, S. (2010). *Galaxy Formation and Evolution*.

Mo, H. J., Mao, S., & White, S. D. M. (1998). The formation of galactic discs. *Monthly Notices of the Royal Astronomical Society*, 295(2), 319–336.

Mohr, J. J., Mathiesen, B., & Evrard, A. E. (1999). Properties of the Intracluster Medium in an Ensemble of Nearby Galaxy Clusters. *The Astrophysical Journal*, 517(2), 627–649.

Montero-Dorta, A. D. & Prada, F. (2009). The SDSS DR6 luminosity functions of galaxies. *Monthly Notices of the Royal Astronomical Society*, 399(3), 1106–1118.

Moore, B., Katz, N., Lake, G., Dressler, A., & Oemler, A. (1996). Galaxy harassment and the evolution of clusters of galaxies. *nature*, 379(6566), 613–616.

Moore, B., Lake, G., & Katz, N. (1998). Morphological Transformation from Galaxy Harassment. *The Astrophysical Journal*, 495(1), 139.

Moretti, A., Bettoni, D., Poggianti, B. M., Fasano, G., Varela, J., D'Onofrio, M., Vulcani, B., Cava, A., Fritz, J., Couch, W. J., Moles, M., & Kjaergaard, P. (2015). VizieR Online Data Catalog: 72 WINGS nearby clusters luminosity functions (Moretti+, 2015). *VizieR Online Data Catalog*, (pp. J/A+A/581/A11).

Mroczkowski, T., Nagai, D., Basu, K., Chluba, J., Sayers, J., Adam, R., Churazov, E., Crites, A., Di Mascolo, L., Eckert, D., Macias-Perez, J., Mayet, F., Perotto, L., Pointecouteau, E., Romero, C., Ruppin, F., Scannapieco, E., & ZuHone, J. (2019). Astrophysics with the Spatially and Spectrally Resolved Sunyaev-Zeldovich Effects. A Millimetre/Submillimetre Probe of the Warm and Hot Universe. *Space Science Reviews*, 215(1), 17.

Muzzin, A., Wilson, G., Lacy, M., Yee, H., & Stanford, S. (2008). The Evolution of Dusty Star Formation and Stellar Mass Assembly in Clusters: Results from the IRAC 3.6, 4.5, 5.8, and 8.0 μm Cluster Luminosity Functions. *The Astrophysical Journal*, 686(2), 966.

Muzzin, A., Yee, H. K. C., Hall, P. B., Ellingson, E., & Lin, H. (2007). Near-Infrared Properties of Moderate-Redshift Galaxy Clusters: Luminosity Functions and Density Profiles. *The Astrophysical Journal*, 659(2), 1106.

Niemack, M. D., Ade, P. A. R., Aguirre, J., Barrientos, F., Beall, J. A., Bond, J. R., Britton, J., Cho, H. M., Das, S., Devlin, M. J., Dicker, S., Dunkley, J., Dünner, R., Fowler, J. W., Hajian, A., Halpern, M., Hasselfield, M., Hilton, G. C., Hilton, M., Hubmayr, J., Hughes, J. P., Infante, L., Irwin, K. D., Jarosik, N., Klein, J., Kosowsky, A., Marriage, T. A., McMahon, J., Menanteau, F., Moodley, K., Nibarger, J. P., Nolta, M. R., Page, L. A., Partridge, B., Reese, E. D., Sievers, J., Spergel, D. N., Staggs, S. T., Thornton, R., Tucker, C., Wollack, E., & Yoon, K. W. (2010). ACTPol: a polarization-sensitive receiver for the Atacama Cosmology Telescope. In W. S. Holland & J. Zmuidzinas (Eds.), *SPIE Proceedings*: SPIE.

Nomoto, K., Kobayashi, C., & Tominaga, N. (2013). Nucleosynthesis in Stars and the Chemical Enrichment of Galaxies. *Annual Review of Astronomy and Astrophysics*, 51(1), 457–509.

Ocvirk, P., Pichon, C., & Teyssier, R. (2008). Bimodal gas accretion in the Horizon–MareNostrum galaxy formation simulation. *Monthly Notices of the Royal Astronomical Society*, 390(4), 1326–1338.

Oemler, Augustus, J. (1974). The Systematic Properties of Clusters of Galaxies. Photometry of 15 Clusters. *The Astrophysical Journal*, 194, 1–20.

Oguri, M. (2014). A cluster finding algorithm based on the multiband identification of red sequence galaxies. *Monthly Notices of the Royal Astronomical Society*, 444(1), 147–161.

Oke, J. B. & Gunn, J. E. (1983). Secondary standard stars for absolute spectrophotometry. *Astrophysical Journal*, 266, 713–717.

Ostriker, E. C., McKee, C. F., & Leroy, A. K. (2010). Regulation of Star Formation Rates in Multiphase Galactic Disks: A Thermal/Dynamical Equilibrium Model. *The Astrophysical Journal*, 721(2), 975–994.

Ostriker, E. C. & Shetty, R. (2011). Maximally Star-forming Galactic Disks. I. Starburst Regulation Via Feedback-driven Turbulence. *The Astrophysical Journal*, 731(1), 41.

Ostriker, J. P. & Tremaine, S. D. (1975). Another evolutionary correction to the luminosity of giant galaxies. *Astrophysical Journal*, 202, L113–L117.

Pan, L., Padoan, P., Haugboelle, T., & Nordlund, A. (2016). The impact of supernova remnants on interstellar turbulence and star formation. In *Supernova Remnants: An Odyssey in Space after Stellar Death* (pp. 146).

Paolillo, M., Andreon, S., Longo, G., Puddu, E., Gal, R., Scaramella, R., Djorgovski, S., & De Carvalho, R. (2001). Luminosity function of clusters of galaxies. *Astronomy & Astrophysics*, 367(1), 59–71.

Park, J., Smith, R., & Yi, S. k. (2018). Star Formation of Merging Disk Galaxies with AGN Feedback Effects. In *American Astronomical Society Meeting Abstracts #231*, volume 231 of *American Astronomical Society Meeting Abstracts* (pp. 222.04).

Patterson, F. S. (1940). The Luminosity Gradient of Messier 33. *Harvard College Observatory Bulletin*, 914, 9–10.

Pearson, W. J., Wang, L., Alpaslan, M., Baldry, I., Bilicki, M., Brown, M. J. I., Grootes, M. W., Holwerda, B. W., Kitching, T. D., Kruk, S., & van der Tak, F. F. S. (2019). Effect of galaxy mergers on star-formation rates. *Astronomy & Astrophysics*, 631, A51.

Peebles, P. J. E. (1982). Large-scale background temperature and mass fluctuations due to scale-invariant primeval perturbations. *Astrophysical Journal*, 263, L1–L5.

Peebles, P. J. E. (1993). *Principles of Physical Cosmology*.

Peebles, P. J. E., Schramm, D. N., Turner, E. L., & Kron, R. G. (1991). The case for the relativistic hot Big Bang cosmology. *Nature*, 352(6338), 769–776.

Penzias, A. A. & Wilson, R. W. (1965). A Measurement of Excess Antenna Temperature at 4080 Mc/s. *Astrophysical Journal*, 142, 419–421.

Perlmutter, S., Aldering, G., Goldhaber, G., Knop, R. A., Nugent, P., Castro, P. G., Deustua, S., Fabbro, S., Goobar, A., Groom, D. E., Hook, I. M., Kim, A. G., Kim, M. Y., Lee, J. C., Nunes, N. J., Pain, R., Pennypacker, C. R., Quimby, R., Lidman, C., Ellis, R. S., Irwin, M., McMahon, R. G., Ruiz-Lapuente, P., Walton, N., Schaefer, B., Boyle, B. J., Filippenko, A. V., Matheson, T., Fruchter, A. S., Panagia, N., Newberg, H. J. M., Couch, W. J., & Project, T. S. C. (1999). Measurements of Ω and Λ from 42 High-Redshift Supernovae. *The Astrophysical Journal*, 517(2), 565–586.

Pillepich, A., Springel, V., Nelson, D., Genel, S., Naiman, J., Pakmor, R., Hernquist, L., Torrey, P., Vogelsberger, M., Weinberger, R., & Marinacci, F. (2017). Simulating galaxy

formation with the IllustrisTNG model. *Monthly Notices of the Royal Astronomical Society*, 473(3), 4077–4106.

Planck Collaboration, Ade, P. A. R., Aghanim, N., Armitage-Caplan, C., Arnaud, M., Ashdown, M., Atrio-Barandela, F., Aumont, J., Aussel, H., Baccigalupi, C., Banday, A. J., Barreiro, R. B., Barrena, R., Bartelmann, M., Bartlett, J. G., Battaner, E., Benabed, K., Benoît, A., Benoit-Lévy, A., Bernard, J. P., Bersanelli, M., Bielewicz, P., Bikmaev, I., Bobin, J., Bock, J. J., Böhringer, H., Bonaldi, A., Bond, J. R., Borrill, J., Bouchet, F. R., Bridges, M., Bucher, M., Burenin, R., Burigana, C., Butler, R. C., Cardoso, J. F., Carvalho, P., Catalano, A., Challinor, A., Chamballu, A., Chary, R. R., Chen, X., Chiang, H. C., Chiang, L. Y., Chon, G., Christensen, P. R., Churazov, E., Church, S., Clements, D. L., Colombi, S., Colombo, L. P. L., Comis, B., Couchot, F., Coulais, A., Crill, B. P., Curto, A., Cuttaia, F., Da Silva, A., Dahle, H., Danese, L., Davies, R. D., Davis, R. J., de Bernardis, P., de Rosa, A., de Zotti, G., Delabrouille, J., Delouis, J. M., Démoclès, J., Désert, F. X., Dickinson, C., Diego, J. M., Dolag, K., Dole, H., Donzelli, S., Doré, O., Douspis, M., Dupac, X., Efstathiou, G., Eisenhardt, P. R. M., Enßlin, T. A., Eriksen, H. K., Feroz, F., Finelli, F., Flores-Cacho, I., Forni, O., Frailis, M., Franceschi, E., Fromenteau, S., Galeotta, S., Ganga, K., Génova-Santos, R. T., Giard, M., Giardino, G., Gilfanov, M., Giraud-Héraud, Y., González-Nuevo, J., Górski, K. M., Grainge, K. J. B., Gratton, S., Gregorio, A., Groeneboom, N., E., Gruppuso, A., Hansen, F. K., Hanson, D., Harrison, D., Hempel, A., Henrot-Versillé, S., Hernández-Monteagudo, C., Herranz, D., Hildebrandt, S. R., Hivon, E., Hobson, M., Holmes, W. A., Hornstrup, A., Hovest, W., Huffenberger, K. M., Hurier, G., Hurley-Walker, N., Jaffe, A. H., Jaffe, T. R., Jones, W. C., Juvela, M., Keihänen, E., Keskitalo, R., Khamitov, I., Kisner, T. S., Kneissl, R., Knoche, J., Knox, L., Kunz, M., Kurki-Suonio, H., Lagache, G., Lähteenmäki, A., Lamarre, J. M., Lasenby, A., Laureijs, R. J., Lawrence, C. R., Leahy, J. P., Leonardi, R., León-Tavares, J., Lesgourgues, J., Li, C., Liddle, A., Liguori, M., Lilje, P. B., Linden-Vørnle, M., López-Caniego, M., Lubin, P. M., Macías-Pérez, J. F., MacTavish, C. J., Maffei, B., Maino, D., Mandolesi, N., Maris, M., Marshall, D. J., Martin, P. G., Martínez-

González, E., Masi, S., Massardi, M., Matarrese, S., Matthai, F., Mazzotta, P., Mei, S., Meinhold, P. R., Melchiorri, A., Melin, J. B., Mendes, L., Mennella, A., Migliaccio, M., Mikkelsen, K., Mitra, S., Miville-Deschênes, M. A., Moneti, A., Montier, L., Morgante, G., Mortlock, D., Munshi, D., Murphy, J. A., Naselsky, P., Nati, F., Natoli, P., Nesvadba, N. P. H., Netterfield, C. B., Nørgaard-Nielsen, H. U., Noviello, F., Novikov, D., Novikov, I., O'Dwyer, I. J., Olamaie, M., Osborne, S., Oxborrow, C. A., Paci, F., Pagano, L., Pajot, F., Paoletti, D., Pasian, F., Patanchon, G., Pearson, T. J., Perdereau, O., Perotto, L., Perrott, Y. C., Perrotta, F., Piacentini, F., Piat, M., Pierpaoli, E., Pietrobon, D., Plaszczynski, S., Pointecouteau, E., Polenta, G., Ponthieu, N., Popa, L., Poutanen, T., Pratt, G. W., Prézeau, G., Prunet, S., Puget, J. L., Rachen, J. P., Reach, W. T., Rebolo, R., Reinecke, M., Remazeilles, M., Renault, C., Ricciardi, S., Riller, T., Ristorcelli, I., Rocha, G., Rosset, C., Roudier, G., Rowan-Robinson, M., Rubiño-Martín, J. A., Rumsey, C., Rusholme, B., Sandri, M., Santos, D., Saunders, R. D. E., Savini, G., Schammel, M. P., Scott, D., Seiffert, M. D., Shellard, E. P. S., Shimwell, T. W., Spencer, L. D., Stanford, S. A., Starck, J. L., Stolyarov, V., Stompor, R., Sudiwala, R., Sunyaev, R., Sureau, F., Sutton, D., Suur-Uski, A. S., Sygnet, J. F., Tauber, J. A., Tavagnacco, D., Terenzi, L., Toffolatti, L., Tomasi, M., Tristram, M., Tucci, M., Tuovinen, J., Türler, M., Umana, G., Valenziano, L., Valiviita, J., Van Tent, B., Vibert, L., Vielva, P., Villa, F., Vittorio, N., Wade, L. A., Wandelt, B. D., White, M., White, S. D. M., Yvon, D., Zacchei, A., & Zonca, A. (2014a). Planck 2013 results. XXIX. The Planck catalogue of Sunyaev-Zeldovich sources. *Astronomy & Astrophysics*, 571, A29.

Planck Collaboration, Ade, P. A. R., Aghanim, N., Armitage-Caplan, C., Arnaud, M., Ashdown, M., Atrio-Barandela, F., Aumont, J., Baccigalupi, C., Banday, A. J., Barreiro, R. B., Bartlett, J. G., Battaner, E., Benabed, K., Benoît, A., Benoit-Lévy, A., Bernard, J. P., Bersanelli, M., Bielewicz, P., Bobin, J., Bock, J. J., Bonaldi, A., Bond, J. R., Borrill, J., Bouchet, F. R., Bridges, M., Bucher, M., Burigana, C., Butler, R. C., Calabrese, E., Cappellini, B., Cardoso, J. F., Catalano, A., Challinor, A., Chamballu, A., Chary, R. R., Chen, X., Chiang, H. C., Chiang, L. Y., Christensen, P. R., Church, S., Clements, D. L.,

Colombi, S., Colombo, L. P. L., Couchot, F., Coulais, A., Crill, B. P., Curto, A., Cuttaia, F., Danese, L., Davies, R. D., Davis, R. J., de Bernardis, P., de Rosa, A., de Zotti, G., Delabrouille, J., Delouis, J. M., Désert, F. X., Dickinson, C., Diego, J. M., Dolag, K., Dole, H., Donzelli, S., Doré, O., Douspis, M., Dunkley, J., Dupac, X., Efstathiou, G., Elsner, F., Enßlin, T. A., Eriksen, H. K., Finelli, F., Forni, O., Frailis, M., Fraisse, A. A., Franceschi, E., Gaier, T. C., Galeotta, S., Galli, S., Ganga, K., Giard, M., Giardino, G., Giraud-Héraud, Y., Gjerløw, E., González-Nuevo, J., Górski, K. M., Gratton, S., Gregorio, A., Gruppuso, A., Gudmundsson, J. E., Haissinski, J., Hamann, J., Hansen, F. K., Hanson, D., Harrison, D., Henrot-Versillé, S., Hernández-Monteagudo, C., Herranz, D., Hildebrandt, S. R., Hivon, E., Hobson, M., Holmes, W. A., Hornstrup, A., Hou, Z., Hovest, W., Huffenberger, K. M., Jaffe, A. H., Jaffe, T. R., Jewell, J., Jones, W. C., Juvela, M., Keihänen, E., Keskitalo, R., Kisner, T. S., Kneissl, R., Knoche, J., Knox, L., Kunz, M., Kurki-Suonio, H., Lagache, G., Lähteenmäki, A., Lamarre, J. M., Lasenby, A., Lattanzi, M., Laureijs, R. J., Lawrence, C. R., Leach, S., Leahy, J. P., Leonardi, R., León-Tavares, J., Lesgourgues, J., Lewis, A., Liguori, M., Lilje, P. B., Linden-Vørnle, M., López-Caniego, M., Lubin, P. M., Macías-Pérez, J. F., Maffei, B., Maino, D., Mandolesi, N., Maris, M., Marshall, D. J., Martin, P. G., Martínez-González, E., Masi, S., Massardi, M., Matarrese, S., Matthai, F., Mazzotta, P., Meinhold, P. R., Melchiorri, A., Melin, J. B., Mendes, L., Menegoni, E., Mennella, A., Migliaccio, M., Millea, M., Mitra, S., Miville-Deschênes, M. A., Moneti, A., Montier, L., Morgante, G., Mortlock, D., Moss, A., Munshi, D., Murphy, J. A., Naselsky, P., Nati, F., Natoli, P., Netterfield, C. B., Nørgaard-Nielsen, H. U., Noviello, F., Novikov, D., Novikov, I., O'Dwyer, I. J., Osborne, S., Oxborrow, C. A., Paci, F., Pagano, L., Pajot, F., Paladini, R., Paoletti, D., Partridge, B., Pasian, F., Patanchon, G., Pearson, D., Pearson, T. J., Peiris, H. V., Perdereau, O., Perotto, L., Perrotta, F., Pettorino, V., Piacentini, F., Piat, M., Pierpaoli, E., Pietrobon, D., Plaszczynski, S., Platania, P., Pointecouteau, E., Polenta, G., Ponthieu, N., Popa, L., Poutanen, T., Pratt, G. W., Prézeau, G., Prunet, S., Puget, J. L., Rachen, J. P., Reach, W. T., Rebolo, R., Reinecke, M., Remazeilles, M., Renault, C., Ricciardi, S., Riller, T., Ristorcelli, I., Rocha,

G., Rosset, C., Roudier, G., Rowan-Robinson, M., Rubiño-Martín, J. A., Rusholme, B., Sandri, M., Santos, D., Savelainen, M., Savini, G., Scott, D., Seiffert, M. D., Shellard, E. P. S., Spencer, L. D., Starck, J. L., Stolyarov, V., Stompor, R., Sudiwala, R., Sunyaev, R., Sureau, F., Sutton, D., Suur-Uski, A. S., Sygnet, J. F., Tauber, J. A., Tavagnacco, D., Terenzi, L., Toffolatti, L., Tomasi, M., Tristram, M., Tucci, M., Tuovinen, J., Türler, M., Umana, G., Valenziano, L., Valiviita, J., Van Tent, B., Vielva, P., Villa, F., Vittorio, N., Wade, L. A., Wandelt, B. D., Wehus, I. K., White, M., White, S. D. M., Wilkinson, A., Yvon, D., Zacchei, A., & Zonca, A. (2014b). Planck 2013 results. XVI. Cosmological parameters. *Astronomy & Astrophysics*, 571, A16.

Planck Collaboration, Ade, P. A. R., Aghanim, N., Arnaud, M., Ashdown, M., Aumont, J., Baccigalupi, C., Banday, A. J., Barreiro, R. B., Barrena, R., Bartlett, J. G., Bartolo, N., Battaner, E., Battye, R., Benabed, K., Benoît, A., Benoit-Lévy, A., Bernard, J. P., Bersanelli, M., Bielewicz, P., Bikmaev, I., Böhringer, H., Bonaldi, A., Bonavera, L., Bond, J. R., Borrill, J., Bouchet, F. R., Bucher, M., Burenin, R., Burigana, C., Butler, R. C., Calabrese, E., Cardoso, J. F., Carvalho, P., Catalano, A., Challinor, A., Chamballu, A., Chary, R. R., Chiang, H. C., Chon, G., Christensen, P. R., Clements, D. L., Colombi, S., Colombo, L. P. L., Combet, C., Comis, B., Couchot, F., Coulais, A., Crill, B. P., Curto, A., Cuttaia, F., Dahle, H., Danese, L., Davies, R. D., Davis, R. J., de Bernardis, P., de Rosa, A., de Zotti, G., Delabrouille, J., Désert, F. X., Dickinson, C., Diego, J. M., Dolag, K., Dole, H., Donzelli, S., Doré, O., Douspis, M., Ducout, A., Dupac, X., Efstathiou, G., Eisenhardt, P. R. M., Elsner, F., Enßlin, T. A., Eriksen, H. K., Falgarone, E., Fergusson, J., Feroz, F., Ferragamo, A., Finelli, F., Forni, O., Frailis, M., Fraisse, A. A., Franceschi, E., Frejsel, A., Galeotta, S., Galli, S., Ganga, K., Génova-Santos, R. T., Giard, M., Giraud-Héraud, Y., Gjerløw, E., González-Nuevo, J., Górski, K. M., Grainge, K. J. B., Gratton, S., Gregorio, A., Gruppuso, A., Gudmundsson, J. E., Hansen, F. K., Hanson, D., Harrison, D. L., Hempel, A., Henrot-Versillé, S., Hernández-Monteagudo, C., Herranz, D., Hildebrandt, S. R., Hivon, E., Hobson, M., Holmes, W. A., Hornstrup, A., Hovest, W., Huffenberger, K. M., Hurier, G., Jaffe, A. H., Jaffe, T. R., Jin, T., Jones, W. C.,

Juvela, M., Keihänen, E., Keskitalo, R., Khamitov, I., Kisner, T. S., Kneissl, R., Knoche, J., Kunz, M., Kurki-Suonio, H., Lagache, G., Lamarre, J. M., Lasenby, A., Lattanzi, M., Lawrence, C. R., Leonardi, R., Lesgourgues, J., Levrier, F., Liguori, M., Lilje, P. B., Linden-Vørnle, M., López-Caniego, M., Lubin, P. M., Macías-Pérez, J. F., Maggio, G., Maino, D., Mak, D. S. Y., Mandolesi, N., Mangilli, A., Martin, P. G., Martínez-González, E., Masi, S., Matarrese, S., Mazzotta, P., McGehee, P., Mei, S., Melchiorri, A., Melin, J. B., Mendes, L., Mennella, A., Migliaccio, M., Mitra, S., Miville-Deschênes, M. A., Moneti, A., Montier, L., Morgante, G., Mortlock, D., Moss, A., Munshi, D., Murphy, J. A., Naselsky, P., Nastasi, A., Nati, F., Natoli, P., Netterfield, C. B., Nørgaard-Nielsen, H. U., Noviello, F., Novikov, D., Novikov, I., Olamaie, M., Oxborrow, C. A., Paci, F., Pagano, L., Pajot, F., Paoletti, D., Pasian, F., Patanchon, G., Pearson, T. J., Perdereau, O., Perotto, L., Perrott, Y. C., Perrotta, F., Pettorino, V., Piacentini, F., Piat, M., Pierpaoli, E., Pietrobon, D., Plaszczynski, S., Pointecouteau, E., Polenta, G., Pratt, G. W., Prézeau, G., Prunet, S., Puget, J. L., Rachen, J. P., Reach, W. T., Rebolo, R., Reinecke, M., Remazeilles, M., Renault, C., Renzi, A., Ristorcelli, I., Rocha, G., Rosset, C., Rossetti, M., Roudier, G., Rozo, E., Rubiño-Martín, J. A., Rumsey, C., Rusholme, B., Rykoff, E. S., Sandri, M., Santos, D., Saunders, R. D. E., Savelainen, M., Savini, G., Schammel, M. P., Scott, D., Seiffert, M. D., Shellard, E. P. S., Shimwell, T. W., Spencer, L. D., Stanford, S. A., Stern, D., Stolyarov, V., Stompor, R., Streblyanska, A., Sudiwala, R., Sunyaev, R., Sutton, D., Suur-Uski, A. S., Sygnet, J. F., Tauber, J. A., Terenzi, L., Toffolatti, L., Tomasi, M., Tramonte, D., Tristram, M., Tucci, M., Tuovinen, J., Umana, G., Valenziano, L., Valiviita, J., Van Tent, B., Vielva, P., Villa, F., Wade, L. A., Wandelt, B. D., Wehus, I. K., White, S. D. M., Wright, E. L., Yvon, D., Zacchei, A., & Zonca, A. (2016a). Planck 2015 results. XXVII. The second Planck catalogue of Sunyaev-Zeldovich sources. *Astronomy & Astrophysics*, 594, A27.

Planck Collaboration, Ade, P. A. R., Aghanim, N., Arnaud, M., Ashdown, M., Aumont, J., Baccigalupi, C., Banday, A. J., Barreiro, R. B., Bartlett, J. G., Bartolo, N., Battaner, E., Battye, R., Benabed, K., Benoît, A., Benoit-Lévy, A., Bernard, J. P., Bersanelli, M.,

Bielewicz, P., Bock, J. J., Bonaldi, A., Bonavera, L., Bond, J. R., Borrill, J., Bouchet, F. R., Boulanger, F., Bucher, M., Burigana, C., Butler, R. C., Calabrese, E., Cardoso, J. F., Catalano, A., Challinor, A., Chamballu, A., Chary, R. R., Chiang, H. C., Chluba, J., Christensen, P. R., Church, S., Clements, D. L., Colombi, S., Colombo, L. P. L., Combet, C., Coulais, A., Crill, B. P., Curto, A., Cuttaia, F., Danese, L., Davies, R. D., Davis, R. J., de Bernardis, P., de Rosa, A., de Zotti, G., Delabrouille, J., Désert, F. X., Di Valentino, E., Dickinson, C., Diego, J. M., Dolag, K., Dole, H., Donzelli, S., Doré, O., Douspis, M., Ducout, A., Dunkley, J., Dupac, X., Efstathiou, G., Elsner, F., Enßlin, T. A., Eriksen, H. K., Farhang, M., Fergusson, J., Finelli, F., Forni, O., Frailis, M., Fraisse, A. A., Franceschi, E., Frejsel, A., Galeotta, S., Galli, S., Ganga, K., Gauthier, C., Gerbino, M., Ghosh, T., Giard, M., Giraud-Héraud, Y., Giusarma, E., Gjerløw, E., González-Nuevo, J., Górski, K. M., Gratton, S., Gregorio, A., Gruppuso, A., Gudmundsson, J. E., Hamann, J., Hansen, F. K., Hanson, D., Harrison, D. L., Helou, G., Henrot-Versillé, S., Hernández-Monteagudo, C., Herranz, D., Hildebrandt, S. R., Hivon, E., Hobson, M., Holmes, W. A., Hornstrup, A., Hovest, W., Huang, Z., Huffenberger, K. M., Hurier, G., Jaffe, A. H., Jaffe, T. R., Jones, W. C., Juvela, M., Keihänen, E., Keskitalo, R., Kisner, T. S., Kneissl, R., Knoche, J., Knox, L., Kunz, M., Kurki-Suonio, H., Lagache, G., Lähteenmäki, A., Lamarre, J. M., Lasenby, A., Lattanzi, M., Lawrence, C. R., Leahy, J. P., Leonardi, R., Lesgourgues, J., Levrier, F., Lewis, A., Liguori, M., Lilje, P. B., Linden-Vørnle, M., López-Caniego, M., Lubin, P. M., Macías-Pérez, J. F., Maggio, G., Maino, D., Mandolesi, N., Mangilli, A., Marchini, A., Maris, M., Martin, P. G., Martinelli, M., Martínez-González, E., Masi, S., Matarrese, S., McGehee, P., Meinhold, P. R., Melchiorri, A., Melin, J. B., Mendes, L., Mennella, A., Migliaccio, M., Millea, M., Mitra, S., Miville-Deschênes, M. A., Moneti, A., Montier, L., Morgante, G., Mortlock, D., Moss, A., Munshi, D., Murphy, J. A., Naselsky, P., Nati, F., Natoli, P., Netterfield, C. B., Nørgaard-Nielsen, H. U., Noviello, F., Novikov, D., Novikov, I., Oxborrow, C. A., Paci, F., Pagano, L., Pajot, F., Paladini, R., Paoletti, D., Partridge, B., Pasian, F., Patanchon, G., Pearson, T. J., Perdereau, O., Perotto, L., Perrotta, F., Pettorino, V., Piacentini, F., Piat, M.,

Pierpaoli, E., Pietrobon, D., Plaszczynski, S., Pointecouteau, E., Polenta, G., Popa, L., Pratt, G. W., Prézeau, G., Prunet, S., Puget, J. L., Rachen, J. P., Reach, W. T., Rebolo, R., Reinecke, M., Remazeilles, M., Renault, C., Renzi, A., Ristorcelli, I., Rocha, G., Rosset, C., Rossetti, M., Roudier, G., Rouillé d'Orfeuil, B., Rowan-Robinson, M., Rubiño-Martín, J. A., Rusholme, B., Said, N., Salvatelli, V., Salvati, L., Sandri, M., Santos, D., Savelainen, M., Savini, G., Scott, D., Seiffert, M. D., Serra, P., Shellard, E. P. S., Spencer, L. D., Spinelli, M., Stolyarov, V., Stompor, R., Sudiwala, R., Sunyaev, R., Sutton, D., Suur-Uski, A. S., Sygnet, J. F., Tauber, J. A., Terenzi, L., Toffolatti, L., Tomasi, M., Tristram, M., Trombetti, T., Tucci, M., Tuovinen, J., Türler, M., Umana, G., Valenziano, L., Valiviita, J., Van Tent, F., Vielva, P., Villa, F., Wade, L. A., Wandelt, B. D., Wehus, I. K., White, M., White, S. D. M., Wilkinson, A., Yvon, D., Zacchei, A., & Zonca, A. (2016b). Planck 2015 results. XIII. Cosmological parameters. *Astronomy & Astrophysics*, 594, A13.

Planck Collaboration, Aghanim, N., Akrami, Y., Ashdown, M., Aumont, J., Baccigalupi, C., Ballardini, M., Banday, A. J., Barreiro, R. B., Bartolo, N., Basak, S., Battye, R., Benabed, K., Bernard, J. P., Bersanelli, M., Bielewicz, P., Bock, J. J., Bond, J. R., Borrill, J., Bouchet, F. R., Boulanger, F., Bucher, M., Burigana, C., Butler, R. C., Calabrese, E., Cardoso, J. F., Carron, J., Challinor, A., Chiang, H. C., Chluba, J., Colombo, L. P. L., Combet, C., Contreras, D., Crill, B. P., Cuttaia, F., de Bernardis, P., de Zotti, G., Delabrouille, J., Delouis, J. M., Di Valentino, E., Diego, J. M., Doré, O., Douspis, M., Ducout, A., Dupac, X., Dusini, S., Efstathiou, G., Elsner, F., Enßlin, T. A., Eriksen, H. K., Fantaye, Y., Farhang, M., Fergusson, J., Fernandez-Cobos, R., Finelli, F., Forastieri, F., Frailis, M., Fraisse, A. A., Franceschi, E., Frolov, A., Galeotta, S., Galli, S., Ganga, K., Génova-Santos, R. T., Gerbino, M., Ghosh, T., González-Nuevo, J., Górski, K. M., Gratton, S., Gruppuso, A., Gudmundsson, J. E., Hamann, J., Handley, W., Hansen, F. K., Herranz, D., Hildebrandt, S. R., Hivon, E., Huang, Z., Jaffe, A. H., Jones, W. C., Karakci, A., Keihänen, E., Keskitalo, R., Kiiveri, K., Kim, J., Kisner, T. S., Knox, L., Krachmalnicoff, N., Kunz, M., Kurki-Suonio, H., Lagache, G., Lamarre, J. M., Lasenby,

A., Lattanzi, M., Lawrence, C. R., Le Jeune, M., Lemos, P., Lesgourgues, J., Levrier, F., Lewis, A., Liguori, M., Lilje, P. B., Lilley, M., Lindholm, V., López-Caniego, M., Lubin, P. M., Ma, Y. Z., Macías-Pérez, J. F., Maggio, G., Maino, D., Mandolesi, N., Mangilli, A., Marcos-Caballero, A., Maris, M., Martin, P. G., Martinelli, M., Martínez-González, E., Matarrese, S., Mauri, N., McEwen, J. D., Meinhold, P. R., Melchiorri, A., Mennella, A., Migliaccio, M., Millea, M., Mitra, S., Miville-Deschênes, M. A., Molinari, D., Montier, L., Morgante, G., Moss, A., Natoli, P., Nørgaard-Nielsen, H. U., Pagano, L., Paoletti, D., Partridge, B., Patanchon, G., Peiris, H. V., Perrotta, F., Pettorino, V., Piacentini, F., Polastri, L., Polenta, G., Puget, J. L., Rachen, J. P., Reinecke, M., Remazeilles, M., Renzi, A., Rocha, G., Rosset, C., Roudier, G., Rubiño-Martín, J. A., Ruiz-Granados, B., Salvati, L., Sandri, M., Savelainen, M., Scott, D., Shellard, E. P. S., Sirignano, C., Sirri, G., Spencer, L. D., Sunyaev, R., Suur-Uski, A. S., Tauber, J. A., Tavagnacco, D., Tenti, M., Toffolatti, L., Tomasi, M., Trombetti, T., Valenziano, L., Valiviita, J., Van Tent, B., Vibert, L., Vielva, P., Villa, F., Vittorio, N., Wandelt, B. D., Wehus, I. K., White, M., White, S. D. M., Zacchei, A., & Zonca, A. (2020). Planck 2018 results. VI. Cosmological parameters. *Astronomy & Astrophysics*, 641, A6.

Poggianti, B. M., Jaffé, Y. L., Moretti, A., Gullieuszik, M., Radovich, M., Tonnesen, S., Fritz, J., Bettoni, D., Vulcani, B., Fasano, G., Bellhouse, C., Hau, G., & Omizzolo, A. (2017). Ram-pressure feeding of supermassive black holes. *Nature*, 548(7667), 304–309.

Popesso, P., Biviano, A., Böhringer, H., & Romaniello, M. (2006). RASS-SDSS Galaxy cluster survey. IV. A ubiquitous dwarf galaxy population in clusters. *Astronomy & Astrophysics*, 445(1), 29–42.

Postman, M., Lubin, L. M., Gunn, J. E., Oke, J. B., Hoessel, J. G., Schneider, D. P., & Christensen, J. A. (1996). The Palomar Distant Clusters Survey. I. The Cluster Catalog. *The Astronomical Journal*, 111, 615.

Predehl, P., Andritschke, R., Arefiev, V., Babyshkin, V., Batanov, O., Becker, W.,

Böhringer, H., Bogomolov, A., Boller, T., Borm, K., et al. (2021). The eROSITA X-ray telescope on SRG. *Astronomy & Astrophysics*, 647, A1.

Puchwein, E. & Springel, V. (2013). Shaping the galaxy stellar mass function with supernova- and AGN-driven winds. *Monthly Notices of the Royal Astronomical Society*, 428(4), 2966–2979.

Puddu, E., Radovich, M., Sereno, M., Bardelli, S., Maturi, M., Moscardini, L., Bellagamba, F., Giocoli, C., Marulli, F., & Roncarelli, M. (2021). AMICO galaxy clusters in KiDS-DR3: Evolution of the luminosity function between z = 0.1 and z = 0.8. *Astronomy & Astrophysics*, 645, A9.

Radovich, M., Poggianti, B., Jaffé, Y. L., Moretti, A., Bettoni, D., Gullieuszik, M., Vulcani, B., & Fritz, J. (2019). GASP – XIX. AGN and their outflows at the centre of jellyfish galaxies. *Monthly Notices of the Royal Astronomical Society*, 486(1), 486–503.

Rakos, K. D., Schombert, J. M., Odell, A. P., & Steindling, S. (2000). Cluster Populations in A115 and A2283. *The Astrophysical Journal*, 540(2), 715.

Reid, B. A. & Spergel, D. N. (2006). Sunyaev-Zel'dovich effect signals in cluster models. *The Astrophysical Journal*, 651(2), 643.

Reid, I. N., Brewer, C., Brucato, R. J., McKinley, W. R., Maury, A., Mendenhall, D., Mould, J. R., Mueller, J., Neugebauer, G., Phinney, J., Sargent, W. L. W., Schombert, J., & Thicksten, R. (1991). THE SECOND PALOMAR SKY SURVEY. *Publications of the Astronomical Society of the Pacific*, 103(665), 661.

Riess, A. G., Filippenko, A. V., Challis, P., Clocchiatti, A., Diercks, A., Garnavich, P. M., Gilliland, R. L., Hogan, C. J., Jha, S., Kirshner, R. P., Leibundgut, B., Phillips, M. M., Reiss, D., Schmidt, B. P., Schommer, R. A., Smith, R. C., Spyromilio, J., Stubbs, C., Suntzeff, N. B., & Tonry, J. (1998). Observational Evidence from Supernovae for an Accelerating Universe and a Cosmological Constant. *The Astronomical Journal*, 116(3), 1009–1038.

Riess, A. G., Macri, L. M., Hoffmann, S. L., Scolnic, D., Casertano, S., Filippenko, A. V., Tucker, B. E., Reid, M. J., Jones, D. O., Silverman, J. M., Chornock, R., Challis, P., Yuan, W., Brown, P. J., & Foley, R. J. (2016). A 2.4% Determination of the Local Value of the Hubble Constant. *The Astrophysical Journal*, 826(1), 56.

Rines, K. & Geller, M. J. (2008). SPECTROSCOPIC DETERMINATION OF THE LUMINOSITY FUNCTION IN THE GALAXY CLUSTERS A2199 AND VIRGO. *The Astronomical Journal*, 135(5), 1837.

Roberts, I. D. & Parker, L. C. (2020). Ram pressure stripping candidates in the coma cluster: evidence for enhanced star formation. *Monthly Notices of the Royal Astronomical Society*, 495(1), 554–569.

Roberts, I. D., Parker, L. C., Gwyn, S., Hudson, M. J., Carlberg, R., McConnachie, A., Cuillandre, J.-C., Chambers, K. C., Duc, P.-A., Furusawa, H., Gavazzi, R., Hill, V., Huber, M. E., Ibata, R., Kilbinger, M., Mei, S., Mellier, Y., Miyazaki, S., Oguri, M., & Wainscoat, R. J. (2022). Ram pressure candidates in UNIONS. *Monthly Notices of the Royal Astronomical Society*, 509(1), 1342–1357.

Rodríguez Montero, F., Davé, R., Wild, V., Anglés-Alcázar, D., & Narayanan, D. (2019). Mergers, starbursts, and quenching in the simba simulation. *Monthly Notices of the Royal Astronomical Society*, 490(2), 2139–2154.

Romer, A. K., Viana, P. T. P., Liddle, A. R., & Mann, R. G. (2001). A Serendipitous Galaxy Cluster Survey with XMM: Expected Catalog Properties and Scientific Applications. *The Astrophysical Journal*, 547(2), 594.

Rood, H. J. & Sastry, G. N. (1971). "Tuning Fork" Classification of Rich Clusters of Galaxies. *Publications of the Astronomical Society of the Pacific*, 83(493), 313.

Roos, N. (1981). *Galaxy mergers*. PhD thesis, University of Leiden, Netherlands.

Rosati, P., Della Ceca, R., Norman, C., & Giacconi, R. (1997). The ROSAT deep cluster survey: the X-ray luminosity function out to z = 0.8. *The Astrophysical Journal*, 492(1), L21.

Rubin, V. C., Ford, W. K., J., & Thonnard, N. (1980). Rotational properties of 21 SC galaxies with a large range of luminosities and radii, from NGC 4605 (R=4kpc) to UGC 2885 (R=122kpc). *Astrophysical Journal*, 238, 471–487.

Rudnick, G., von der Linden, A., Pelló, R., Aragón-Salamanca, A., Marchesini, D., Clowe, D., Lucia, G. D., Halliday, C., Jablonka, P., Milvang-Jensen, B., Poggianti, B., Saglia, R., Simard, L., White, S., & Zaritsky, D. (2009). THE REST-FRAME OPTICAL LUMINOSITY FUNCTION OF CLUSTER GALAXIES AT z $<$ 0.8 AND THE ASSEMBLY OF THE CLUSTER RED SEQUENCE*. *The Astrophysical Journal*, 700(2), 1559.

Ruhl, J., Ade, P. A. R., Carlstrom, J. E., Cho, H.-M., Crawford, T., Dobbs, M., Greer, C. H., w. Halverson, N., Holzapfel, W. L., Lanting, T. M., Lee, A. T., Leitch, E. M., Leong, J., Lu, W., Lueker, M., Mehl, J., Meyer, S. S., Mohr, J. J., Padin, S., Plagge, T., Pryke, C., Runyan, M. C., Schwan, D., Sharp, M. K., Spieler, H., Staniszewski, Z., & Stark, A. A. (2004). The South Pole Telescope. In J. Zmuidzinas, W. S. Holland, & S. Withington (Eds.), *Millimeter and Submillimeter Detectors for Astronomy II*: SPIE.

Rykoff, E. S., Rozo, E., Busha, M. T., Cunha, C. E., Finoguenov, A., Evrard, A., Hao, J., Koester, B. P., Leauthaud, A., Nord, B., Pierre, M., Reddick, R., Sadibekova, T., Sheldon, E. S., & Wechsler, R. H. (2014). redMaPPer. I. Algorithm and SDSS DR8 Catalog. *The Astrophysical Journal*, 785(2), 104.

Rykoff, E. S., Rozo, E., Hollowood, D., Bermeo-Hernandez, A., Jeltema, T., Mayers, J., Romer, A. K., Rooney, P., Saro, A., Cervantes, C. V., & et al. (2016). THE REDMAPPER GALAXY CLUSTER CATALOG FROM DES SCIENCE VERIFICATION DATA. *The Astrophysical Journal Supplement Series*, 224(1), 1.

Salucci, P., Lapi, A., Tonini, C., Gentile, G., Yegorova, I., & Klein, U. (2007). The universal

rotation curve of spiral galaxies – II. The dark matter distribution out to the virial radius. *Monthly Notices of the Royal Astronomical Society*, 378(1), 41–47.

Sandage, A. (1961). The Ability of the 200-INCH Telescope to Discriminate Between Selected World Models. *Astrophysical Journal*, 133, 355.

Sarazin, C. L. (1986). X-ray emission from clusters of galaxies. *Rev. Mod. Phys.*, 58, 1–115.

Sarmento, R. & Scannapieco, E. (2022). The Effects of Radiative Feedback and Supernova-induced Turbulence on Early Galaxies. *The Astrophysical Journal*, 935(2), 174.

Schaller, G., Schaerer, D., Meynet, G., & Maeder, A. (1992). New Grids of Stellar Models from 0.8-SOLAR-MASS to 120-SOLAR-MASSES at Z=0.020 and Z=0.001. *Astronomy and Astrophysics Supplement Series*, 96, 269.

Schawinski, K., Urry, C. M., Simmons, B. D., Fortson, L., Kaviraj, S., Keel, W. C., Lintott, C. J., Masters, K. L., Nichol, R. C., Sarzi, M., Skibba, R., Treister, E., Willett, K. W., Wong, O. I., & Yi, S. K. (2014). The green valley is a red herring: Galaxy Zoo reveals two evolutionary pathways towards quenching of star formation in early- and late-type galaxies. *Monthly Notices of the Royal Astronomical Society*, 440(1), 889–907.

Schechter, P. (1976). An analytic expression for the luminosity function for galaxies. *The Astrophysical Journal*, 203, 297–306.

Schlegel, D., Dey, A., Herrera, D., Juneau, S., Landriau, M., Lang, D., Meisner, A., Moustakas, J., Myers, A., Schlafly, E., Valdes, F., Weaver, B., Zhang, M., Zhou, R., & DESI Legacy Imaging Surveys Team (2021). DESI Legacy Imaging Surveys Data Release 9. In *American Astronomical Society Meeting Abstracts*, volume 53 of *American Astronomical Society Meeting Abstracts* (pp. 235.03).

Schneider, D. P., Schmidt, M., & Gunn, J. E. (1993). The Palomar Transit GRISM Survey. In *American Astronomical Society Meeting Abstracts*, volume 183 of *American Astronomical Society Meeting Abstracts* (pp. 72.03).

Schulze, F., Remus, R.-S., Dolag, K., Burkert, A., Emsellem, E., & van de Ven, G. (2018). Kinematics of simulated galaxies - I. Connecting dynamical and morphological properties of early-type galaxies at different redshifts. *Monthly Notices of the Royal Astronomical Society*, 480(4), 4636–4658.

Schwartz, D. A. (2004). THE DEVELOPMENT AND SCIENTIFIC IMPACT OF THE CHANDRA X-RAY OBSERVATORY. *International Journal of Modern Physics D*, 13(07), 1239–1247.

Sehgal, N., Bode, P., Das, S., Hernandez-Monteagudo, C., Huffenberger, K., Lin, Y.-T., Ostriker, J. P., & Trac, H. (2010). SIMULATIONS OF THE MICROWAVE SKY. *The Astrophysical Journal*, 709(2), 920.

Seigar, M. S., Graham, A. W., & Jerjen, H. (2007). Intracluster light and the extended stellar envelopes of cD galaxies: an analytical description. *Monthly Notices of the Royal Astronomical Society*, 378(4), 1575–1588.

Sheen, Y.-K., Smith, R., Jaffé, Y., Kim, M., Yi, S. K., Duc, P.-A., Nantais, J., Candlish, G., Demarco, R., & Treister, E. (2017). Discovery of Ram-pressure Stripped Gas around an Elliptical Galaxy in Abell 2670. *The Astrophysical Journal Letters*, 840(1), L7.

Silk, J., Di Cintio, A., & Dvorkin, I. (2014). Galaxy Formation. In *Proceedings of the International School of Physics 'Enrico Fermi' Course 186 'New Horizons for Observational Cosmology' Vol. 186*, volume 186 (pp. 137–187).

Silva, A., Marchesini, D., Silverman, J. D., Martis, N., Iono, D., Espada, D., & Skelton, R. (2021). Galaxy Mergers up to z $<$ 2.5. II. AGN Incidence in Merging Galaxies at Separations of 3 - 15 kpc. , 909(2), 124.

Smethurst, R. J., Lintott, C. J., Simmons, B. D., Schawinski, K., Marshall, P. J., Bamford, S., Fortson, L., Kaviraj, S., Masters, K. L., Melvin, T., Nichol, R. C., Skibba, R. A., & Willett, K. W. (2015). Galaxy Zoo: evidence for diverse star formation histories through the green valley. *Monthly Notices of the Royal Astronomical Society*, 450(1), 435–453.

Smith, G. P., Treu, T., Ellis, R. S., Moran, S. M., & Dressler, A. (2005). Evolution since z = 1 of the Morphology-Density Relation for Galaxies. *The Astrophysical Journal*, 620(1), 78–87.

Smith, K. L., Koss, M., Mushotzky, R., Wong, O. I., Shimizu, T. T., Ricci, C., & Ricci, F. (2020). Significant Suppression of Star Formation in Radio-quiet AGN Host Galaxies with Kiloparsec-scale Radio Structures. *The Astrophysical Journal*, 904(2), 83.

Somerville, R. S., Hopkins, P. F., Cox, T. J., Robertson, B. E., & Hernquist, L. (2008). A semi-analytic model for the co-evolution of galaxies, black holes and active galactic nuclei. *Monthly Notices of the Royal Astronomical Society*, 391(2), 481–506.

Spitzer, Lyman, J. & Baade, W. (1951). Stellar Populations and Collisions of Galaxies. *The Astrophysical Journal*, 113, 413.

Sridhar, S., Song, Y.-S., Ross, A. J., Zhou, R., Newman, J. A., Chuang, C.-H., Blum, R., Gaztañaga, E., Landriau, M., & Prada, F. (2020). Clustering of LRGs in the DECaLS DR8 Footprint: Distance Constraints from Baryon Acoustic Oscillations Using Photometric Redshifts. *The Astrophysical Journal*, 904(1), 69.

Staniszewski, Z., Ade, P. A. R., Aird, K. A., Benson, B. A., Bleem, L. E., Carlstrom, J. E., Chang, C. L., Cho, H.-M., Crawford, T. M., Crites, A. T., de Haan, T., Dobbs, M. A., Halverson, N. W., Holder, G. P., Holzapfel, W. L., Hrubes, J. D., Joy, M., Keisler, R., Lanting, T. M., Lee, A. T., Leitch, E. M., Loehr, A., Lueker, M., McMahon, J. J., Mehl, J., Meyer, S. S., Mohr, J. J., Montroy, T. E., Ngeow, C.-C., Padin, S., Plagge, T., Pryke, C., Reichardt, C. L., Ruhl, J. E., Schaffer, K. K., Shaw, L., Shirokoff, E., Spieler, H. G., Stalder, B., Stark, A. A., Vanderlinde, K., Vieira, J. D., Zahn, O., & Zenteno, A. (2009). GALAXY CLUSTERS DISCOVERED WITH a SUNYAEV-ZEL'DOVICH EFFECT SURVEY. *The Astrophysical Journal*, 701(1), 32–41.

Steinborn, L. K., Hirschmann, M., Dolag, K., Shankar, F., Juneau, S., Krumpe, M., Remus, R.-S., & Teklu, A. F. (2018). Cosmological simulations of black hole growth II: how

(in)significant are merger events for fuelling nuclear activity? *Monthly Notices of the Royal Astronomical Society*, 481(1), 341–360.

Stott, J. P., Smail, I., Edge, A. C., Ebeling, H., Smith, G. P., Kneib, J.-P., & Pimbblet, K. A. (2007). An Increase in the Faint Red Galaxy Population in Massive Clusters since $z \sim 0.5$. *The Astrophysical Journal*, 661(1), 95–101.

Strateva, I., Ivezić, Ž., Knapp, G. R., Narayanan, V. K., Strauss, M. A., Gunn, J. E., Lupton, R. H., Schlegel, D., Bahcall, N. A., Brinkmann, J., Brunner, R. J., Budavári, T., Csabai, I., Castander, F. J., Doi, M., Fukugita, M., Győry, Z., Hamabe, M., Hennessy, G., Ichikawa, T., Kunszt, P. Z., Lamb, D. Q., McKay, T. A., Okamura, S., Racusin, J., Sekiguchi, M., Schneider, D. P., Shimasaku, K., & York, D. (2001). Color Separation of Galaxy Types in the Sloan Digital Sky Survey Imaging Data. *The Astronomical Journal*, 122(4), 1861–1874.

Sunyaev, R. A. & Zeldovich, Y. B. (1970). Small-Scale Fluctuations of Relic Radiation. *Astrophysics and Space Science*, 7(1), 3–19.

Sunyaev, R. A. & Zeldovich, Y. B. (1972). The Observations of Relic Radiation as a Test of the Nature of X-Ray Radiation from the Clusters of Galaxies. *Comments on Astrophysics and Space Physics*, 4, 173.

Sweet, S. M., Drinkwater, M. J., Meurer, G., Kilborn, V., Audcent-Ross, F., Baumgardt, H., & Bekki, K. (2015). Kinematics of dwarf galaxies in gas-rich groups, and the survival and detectability of tidal dwarf galaxies. *Monthly Notices of the Royal Astronomical Society*, 455(3), 2508–2528.

Swetz, D. S., Ade, P. A. R., Amiri, M., Appel, J. W., Battistelli, E. S., Burger, B., Chervenak, J., Devlin, M. J., Dicker, S. R., Doriese, W. B., Dünner, R., Essinger-Hileman, T., Fisher, R. P., Fowler, J. W., Halpern, M., Hasselfield, M., Hilton, G. C., Hincks, A. D., Irwin, K. D., Jarosik, N., Kaul, M., Klein, J., Lau, J. M., Limon, M., Marriage, T. A., Marsden, D., Martocci, K., Mauskopf, P., Moseley, H., Netterfield, C. B., Niemack, M. D., Nolta,

M. R., Page, L. A., Parker, L., Staggs, S. T., Stryzak, O., Switzer, E. R., Thornton, R., Tucker, C., Wollack, E., & Zhao, Y. (2011). OVERVIEW OF THE ATACAMA COSMOLOGY TELESCOPE: RECEIVER, INSTRUMENTATION, AND TELESCOPE SYSTEMS. *The Astrophysical Journal Supplement Series*, 194(2), 41.

Thomas, J., Saglia, R. P., Bender, R., Thomas, D., Gebhardt, K., Magorrian, J., Corsini, E. M., Wegner, G., & Seitz, S. (2011). Dynamical masses of early-type galaxies: a comparison to lensing results and implications for the stellar initial mass function and the distribution of dark matter. *Monthly Notices of the Royal Astronomical Society*, 415(1), 545–562.

Thornton, R. J., Ade, P. A. R., Aiola, S., Angilè, F. E., Amiri, M., Beall, J. A., Becker, D. T., Cho, H.-M., Choi, S. K., Corlies, P., Coughlin, K. P., Datta, R., Devlin, M. J., Dicker, S. R., Dünner, R., Fowler, J. W., Fox, A. E., Gallardo, P. A., Gao, J., Grace, E., Halpern, M., Hasselfield, M., Henderson, S. W., Hilton, G. C., Hincks, A. D., Ho, S. P., Hubmayr, J., Irwin, K. D., Klein, J., Koopman, B., Li, D., Louis, T., Lungu, M., Maurin, L., McMahon, J., Munson, C. D., Naess, S., Nati, F., Newburgh, L., Nibarger, J., Niemack, M. D., Niraula, P., Nolta, M. R., Page, L. A., Pappas, C. G., Schillaci, A., Schmitt, B. L., Sehgal, N., Sievers, J. L., Simon, S. M., Staggs, S. T., Tucker, C., Uehara, M., van Lanen, J., Ward, J. T., & Wollack, E. J. (2016). THE ATACAMA COSMOLOGY TELESCOPE: THE POLARIZATION-SENSITIVE ACTPol INSTRUMENT. *The Astrophysical Journal Supplement Series*, 227(2), 21.

Toft, S., Mainieri, V., Rosati, P., Lidman, C., Demarco, R., Nonino, M., & Stanford, S. (2004). K-band luminosity function of the $z = 1.237$ cluster of galaxies RDCS J1252. 9-2927. *Astronomy & Astrophysics*, 422(1), 29–38.

Tonry, J. L. (1987). Properties of CD galaxies. In P. T. de Zeeuw (Ed.), *Structure and Dynamics of Elliptical Galaxies*, volume 127 (pp. 89–98).

Tremaine, S. D. & Richstone, D. O. (1977). A test of a statistical model for the luminosities of bright cluster galaxies. *The Astrophysical Journal*, 212, 311–316.

Tully, R. B., Mould, J. R., & Aaronson, M. (1982). A color-magnitude relation for spiral galaxies. *The Astrophysical Journal*, 257, 527–537.

Uson, J. M. (1986). The Sunyaev-Zel'dovich effect: measurements and implications. *National Radio Astronomy Observatory Workshop*, 16, 255–260.

Valotto, C. A., Nicotra, M. A., Muriel, H., & Lambas, D. G. (1997). The luminosity function of galaxies in clusters. *The Astrophysical Journal*, 479(1), 90.

van den Bergh, S. (1978). The Luminosity Function of Clusters of Galaxies. *Astrophysics and Space Science*, 53(2), 415–419.

van Haarlem, M. P., Frenk, C. S., & White, S. D. M. (1997). Projection effects in cluster catalogues. *Monthly Notices of the Royal Astronomical Society*, 287(4), 817–832.

van Houdt, J., van der Wel, A., Bezanson, R., Franx, M., d'Eugenio, F., Barisic, I., Bell, E. F., Gallazzi, A., de Graaff, A., Maseda, M. V., et al. (2021). Stellar Dynamical Models for 797 $z \sim 0.8$ Galaxies from LEGA-C. *The Astrophysical Journal*, 923(1), 11.

Vaughan, S. P., Tiley, A. L., Davies, R. L., Prichard, L. J., Croom, S. M., Bureau, M., Stott, J. P., Bunker, A., Cappellari, M., Ansarinejad, B., & Jarvis, M. J. (2020). K-CLASH: Strangulation and ram pressure stripping in galaxy cluster members at $0.3 < z < 0.6$. *Monthly Notices of the Royal Astronomical Society*, 496(3), 3841–3861.

Vecchia, C. D. & Schaye, J. (2012). Simulating galactic outflows with thermal supernova feedback. *Monthly Notices of the Royal Astronomical Society*, 426(1), 140–158.

Veillet, C. (2007). CFHTLS. In *American Astronomical Society Meeting Abstracts #210*, volume 210 of *American Astronomical Society Meeting Abstracts* (pp. 62.02).

Vikhlinin, A., Kravtsov, A. V., Burenin, R. A., Ebeling, H., Forman, W. R., Hornstrup, A., Jones, C., Murray, S. S., Nagai, D., Quintana, H., & Voevodkin, A. (2009). CHANDRA CLUSTER COSMOLOGY PROJECT III: COSMOLOGICAL PARAMETER CONSTRAINTS. *The Astrophysical Journal*, 692(2), 1060.

Villa, G., Page, C. G., Turner, M. J. L., Cooke, B. A., Ricketts, M. J., Pounds, K. A., & Adams, D. J. (1976). The Ariel V Sky Survey Instrument and new Observations of the Milky Way. *Monthly Notices of the Royal Astronomical Society*, 176(3), 609–620.

Visvanathan, N. (1981). Are we falling into the Virgo Cluster? *Publications of the Astronomical Society of Australia*, 4(2), 172–177.

Visvanathan, N. & Sandage, A. (1977). The color - absolute magnitude relation for E and S0 galaxies. I. Calibration and tests for universality using Virgo and eight other nearby clusters. *Astrophysical Journal*, 216, 214–226.

Voges, W., Aschenbach, B., Boller, T., Bräuninger, H., Briel, U., Burkert, W., Dennerl, K., Englhauser, J., Gruber, R., Haberl, F., Hartner, G., Hasinger, G., Kürster, M., Pfeffermann, E., Pietsch, W., Predehl, P., Rosso, C., Schmitt, J. H. M. M., Trümper, J., & Zimmermann, H. U. (1999). The ROSAT all-sky survey bright source catalogue. *arXiv preprint astro-ph/9909315*, 349, 389–405.

Voit, G. M. (2005). Tracing cosmic evolution with clusters of galaxies. *Reviews of Modern Physics*, 77(1), 207–258.

von der Linden, A., Wild, V., Kauffmann, G., White, S. D. M., & Weinmann, S. (2010). Star formation and AGN activity in SDSS cluster galaxies. *Monthly Notices of the Royal Astronomical Society*, 404(3), 1231–1246.

Vulcani, B., Poggianti, B. M., Gullieuszik, M., Moretti, A., Tonnesen, S., Jaffé , Y. L., Fritz, J., Fasano, G., & Bettoni, D. (2018). Enhanced Star Formation in Both Disks and Ram-pressure-stripped Tails of GASP Jellyfish Galaxies. *The Astrophysical Journal*, 866(2), L25.

Weinmann, S. M., van den Bosch, F. C., Yang, X., & Mo, H. J. (2006). Properties of galaxy groups in the Sloan Digital Sky Survey - I. The dependence of colour, star formation and morphology on halo mass. *Monthly Notices of the Royal Astronomical Society*, 366(1), 2–28.

Wen, Z. L. & Han, J. L. (2015). Dependence of the bright end of composite galaxy luminosity functions on cluster dynamical states. *Monthly Notices of the Royal Astronomical Society*, 448(1), 2–8.

Wen, Z. L., Han, J. L., & Liu, F. S. (2009). GALAXY CLUSTERS IDENTIFIED FROM THE SDSS DR6 AND THEIR PROPERTIES. *The Astrophysical Journal Supplement Series*, 183(2), 197–213.

White, S. D. M. (1980). Tidal Interactions and the Merging of Galaxies. *Philosophical Transactions of the Royal Society of London Series A*, 296(1419), 347–349.

Williamson, R., Benson, B. A., High, F. W., Vanderlinde, K., Ade, P. A. R., Aird, K. A., Andersson, K., Armstrong, R., Ashby, M. L. N., Bautz, M., Bazin, G., Bertin, E., Bleem, L. E., Bonamente, M., Brodwin, M., Carlstrom, J. E., Chang, C. L., Chapman, S. C., Clocchiatti, A., Crawford, T. M., Crites, A. T., de Haan, T., Desai, S., Dobbs, M. A., Dudley, J. P., Fazio, G. G., Foley, R. J., Forman, W. R., Garmire, G., George, E. M., Gladders, M. D., Gonzalez, A. H., Halverson, N. W., Holder, G. P., Holzapfel, W. L., Hoover, S., Hrubes, J. D., Jones, C., Joy, M., Keisler, R., Knox, L., Lee, A. T., Leitch, E. M., Lueker, M., Luong-Van, D., Marrone, D. P., McMahon, J. J., Mehl, J., Meyer, S. S., Mohr, J. J., Montroy, T. E., Murray, S. S., Padin, S., Plagge, T., Pryke, C., Reichardt, C. L., Rest, A., Ruel, J., Ruhl, J. E., Saliwanchik, B. R., Saro, A., Schaffer, K. K., Shaw, L., Shirokoff, E., Song, J., Spieler, H. G., Stalder, B., Stanford, S. A., Staniszewski, Z., Stark, A. A., Story, K., Stubbs, C. W., Vieira, J. D., Vikhlinin, A., & Zenteno, A. (2011). A SUNYAEV-ZEL'DOVICH-SELECTED SAMPLE OF THE MOST MASSIVE GALAXY CLUSTERS IN THE 2500 $\deg^2$ SOUTH POLE TELESCOPE SURVEY. *The Astrophysical Journal*, 738(2), 139.

Woods, R. M., Wadsley, J., Couchman, H. M. P., Stinson, G., & Shen, S. (2014). The role of cold flows and reservoirs in galaxy formation with strong feedback. *Monthly Notices of the Royal Astronomical Society*, 442(1), 732–740.

Wright, E. L., Eisenhardt, P. R. M., Mainzer, A. K., Ressler, M. E., Cutri, R. M., Jarrett, T., Kirkpatrick, J. D., Padgett, D., McMillan, R. S., Skrutskie, M., Stanford, S. A., Cohen, M., Walker, R. G., Mather, J. C., Leisawitz, D., Gautier, Thomas N., I., McLean, I., Benford, D., Lonsdale, C. J., Blain, A., Mendez, B., Irace, W. R., Duval, V., Liu, F., Royer, D., Heinrichsen, I., Howard, J., Shannon, M., Kendall, M., Walsh, A. L., Larsen, M., Cardon, J. G., Schick, S., Schwalm, M., Abid, M., Fabinsky, B., Naes, L., & Tsai, C.-W. (2010). The Wide-field Infrared Survey Explorer (WISE): Mission Description and Initial On-orbit Performance. *The Astronomical Journal*, 140(6), 1868–1881.

Wu, P.-F., van der Wel, A., Bezanson, R., Gallazzi, A., Pacifici, C., Straatman, C. M. S., Barišić, I., Bell, E. F., Chauke, P., D'Eugenio, F., Franx, M., Muzzin, A., Sobral, D., & van Houdt, J. (2020). The Colors and Sizes of Recently Quenched Galaxies: A Result of Compact Starburst before Quenching. *The Astrophysical Journal*, 888(2), 77.

Yan, H., Li, H., Wang, S., Zong, W., Yuan, H., Xiang, M., Huang, Y., Xie, J., Dong, S., Yuan, H., Bi, S., Chu, Y., Cui, X., Deng, L., Fu, J., Han, Z., Hou, J., Li, G., Liu, C., Liu, J., Liu, X., Luo, A., Shi, J., Wu, X., Zhang, H., Zhao, G., & Zhao, Y. (2022). Overview of the LAMOST survey in the first decade. *The Innovation*, 3, 100224.

Yang, Y., Zhou, X., Yuan, Q., Jiang, Z., Ma, J., Wu, H., & Chen, J. (2004). Large-field multicolor study of A168: Subclusters, dynamics, and luminosity functions. *The Astrophysical Journal*, 600(1), 141.

Yee, H., Gladders, M., Gilbank, D., Majumdar, S., Hoekstra, H., Ellingson, E., et al. (2007). The Red-Sequence Cluster Surveys. *arXiv preprint astro-ph/0701839*.

Yee, H. K. C. & Gladders, M. D. (2002). Optical Surveys for Galaxy Clusters. In L.-W. Chen, C.-P. Ma, K.-W. Ng, & U.-L. Pen (Eds.), *AMiBA 2001: High-Z Clusters, Missing Baryons, and CMB Polarization*, volume 257 of *Astronomical Society of the Pacific Conference Series* (pp. 109).

Yoachim, P. & Dalcanton, J. J. (2006). Structural Parameters of Thin and Thick Disks in Edge-on Disk Galaxies. *The Astronomical Journal*, 131(1), 226–249.

Zhang, Y., Miller, C. J., Rooney, P., Bermeo, A., Romer, A. K., Vergara Cervantes, C., Rykoff, E. S., Hennig, C., Das, R., McKay, T., Song, J., Wilcox, H., Bacon, D., Bridle, S. L., Collins, C., Conselice, C., Hilton, M., Hoyle, B., Kay, S., Liddle, A. R., Mann, R. G., Mehrtens, N., Mayers, J., Nichol, R. C., Sahlén, M., Stott, J., Viana, P. T. P., Wechsler, R. H., Abbott, T., Abdalla, F. B., Allam, S., Benoit-Lévy, A., Brooks, D., Buckley-Geer, E., Burke, D. L., Carnero Rosell, A., Carrasco Kind, M., Carretero, J., Castander, F. J., Crocce, M., Cunha, C. E., D'Andrea, C. B., da Costa, L. N., Diehl, H. T., Dietrich, J. P., Eifler, T. F., Flaugher, B., Fosalba, P., García-Bellido, J., Gaztanaga, E., Gerdes, D. W., Gruen, D., Gruendl, R. A., Gschwend, J., Gutierrez, G., Honscheid, K., James, D. J., Jeltema, T., Kuehn, K., Kuropatkin, N., Lima, M., Lin, H., Maia, M. A. G., March, M., Marshall, J. L., Melchior, P., Menanteau, F., Miquel, R., Ogando, R. L. C., Plazas, A. A., Sanchez, E., Schubnell, M., Sevilla-Noarbe, I., Smith, M., Soares-Santos, M., Sobreira, F., Suchyta, E., Swanson, M. E. C., Tarle, G., Walker, A. R., & Collaboration), D. (2019). Galaxies in X-ray selected clusters and groups in Dark Energy Survey data – II. Hierarchical Bayesian modelling of the red-sequence galaxy luminosity function. *Monthly Notices of the Royal Astronomical Society*, 488(1), 1–17.

Zinger, E., Dekel, A., Kravtsov, A. V., & Nagai, D. (2018). Quenching of satellite galaxies at the outskirts of galaxy clusters. *Monthly Notices of the Royal Astronomical Society*, 475(3), 3654–3681.

Zwicky, F. (1933). Die Rotverschiebung von extragalaktischen Nebeln. *Helvetica Physica Acta*, 6, 110–127.

Zwicky, F., Herzog, E., Wild, P., Karpowicz, M., & Kowal, C. T. (1961). *Catalogue of galaxies and of clusters of galaxies, Vol. I.*